THE INFLUENCE OF UNSTEADY PRESSURE GRADIENTS ON COMPARTMENTALIZATION REQUIREMENTS FOR PRESSURE-EQUALIZED RAINSCREENS

Final Report

D. INCULET

D. SURRY

JUNE 1996

BOUNDARY LAYER WIND TUNNEL LABORATORY
THE UNIVERSITY OF WESTERN ONTARIO
FACULTY OF ENGINEERING SCIENCE
LONDON, ONTARIO, CANADA
N6A 5B9

CONTENTS

EXECUTIVE SUMMARY

Seeking to improve the design of pressure-equalized rainscreens in high rise residential buildings, Canada Mortgage and Housing Corporation has sponsored this research on unsteady exterior pressure gradients. The work is intended for use in selecting compartment sizes in a pressure-equalized rainscreen, aimed at minimizing differential pressures across the rainscreen which are caused by these pressure gradients. The report details the following components:

1. Building and testing of a simple building model in the wind tunnel, fitted with a dense coverage of pressure taps on two faces. A comprehensive test program studying the effects of wind angle, upstream exposure, building height and face aspect ratio on the unsteady pressures was conducted. Possible effects caused by a similar sized building placed upstream were also tested.
2. Seeking an analysis method (affected in part by the results) which would provide designers with the necessary information for compartment sizing, orthogonal decomposition as well as a simple gust factor approach were explored. A method for calculating the gradients from the discrete pressures was necessarily developed.
3. Analysis of a portion of the data set, intended to show some results of the methods employed and the extent of the problem.

Some very preliminary recommendations for unsteady horizontal and vertical gradients have been made using a combination of the orthogonal decomposition results and actual peak unsteady values. The maximum recommended non-dimensional horizontal pressure gradient is 25.0, found at the vertical edges; the maximum vertical pressure gradient is 30.0, located at the top edge of the building. These must be superimposed on the mean gradients. These recommendations have been developed using only a small portion of the data set and it is not yet known if they are applicable over a range of simple building geometries.

RÉSUMÉ

La Société canadienne d'hypothèques et de logement a parrainé cette recherche portant sur les gradients instables de pression extérieure dans le but d'améliorer les écrans pare-pluie à pression équilibrée mis en oeuvre dans les tours d'habitation. Les travaux avaient pour but d'aider au choix des dimensions des compartiments d'un écran pare-pluie à pression équilibrée afin de réduire au minimum les différences de pression causées à l'écran pare-pluie par ces gradients de pression. Le rapport fait état des éléments suivants :

1. Construction et essai en soufflerie d'un modèle de bâtiment simple équipé, sur deux faces, d'une panoplie de prises de pression. Essai complet visant l'étude des effets qu'ont, sur l'instabilité des pressions, l'angle du vent, l'exposition au vent, la hauteur du bâtiment et le facteur de forme de la face. Les effets possibles causés par un bâtiment comparable situé en amont sont également examinés.
2. Recherche d'une méthode analytique (en partie modifiée par les résultats) pouvant offrir aux concepteurs les données requises pour établir la taille des compartiments, la décomposition orthogonale ainsi que la méthode du simple coefficient de rafale. Une méthode devant permettre le calcul des gradients à partir des pressions discrètes a nécessairement été mise au point.
3. Analyse d'une partie des séries de données dans le but de démontrer certains résultats obtenus avec les méthodes utilisées de même que l'étendue du problème.

Certaines recommandations très préliminaires relativement aux gradients horizontaux et verticaux instables ont été formulées à partir des résultats de la décomposition orthogonale associés avec les valeurs instables réelles de pointe. Le gradient de pression horizontal non dimensionnel maximum recommandé est de 25,0, observé aux rives verticales; le gradient de pression vertical maximum recommandé est de 30,0, celui-là étant situé à la rive supérieure du bâtiment. Ces valeurs doivent être superposées à celles des gradients moyens. Ces recommandations sont fondées sur une petite partie des données seulement, et on ne sait pas encore si elles peuvent s'appliquer à un éventail de géométries de bâtiment simples.

CMHC SCHL

Helping to house Canadians

Question habitation, comptez sur nous

National Office

700 Montreal Road
Ottawa, Ontario
K1A 0P7

Bureau national

700 chemin de Montréal
Ottawa (Ontario)
K1A 0P7

Puisqu'on prévoit une demande restreinte pour ce document de recherche, seul le sommaire a été traduit.

La SCHL fera traduire le document si la demande le justifie.

Pour nous aider à déterminer si la demande justifie que ce rapport soit traduit en français, veuillez remplir la partie ci-dessous et la retourner à l'adresse suivante :

Le Centre canadien de documentation sur l'habitation
La Société canadienne d'hypothèques et de logement
700, chemin de Montréal, bureau C1-200
Ottawa (Ontario)
K1A 0P7

TITRE DU RAPPORT : _____

_____

Je préférerais que ce rapport soit disponible en français.

NOM _____

ADRESSE _____
rue app.

_____
ville province code postal

No de télephone ( ) _____

TEL: (613) 748-2000

Canada Mortgage and Housing Corporation Société canadienne d'hypothèques et de logement

Canada

ACKNOWLEDGEMENTS

This study of rain simulation and wetting patterns on buildings was initiated by Canada Mortgage and Housing Corporation. The financial contributions of both Canada Mortgage and Housing Corporation and the Natural Sciences and Engineering Research Council of Canada are acknowledged.

Acknowledgement is made of the contributions by various members of the Laboratory staff: Mr. A. Burggraaf and Mr. S. Norman helped with the tubing of the model; Mr. G. Dafoe and Mr. S. Norman helped with the wind tunnel set-up. The model was constructed by members of the University Machine Shop. The report was finally assembled by Mrs. Tanya Spruyt and Mr. Jon Southen.

Finally, the authors would like to acknowledge the general direction, advice and encouragement received from Dr. A. G. Davenport, Director of the Boundary Layer Wind Tunnel Laboratory.

1 Introduction

The need for compartmentalization of the cavities within pressure-equalized rainscreens has been widely recognized [11,12], in order to limit the pressure differences that can develop across ventilation holes. Problems can arise when there are non-uniform external pressures, since the cavity pressures tend to be very nearly uniform, even when they are time-varying. External pressure non-uniformities can arise due both to mean spatial effects and to unsteady effects. Criteria have been suggested based primarily on existing knowledge of the gradients of mean pressures, together with the pressure differences that arise from phase differences associated with the dynamic response of the cavity to uniform unsteady external pressures; however, there has been little recognition that gustiness will also contribute directly to the external pressure differences that may exist across a compartment.

Improved design of pressure-equalized wall systems and quantification of all aspects of the pressure differences that may exist across the outer rainscreen motivated Canada Mortgage and Housing Corporation to sponsor several wide-ranging studies related to these problems. Most have already been reported separately. These include:

1) A study of rain-wetting patterns on buildings using wind tunnel simulations [4]
2) Measurement of mean and unsteady pressure distributions close to edges [8]
3) A summary of mean pressure gradients derived from archived tests on real buildings [6]
4) A preliminary study of the combined statistics of wind and rain [9]

On the basis of the above data, preliminary guidelines have been suggested as recorded in Appendix A.

It is the purpose of this report to examine a comprehensive set of unsteady pressure data measured on very carefully constructed models, in order to provide improved suggestions for the influence of the unsteady gradients, based on a simplified initial analysis of the data. In the long term, a more detailed analysis of the complete data set will form part of the senior author's PhD. thesis.

Eventually, in order to set reasonable criteria for compartmentalization, the dynamics of the compartment must be considered, together with criteria on the residual mean and unsteady pressure differences that can be tolerated by a successful rainscreen.

2 Scope of the Experimental Work

The wind tunnel measurements conducted in this study were intended to yield a representative picture of unsteady gradients on simple building geometries. It is a study on the complexities of one building. This would augment the work on *mean* pressure gradients and the complexities of shape [6].

To measure the time-varying pressure field over an entire building face, it was required to use the new "solid state" pressure sensing equipment at the Boundary Layer Wind Tunnel Laboratory. This allows simultaneous pressure measurement and hence, the calculation of *instantaneous* pressure gradients on the building face. An adequate coverage of pressure taps on the model is

required to "capture" the gradients as accurately as possible. It should be mentioned that it was ultimately necessary to redesign the model and retest due to small inaccuracies in the first model which, while fairly inconsequential to the pressures themselves, caused unforeseen yet significant inaccuracies in the calculation of gradients. The inaccuracies involved a slight misalignment of the tap positions near the edges, and varying sizes of tap holes - the result of an existing model being fitted with additional taps at a later stage.

2.1 Wind Tunnel Model

The basic pressure model used was a simple block type building having a height:width:depth (H:W:D) ratio of 3:2:1. Hence, the two instrumented faces had aspect ratios H:W of 3:2 and 3:1. The length scaling of 1:200 used resulted in this representing a building approximately 60 metres high, 40 metres wide, and 20 metres deep.

The wide face was instrumented with 509 pressure taps, 330 of these being placed on a 15X22 even grid. This basic grid spacing represented 2.9 m in full-scale. (It should be noted that this grid is based on the assumption that taps may be placed exactly at the model edges. In fact, the first line of taps was necessarily 2.5 mm model-scale or 0.5 m full-scale in from the edge, requiring extrapolation of results to achieve the even grid). Two extra grid lines were added at the side and top edges of the face, giving a 1.45 m full-scale spacing to a distance of 5.8 m towards the centre of the building (representing approximately 15% of the face width). The resulting grid was thus 19X24 (456 taps). The additional taps were intended for possible correlation studies. The narrow face was instrumented with 390 pressure taps. A 15X22 even grid was again used, with two extra grid lines added at the top edge to give a 15X24 grid. The grid spacing for this face resulted in a 1.45 m full-scale spacing across the entire width. Again, the additional taps will be used for correlation studies. The extra grid lines towards the edges were aimed at capturing more accurately the steeper gradients expected there. The number of taps used on each face required that the two faces be tested separately.

The basic tap spacing of 2.9 m full-scale was selected on the basis of it being a practical compartment size within the limitations of the instrumentation (a maximum of 512 taps are available to be scanned simultaneously). It was also expected to be, approximately, the spatial dimension of the smallest gust which could be measured. This was based on a maximum model-scale frequency response of the tubing system of 200 Hz and a relatively low wind tunnel speed of 10.7 m/s at gradient. The tubing system was especially designed for this study.

In addition to testing the "basic" model described above, two more heights were also tested by dropping the model beneath the wind tunnel floor. The extra heights represented 40 m and 20 m full-scale. Of course, the number of taps used in these tests was reduced. The additional aspect ratios H:W of the wide face were consequently 1:1 and 1:2 ; those of the narrow face were 2:1 and 1:1. That the 1:1 ratio is repeated for both faces will allow an interesting comparison.

2.2 Wind Tunnel Experiments

2.2.1 Wind Profiles

Two upstream exposures were used for the tests, representing an "open country" and a "suburban" terrain. The resulting profiles are shown in Figure 2.1. The power law exponents were

0.16 and 0.23 for the open and suburban exposures respectively; the roughness lengths, z_o, were 0.035 m and 0.38 m.

It must be noted that the pressure tests for the suburban, perpendicular wind case showed an asymmetry in the results (the pressures on one side of the building face were consistently lower than on the other). Consequently, a horizontal profile at the 30 m height full-scale was taken for both exposures. These horizontal profiles are shown in Figure 2.2. It is clear that there is a horizontal gradient across the tunnel and across the building width which is consistent with this observation. There is not such a definable gradient for the open exposure. An explanation for the gradient across the tunnel is, as yet, unconfirmed. However, due to this problem, the pressure results for the open country exposure will be treated as the base case, with the suburban exposure case providing an indication of the variation which may be expected due to changes in terrain roughness.

2.2.2 Wind Spectra

Wind spectra were measured for both exposures at 10 m full-scale and at all three building heights. Those at 10 m and 60 m are shown in Figures 2.3 and 2.4. The comparison with ESDU 74031 shows good agreement.

2.2.3 Pressure Tests

Pressure tests were carried out for the three model configurations described in Section 2.1. Angles from 0 to 180 degrees (representing windward to leeward faces respectively) were tested using increments of 10 degrees. As indicated in Section 2.2.1, both an open country and a suburban exposure were tested. Sampling was conducted for two minutes (representing up to one hour in full-scale) at a frequency of 500 Hz. The wind speed was 10.7 m/s at gradient in the wind tunnel.

Assuming a full-scale velocity of 20.0 m/s at 10 m, the velocity scaling, V_{MS}/V_{FS}, is 0.28 for the open country case and 0.23 for the suburban case. Thus, the frequency scaling f_{MS}/f_{FS} is 56:1 for the open country case and 47:1 for the suburban case. If a full-scale velocity of 30.0 m/s is of interest, the frequency scaling decreases to 37:1 and 31:1 for the open country and suburban cases respectively. Lower full-scale velocities may be of interest since a large portion of rainfall occurs at lower wind speeds [9].

Tests to illustrate possible interference effects caused by an identical upstream building were also conducted. The wide face was tested for the 40 m full-scale building height in the 0 degree orientation. Only the open exposure was used since that has been shown to give the worst comparative effects [7]. The upstream building was placed at 6 different positions:

[1]] Positions 1, 2 and 3 were directly upstream of the test building at centre-to-centre distances of 40m, 80m and 160m (in full-scale) respectively.

[2]] Positions 4, 5 and 6 were half the building width off-centre (*i.e.*. displaced sideways by 20m) at the same centre-to-centre upstream distances of 40m, 80m and 160m (in full-scale). The *left* half of the building face was left unshielded directly.

3 Method of Analysis

Two methods of analysing the data have been examined. The first consists of a method known as "proper orthogonal decomposition" which breaks the pressure or pressure gradient distribution down to a linear combination of "orthonormal" shape functions, similar, in principle, to a two-dimensional Fourier series. The technique was used to extract the unsteady pressure and pressure gradient distribution shapes that are common to all instantaneous distributions. The acquired series of shape functions normally converge rapidly and allow for simplification of the description of the pressure and pressure gradient fields by dropping the higher order shape functions which are usually far less significant. The second approach is that of a simple "gust factor" which relates the peak pressures and pressure gradients to their respective means.

All pressure coefficients, C_p, (collected referenced to a 1.5m height in the wind tunnel) were referenced to the mean dynamic pressure at roof height in the approaching flow. That is, $C_p = \frac{P - P_o}{1/2 \rho V_H^2}$, where P is the local pressure on the wall surface, P_o and V_H are the reference static pressure and roof height velocity, respectively, in the undisturbed free stream, and ρ is the density of air. The pressure gradients were defined in a similar non-dimensional fashion as $G_H = \frac{\partial C_p}{\partial (x/W)}$ and $G_V = \frac{\partial C_p}{\partial (y/H)}$, where x and y are the horizontal and vertical co-ordinates and W and H are the face width and height respectively. To illustrate, a typical non-dimensional horizontal gradient of 10 with a building width of 40 m would imply a ΔC_p per metre equal to 0.25 (*i.e.* 10/40). With a wind speed of, say 20 m/s at building height, and, consequently a wind pressure of about 240 Pa, this further implies a pressure gradient per metre of 60 Pa/m (*i.e.* 0.25x240).

3.1 Orthogonal Decomposition of Unsteady Pressures and Pressure Gradients

The complete two-minute (model-scale) simultaneous time histories of pressures at the grid locations were used in the orthogonal decomposition. Each wind angle and upstream exposure for each building face and height represented a different case. At each time increment, the instantaneous horizontal and vertical pressure gradients were calculated for each grid (tap) location. The sampling time and frequency resulted in 60,000 time increments. A spline fitting routine was used for the calculations. As indicated in Section 2.1, there was a slight deviation from the even grid at the side and top edges as obvious physical restraints prevent a tap from being located exactly at the model edge - the edge values for the pressures and pressure gradients were in fact extrapolated, giving the even grid of values. The point should be emphasized that, due to the regular grid of tap locations, only the *gradients* were required to be calculated - the C_p's used were those directly measured (this is in contrast to the analysis scheme required with the first model since its grid of taps was not entirely regular and required that some of the C_p's be calculated with the spline fitting routine).

The mean C_p was calculated for each tap location and removed from the total unsteady signal measured at that tap. Similarly, the mean G_H and G_V were calculated and removed from the total unsteady signals of horizontal and vertical pressure gradients respectively. Hence, the signals which were analyzed by orthogonal decomposition were only the unsteady portion of the total signals. It was believed that this method would allow one to more easily combine the results of this *unsteady* pressure work with those of the *mean* pressures and pressure gradients previously

studied [6]. That work dealt with the question of finding mean pressure and pressure gradients representative for many different building geometries and sitings.

The orthogonal decomposition technique (an eigenvector finding process) was then applied to the ensemble of time increments for one building face, height, angle and exposure. In this way, the common shape functions for the unsteady pressures, horizontal pressure gradients and vertical pressure gradients were extracted for one building configuration and wind angle. The shape functions were normalized so that the sum of their grid nodal values squared and averaged over all nodes was equal to unity.

For each time increment, the actual distribution of the instantaneous unsteady pressure or pressure gradients can be represented by a linear combination of their shape functions as follows:

$$F\left(x',y',t\right) = A_1(t) f_1\left(x',y'\right) + A_2(t) f_2\left(x',y'\right) + A_3(t) f_3\left(x',y'\right) + \cdots + A_N(t) f_N\left(x',y'\right) \qquad (1)$$

where $x' = x/W$ and $y' = y/H$ are the normalized co-ordinates, t is the time increment, $F(x',y',t)$ denotes any one of the pressures, horizontal gradients or vertical gradients, $f_i(x',y')$, $i=1,2,3 \ldots N$, are the common shape functions, and factors $A_i(t)$, $i=1,2,3 \ldots N$, are the amplitudes of the common shape functions (i.e.. modal amplitudes) for the time increment under consideration. The subscript *"i"* refers to mode number. Since the statistical mean of the pressures and pressure gradients has been removed, the mean amplitudes of the shape functions, $\overline{A_i}$, should have a zero value. The root-mean-square of the shape function amplitudes, $\tilde{A}_i$, will be non-zero.

The mode numbering was chosen so that the mode with the smallest number contributes the largest fraction of the total energy in the ensemble of actual instantaneous distributions (i.e., it has the highest "collective energy ratio"); higher number modes contribute progressively less and less of the energy. The number of modes (N) is equivalent to the number of grid nodes although it is hoped that only the first few will provide most of the energy. The collective energy ratio, $cer(i)$, the approximated-to-actual ratio of total energy summed over all nodes and time increments for a particular mode, can be calculated more simply from the eigenvalues associated with the eigenvectors (mode shape functions):

$$cer(i) = \frac{N\,\overline{A_i(t)^2}}{\sum_{i_{node}=1}^{N} \overline{C_p(i_{node},t)^2}} = \frac{\lambda_i}{\sum_{i=1}^{N} \lambda_i} \quad \text{(the overbar indicates an average over all time increments)} \qquad (2)$$

The "nodal energy ratio", $ner(i_{node},i)$, can be expressed in a similar fashion and can be used to determine which mode shapes contribute the most energy to specific grid nodes on the face:

$$ner(i_{node},i) = \frac{\overline{\left[A_i(t) * f_i\left(x',y'\right)\right]^2}}{\overline{C_p(i_{node},t)^2}} \qquad (3)$$

The orthogonal decomposition can be conducted for the entire signal (*i.e.*. from 0 to 200 Hz model-scale) and for the same signal after various filters have been applied. These filters may take the form of lowpass or bandpass filters.

To extend the analysis to information useful for design, it is necessary to combine the modes. Following the approach of Ho [3] and Lin [6], reliability theory can be used with the statistical results of the first few modes to arrive at a composite result with a prescribed safety index (reliability index β). Assuming a normal distribution of $F(x',y')$ at a point (x',y'), a representative value for this point, $F_r(x',y')$, can be calculated as follows:

$$F_r\left(x',y'\right) = \bar{F}\left(x',y'\right) \pm \beta\tilde{F}\left(x',y'\right) \tag{4}$$

where $\bar{F}\left(x',y'\right)$ and $\tilde{F}\left(x',y'\right)$ are the average and standard deviation respectively of $F(x',y')$ over all time increments calculated at point (x',y'). From Equation (1) and the properties of orthogonal decomposition (*i.e.*. $\overline{A_iA_j} = 0$ when $i \neq j$),

$$\bar{F}(x',y') = \bar{A}_1 f_1\left(x',y'\right) + \bar{A}_2 f_2\left(x',y'\right) + \bar{A}_3 f_3\left(x',y'\right) + \ldots + \bar{A}_N f_N\left(x',y'\right) \tag{5}$$

$$\overline{F^2}(x',y') = \overline{A_1^2 f_1^2}\left(x',y'\right) + \overline{A_2^2 f_2^2}\left(x',y'\right) + \overline{A_3^2 f_3^2}\left(x',y'\right) + \ldots + \overline{A_N^2 f_N^2}\left(x',y'\right) \tag{6}$$

and

$$\tilde{F}\left(x',y'\right) = \sqrt{\overline{F^2}\left(x',y'\right) - \bar{F}^2\left(x',y'\right)} \tag{7}$$

This approach provides a uni-reliability of $P_r = \Phi\left(\beta\right)$ where $\Phi(\ )$ is the standardized cumulative normal distribution function (see Table A.1 of [1], for example) and β the prescribed safety or reliability index. A simplified and approximate representation can be obtained by dropping the higher order modes, depending on the accuracy needed. The collective and nodal energy ratios may be referred to in considering the number of modes to use.

Equations (4,5,6, and 7) above are further simplified in this study by the fact that the mean pressures and pressure gradients have been removed from the signal. With $\bar{A}_n = 0$, Equation (7) simplifies to:

$$\tilde{F}\left(x',y'\right) = \sqrt{\overline{F^2}\left(x',y'\right)} \tag{8}$$

and $\bar{F}\left(x',y'\right)$ in Equation (4) becomes the statistical mean which was removed from the signal, or a mean which is, itself, based on reliability theory such as that developed in [6].

3.2 Simple Relationships between Mean and Unsteady Pressures and Pressure Gradients

The orthogonal decomposition analysis described in Section 3.1 uses considerable computer time. Also, preliminary results showed that the energy extraction in the first modes can be relatively low for the horizontal and vertical pressure gradients (however, see Sections 4.2.2 and 4.4 for comments on the limitations of the gradient calculations and the effects of lowpass filtering). Consequently, a simple method of describing *peak* pressure gradients was sought.

Taking the established idea of a "gust factor" which relates peak pressures to mean pressures, it was examined whether there is a relationship between peak and mean pressure gradients. To this end, a horizontal gust factor, G_H, and a vertical gust factor, G_V, were calculated as follows:

$$G_H = \frac{\hat{g}_H}{\bar{g}_H}; \quad G_V = \frac{\hat{g}_V}{\bar{g}_V} \tag{9}$$

where $\hat{g}_H$ and $\hat{g}_V$ are peak horizontal and vertical gradients respectively, and $\bar{g}_H$ and $\bar{g}_V$ are mean horizontal and vertical gradients respectively.

No statistical analysis to arrive at the peak gradients was conducted at this time which likely results in more variability than necessary. Instead, the actual peaks calculated for the two-minute

time history were used. The simple relationship shown in Equation (9) has the obvious problem that numerical difficulties will arise when the mean gradients approach zero (as they are expected to do, for example, at the centre of the windward face). Albeit, there may be some value in this approach where the gradients have their highest values and are thus of the greatest concern.

Again, it is possible to apply a digital filter, either lowpass or bandpass, to examine the frequency content of the peaks.

4 Results and Discussion

The analysis described in Section 3 has, thus far, been applied to a very small portion of the acquired data. It has been used on the wide face of the tallest building model (H:W of 3:2). Four wind angles have been examined for the "base case" of open country exposure - 0, 30, 60 and 90 degrees. For comparison, the 0 degree wind angle has also been examined for the same building face in the suburban exposure. It is believed that this is an adequate data base to validate the analysis method and to arrive at some preliminary conclusions.

4.1 Instantaneous Pressure and Pressure Gradient Contours

The advantage of using the new pressure scanner technology is that it allows an *instantaneous* picture of the pressures over the building face. This, in turn, allows the calculation of instantaneous pressure gradients. While any one instant in time does not give the statistical information required for design purposes, it does provide some insight into the process. To this end, three instantaneous distributions have been chosen randomly from the 2-minute time series of the 0 degree wind angle data. The results are taken at time increments of 10, 20 and 60 seconds into the 2-minute time series. The total signal is used. The open country exposure results of pressure, horizontal gradients and vertical gradients are shown in Figures 4.1a, 4.1b. and 4.1c respectively, and suburban exposure results are shown in Figures 4.2a, 4.2b. and 4.2c respectively. The mean distribution for each is shown in the top left graph of each figure to allow one to easily see the deviation from the mean. The instantaneous distributions are indicated as "inst" in each graph.

Figure 4.1a shows a maximum pressure coefficient of about 0.8, 0.4, or 0.6, depending on the time increment. The distribution in the centre region of the building can vary substantially from the mean distribution (see, in particular, the top right graph where the highest pressure coefficient is located at half the building height and at $x/W \approx 0.7$) A noticeable feature of all three time increments, however, is the rapid decline in pressure coefficients near the top and side edges, regardless of the interior distribution or the level of pressure coefficients.

Referring to Figures 4.1b and 4.1c which show the horizontal and vertical gradients, respectively, for the same time increments, the latter observation becomes quite clear. The central 80% of the building width sees relatively small *horizontal* gradients (a value less than 2), even for the highly unsymmetrical pressure coefficient distribution mentioned above. However, at about 10% of the building width in from the edges, the horizontal gradients get progressively larger as they approach the vertical edges. Similarly, the bottom 90% of the building height is exposed to *vertical* pressure gradients nearing a value of zero; for the most part, these gradients rapidly increase in the zone representing the top 10% (or slightly less) of the building. Being

instantaneous, there are small regions where the gradients decrease somewhat as the edge is approached. The vertical gradients near the top edge appear to have, in general, higher values than the horizontal gradients near the vertical edges. This may well be geometry dependent and must be examined further.

Similar observations may be made for the suburban exposure case although there seems to be considerably more variability between the time increments chosen. Of note are the vertical gradient distributions shown in the bottom two graphs of Figure 4.2c. One distribution has a maximum gradient of about 16, while the other sees a gradient of 32. Recall that these are randomly chosen time increments and merely show some of the variability which is possible.

Overall, it can be stated that the instantaneous distributions of *gradients* are very similar in form to their mean distributions (more so than their pressure distribution counterparts), albeit not as "smooth" in nature.

4.2 Orthogonal Decomposition

The following discussion of results of the orthogonal decomposition analysis will begin with a description of the mean pressures and pressure gradients. It is important to document these mean values since they have been removed from the total signal. In addition, it will allow an appreciation for the magnitude of the unsteady values. The portion of the total energy in the signals comprised by these means will be examined. Secondly, the first 3 *shapes* of the unsteady pressures and pressure gradients will be examined with a look at their collective energy ratios. Finally, the unsteady pressure and pressure gradient contours resulting from the reliability analysis with the first 3 modes and a safety index of 3.0 will be presented. Their nodal energy ratios will be discussed. Emphasis will be placed on the 0 degree wind angle, and, to a lesser extent, on the 30 and 60 degree wind angles. This is due to the fact that rain wetting studies [4,5] have shown 0 degrees to be the most important angle, but that angles of 30 and 60 degrees also result in some wetting. The 90 degree wind angle is included for completeness, although the rain wetting studies have shown this face to remain relatively dry.

4.2.1 Mean Pressure and Pressure Gradient Contours

Mean Pressures

The top left graph in each of Figures B.1 to B.4 in Appendix B (indicated as "Mn") shows the mean distribution of pressures for wind angles of 0, 30, 60 and 90 degrees respectively, for the open country case. This is the mean distribution which has been removed from the total signal . The case of the 0 degree wind shows the classic distribution one would expect, with a maximum C_p of about 0.7 in the central portion of the building face near the top. The C_p's near the edges are slightly negative (approaching -0.1 and -0.2 at the vertical edges). This indicates that the tap grid was chosen densely enough and near enough to the edges to capture this feature which is often missed by the typical resolutions used in a standard pressure test. The distribution is perhaps not as smooth as one may expect, but could indicate minor differences in the approach flow, in the taps, the calibrations used during testing, or simply a result of the interpolation used in the plotting program. It is not expected to introduce any appreciable error into the results. At a wind angle of 30 degrees, the maximum C_p is still about 0.7 but its location is shifted upstream, again as expected. At the 60 degree wind angle, the maximum C_p is only 0.2 and a large portion of the face experiences a negative C_p. At 90 degrees, the entire face is subjected to a negative C_p, with

values becoming less negative as the downstream edge is approached (values range from approximately -0.8 to -0.3).

Mean Horizontal Pressure Gradients

The top left graph in each of Figures B.5 to B.8 gives results for the mean horizontal pressure gradients, again at wind angles of 0, 30, 60 and 90 degrees, respectively, for the open country case. The high mean horizontal gradients for the 0 degree wind angle are concentrated along the vertical edges of the building with a maximum value of approximately 14 (+14 on the left side and -14 on the right side due to the convention used). At a distance of $x/W \approx 0.06$ in from both vertical edges, these mean gradients have reduced to a value of about 4 (recall, that for a 40m wide building, this still represents a change of 0.1 C_p over a 1m distance). Of course, along the centreline of the building, the gradient for this symmetrical case should be zero and it is very nearly so. The mean gradients for the 30 degree wind reduce to a maximum of about 10 (again, at the vertical edges). For the 60 degree wind, the maximum mean gradient is only about 3, but it occurs slightly downstream of the leading edge, at about $x/W = 0.08$, and towards the top of the building. It occurs again right at the downstream edge. The mean gradients for the 90 degree wind are rather inconsequential, with values very nearly zero over most of the face. The exceptions are some small isolated regions at distances closer than $x/W = 0.04$ in from both vertical edges where values reach about 3.

Mean Vertical Pressure Gradients

Results for the mean vertical pressure gradients are given in the top left graph of Figures B.9 to B.12 for wind angles of 0, 30, 60 and 90 degrees, respectively, for the open country case. For the 0 degree wind angle, the high mean vertical gradients (values greater than 4) are concentrated near the top edge of the building at $y/H \geq 0.94$. The maximum value is about 20. At a wind angle of 30 degrees, this zone is approximately the same size, but values near the upstream corner approach 32, while those at the downstream corner are reduced to about 12. The 60 degree wind angle also results in higher vertical gradients at the upstream corner than the downstream, but the values are reduced to about 16 and 4 respectively. At 90 degrees, the vertical gradients are essentially zero everywhere on the face.

Effect of Exposure

Figures B.13 ,B.14 and B.15 give results of mean pressures, horizontal gradients and vertical gradients, respectively, for the suburban exposure and 0 degree wind angle. Unfortunately, as mentioned in Section 2.2.1, the wind profile was not symmetric across the tunnel for this case and the results of this are visible in the mean distributions. Nevertheless, they are adequate to show some effects of the increase in terrain roughness. The C_p's are slightly lower in the suburban case, but still approach the same negative values towards the edges. The mean horizontal and vertical gradients are *very* similar to their open country exposure counterparts.

Energy Contribution of Mean Component

Appendix C contains graphs showing the contributions of the mean energy at a location on the face as a fraction of the total energy at that location. These are the top left graphs of each figure, indicated as "-me". The bottom left graphs in each figure, also indicated by "-me" are for a filtered signal and will be discussed later in Section 4.4. Some smoothing was required for the plots of horizontal and vertical gradients; it was not used with the pressure coefficients.

From Figure C.1, it can be seen that for a 0 degree wind in the open country case, the pressures in the central portion of the face ($0.08 < x/W < 0.92$ and $y/H < 0.92$) derive most of their energy from the means (> 80%). Towards the edges however, the means contribute less and less to the energy, reaching about only 30% at the edges. At a 30 degree wind angle (Figure C.2), a large portion of the face has pressure coefficients where the mean contributes greater than 70% of the total energy, but the means nearer the downstream edge and top edge contribute only a small fraction as they pass from positive to negative values. At 60 degrees (Figure C.3), the means become even less important over a larger region. However, at 90 degrees (Figure C.4), the mean pressure coefficients contribute greater than 70% of the energy over most of the face (recall that the means are high negative).

More at issue for compartmentalization purposes are the pressure gradients. Figure C.5 shows the contribution of the mean horizontal pressure gradients to the total energy of these gradients for the 0 degree wind angle and the open country exposure. In contrast to the C_p's, the mean horizontal gradients contribute a larger portion of the energy near the vertical edges (*i.e.*, where the mean gradients are high) than in the building centre. At distances closer than $x/W = 0.06$ to the vertical edges, the means contribute greater than 80% of the total energy. The exception to this is the top corners where the mean gradients drop in magnitude. Approaching the building centreline, the contribution drops gradually from the 80% to about 10%. Figure C.6 shows that, for a wind angle of 30 degrees, the contribution of the mean gradients at the leading edge is less than 60%. The mean gradients are still relatively high in this region and this indicates that the unsteady gradients will hold some importance here. At 60 degrees (Figure C.7), the means contribute little energy at the upstream half of the face, likely due to the reattachment mechanism of the flow. Recall too that the mean horizontal gradients for this angle are relatively small. For the 90 degree wind angle (Figure C.8), the contribution by the mean gradients is essentially zero.

Figure C.9 shows the contribution of the mean vertical pressure gradients for 0 degrees and an open country exposure. At values of $y/H \geq 0.94$, the mean gradients contribute more than 65% of the energy, with the larger values being closer to the edge. This places greater importance on the unsteady vertical gradients at the top edge than the unsteady horizontal gradients at the vertical edges.

The effects of a rougher exposure are demonstrated in Figures C.13, C.14 and C.15. As expected, the means contribute less to the total energy compared to the open country case, and this increases the importance of the *unsteady* pressures and pressure gradients in rougher terrain.

4.2.2 Unsteady Pressure and Pressure Gradient Contours from Orthogonal Decomposition

Shape functions for the first 3 modes of the *unsteady* portion of the pressure and pressure gradient signals are given in Figures B.1 to B.15. Modes 1, 2 and 3 are indicated as M1, M2 and M3 respectively. They will be discussed only briefly here, as the more useful information for design is contained in Section 4.2.3. The root-mean-square amplitude of the shapes is given in Table B.1.

Unsteady Pressure Shapes

Figures B.1 to B.4 show results of the analysis on the pressure coefficients for wind angles of 0, 30, 60 and 90 degrees respectively, for the open country case. The most noticeable feature of

these shapes is that for the 0 and 30 degree wind angles, the first shape is very similar to the simple mean distribution (although much smoother). For the 60 degree case, the maximum unsteady pressure appears to have moved towards the upstream edge, relative to the location of the maximum mean pressure. For the 90 degree case, it is difficult to compare the first unsteady shape with the mean distribution, but there appears to be some differences in the shape of the distribution.

Unsteady Horizontal Pressure Gradient Shapes

Figures B.5 to B.8 give shape functions for the unsteady portion of the horizontal pressure gradients for wind angles of 0, 30, 60 and 90 degrees, again for the open country case. As with the pressures, the first shapes for the 0 and 30 degree wind angles are much like the mean distributions. All three modes for these angles concentrate on information at the vertical edges. For the 60 degree wind angle, the shapes give information primarily near the upstream edge, where, as previously mentioned, reattachment may be occurring.

Unsteady Vertical Pressure Gradient Shapes

Figures B.9 to B.12 show the shape functions for vertical pressure gradients at wind angles of 0, 30, 60 and 90 degrees respectively, in open country. For angles of 0 and 30 degrees, the first shapes are, again, similar to their mean counterparts. The second shapes supply more information near the top edge; the third shapes seem to provide little in the way of a recognisable shape. For angles of 60 and 90 degrees, the first shapes again give information primarily along the top edge.

Effect of Exposure

Results from the suburban exposure test at 0 degrees are given in Figures B.13, B.14 and B.15 for pressures, horizontal gradients and vertical gradients respectively. Like the open country case, the first shape of the pressure is similar to its mean distribution. The second and third shapes are, unfortunately not symmetric as they are in the open country case due to the horizontal gradient across the tunnel. For the gradients, all three shapes are virtually identical in form to their open country counterparts.

Collective Energy Ratios

The collective energy ratios for each of the shapes described above are given in Table B.2. Recall that these give the fraction of the total *unsteady* energy, averaged over all nodes, which is contained in each shape. It is seen, for example, that for the pressures at a 0 degree wind angle and in an open country exposure, the first shape contributes 58% of the total unsteady energy. The second and third shapes contribute much less, only 12% and 9% respectively. However, this means that by combining the three shapes, 79% of the unsteady energy is accounted for. The orthogonal decomposition analysis of gradients is much less effective at extracting the energy - the first shape of the horizontal gradients extracts 32% of the energy; the second and third shapes extract 11% and 4% respectively. Hence, the combination of the three shapes gives 47% of the energy. However, it must be recalled that this includes energy in the large central region of the face where the gradients are typically small. It will be seen in Section 4.2.3 when examining nodal energies that the energy extraction is more efficient towards the edges where the gradients are high. Similar to the horizontal gradients, the first shape of the vertical gradients extracts 29% of the unsteady energy while the second and third shapes account for 5% and 4% respectively, giving a combined total of 38%. The extraction of energy for the 90 degree wind angle is

extremely poor for the gradients. The inclusion of additional modes is not considered practical as their individual energy contributions are very small.

The increase in terrain roughness, giving more unsteady energy, allows a greater efficiency in its extraction. The suburban exposure at 0 degrees gives combined energy extractions (3 modes combined) of 85%, 51% and 43% for the pressures, horizontal gradients and vertical gradients respectively.

The effects of lowpass filtering on the energy extraction will be discussed in Section 4.4. It is particularly important for the gradients since these are calculated quantities and their accuracy is limited by the pressure tap spacing and the spline fit used.

4.2.3 Reliability Analysis with First 3 Modes

Using Equation 4, representative values for the unsteady pressures and gradients ($F_r(x',y')$) were determined. The mean values in Equation 4 ($\bar{F}(x',y')$) were neglected in the calculations as this section is intended to focus on the unsteady portion of the signal. As indicated in Section 3.1, it is optional which mean might be included in the equation - a "true" mean or a mean which is based on reliability theory. A reliability index of 3.0 was used which suggests a probability of 0.99 that the unsteady pressures or gradients will not be exceeded. However, only the first 3 modes were used and it must be cautioned that, as indicated in Section 4.2.2, the energy extraction is not adequate to ensure such a probability.

Expected Unsteady Pressures

The values for $F_r(x',y')$ where F is the unsteady pressure coefficient are given in the top graph of Figures 4.3, 4.4, 4.5 and 4.6 for wind angles of 0, 30, 60 and 90 degrees respectively, all for the open country exposure. The expected maximum unsteady pressure coefficient for the 0 degree angle is seen to be 0.8 in Figure 4.3, the minimum is about 0.3. The shape of the distribution is much like the classic shape of the mean pressures. Since positive acting pressures will more likely drive water through the rainscreen than will suctions, these values should be considered as positive acting. By adding these to the negative mean pressures at the edges then, the pressure coefficients found there will become positive (using the mean pressure distribution which was actually measured, not a reliability based distribution). The gust factor at the point of maximum pressure has a value of about 2. At the 30 degree wind angle, the maximum and minimum unsteady pressure coefficients are about 0.7 and 0.2 respectively. The unsteady pressures for the 60 degree wind angle are, perhaps the most interesting in that their form is shifted from that of the mean pressures and their values are high relative to the mean pressure values. The maximum unsteady pressure coefficient is about 1.0 and located in a zone where the mean pressure coefficients are approximately zero. At 90 degrees, the unsteady pressure coefficients are high, but not likely high enough to cause a substantial positive acting pressure when combined with the mean pressures.

Expected Unsteady Horizontal Pressure Gradients

The unsteady horizontal pressure gradients are given in the bottom left graph of Figures 4.3, 4.4, 4.5 and 4.6 for wind angles of 0, 30, 60 and 90 degrees respectively, all for the open country exposure. The unsteady horizontal gradients have an expected maximum value of about 10 at the vertical edges; by $x/W = 0.06$, this value has dropped to 4. Using the mean horizontal gradients acquired in this test, this suggests a gust factor of approximately 2 in this region, ie the total is

twice the mean gradient. At 30 degrees (Figure 4.4), the maximum unsteady horizontal gradient is 14, located at the upstream edge; at the downstream edge it is 6. This suggests a gust factor of 2.8 at the upstream edge. The unsteady horizontal gradients for a wind angle of 60 degrees are extremely high (see Figure 4.5), reaching values of 36 in the upstream corner. The gust factors are, consequently, very high as well. Downstream of $x/W = 0.16$, the unsteady gradients are less than 4. At 90 degrees, the unsteady gradients have values of only about 3.

Expected Unsteady Vertical Pressure Gradients

The unsteady vertical pressure gradients are given in the bottom right graph of Figures 4.3, 4.4, 4.5 and 4.6 for wind angles of 0, 30, 60 and 90 degrees, respectively, and for the open country exposure. The maximum unsteady vertical gradient is expected to be 20 at the top edge; at $y/H = 0.95$, this is reduced to 4. These results indicate a gust factor of approximately 2 (*i.e.* the unsteady gradients have about the same magnitude as the mean gradients). At 30 degrees, the unsteady vertical gradients are expected to be very high at the upstream corner, similar to the means. The expected values reach 32, again indicating a gust factor of about 2. A similar situation exists for the 60 degree wind except that the expected unsteady vertical gradient reaches a value of 38 in the top corner, resulting in a gust factor of about 3. At 90 degrees, results show that very high unsteady vertical gradients can be expected along the top edge, primarily in the middle region. Values for these gradients may reach 34.

Effect of Exposure

Figure 4.7 shows the representative unsteady pressures and gradients for the suburban exposure and a 0 degree wind angle. The maximum expected unsteady pressure coefficient is increased to about 1.1 from the value of 0.8 in the open country situation. The minimum is 0.5 in lieu of 0.3. Hence, as expected, the rougher terrain results in higher unsteady pressures and, consequently, higher positive pressures to drive water through the rainscreen. The gust factors are higher than with the smoother terrain since the mean pressure coefficients were smaller in that case. The gust factor at the point of maximum pressure has a value of about 2.5. The expected unsteady horizontal gradients are also higher, reaching a value of 16 at the vertical edges. However, like the open country case, this value drops to 4 at $x/W = 0.06$. The maximum expected vertical gradient is 26 at the top edge (in lieu of 20 in the open country situation); this too is reduced to 4 at $y/H = 0.95$. The gust factors along the vertical edges for the horizontal gradients and along the top edge for the vertical gradients are about 2.3.

Nodal Energy Ratios of Combined First 3 Modes

The top right graph in Figures C.1 to C.15 shows the nodal energy ratios for the first three modes combined. These are calculated by Equation 3 and summed over the 3 modes. It is apparent from these graphs that the energy extraction is most efficient in locations where the signal is high.

Figures C.1 to C.4 describe the nodal energy ratios for pressures at 0, 30, 60 and 90 degrees, respectively, for the open country exposure. Examining the nodal energy ratios for a 0 degrees wind angle and recalling from Section 4.2.2 that the collective energy ratio for the 3 modes was 79%, it is seen that this is exceeded in the central portion of the face - the nodal energy ratios here are 90%. It is not until the zone $x/W \leq 0.12$ and $y/H \geq 0.96$ that the nodal energy ratios are as low as 80% and at the very edge, they are approximately 40% over most of the length.

Figures C.5 to C.8 show nodal energy ratios for the horizontal gradients at 0, 30, 60 and 90 degrees, again for the open country exposure. At a wind angle of 0 degrees, the nodal energy ratios are between 40% and 70% in the high unsteady gradient zone ($x/W \leq 0.06$). The unsteady gradients account for about 20% of the total energy in this zone. Recall that the collective energy ratio was 47%. At 30 degrees, at the upstream edge where the mean gradient has a value of about 8, the unsteady portion of the signal accounts for 40% of the total energy, and the nodal energy ratios here are about 70%. Hence, the unsteady gradients shown in Figure 4.4 have an important contribution here. However, it is true that at 60 degrees, near the upstream edge where the unsteady energy accounts for about 90% of the total energy, the nodal energy ratios range from only 10 to 60%, with most of them less than 40%. This appears to be a rather unstable region. At 90 degrees, the nodal energy ratios are less than 30% over most of the face.

Figures C.9 to C.12 give nodal energy ratios for the vertical gradients at 0, 30, 60 and 90 degrees. For the 0 degree wind angle the nodal energy ratios are between 40% and 70% in the high unsteady gradient zone ($y/H \geq 0.95$), compared to a collective energy ratio of only 38%. The unsteady gradients account for 20 to 30% of the total energy in this zone

The effect of an increase in terrain roughness can be seen in Figures C.13 to C.15. In almost all locations, the nodal energy ratios are increased compared to their open country counterparts. This is expected, given the results of the collective energy ratios.

4.3 Peak Pressure Gradients and Gust Factors

Measured Peak Pressure Gradients

Shown in Figures 4.8 to 4.12 are contour plots of the peak gradients with their means subtracted. The peak gradients were chosen such that their sign was the same as that of their respective mean gradients. The absolute values of these quantities have been used to avoid more scatter in the plots caused by the fact that, near small mean gradients, the sign of the mean gradients fluctuates from one location to another. Smoothing has been carried out once for these contour plots. Ideally, these peaks should be similar in absolute value to the expected values from the orthogonal decomposition analysis reported in Section 4.2.3.

The results show peak horizontal gradients (*less their mean*) of about 20 at the vertical edges for the open country case at 0 degrees. The central region sees minimum peak horizontal gradients of about 4. With the suburban exposure, these values are increased to about 30 and 5 respectively. At 30 degrees the maximum peaks are found at the upstream edge with values of about 24; at 60 degrees, the peak increases to approximately 50 at the upstream edge. Minimum peaks of about 4 are still found for these angles. At 90 degrees, the peaks are calculated to be extremely high over large areas of the face, with values between 15 and 50. They are possibly very rare events or poorly correlated as the expected values from the orthogonal decomposition analysis do not suggest such values.

Peak vertical gradients are seen to be about 30 at the top edge for the 0 degree wind angle with an open country exposure. Minimum values of about 7 are found in the central region of the face. Corresponding values for the suburban case are about 40 and 9 respectively. An interesting feature of these results when compared to the orthogonal decomposition results is the presence of relatively high peaks near the base of the building. These reach values of 14 and 19 for the open country and suburban exposures respectively. At 30 and 60 degree wind angles, the maximum

peak vertical gradients are found at the upstream corner and have values of about 40 and 50 respectively. The minimum peak values on the face are about 6 and 5 respectively. Like the horizontal gradients, peak vertical gradients for the 90 degree wind angle are high over the entire face with values between approximately 20 and 50.

An important observation can be made for the 0 degree wind angle in comparing the peak gradient contours with the contours of expected gradients from the orthogonal decomposition analysis. Generally, with the peak gradients, values increase near the top corners relative to the edges for the same x/W (for horizontal gradients) and y/H (for vertical gradients). However, with the expected gradients, the values *decreased* at the corners relative to further along the edges for the same x/W and y/H values. Referring to the figures in Appendix C, it is seen that the orthogonal decomposition analysis would have underestimated these peaks since the nodal energy ratios in the top corners were poor. In addition, the unsteady energy accounts for a greater portion of the total energy in the corners than it does further along the edges. The use of additional mode shapes would have been required to capture these peaks.

Gust Factors

Gust factors for the horizontal and the vertical pressure gradients were calculated using Equation 9. The peak gradients were chosen such that their sign was the same as that of their respective mean gradients. Resulting contour plots of these gust factors for the 0 degree wind angle are shown in Figures 4.13 and 4.14 . The raw results have been smoothed in the contour plotting program 4 times as they proved to be very difficult to decipher without this.

As mentioned in Section 3.2, the practical applications of the gust factor are limited in regions where the mean pressure gradients are very low and thus the gust factors are calculated to be extremely high (greater than, say, 10). In the central 40% of the face shown in Figure 4.13 and 4.14, the gust factors for the horizontal gradients exceed 10. In this region, most of the peak gradients (less their mean) are less than about 6. It might be tempting to assume that regions of high gust factors and therefore low means can be handled by assuming some maximum peak gradient. Unfortunately, not all locations with small mean gradients have correspondingly low peak gradients. Take, for example, the upstream edge for the 60 degree wind angle with open country exposure. Here, the mean horizontal gradients are approximately 0 at $x/W=0.2$ (see Figure B.7). However, at that same location, the peak gradients less their mean are approximately 15 (see Figure 4.10a). A general rule does not seem to be easily applicable.

Regions closer to the edges have both horizontal and vertical gust factor values closer to 4 or 5 except near the corners where they approach 20. To avoid overdesign, a graduated gust factor would be required (there is not one value which seems practical to apply to the entire face). Whether this is a practical approach to follow requires further investigation of the data base including other building heights and aspect ratios.

4.4 Effects of Lowpass Filtering

A lowpass filter at 20 Hz (model scale) was applied to the data. This represents, as an example, 0.54 Hz in full-scale for a 30 m/s wind speed at 10m in open country. As a first step, this cut-off frequency was chosen by examining the coherence between the horizontal gradients at several grid locations. The filter was applied to the pressure coefficient data itself, from which the gradients were calculated - it was not applied to the calculated gradients.

The general effect of the filter is, of course, to reduce the unsteady portion of the signal. The instantaneous contours of Figures 4.1 and 4.2 are shown again in Appendix D, this time with the 20 Hz lowpass filter. It is seen that, while the form remains relatively similar, they are somewhat smoother and, generally, have lower values.

The filtered shape functions are shown in Appendix E. For most angles, the first 3 shapes are virtually identical to their unfiltered counterparts. The amplitudes are reduced (for the first mode, typically by 2 to 20%) however and, consequently, the expected pressures and gradients from the orthogonal decomposition are reduced. The amplitudes are given in Table E.1. The collective energy ratios are increased, particularly for the gradients, since the total unsteady signal is smaller. They are given in Table E.2. It is seen, for example, that for a 0 degree wind angle in the open country exposure, 80% and 71% of the total unsteady energy is extracted in the first three modes for the horizontal and vertical gradients respectively. This is increased from 47% and 38% respectively in the unfiltered case.

Reliability analysis using the first 3 filtered modes results in the expected values shown in Appendix F. For the 0 and 30 degree wind angles, the expected horizontal and vertical gradients are changed very little from the unfiltered versions since the first modes have amplitudes within 94% of one another. The nodal energy ratios are increased quite substantially; they are shown in the bottom graphs of Figures C.1 to C.15.

Finally, the peak gradients calculated after filtering are given in Appendix G. It is seen that, for example, the maximum horizontal gradient for the open country exposure at 0 degrees is reduced to about 15 and the maximum vertical peak gradient is reduced to about 24 (from 20 and 30 respectively).

5 Conclusions and Future Work

It was hoped and assumed that the orthogonal decomposition analysis would provide the answers to this problem. In most uses known to the authors, it has proven to be a very effective method, extracting most of the energy from a process in the first few modes. This is true in the current situation when the means are included such that the first mode actually has a mean component in addition to the unsteady component. However, when dealing with only the unsteady component of the signal as has been done herein, the energy extraction has not been as effective. While about 80% of the energy of the pressure coefficients is removed in the first 3 modes (except for the angle of 90 degrees), less than 50% of the *gradient* energy is removed in these first 3 modes. The gradient energy extraction is improved to 70-80% when the lowpass filter is used (except for the angles of 60 and 90 degrees). One fortuitous result is, however, that the nodal energy ratios are greater in areas of high gradients where they are, of course, more important.

This being said, orthogonal decomposition is, to date, the best analysis method used in this problem of unsteady gradients. The gust factor is not believed to have yielded results which may be simply applied in a blanket fashion - and this is typically the premise of such an approach. Consequently, to arrive at some *preliminary* recommendations at this time, a combination of the orthogonal decomposition results and of the actual peak unsteady values will be used. Further, it must be emphasized that the substantial data base has, as yet, been analysed insufficiently to arrive at guidelines applicable to the many building shapes which have been tested.

The preliminary recommendations for unsteady horizontal and vertical pressure gradients are given in Table 5.1. They are based, primarily on the unfiltered data for an open country exposure, with some allowance for the effects of a suburban exposure. In many cases, the effect of the filtering is negligible, and given the other uncertainties, it is more prudent to use the unfiltered data. While use of the open country exposure does not yield the most conservative results, wind angles of 30 and 60 degrees were found to have some of the higher unsteady gradients and these angles had not been analysed for the suburban case. However, the 60 degree angle has wetting intensities less than the 0 degree wind angle [4] and, in the interest of not overdesigning, some of the very high peak gradients at 60 degrees are not integrated into the recommendations. The recommendations do, in these cases, exceed the expected values from the orthogonal decomposition results for all but an *extremely* small region at the top corners.

When the results of Table 5.1 are compared with the detailed mean gradient data included in Appendix A, a surprisingly similar pattern can be seen. Near the edges, the magnitudes are large and of similar size. In central regions, where the magnitudes are not as significant, the mean approaches zero whereas the unsteady gradients approach a constant value.

Thus, to a reasonable approximation, the following constitutes an approximation to the total pressure gradients in various regions.

a) Within 10% of the vertical edges, the total horizontal gradients can be estimated as 1.7 times the mean gradients.

b) Within 10% of the top edge, the total vertical gradients can be estimated as 2.0 times the mean gradients.

c) In the interior of the face away from these edge regions, the total normalized horizontal gradient can be taken as 15, and the normalized vertical gradient can be taken as 20.

Future work on this topic of unsteady gradients is critical to arrive at solid guidelines which can be used with confidence. It is the intent of the authors to carry out the following, using the acquired data base:

1. The limitations of the gradient calculations must be established. That is, what is the effect of the spline fit and the tap spacing on the accuracy of these calculations.
2. The spectra of gradients must be further examined to determine the energy content as a function of frequency. This must await the results of 1. above. This will aid in deciding whether a filter is appropriate, and if so, at what frequency.
3. The orthogonal decomposition analysis may be limited to smaller regions such as edges and corners to possibly obtain better energy extraction in these regions.
4. Ultimately, the worst case over all angles relevant to the rain wetting mechanism should be obtained.
5. The final analysis method chosen must be extended to the entire data base to ensure that the guidelines are applicable to a range of simple buildings.
6. The upstream interference effects data must be studied to gain insight into the variations which may be expected when a building is not located in a uniform exposure.
7. Effects of compartment dynamics, and of tolerable pressure differences must also be considered in setting final compartmentalization guidelines.

REFERENCES

[1] Benjamin, J.R. and Cornell, C.A. "Probability, Statistics, and Decision for Civil Engineers", McGraw-Hill, 1970.

[2] CAN/CSA-A440-M90 (1990), Windows, A National Standard of Canada.

[3] Ho, T.C.E. " Statistical Analysis of Peak Pressure Distributions on Tall Buildings", M.E.Sc. Thesis, The University of Western Ontario, 1985

[4] Inculet, D. and Surry, D. "Simulation of Wind-Driven Rain and Wetting Patterns on Buildings", BLWT-SS30-1994, The University of Western Ontario, November 1994.

[5] Inculet, D., Surry, D. and Skerlj, P.F. "The Experimental Simulation of Wind and Rain Effects on the Building Envelope", International Conference on Building Envelope Systems and Technology Forum on Building Envelope Research, Singapore, December 7-8, 1994.

[6] Lin, J.X., Surry, D. and Inculet, D.R. "A Study of the Characteristic Shapes of Mean Pressures and their Gradients on Buildings in Realistic Surroundings", BLWT-SS3-1995, The University of Western Ontario, March 1995.

[7] Sanni, R.A., Surry, D. and Davenport, A.G. "Wind Loading on Intermediate Height Buildings", Canadian Journal of Civil Engineering, Vol.19, No.1, February 1992.

[8] Skerlj, P.F. and Surry, D. "A Study of Mean Pressure Gradients, Mean Cavity Pressures, and Residual Mean Pressures across a Rainscreen for a Representative Building", BLWT-SS23-1994, The University of Western Ontario, September 1994.

[9] Surry, D., Skerlj, P.F. and Mikitiuk, M.J. "Climatic Relationships Between Wind and Rain", BLWT-SS22-1994, The University of Western Ontario, September 1994.

[10] Surry, D., Inculet, D.R., Skerlj, P.F., Lin, J-X., and Davenport, A.G. "Wind, Rain and the Building Envelope: A Status Report of Ongoing Research at the University of Western Ontario", Journal of Wind Engineering and Industrial Aerodynamics, Vol.53, pp.19-36, 1994

[11] Baskaran, A. "Review of Design Guidelines for Pressure-Equalized Rainscreen Walls", Internal Report No. 629, National Research Council, Institute for Research in Construction, Ottawa, Canada, 1992.

[12] Inculet, D.R. "Pressure-Equalization of Rainscreen Cladding", M.E.Sc. Thesis, The University of Western Ontario, 1990.

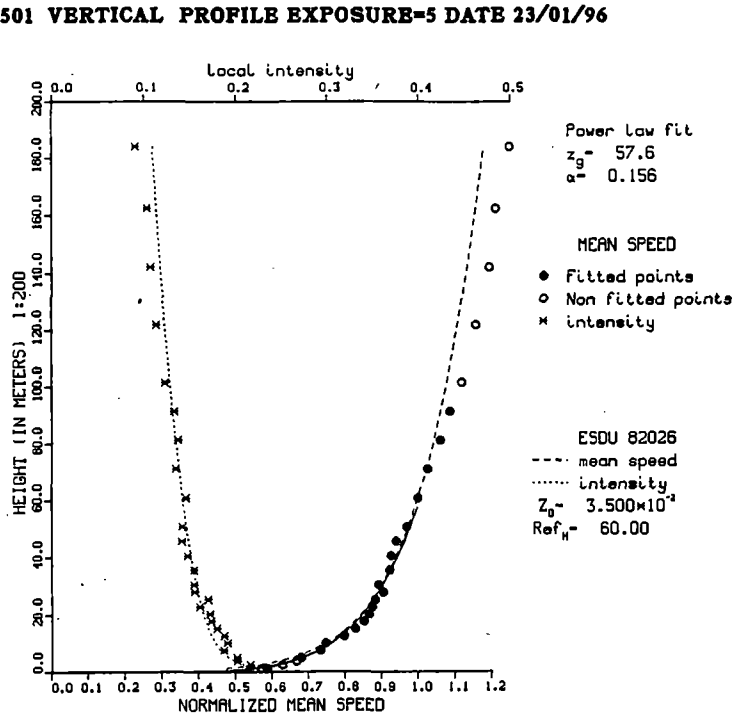

Figure 2.1a. Mean Speed and Turbulence Intensity Profiles at the Test Site (Open Country Exposure)

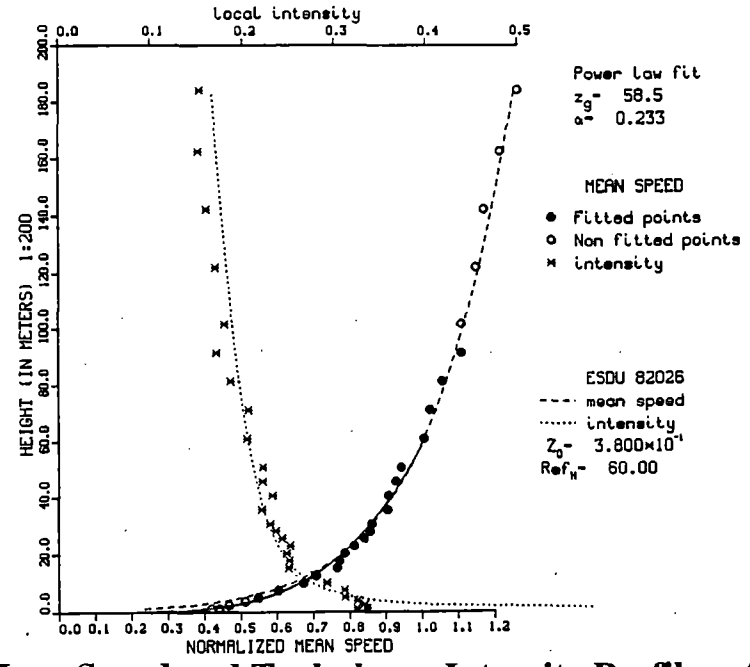

Figure 2.1b. Mean Speed and Turbulence Intensity Profiles at the Test Site (Suburban Exposure)

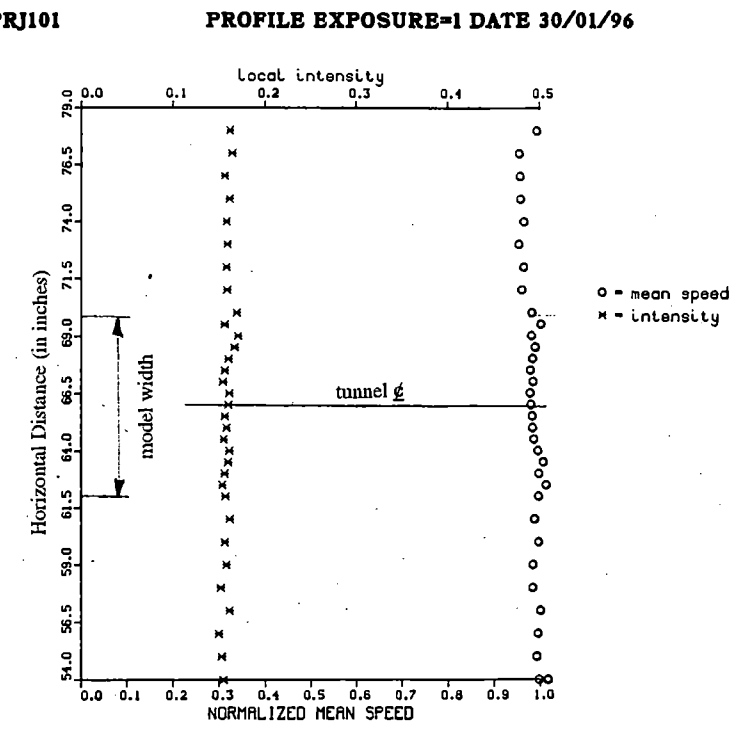

Figure 2.2a. Horizontal Mean Speed and Turbulence Intensity Profiles (Open Country Exposure)

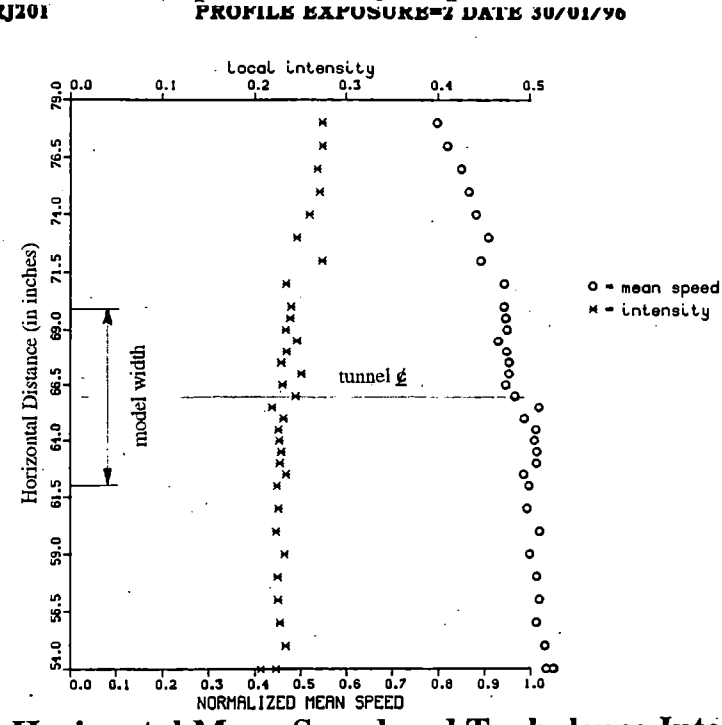

Figure 2.2b. Horizontal Mean Speed and Turbulence Intensity Profiles (Suburban Exposure)

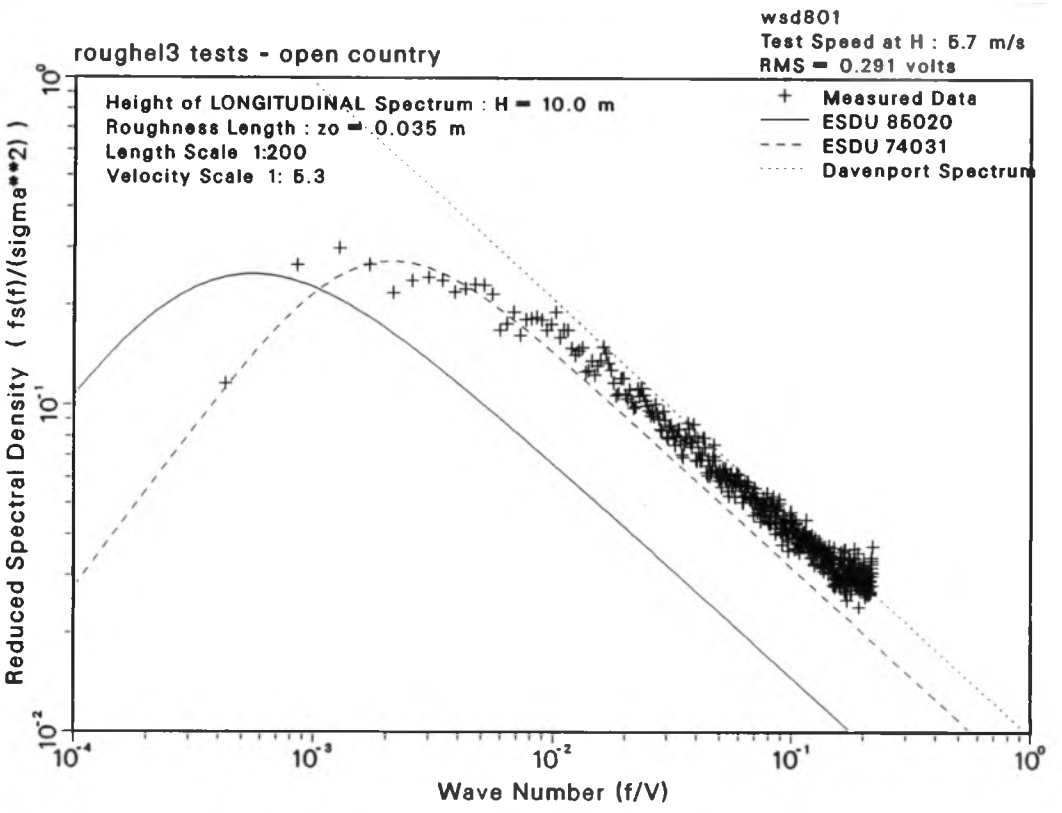

Figure 2.3a. Wind Spectra at 10m Full-scale (Open Country Exposure)

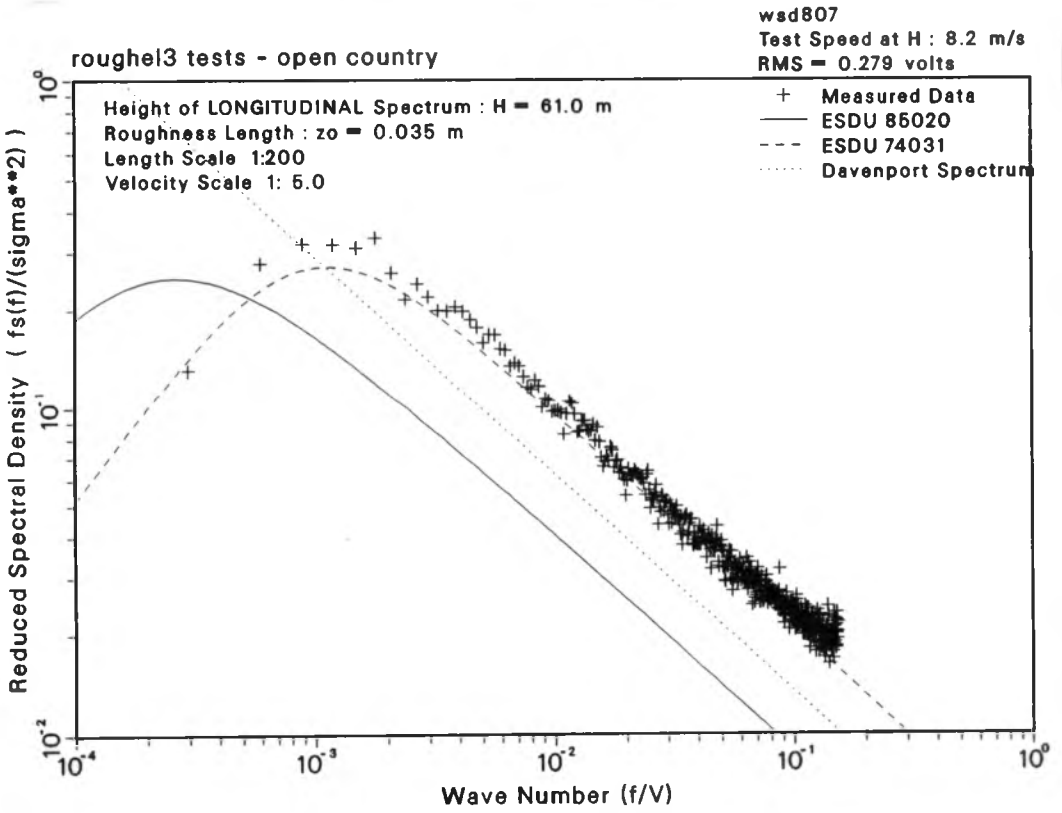

Figure 2.3b. Wind Spectra at 61m Full-scale (Open Country Exposure)

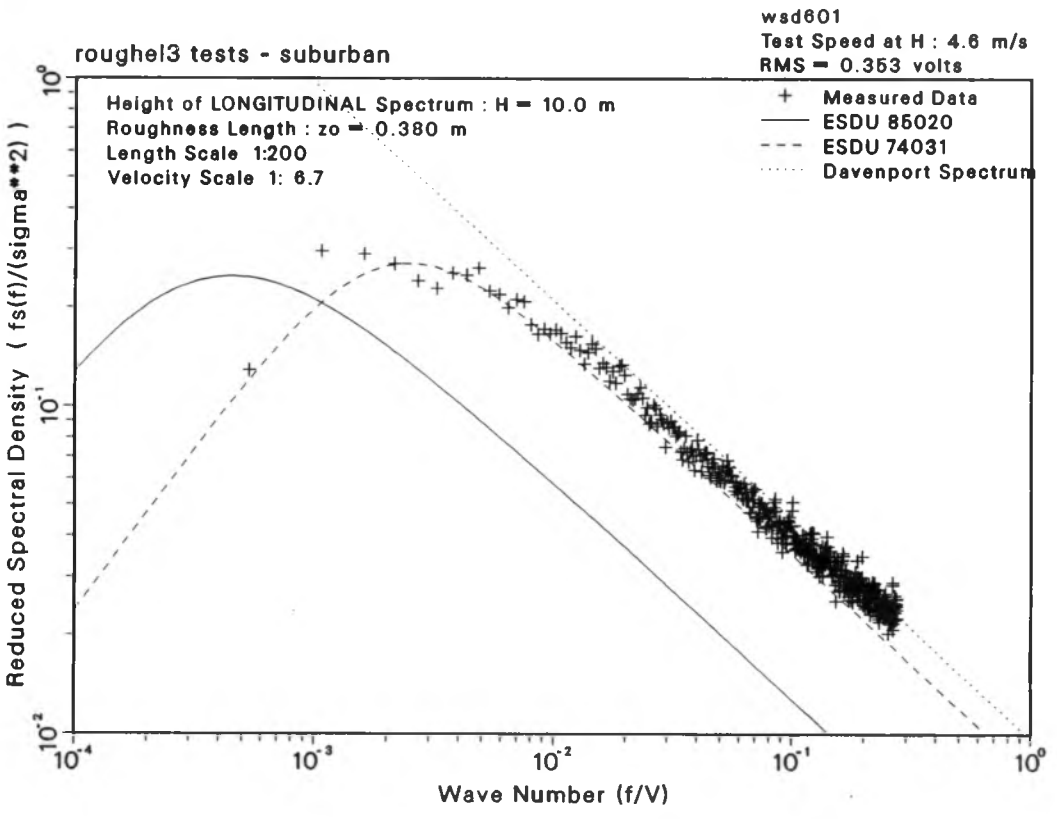

Figure 2.4a. Wind Spectra at 10m Full-scale (Suburban Exposure)

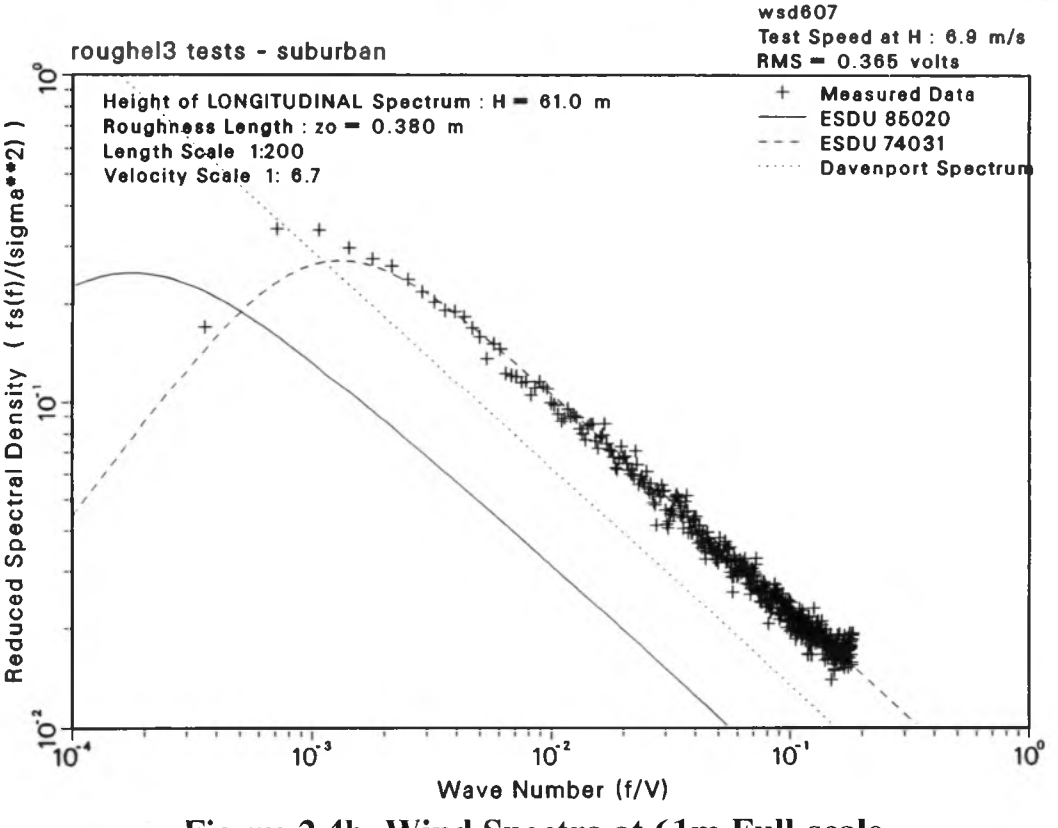

Figure 2.4b. Wind Spectra at 61m Full-scale (Suburban Exposure)

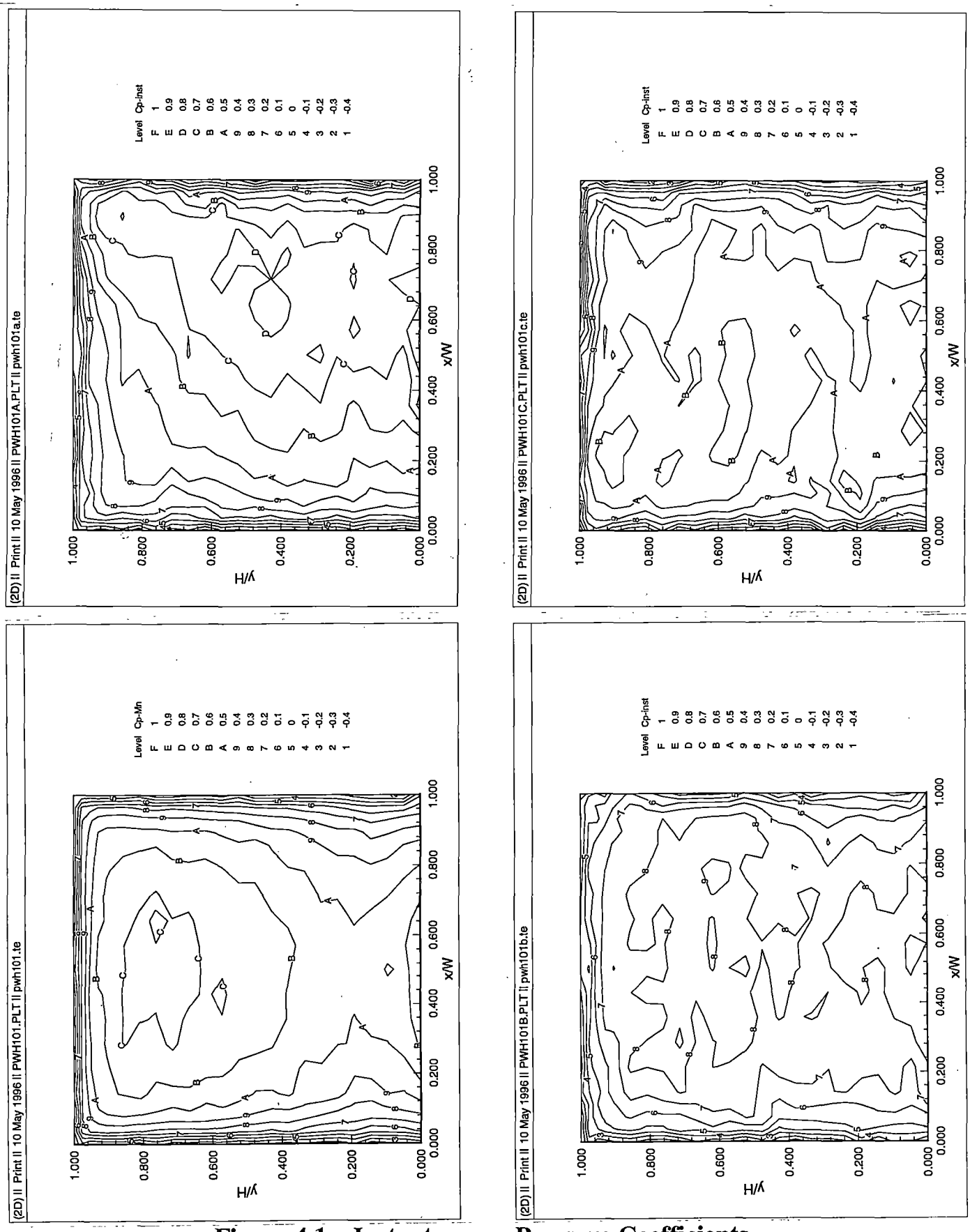

Figure 4.1a. Instantaneous Pressure Coefficients

(0 degrees, open country)

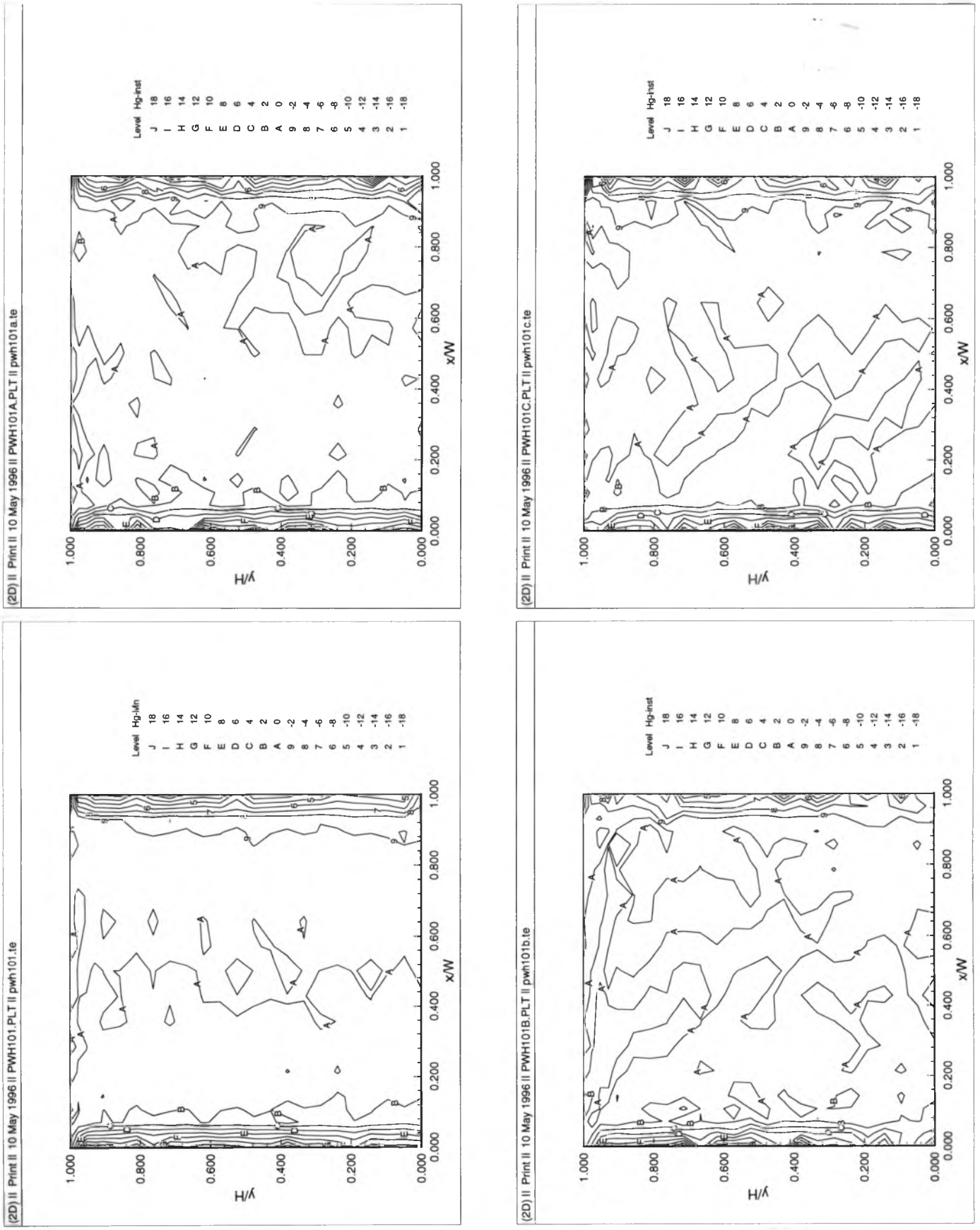

Figure 4.1b. Instantaneous Horizontal Pressure Gradients

(0 degrees, open country)

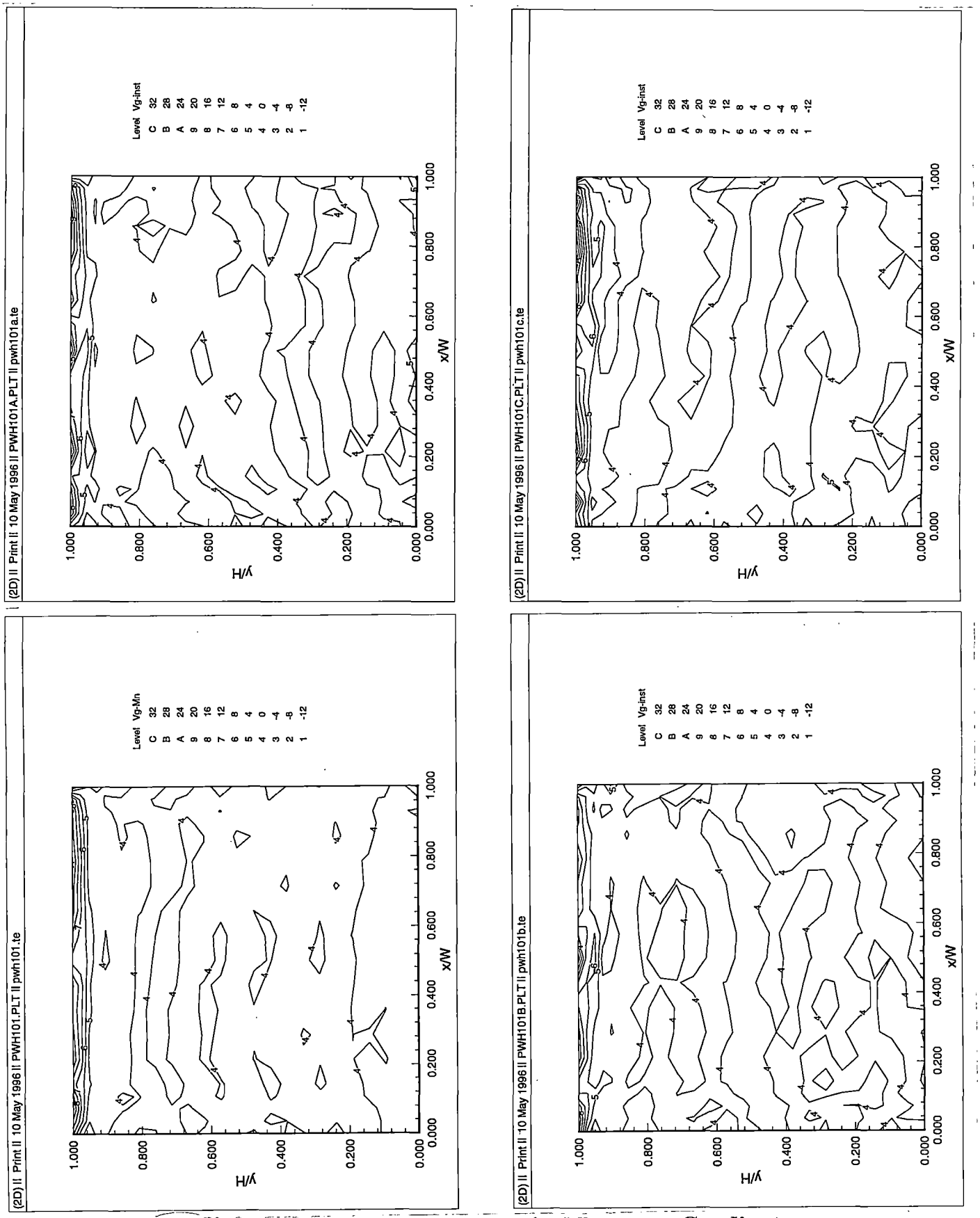

Figure 4.1c. Instantaneous Vertical Pressure Gradients

(0 degrees, open country)

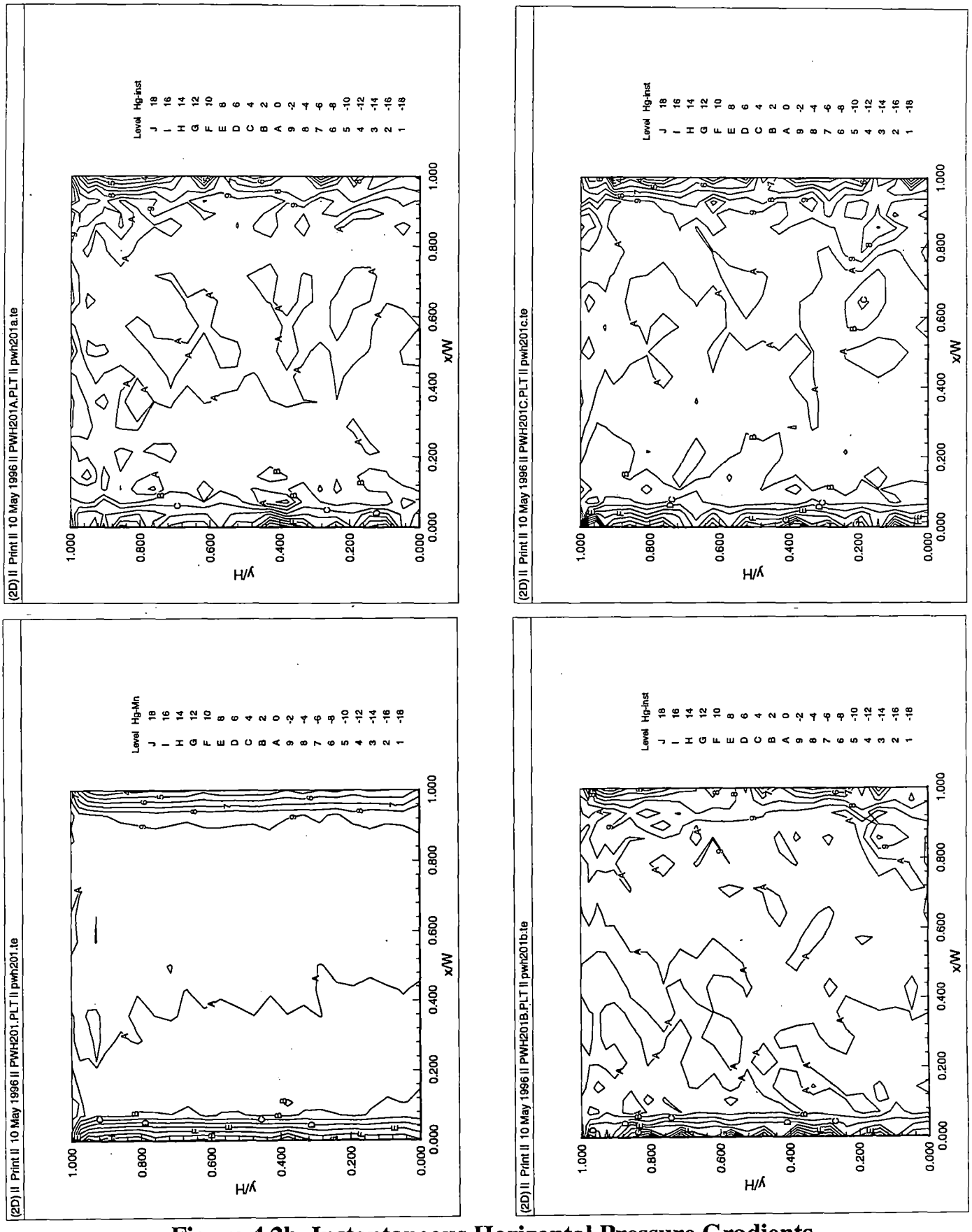

Figure 4.2b. Instantaneous Horizontal Pressure Gradients

(0 degrees, suburban)

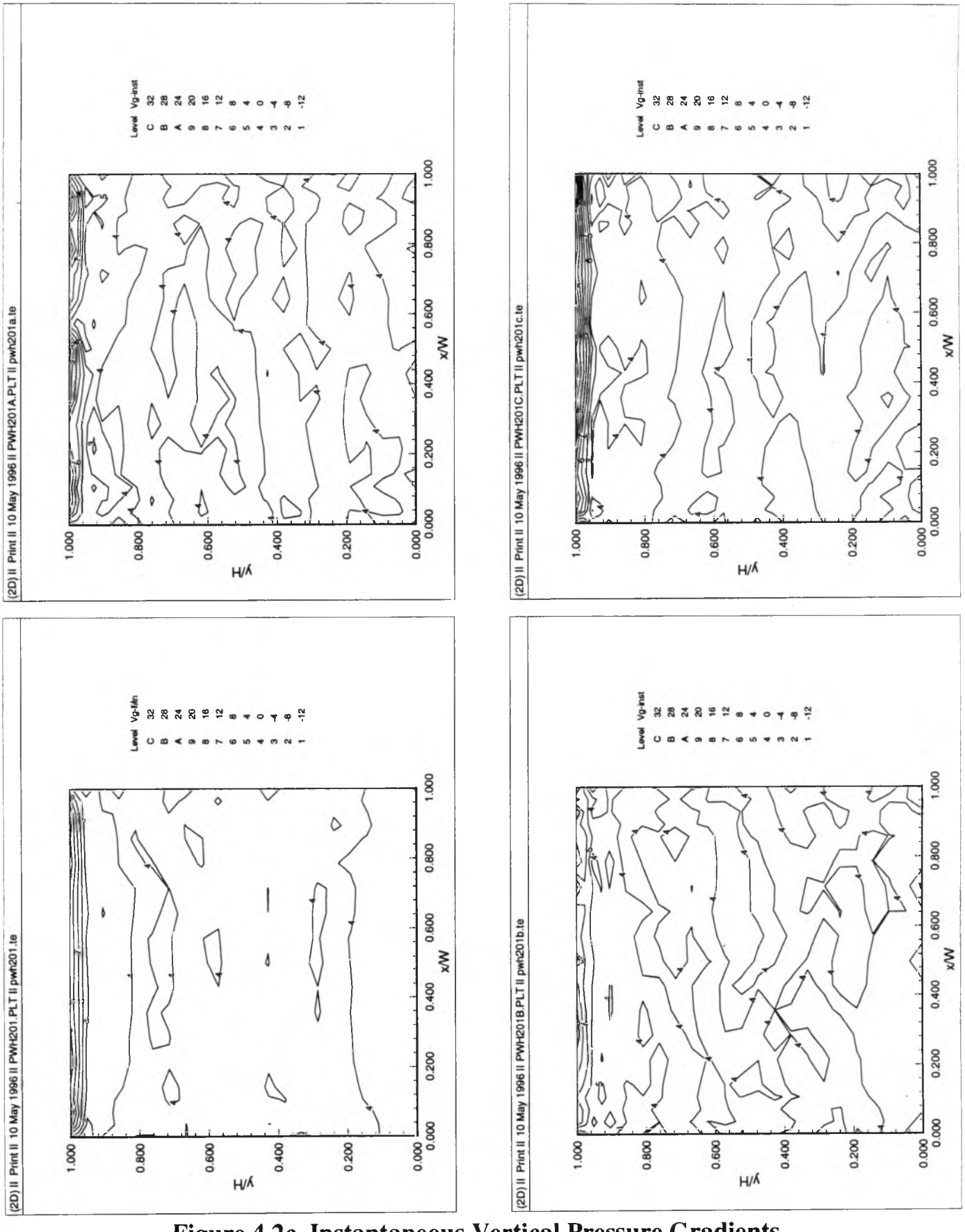

Figure 4.2c. Instantaneous Vertical Pressure Gradients

(0 degrees, suburban)

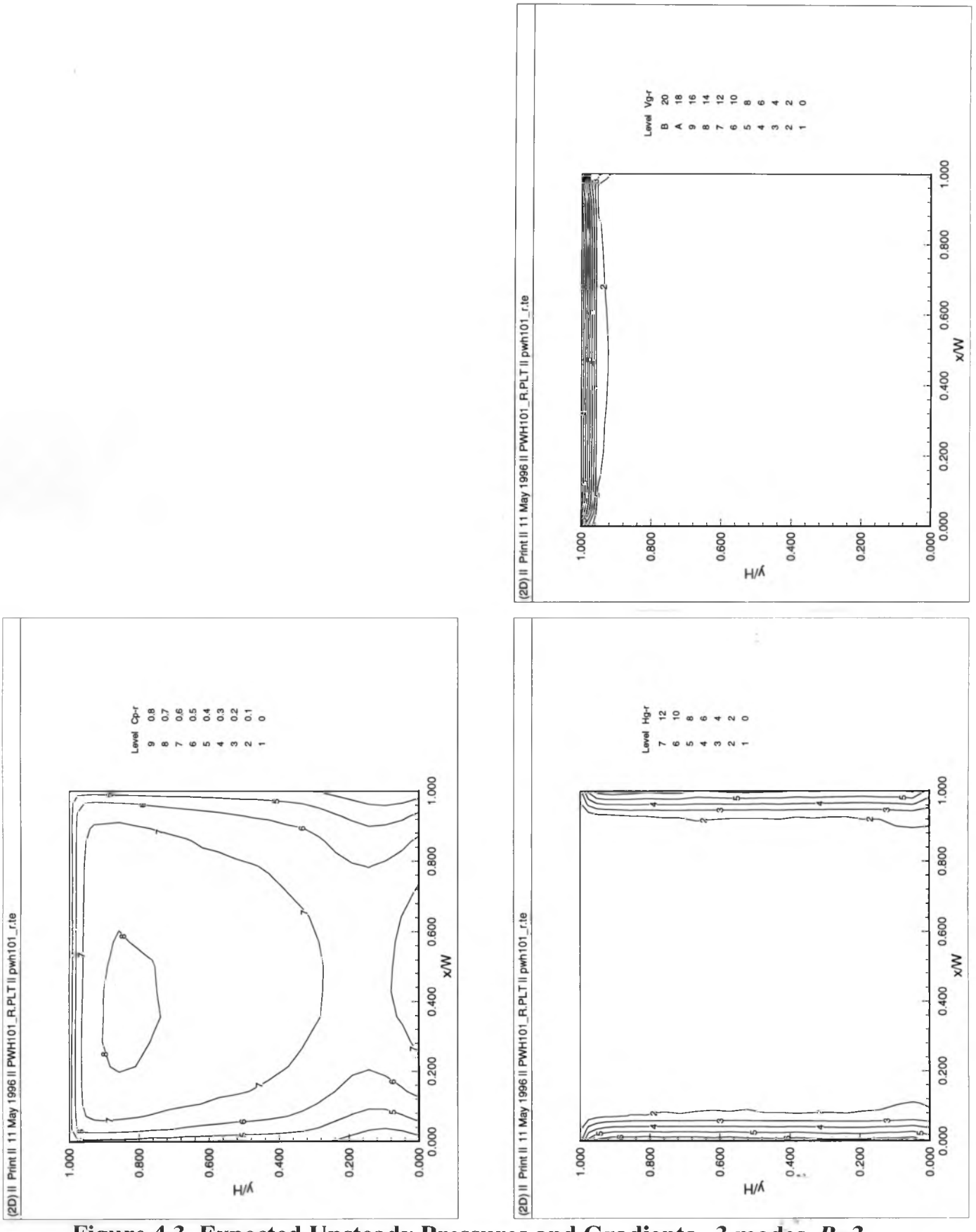

Figure 4.3. Expected Unsteady Pressures and Gradients , 3 modes, B=3

(0 degrees, open country)

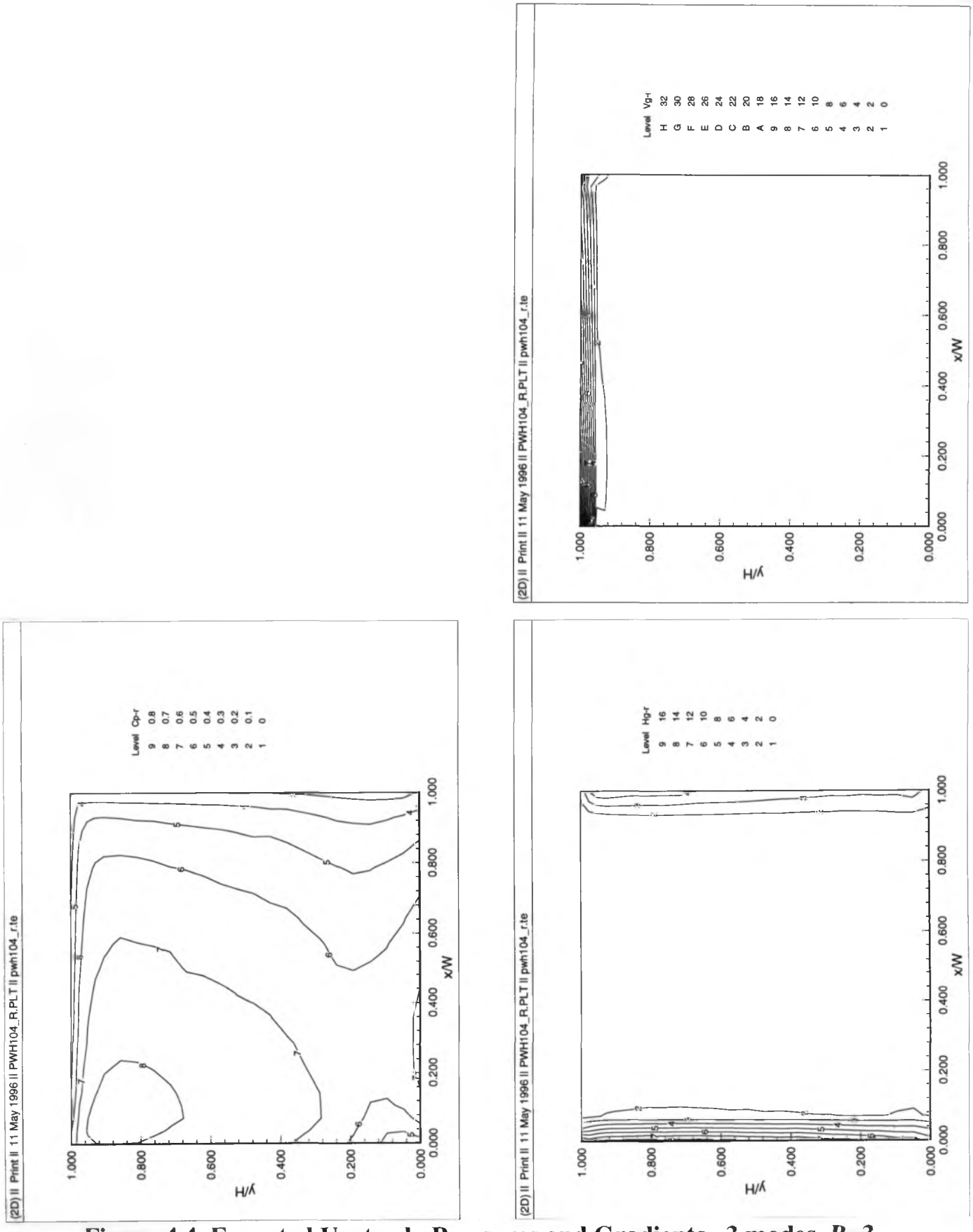

Figure 4.4. Expected Unsteady Pressures and Gradients , 3 modes, B=3 (30 degrees, open country)

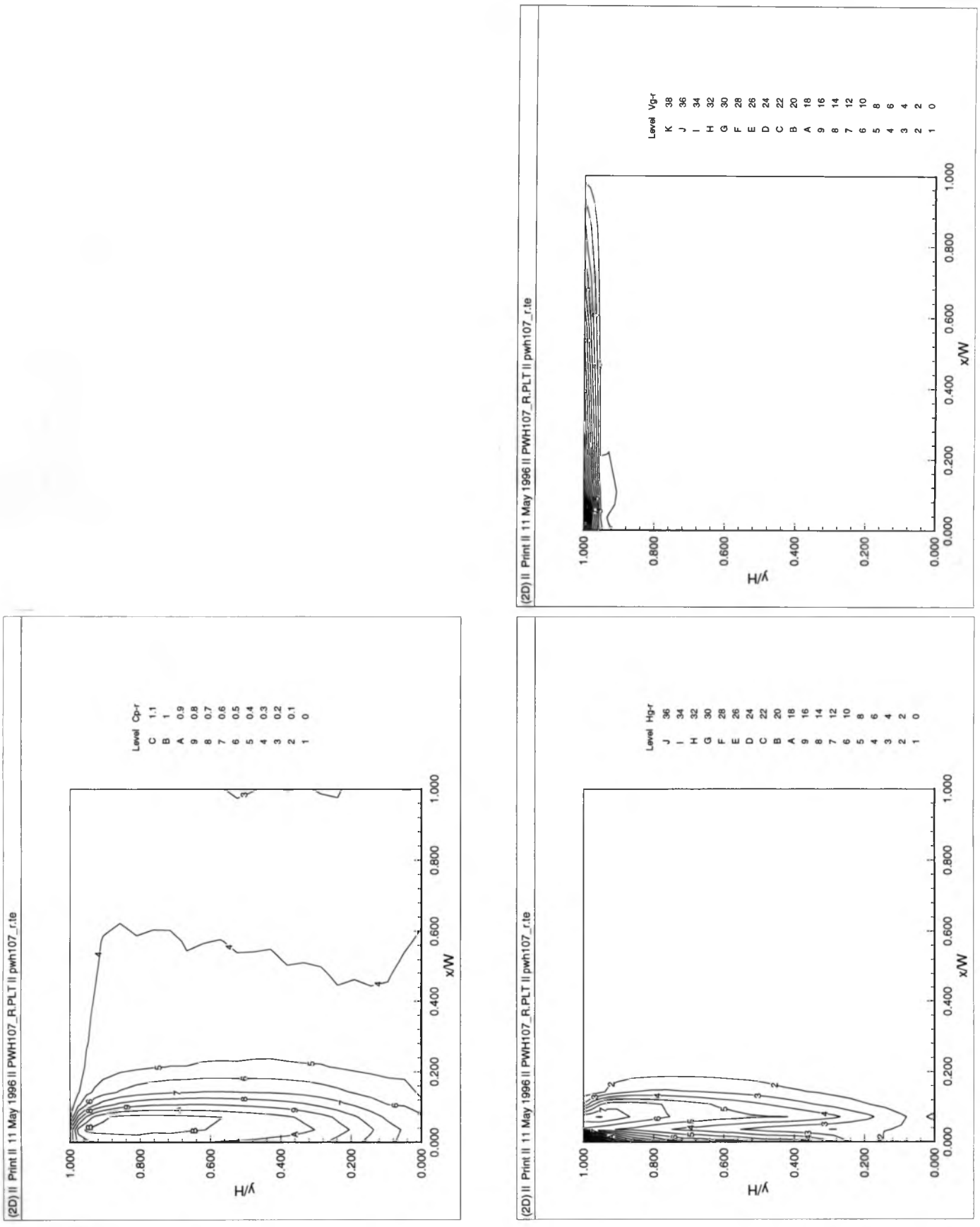

Figure 4.5. Expected Unsteady Pressures and Gradients , 3 modes, *B*=3 (60 degrees, open country)

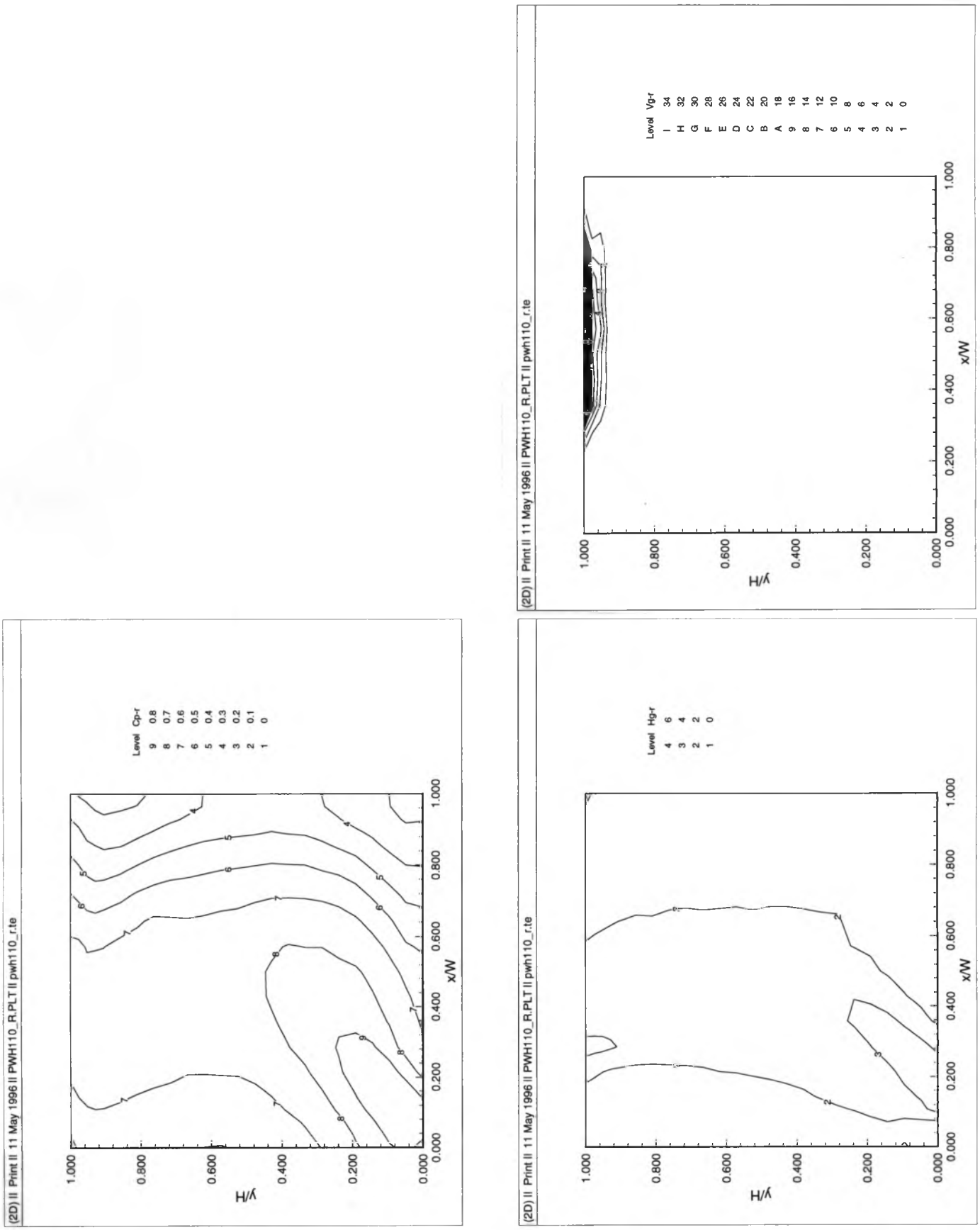

Figure 4.6. Expected Unsteady Pressures and Gradients , 3 modes, *B*=3

(90 degrees, open country)

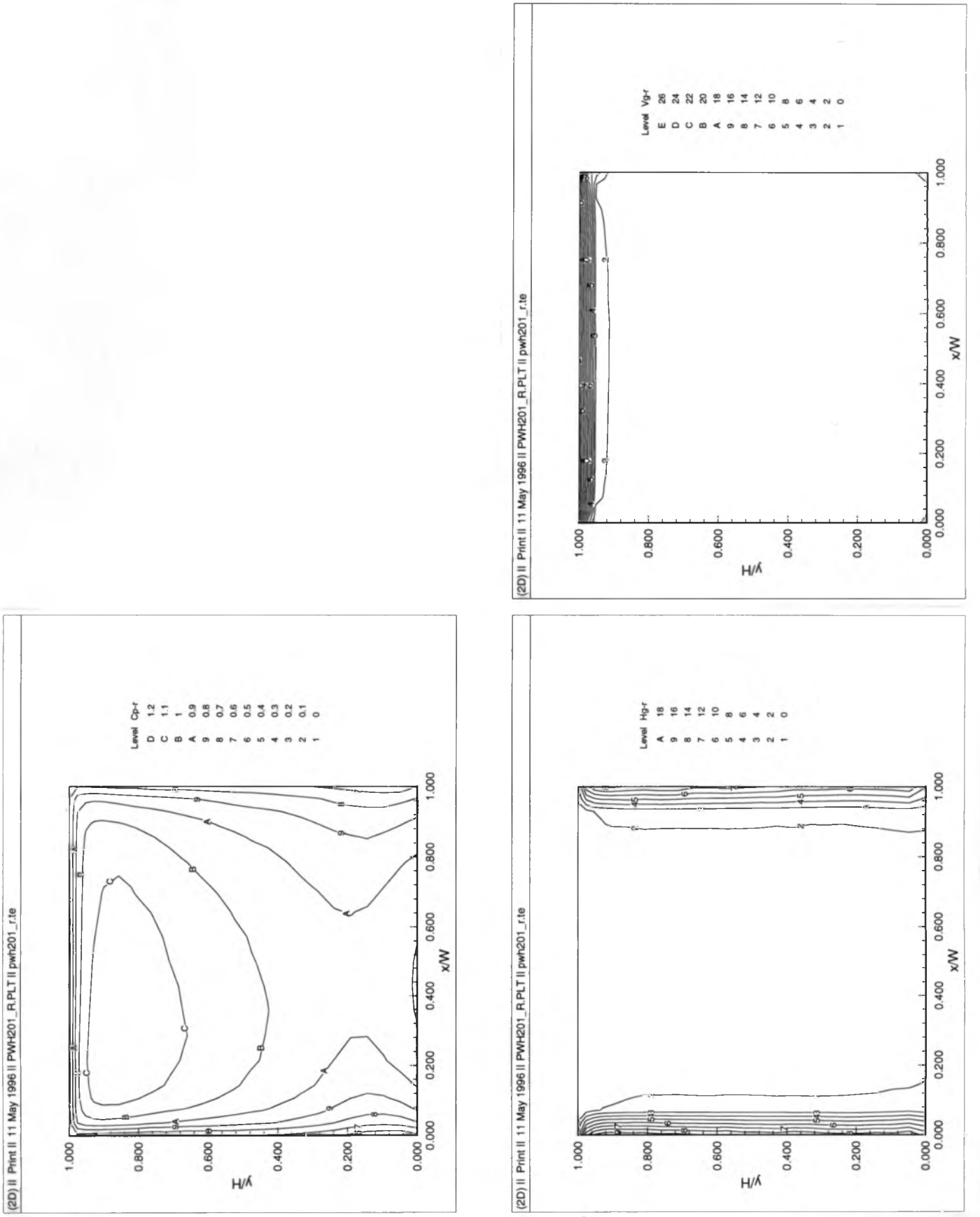

Figure 4.7. Expected Unsteady Pressures and Gradients , 3 modes, *B*=3

(0 degrees, suburban)

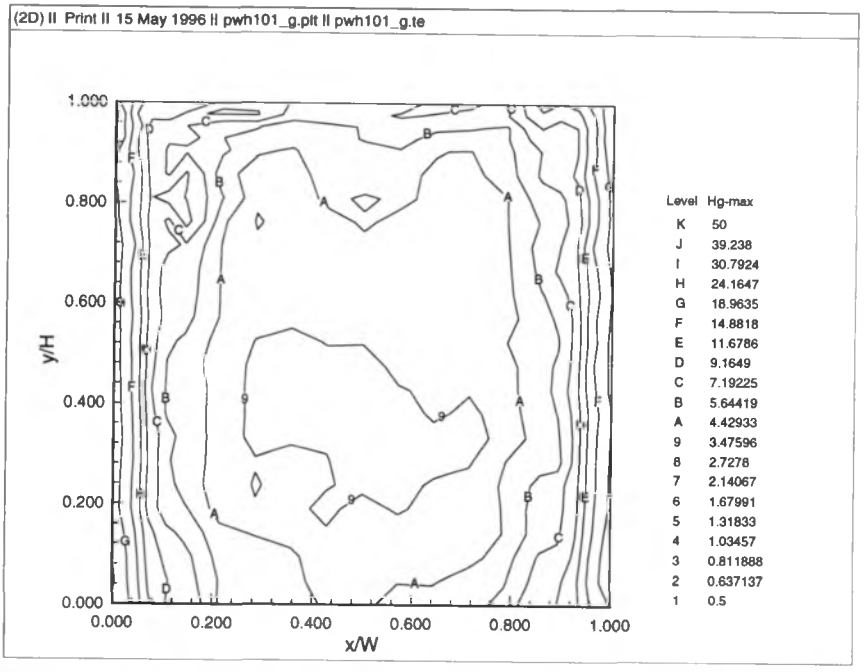

Figure 4.8a. Peak Unsteady Horizontal Pressure Gradients (0 degrees, open country)

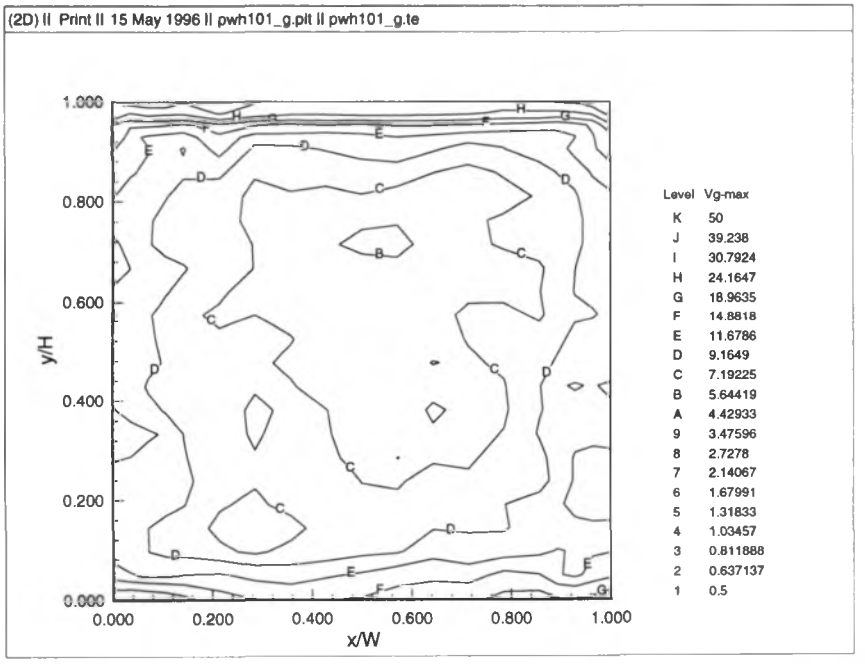

Figure 4.8b. Peak Unsteady Vertical Pressure Gradients (0 degrees, open country)

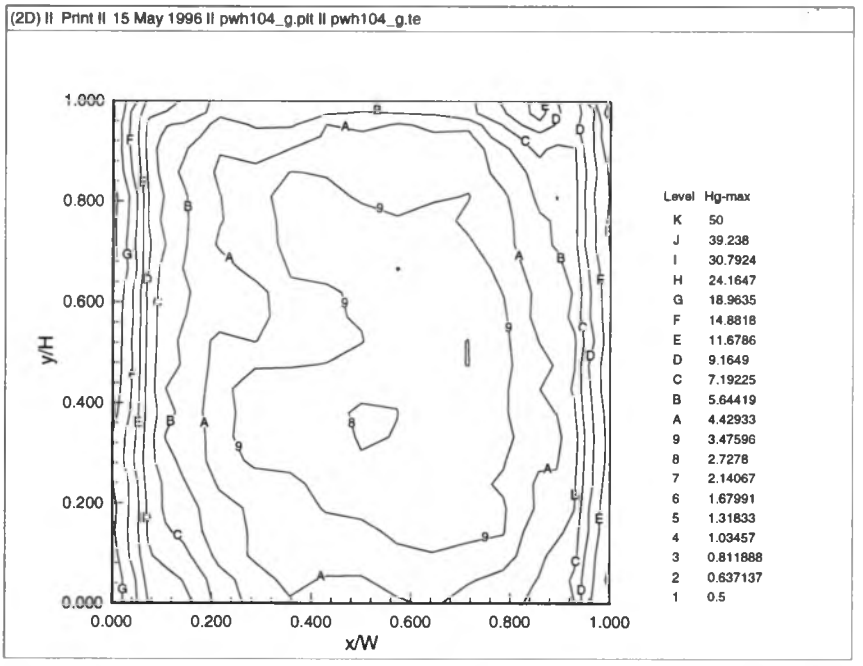

Figure 4.9a. Peak Unsteady Horizontal Pressure Gradients (30 degrees, open country)

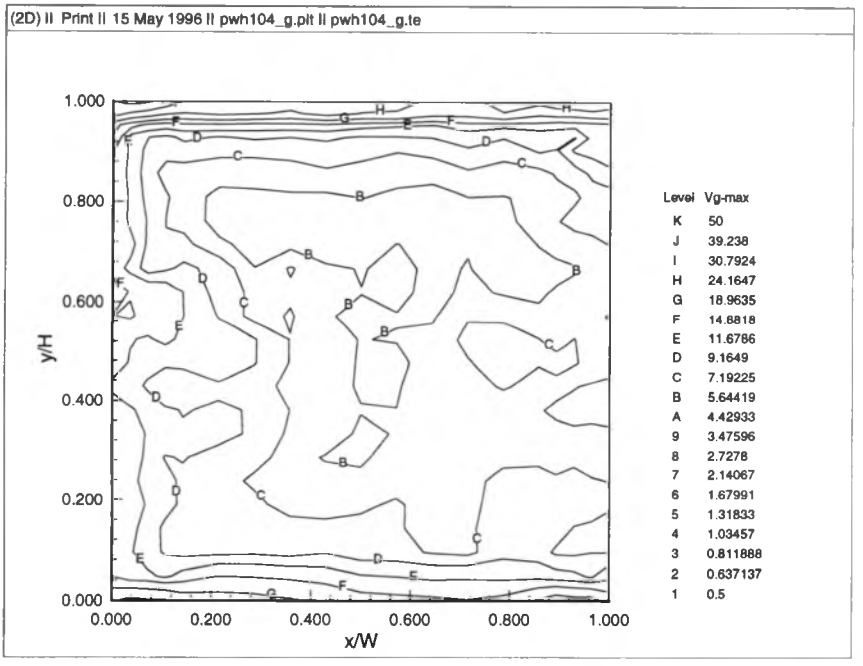

Figure 4.9b. Peak Unsteady Vertical Pressure Gradients (30 degrees, open country)

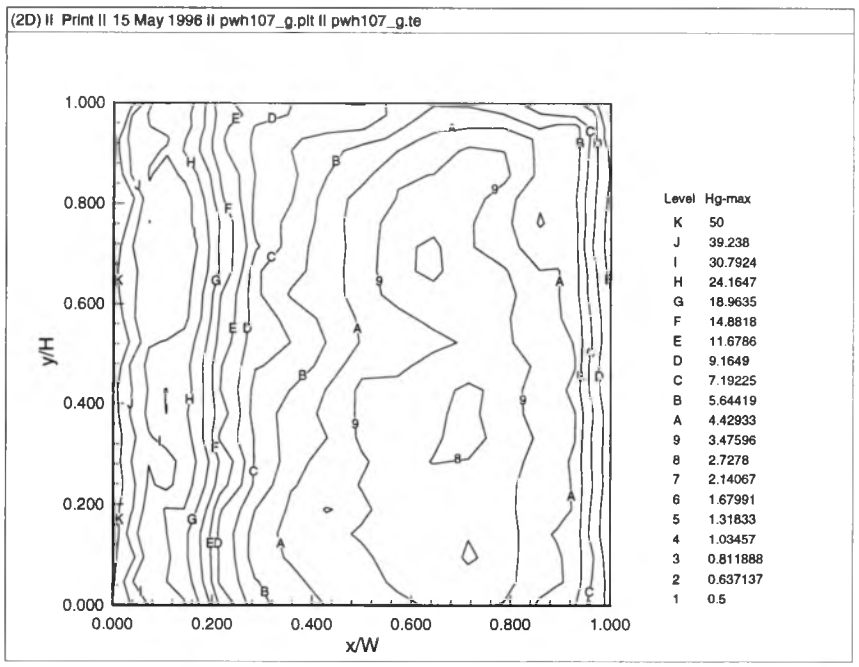

Figure 4.10a. Peak Unsteady Horizontal Pressure Gradients (60 degrees, open country)

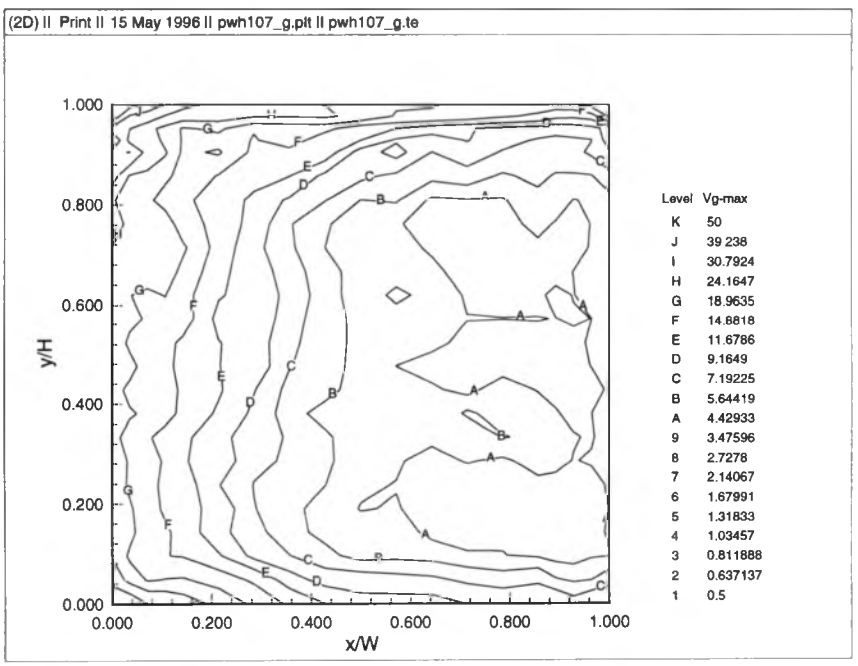

Figure 4.10b. Peak Unsteady Vertical Pressure Gradients (60 degrees, open country)

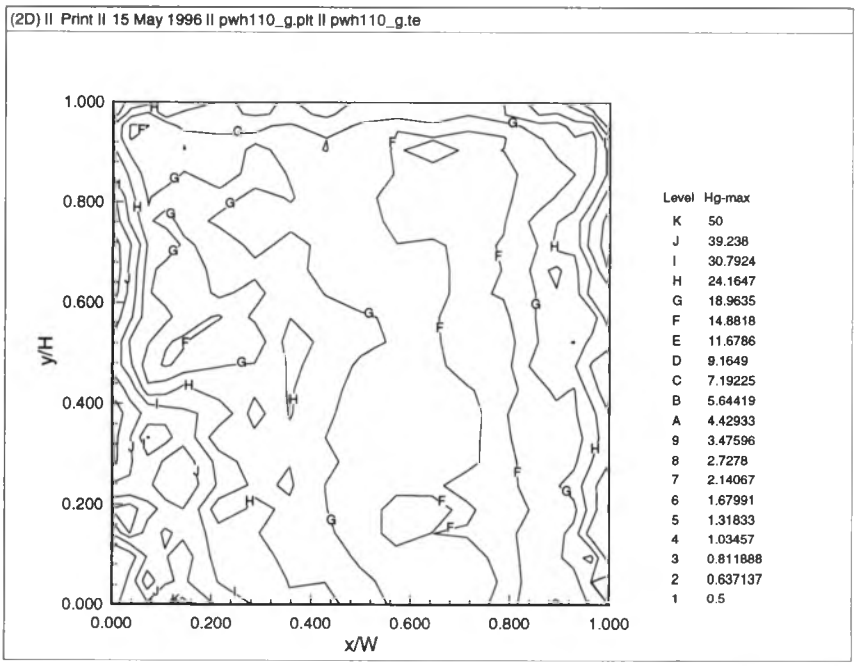

Figure 4.11a. Peak Unsteady Horizontal Pressure Gradients (90 degrees, open country)

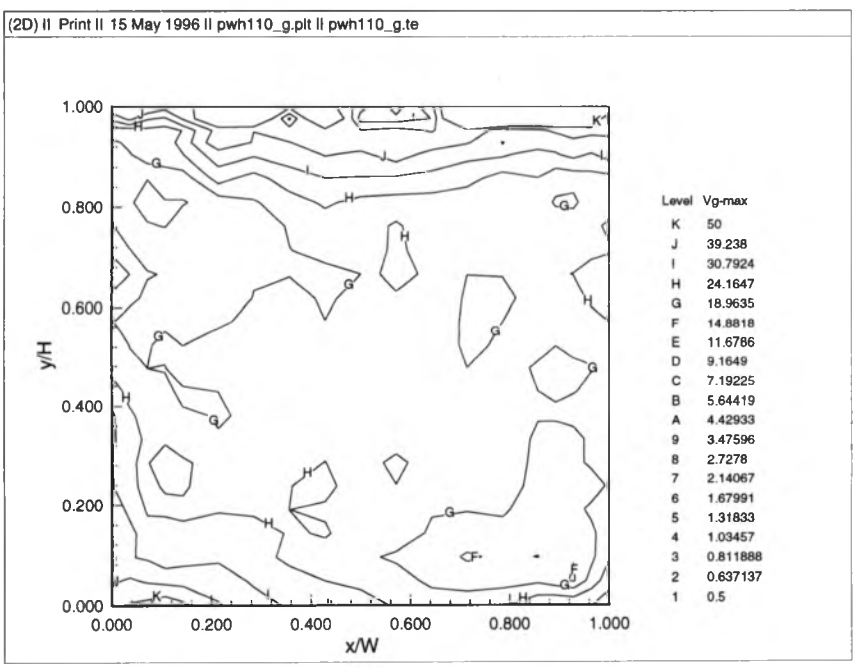

Figure 4.11b. Peak Unsteady Vertical Pressure Gradients (90 degrees, open country)

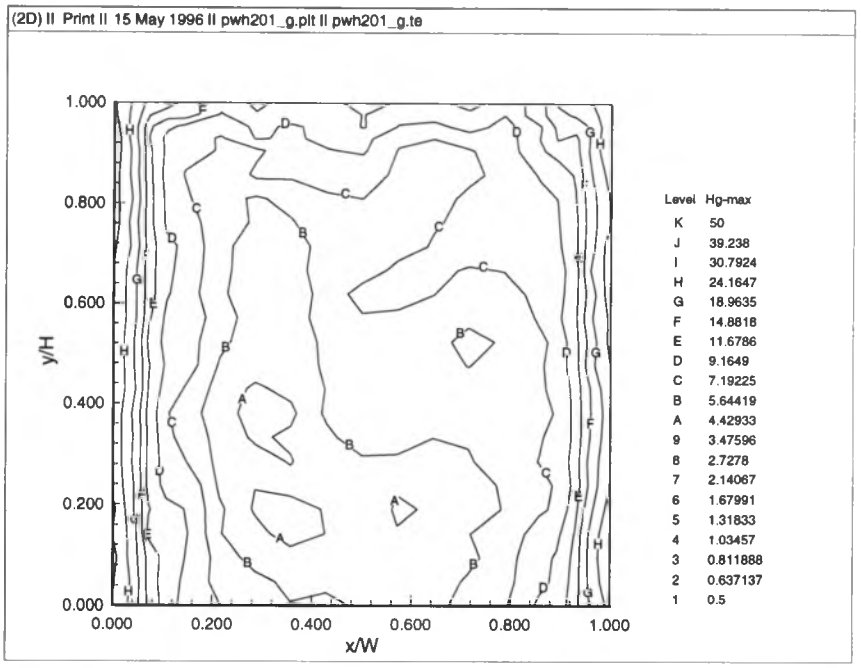

Figure 4.12a. Peak Unsteady Horizontal Pressure Gradients (0 degrees, suburban)

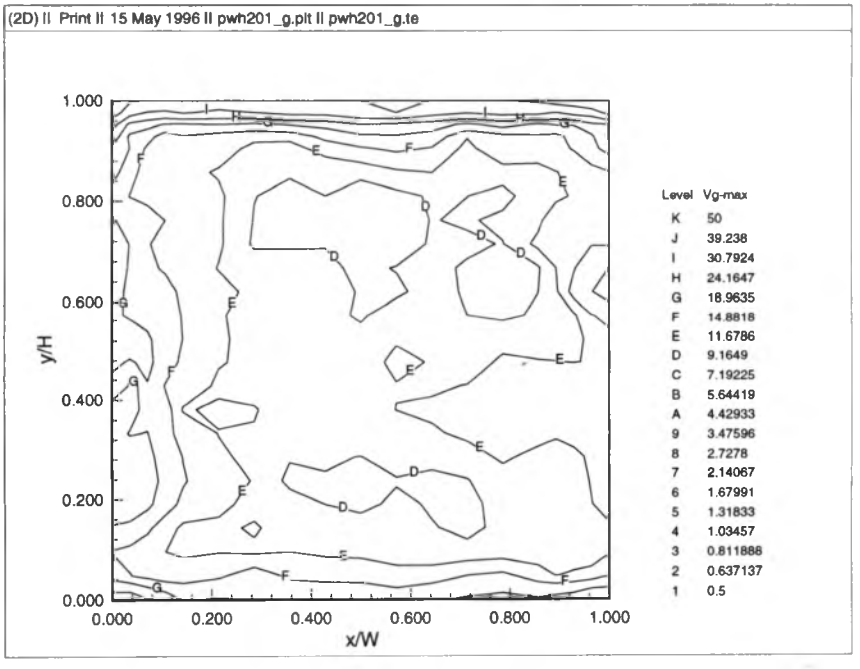

Figure 4.12b. Peak Unsteady Vertical Pressure Gradients (0 degrees, suburban)

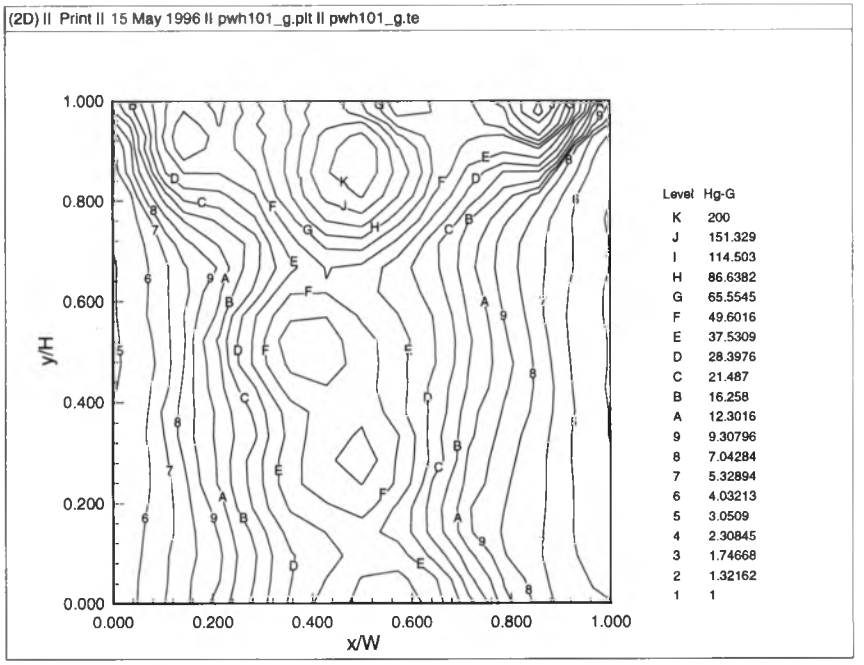

Figure 4.13a. Gust Factors for Horizontal Pressure Gradients (0 degrees, open country)

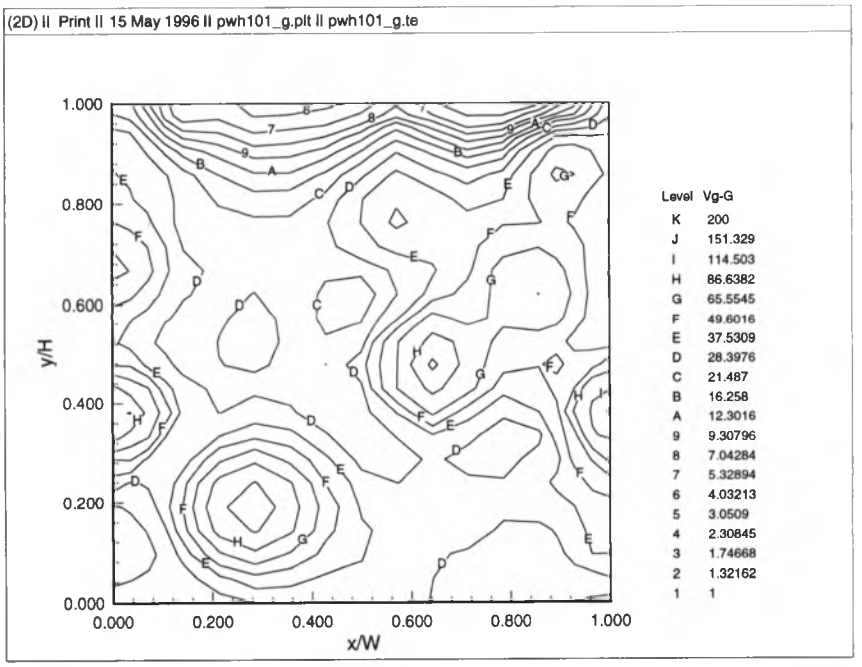

Figure 4.13b. Gust Factors for Vertical Pressure Gradients (0 degrees, open country)

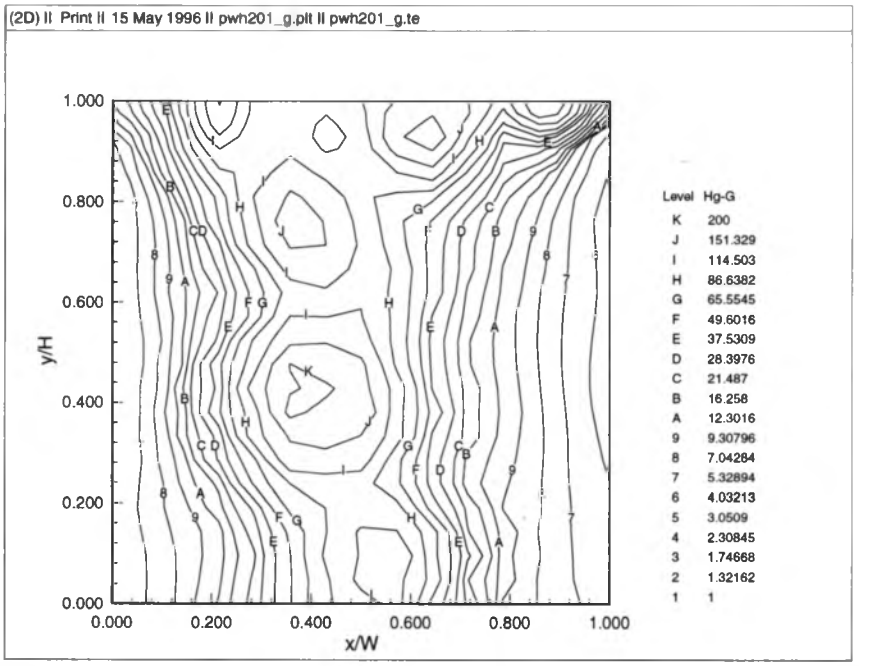

Figure 4.14a. Gust Factors for Horizontal Pressure Gradients (0 degrees, suburban)

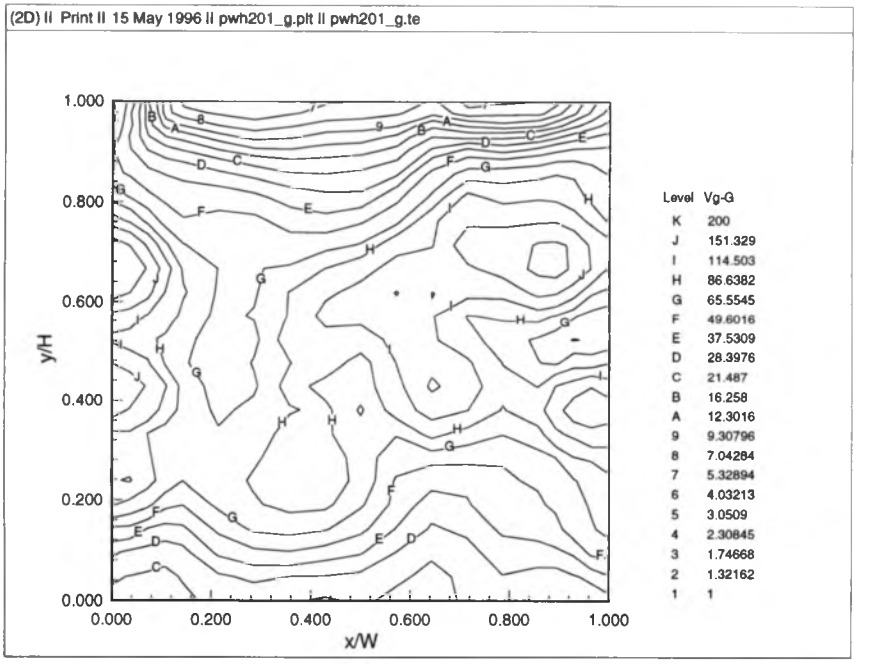

Figure 4.14b. Gust Factors for Vertical Pressure Gradients (0 degrees, suburban)

Horizontal Gradients (constant with x')	
x'	dCp / dx'
1.00	25.0
0.98	20.0
0.96	15.0
0.94	13.0
0.92	11.0
0.90	9.0
0.85	8.0
0.80	7.0
0.70	6.0
0.60	5.0
0.50	5.0
0.40	5.0
0.30	6.0
0.20	7.0
0.15	8.0
0.10	9.0
0.08	11.0
0.06	13.0
0.04	15.0
0.02	20.0
0.00	25.0

Vertical Gradients (constant with y')	
y'	dCp / dy'
1.00	30.0
0.98	25.0
0.96	21.0
0.94	18.0
0.92	15.0
0.90	13.0
0.85	11.0
0.80	9.0
0.70	9.0
0.60	9.0
0.50	9.0
0.40	9.0
0.30	9.0
0.20	9.0
0.10	12.0
0.00	15.00

Note: peak gradients at a 60 degree wind angle are significantly higher

* x'= x/W; y'= y/H

Table 5.1. <u>Preliminary</u> Recommended Unsteady Horizontal and Vertical Pressure Gradients

APPENDIX A

DESIGN GUIDELINES FOR COMPARTMENTALIZATION OF PRESSURE-EQUALIZED RAINSCREEN WALLS

Boundary Layer Wind Tunnel Laboratory
The University of Western Ontario

DRAFT 2

A pressure-equalized rainscreen (PER) wall consists of an exterior rainscreen, a cavity (vented to the exterior), and an interior air barrier system.

The primary purpose of pressure equalization (PE) is to reduce the pressure difference across the rainscreen that is available to drive water into the cavity. Secondarily, PE may reduce the net wind loads on the rainscreen. The degree of PE is a function of many parameters, but it is inherently limited by the gradients of exterior pressures.

Compartmentalization is accomplished by designing the air barrier system to form multiple compartments and hence limiting the vertical and horizontal extent of any one compartment.

Detailed design can be accomplished on the basis of the non-dimensional gradients provided on the following page. The simple guidelines below have been established to limit the mean pressure difference across a panel to approximately 50 Pa under a DRWP of 250 Pa at the top of the building.† For parameters differing significantly from these, the detailed approach should be followed.

On planar walls of width B and height H, compartments should be designed with the maximum dimensions given below

Region	Vertical Size	Horizontal Size
Within .03 H of top edge	*	*
Within .03 B of side edge	*	*
.03 B - .10 B	.05 H or 1m	.02 B or 1m
.90 H - .97 H	.02 H or 1m	.05 B or 1m
.10 B - .20 B	.05 H or 1m	.04 B or 1m
.80 H - .90 H	.04 H or 1m	.05 B or 1m
.20 B - .50 H	.1 H or 1m	.08 B or 1m
0 - .80 H	.08 H or 1m	.1 B or 1m

* Within these regions, gradients are extreme and PE is unlikely to be obtained within the same tolerance as other regions of the wall. Special design precautions should be observed to minimize the consequences of leakage.

In addition to the above requirements, use of these specifications assumes the design of the PER system is consistent with accepted PER design guidelines with regard to venting, cavity size, and air barrier leakage. In particular, no deliberate PER vents shall be placed within 0.01B of a side edge or 0.01H of a top edgeand no compartment should extend to both sides of an edge.

---

† The unsteady results reported in the main text imply that the total peak pressure difference may then be as large as 100 Pa.

APPENDIX A - continued
(After Table 9, reference 3)

Data for the Zone Diagrams of Simplified Horizontal and Vertical Gradients for the Worst Case over All Wind Angles, Based on the Results of Utilizing the First 5 Modes with a Reliability Index of 3.0

Horizontal Gradients (Constant with y')		Vertical Gradients (Constant with x')	
x'	|dCp/dx'|	y'	|dCp/dy'|
0.00	32.0	0.00	8.0
0.01	30.0	0.01	7.7
0.02	28.0	0.02	7.4
0.03	26.0	0.03	7.1
0.04	24.0	0.04	6.8
0.05	22.0	0.05	6.5
0.06	20.0	0.06	6.2
0.07	18.0	0.07	5.9
0.08	16.0	0.08	5.6
0.09	14.0	0.09	5.3
0.10	12.0	0.10	5.0
0.15	9.0	0.15	4.0
0.20	6.0	0.20	3.0
0.30	3.0	0.30	2.0
0.40	2.0	0.40	1.5
0.50	0.0	0.50	1.0
0.60	2.0	0.60	1.0
0.70	3.0	0.70	2.0
0.80	6.0	0.80	4.0
0.85	9.0	0.85	8.0
0.90	12.0	0.90	12.0
0.91	14.0	0.91	14.0
0.92	16.0	0.92	16.0
0.93	18.0	0.93	18.0
0.94	20.0	0.94	20.0
0.95	22.0	0.95	22.0
0.96	24.0	0.96	24.0
0.97	26.0	0.97	26.0
0.98	28.0	0.98	28.0
0.99	30.0	0.99	30.0
1.00	32.0	1.00	32.0

For a building face B wide and H high

$$\Delta p \text{ across a panel of width } \Delta B = \left|\frac{dC_p}{dx'}\right| \frac{\Delta B}{B} \cdot C_e(H) \cdot (DRWP$$

$$\Delta p \text{ across a panel of height } \Delta H = \left|\frac{dC_p}{dy'}\right| \frac{\Delta H}{H} \cdot C_e(H) \cdot (DRWP$$

e.g. if $C_e(H) \cdot (DRWP) =$ 250 Pa, B = 50m, and we have a panel of ΔB = 2m at $y' = y/H = .5$, $x' = x/B = .05$

then $\left|\frac{dC_p}{dx'}\right| = 22$ and $\Delta p = 22 \times \left(\frac{2}{50}\right) \times 250 = 22$ Pa

APPENDIX B

TABLE B.1 - MODAL AMPLITUDES

TABLE B.2 - COLLECTIVE ENERGY RATIOS

MEANS AND 1ST 3 MODE SHAPES

(UNFILTERED)

Open Country Exposure:

Wind Angle	Pressure Coefficients				Horizontal Gradients				Vertical Gradients			
	mode 1	mode 2	mode 3	mode 4	mode 1	mode 2	mode 3	mode 4	mode 1	mode 2	mode 3	mode 4
0	0.158	0.07	0.063	0.039	1.112	0.659	0.376	0.316	1.208	0.524	0.438	0.399
30	0.152	0.071	0.053	0.034	1.186	0.477	0.363	0.278	1.365	0.644	0.419	0.383
60	0.137	0.053	0.047	0.033	1.109	0.866	0.734	0.651	1.203	0.673	0.537	0.405
90	0.147	0.088	0.071	0.053	0.444	0.415	0.348	0.355	0.739	0.66	0.628	0.593

Suburban Exposure:

Wind Angle	Pressure Coefficients				Horizontal Gradients				Vertical Gradients			
	mode 1	mode 2	mode 3	mode 4	mode 1	mode 2	mode 3	mode 4	mode 1	mode 2	mode 3	mode 4
0	0.283	0.087	0.08	0.067	1.555	0.726	0.497	0.384	1.66	0.709	0.534	0.497

Table B.1 Root-Mean-Square Modal Amplitudes (unfiltered signals)

* wide face of building, aspect ratio H:W of 3:2

Open Country Exposure:

Wind Angle	Pressure Coefficients				Horizontal Gradients				Vertical Gradients			
	mode 1	mode 2	mode 3	mode 4	mode 1	mode 2	mode 3	mode 4	mode 1	mode 2	mode 3	mode 4
0	0.583	0.115	0.094	0.035	0.319	0.112	0.037	0.026	0.287	0.054	0.038	0.032
30	0.604	0.133	0.074	0.03	0.381	0.062	0.036	0.022	0.351	0.078	0.033	0.028
60	0.596	0.088	0.07	0.034	0.136	0.083	0.059	0.047	0.244	0.076	0.049	0.029
90	0.374	0.134	0.088	0.049	0.034	0.029	0.022	0.022	0.052	0.042	0.038	0.034

Suburban Exposure:

Wind Angle	Pressure Coefficients				Horizontal Gradients				Vertical Gradients			
	mode 1	mode 2	mode 3	mode 4	mode 1	mode 2	mode 3	mode 4	mode 1	mode 2	mode 3	mode 4
0	0.726	0.068	0.059	0.041	0.387	0.084	0.039	0.024	0.336	0.062	0.035	0.03

Table B.2 Collective Energy Ratios (unfiltered signals)

* wide face of building, aspect ratio H:W of 3:2

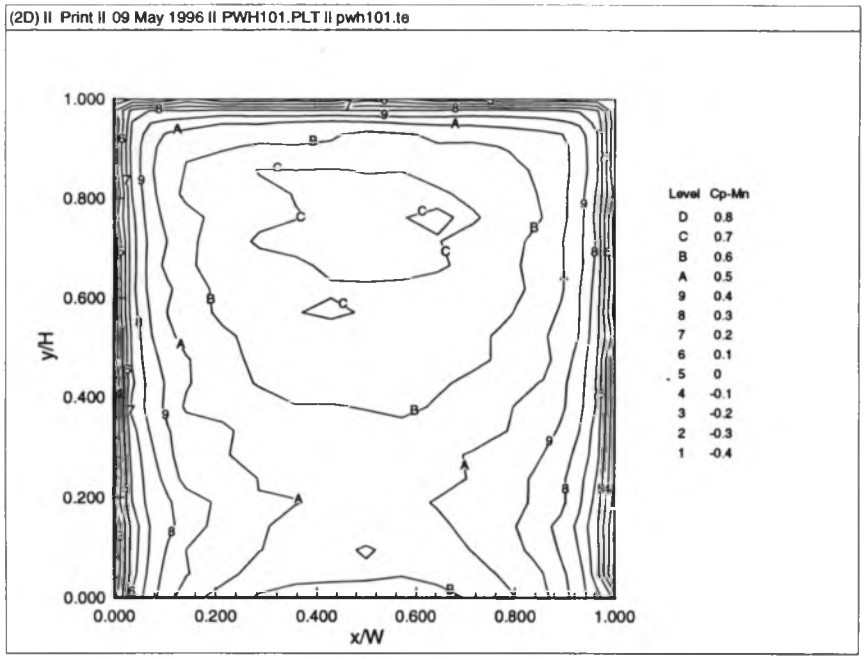

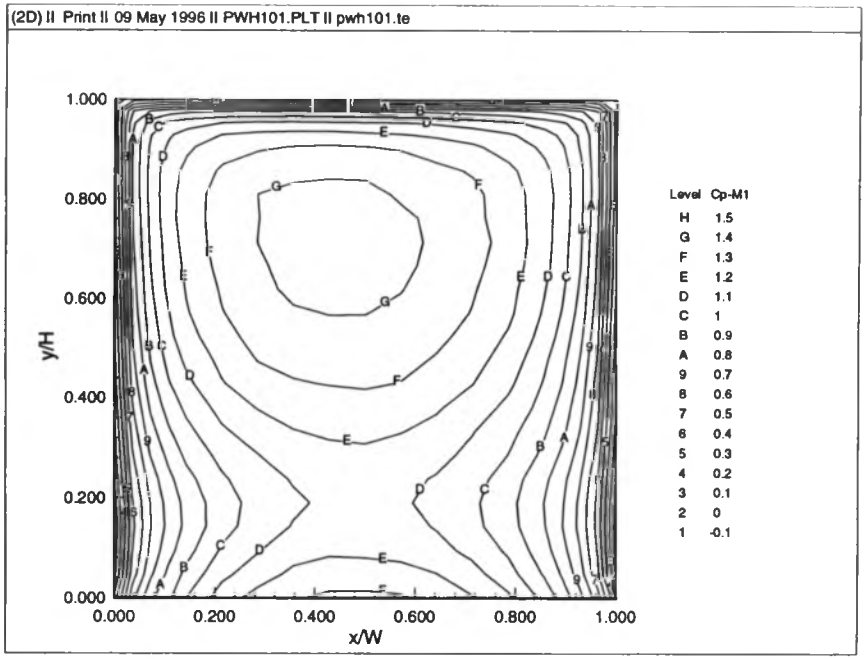

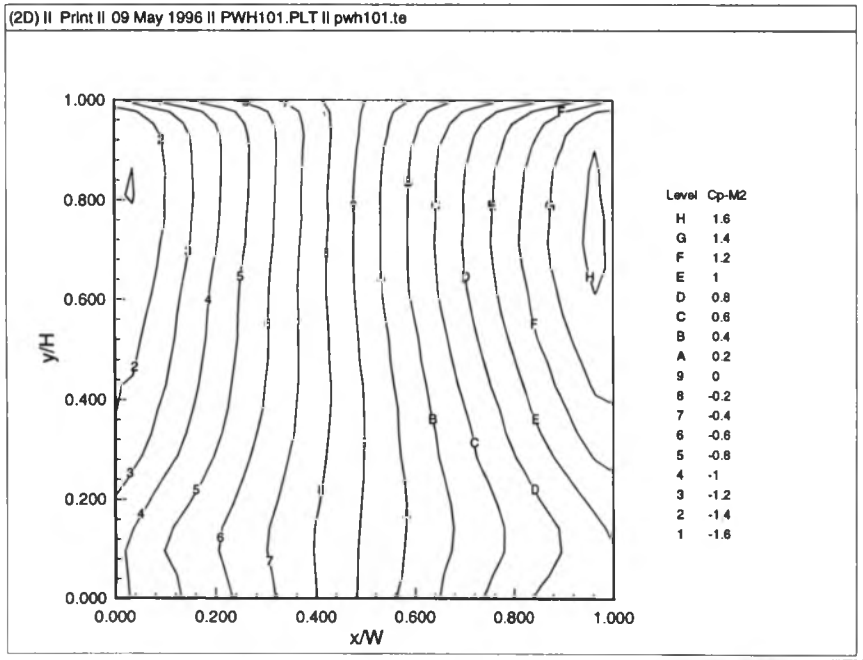

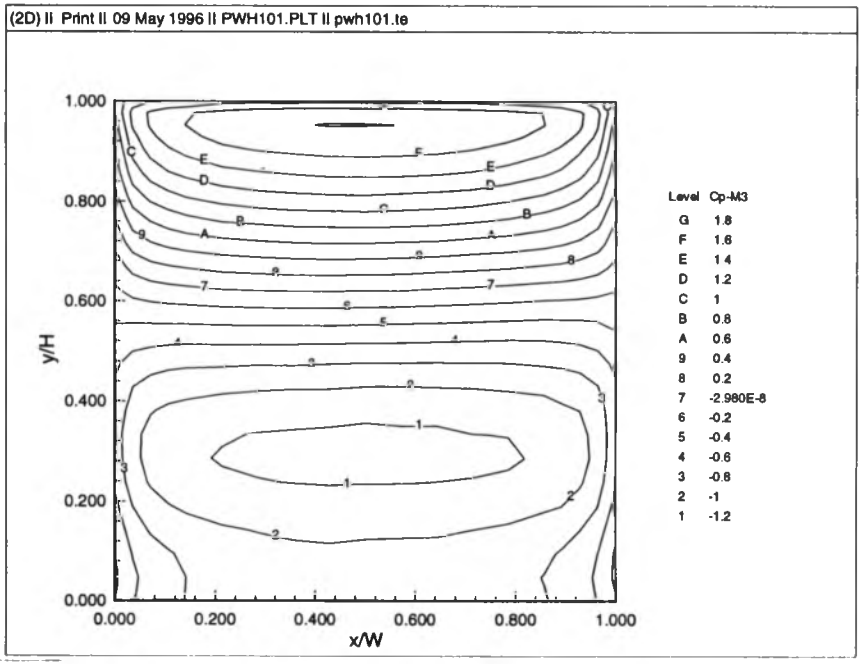

Figure B.1. Means and 1st 3 Mode Shapes of Pressure Coefficients

(0 degrees, open country)

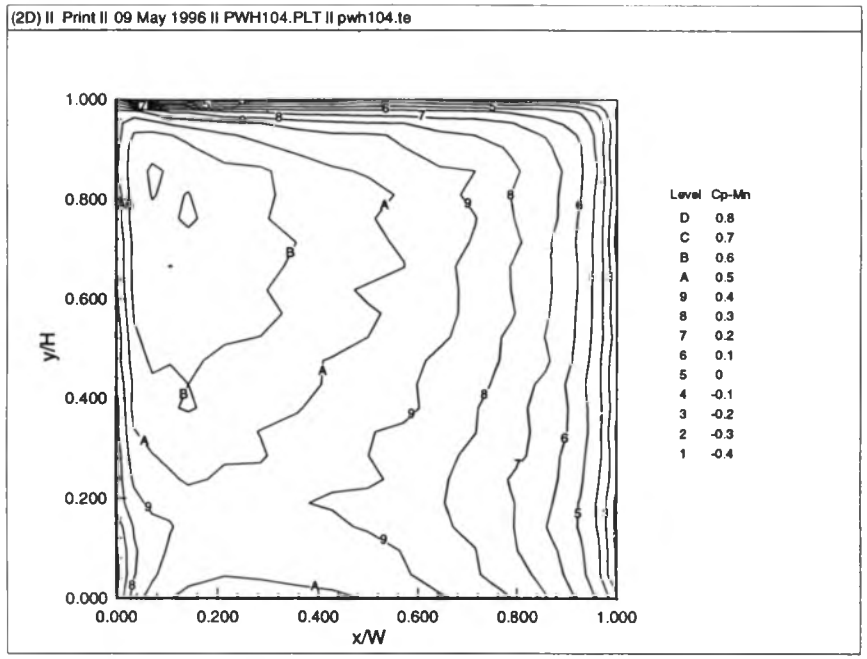

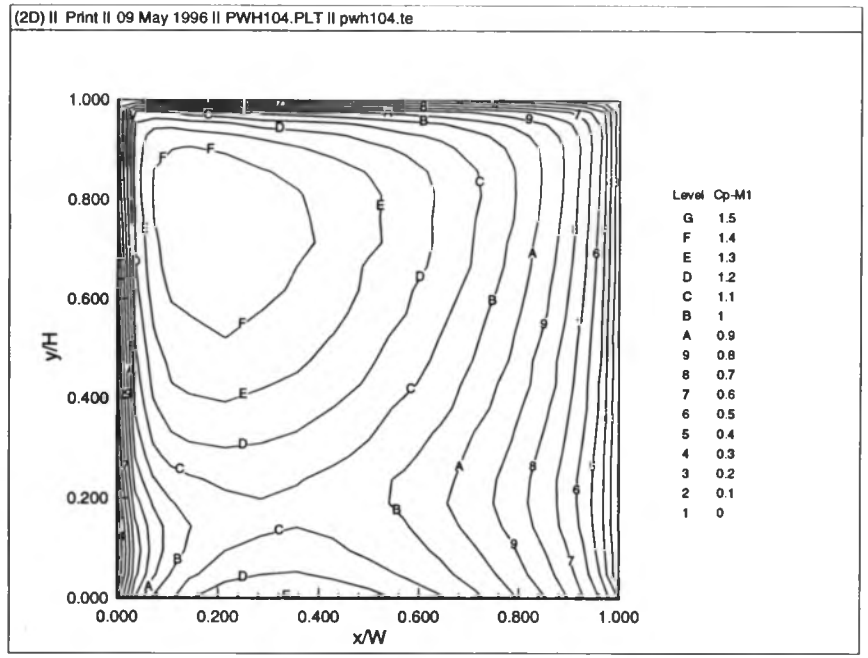

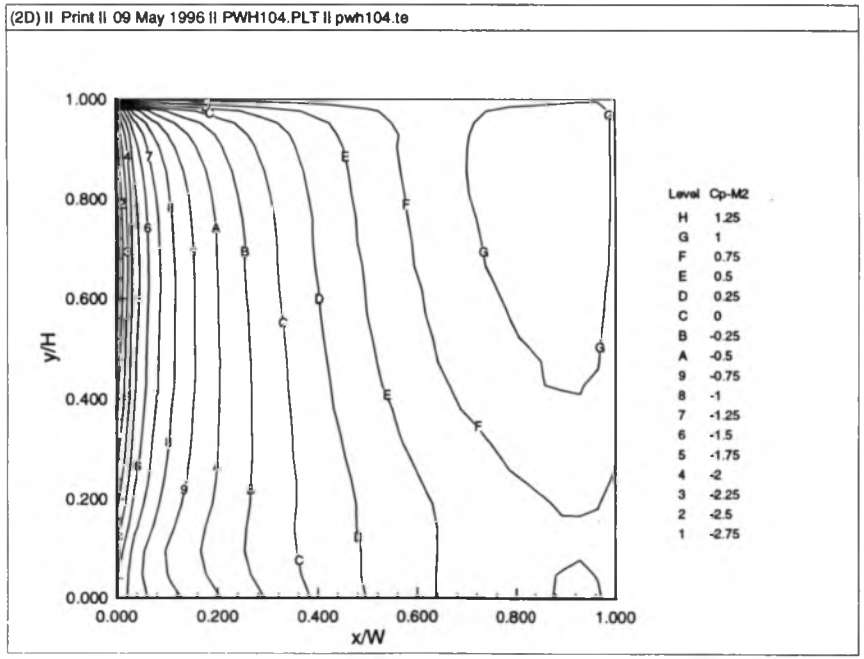

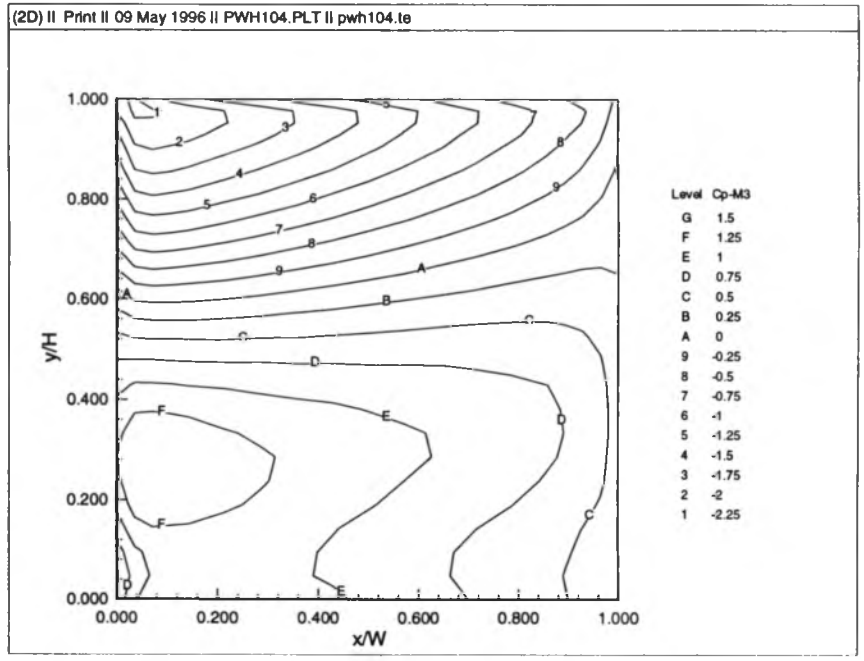

Figure B.2. Means and 1st 3 Mode Shapes of Pressure Coefficients

(30 degrees, open country)

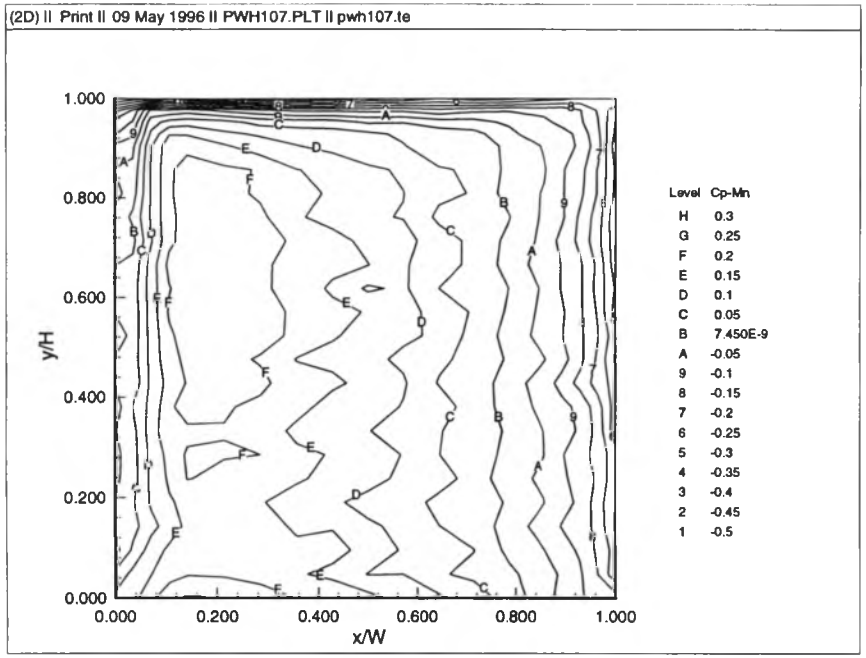

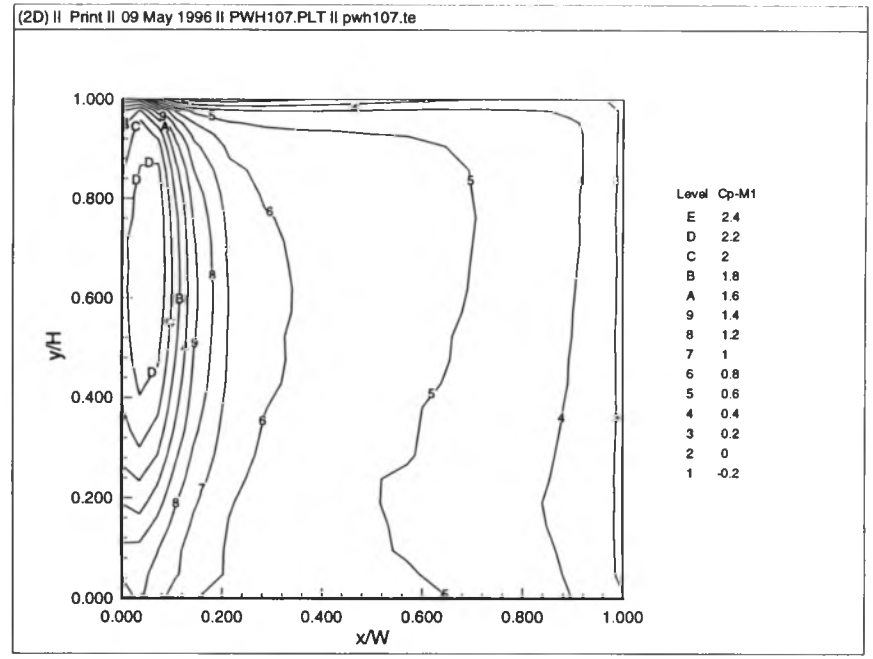

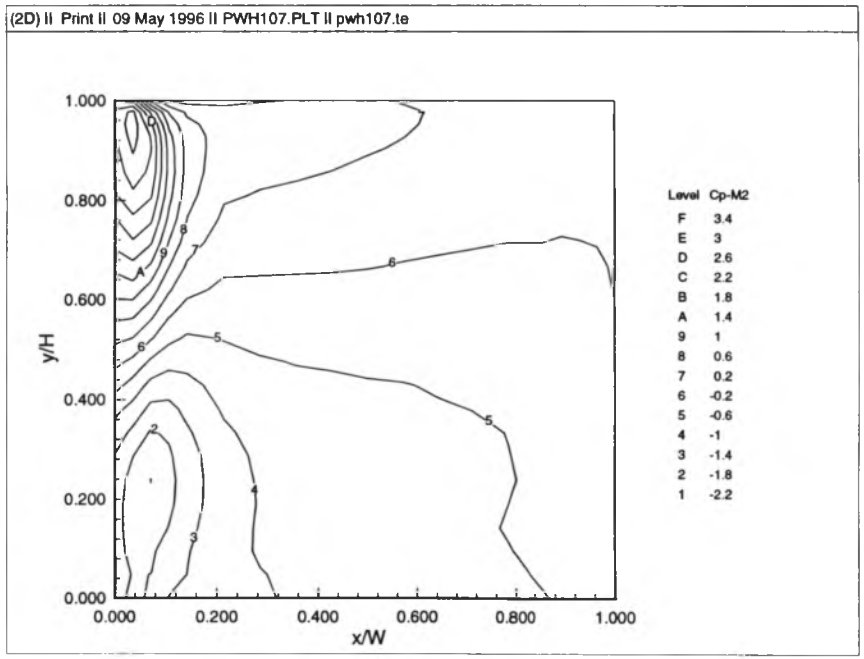

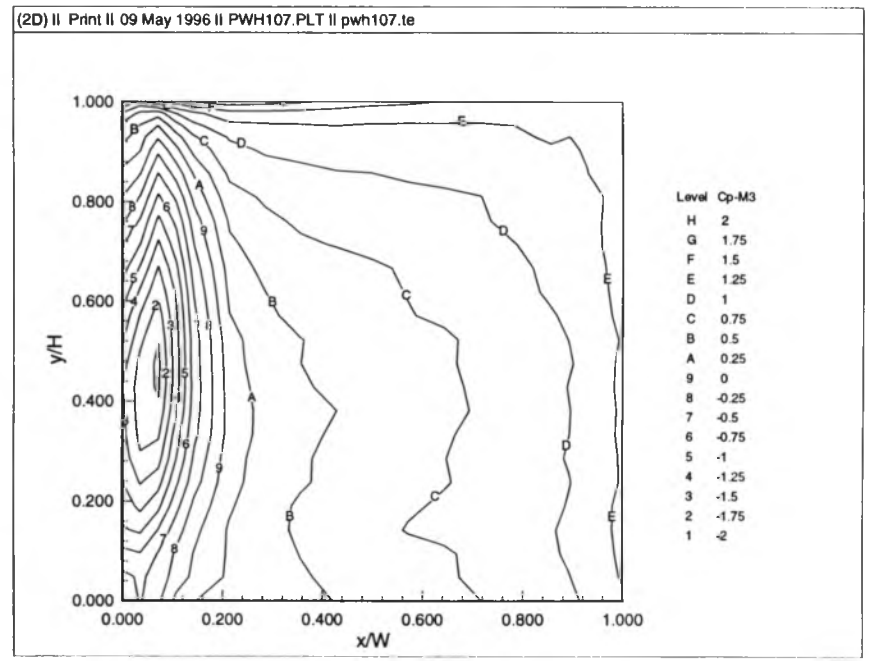

Figure B.3. Means and 1st 3 Mode Shapes of Pressure Coefficients

(60 degrees, open country)

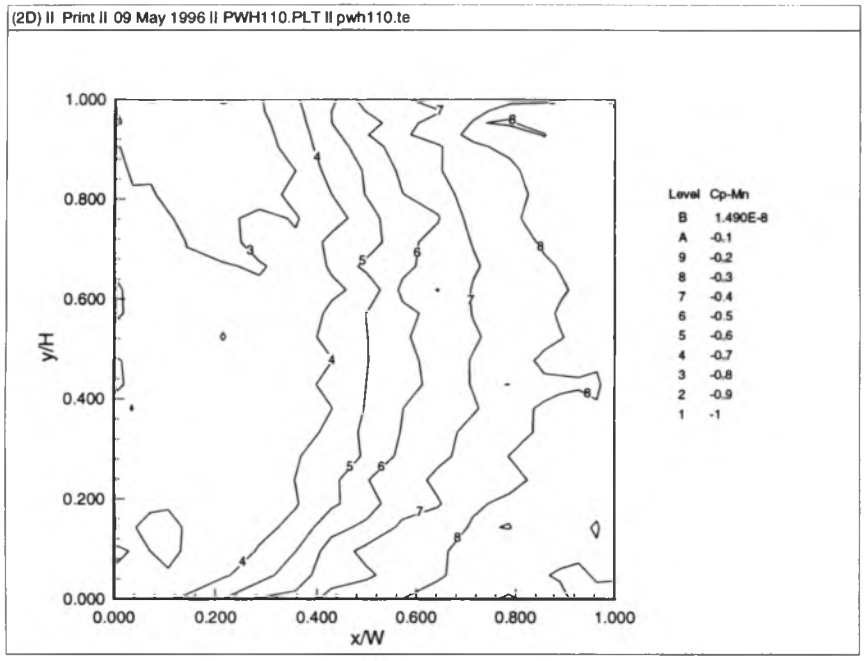

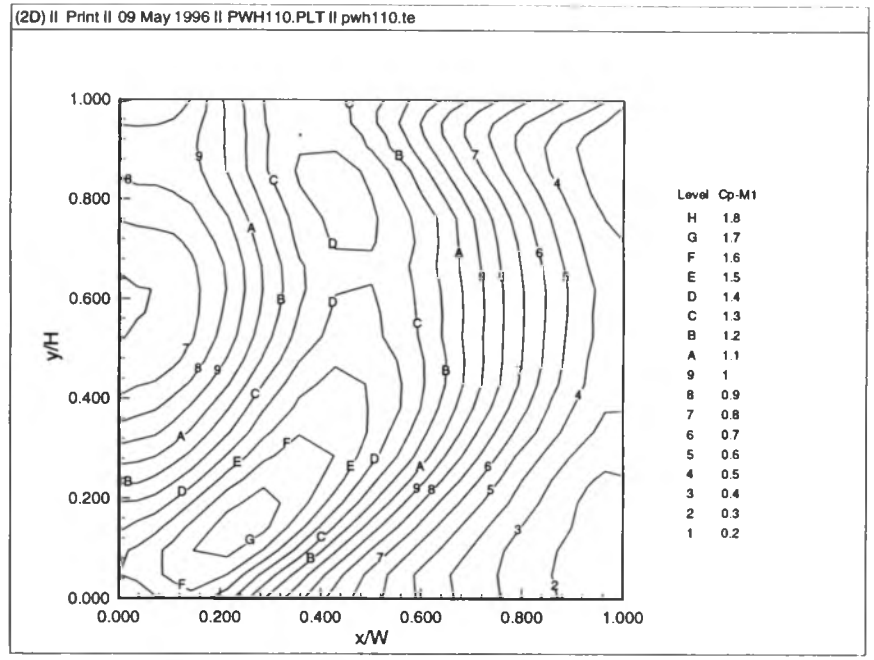

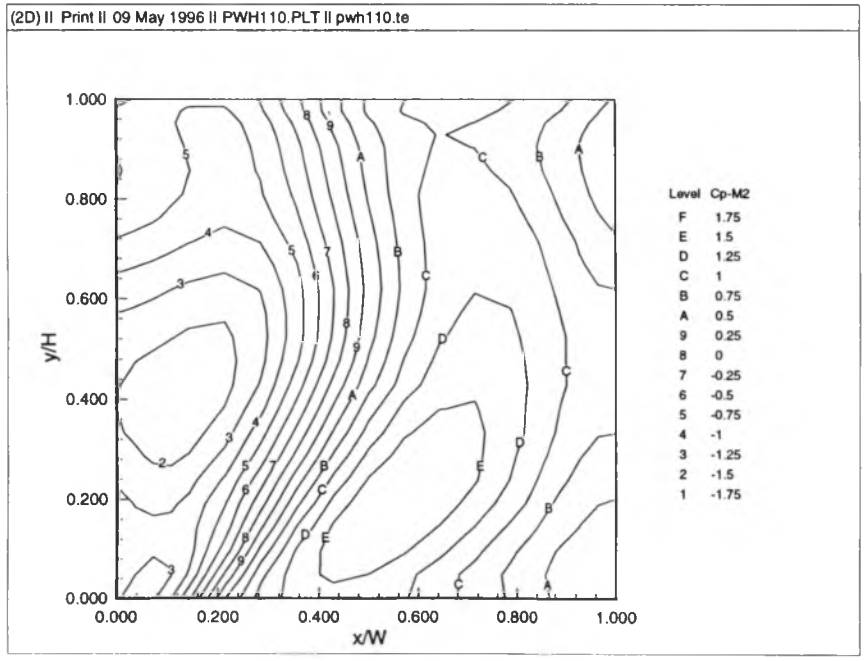

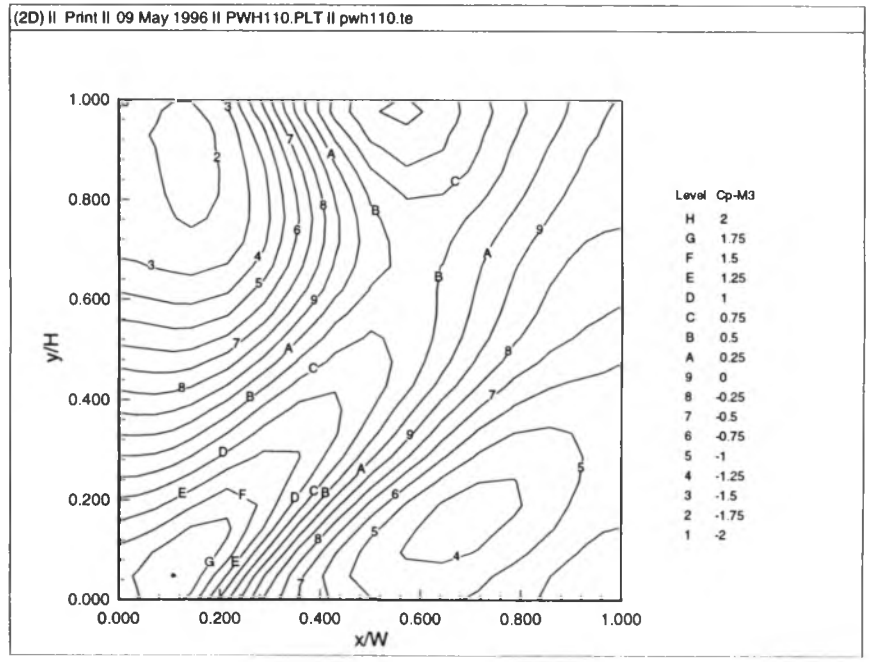

Figure B.4. Means and 1st 3 Mode Shapes of Pressure Coefficients

(90 degrees, open country)

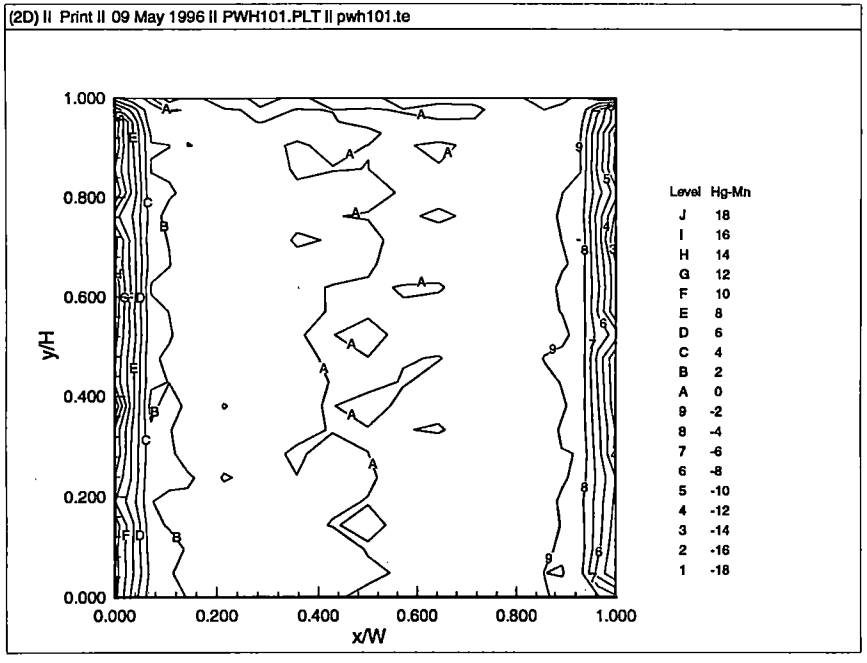

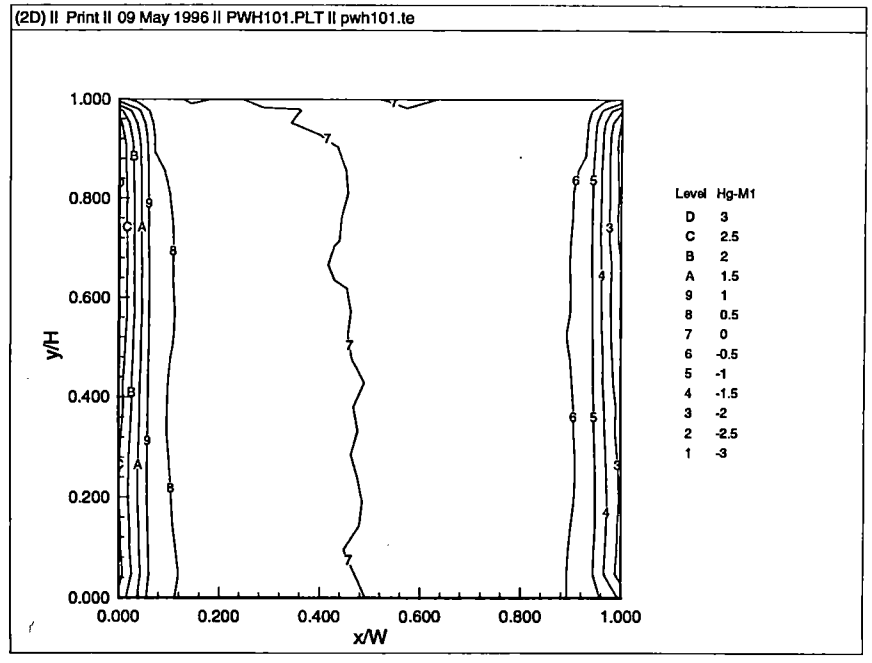

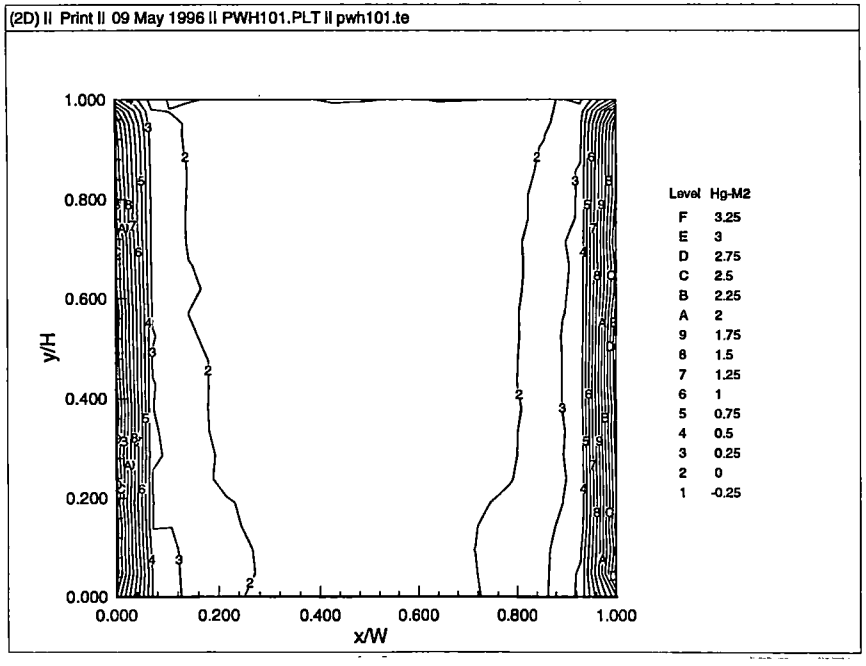

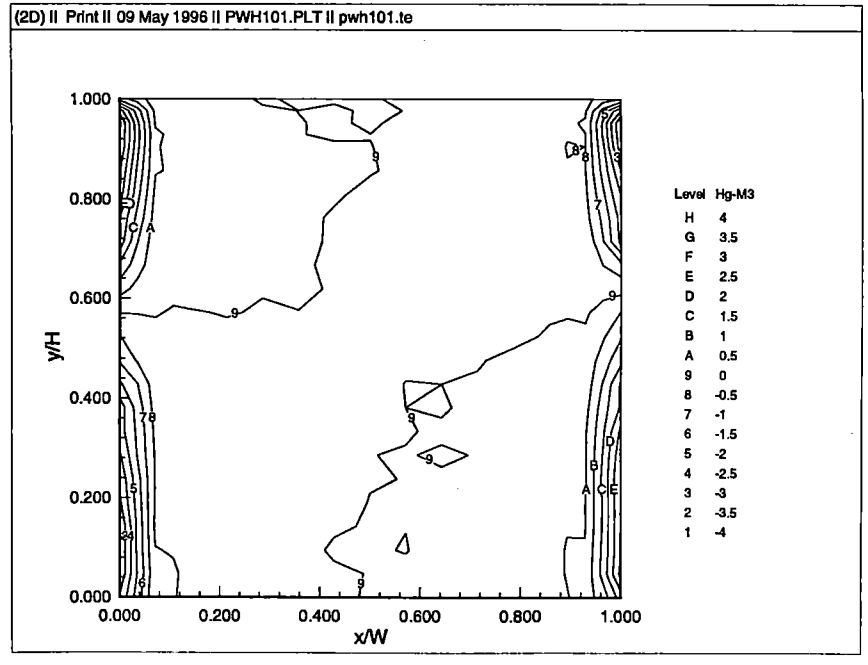

Figure B.5. Means and 1st 3 Mode Shapes of Horizontal Pressure Gradients

(0 degrees, open country)

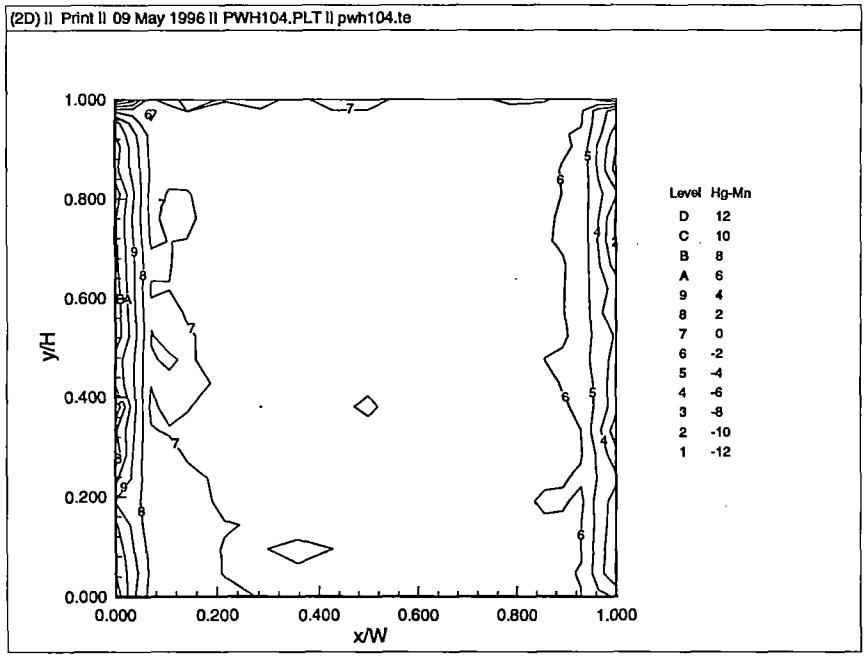

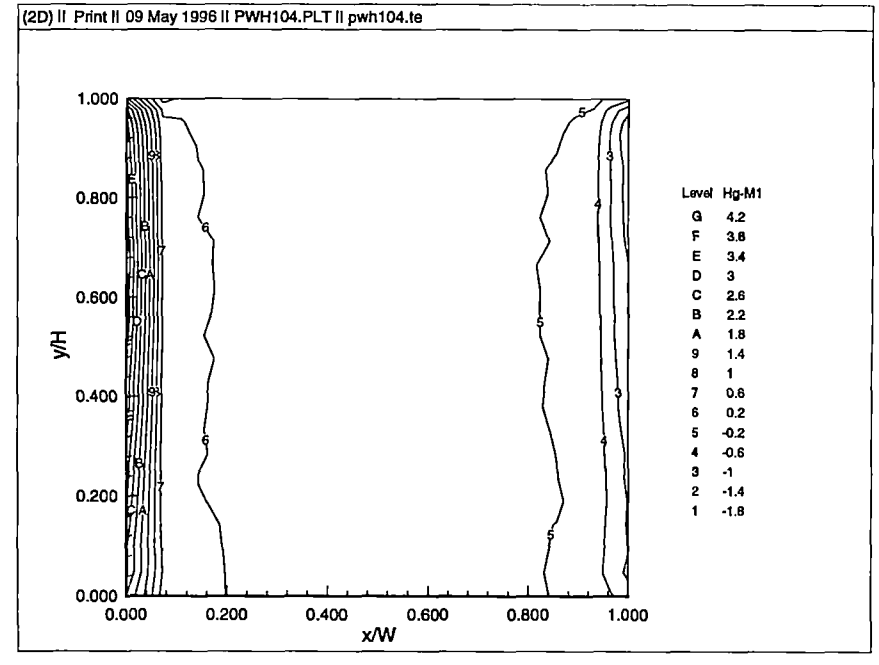

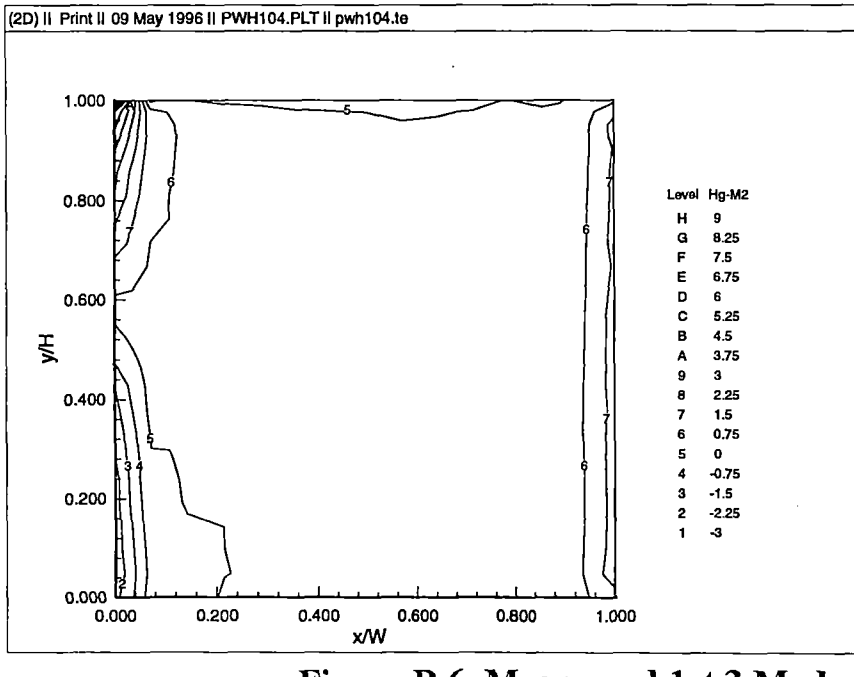

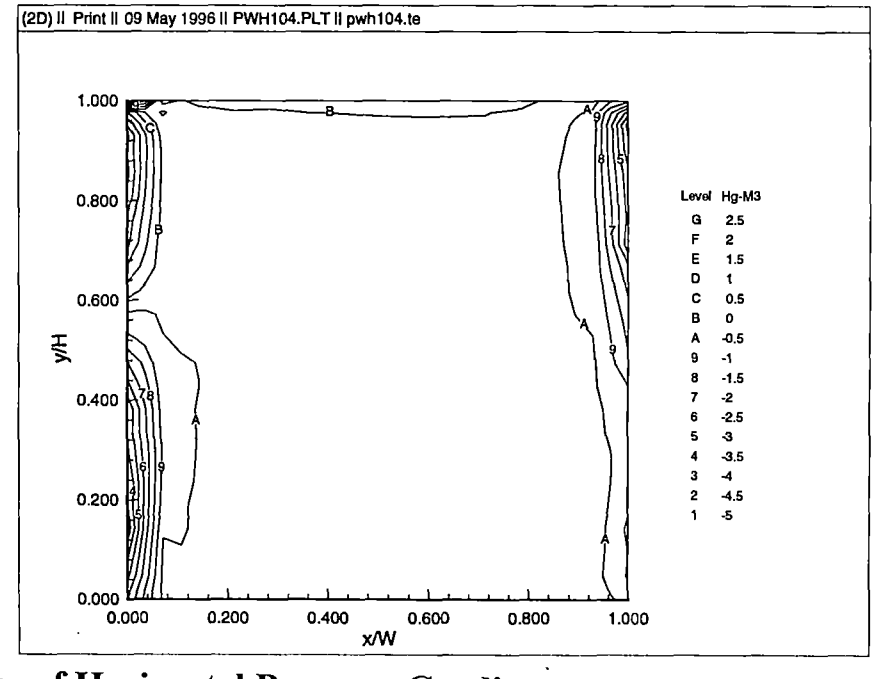

Figure B.6. Means and 1st 3 Mode Shapes of Horizontal Pressure Gradients

(30 degrees, open country)

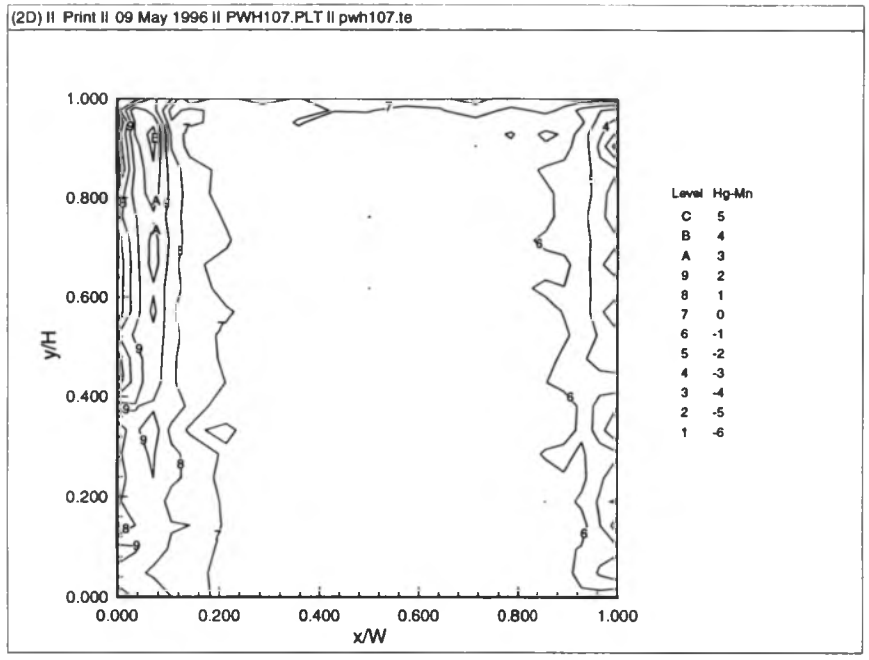

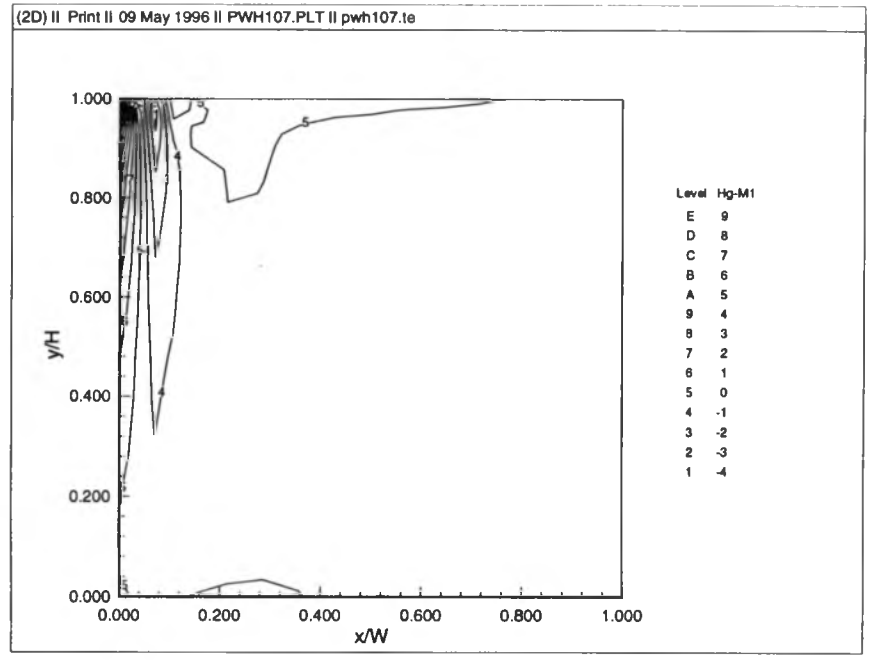

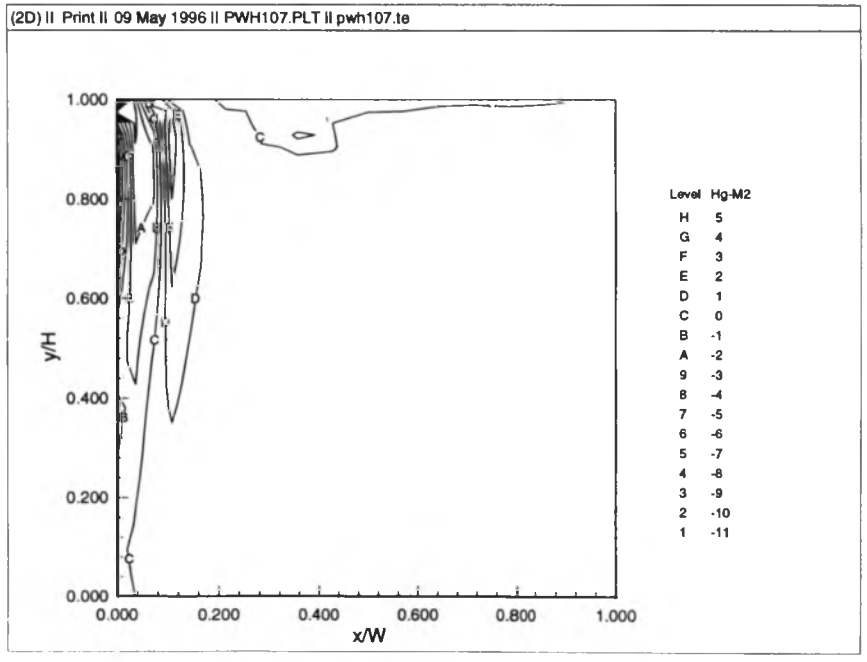

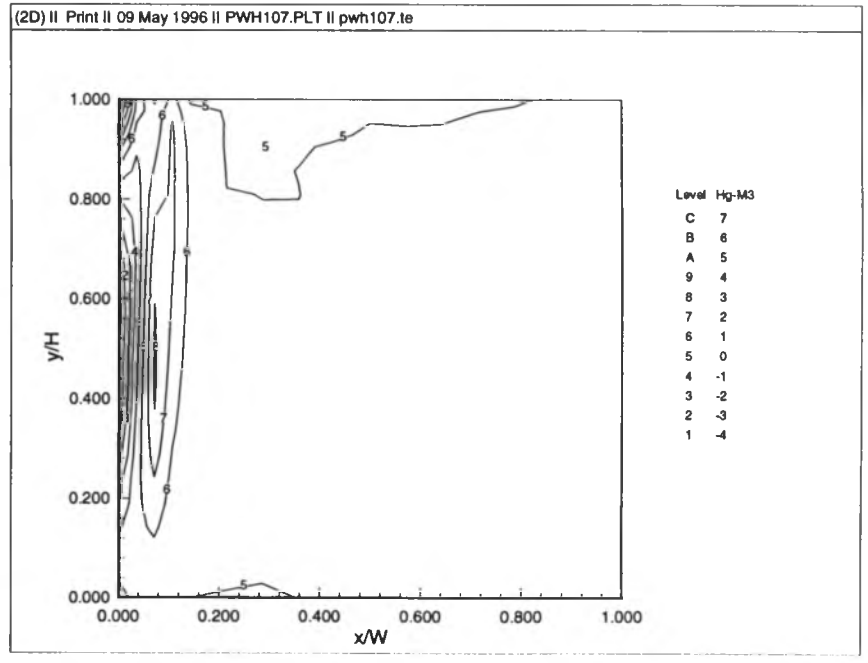

Figure B.7. Means and 1st 3 Mode Shapes of Horizontal Pressure Gradients (60 degrees, open country)

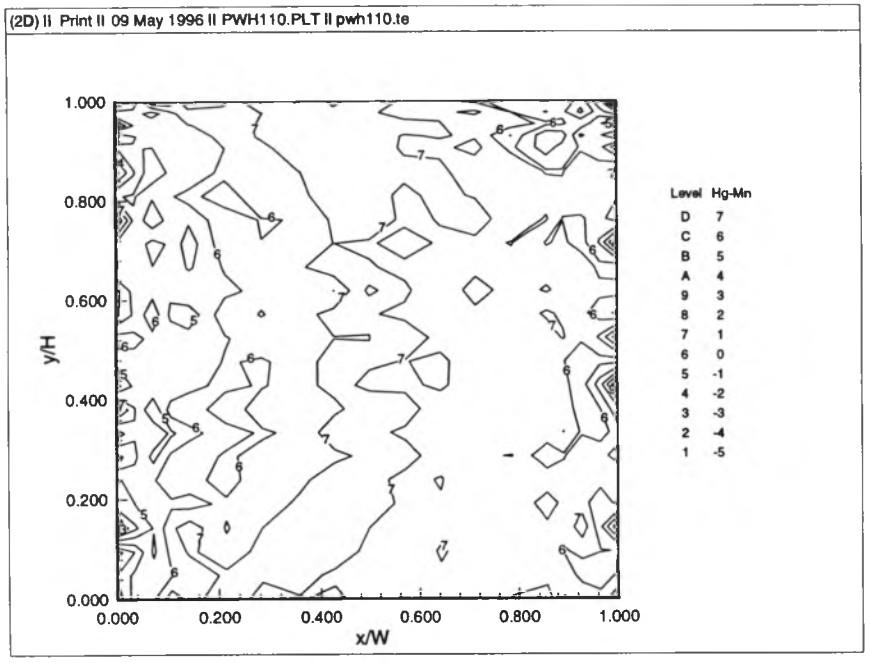

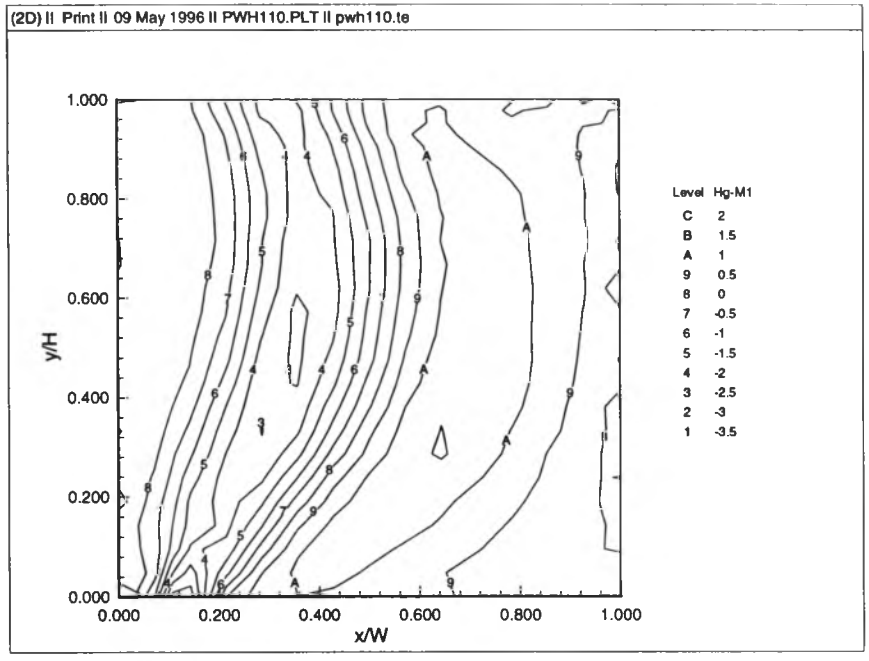

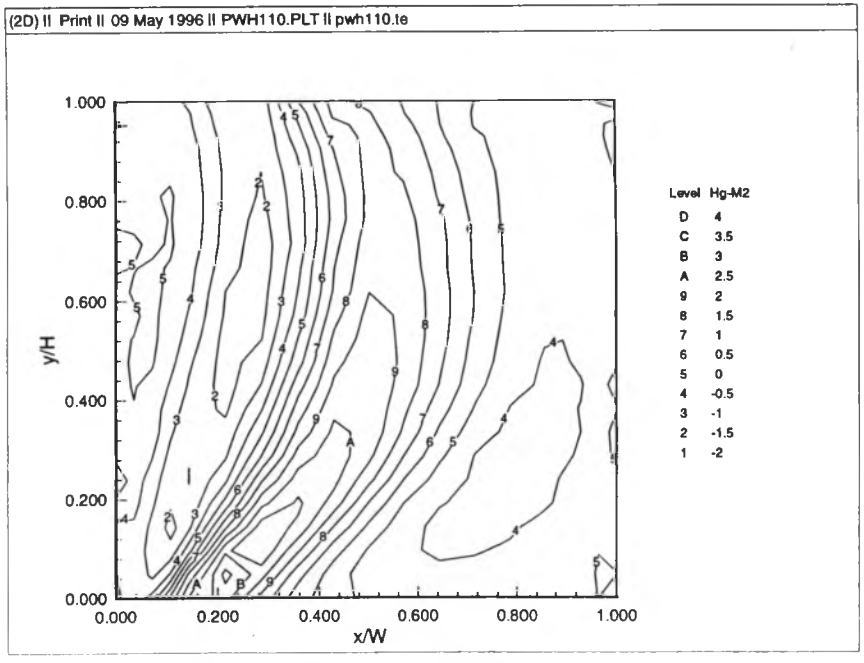

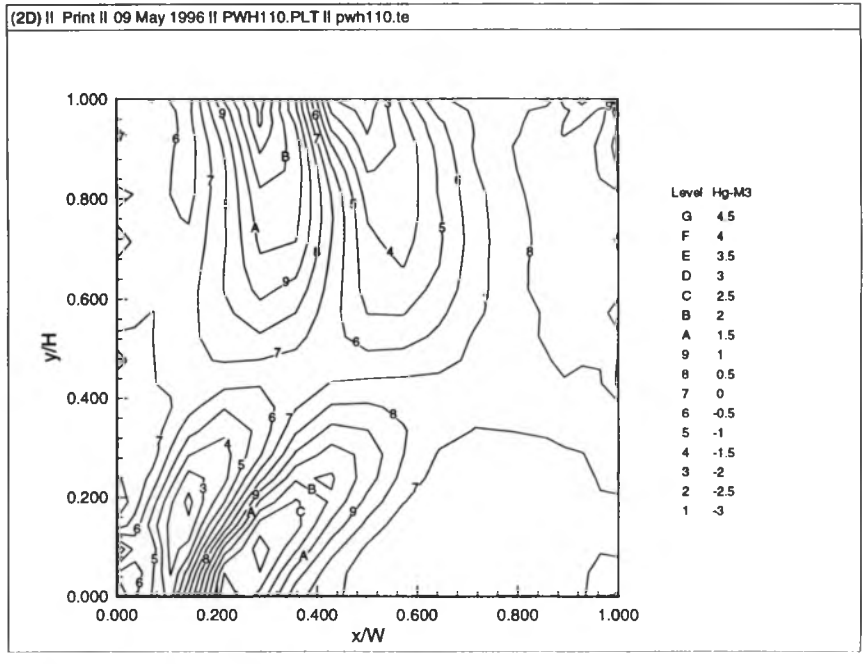

Figure B.8. Means and 1st 3 Mode Shapes of Horizontal Pressure Gradients

(90 degrees, open country)

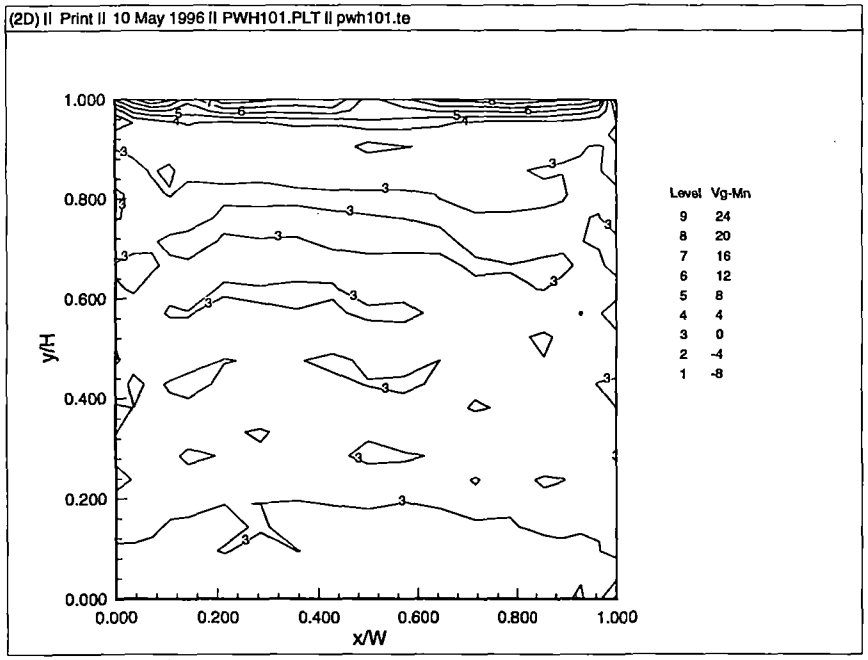

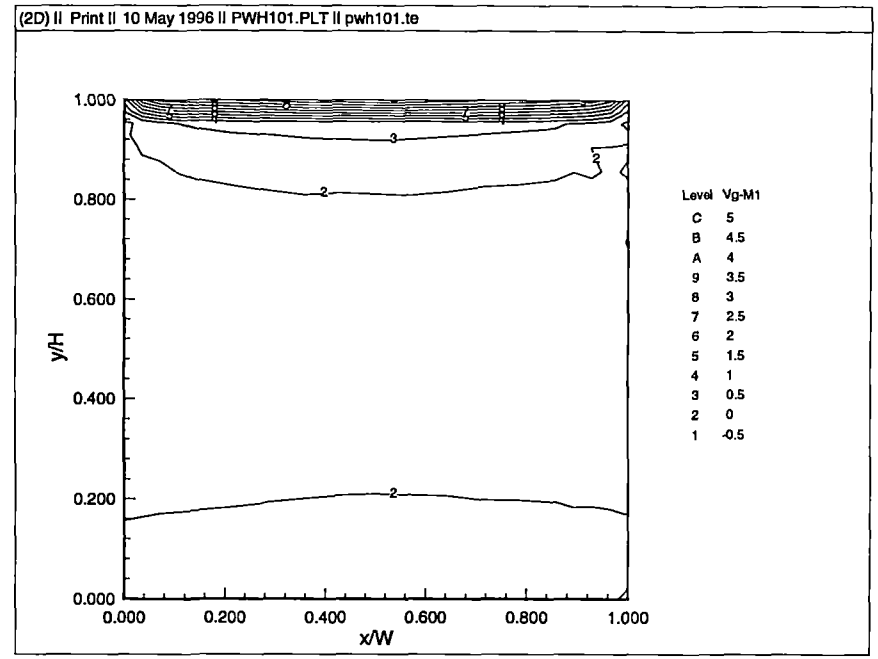

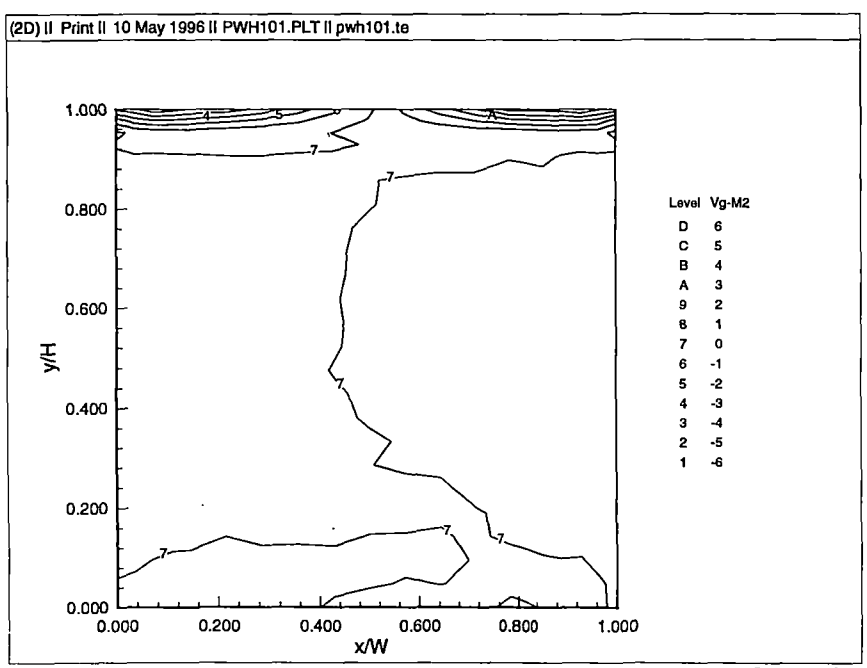

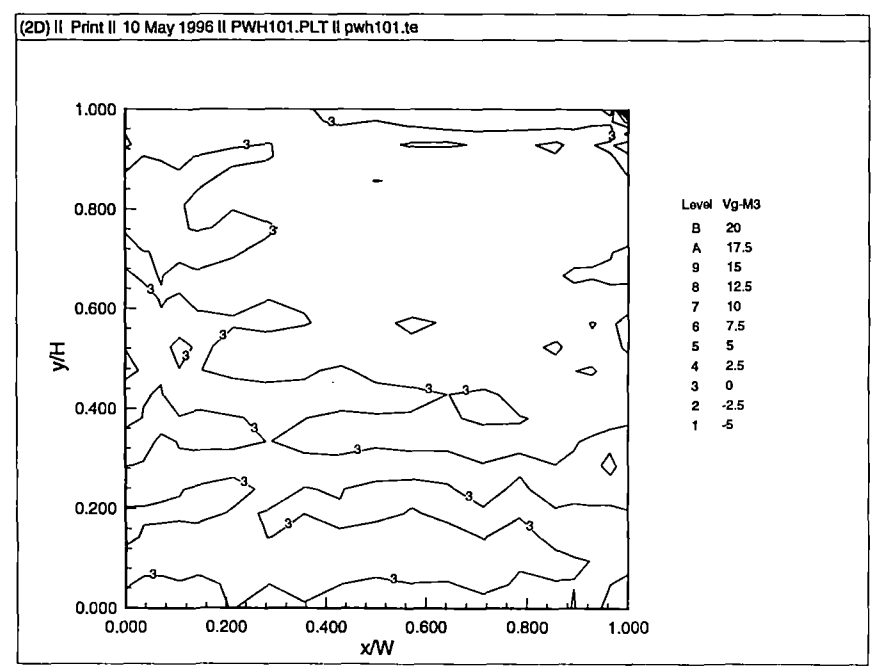

Figure B.9. Means and 1st 3 Mode Shapes of Vertical Pressure Gradients

(0 degrees, open country)

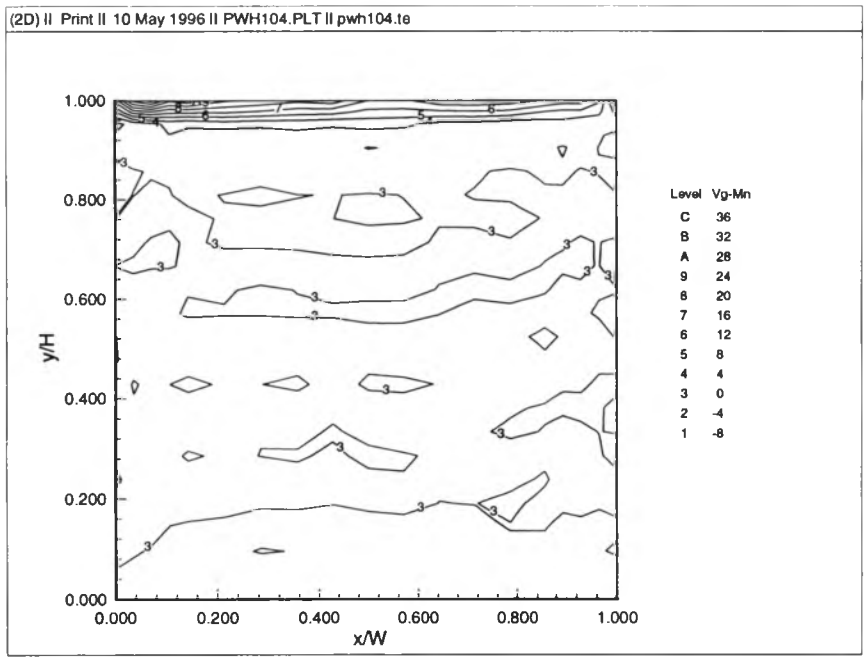

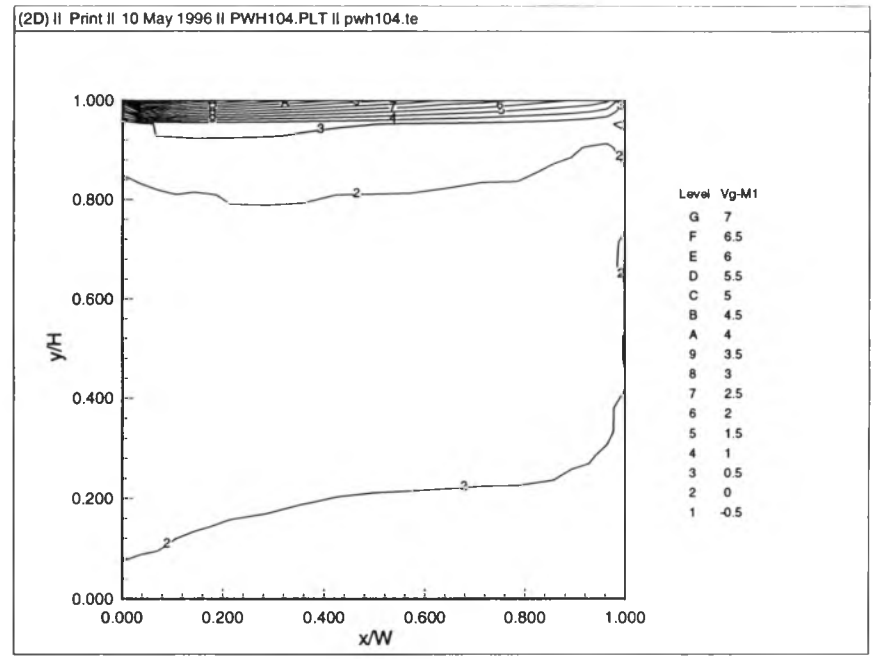

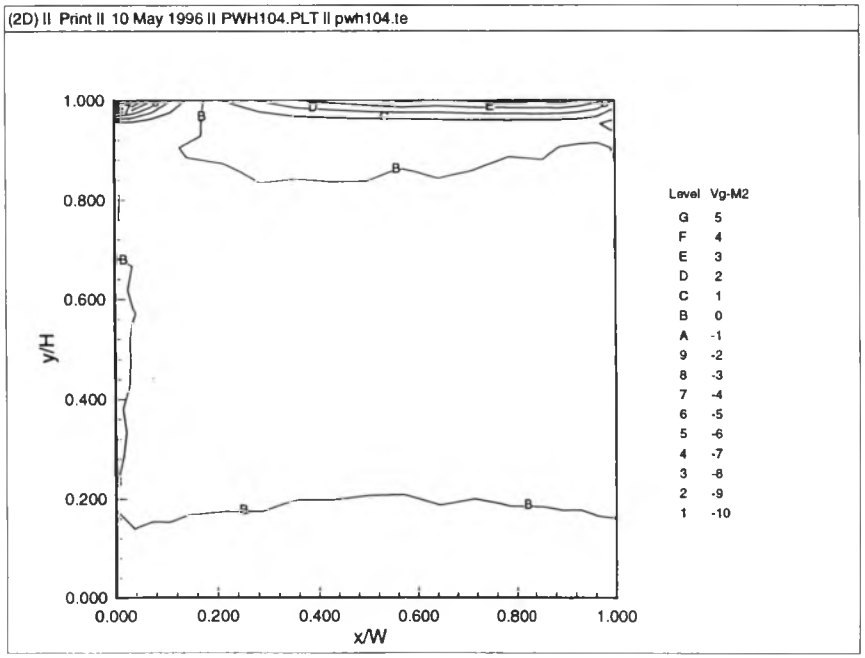

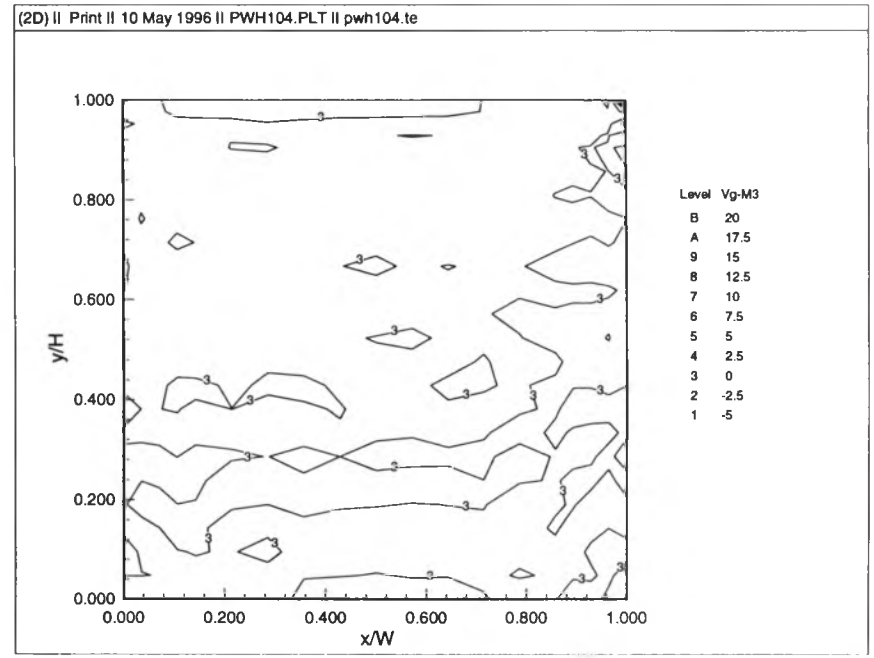

Figure B.10. Means and 1st 3 Mode Shapes of Vertical Pressure Gradients

(30 degrees, open country)

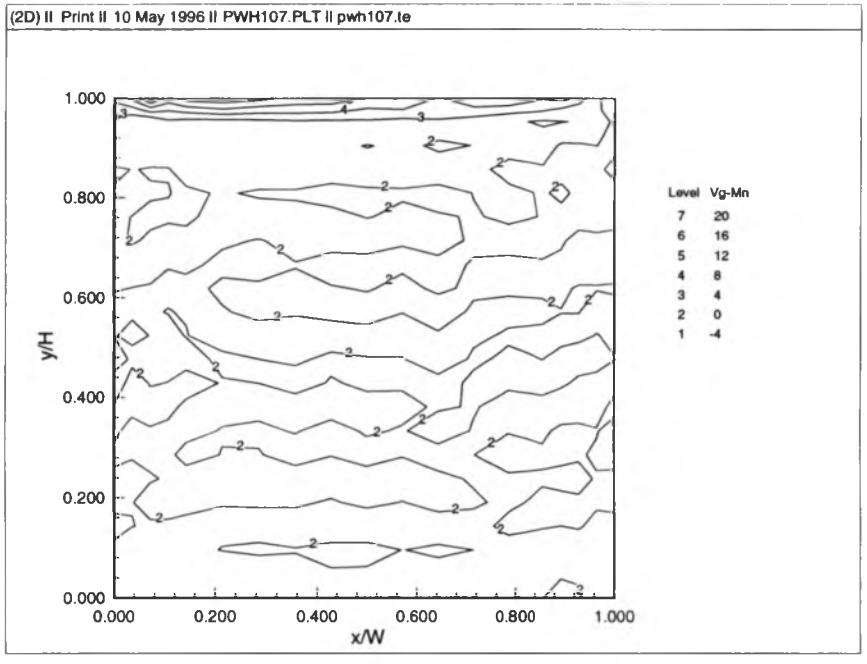

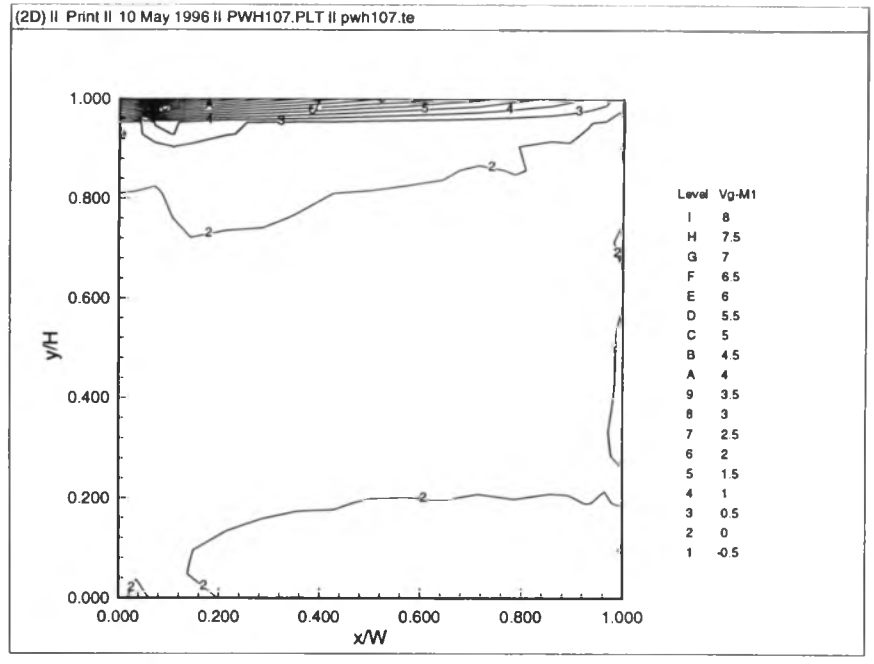

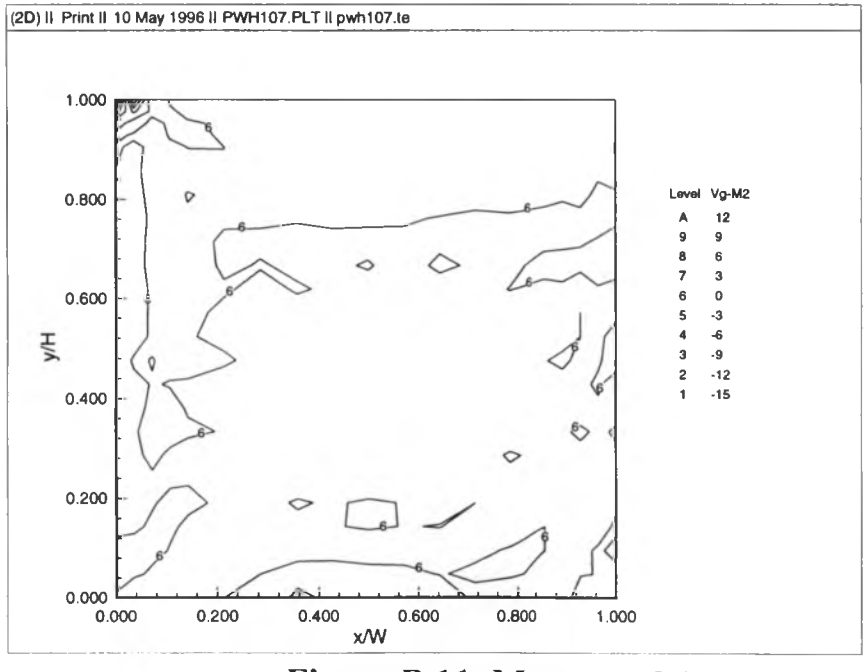

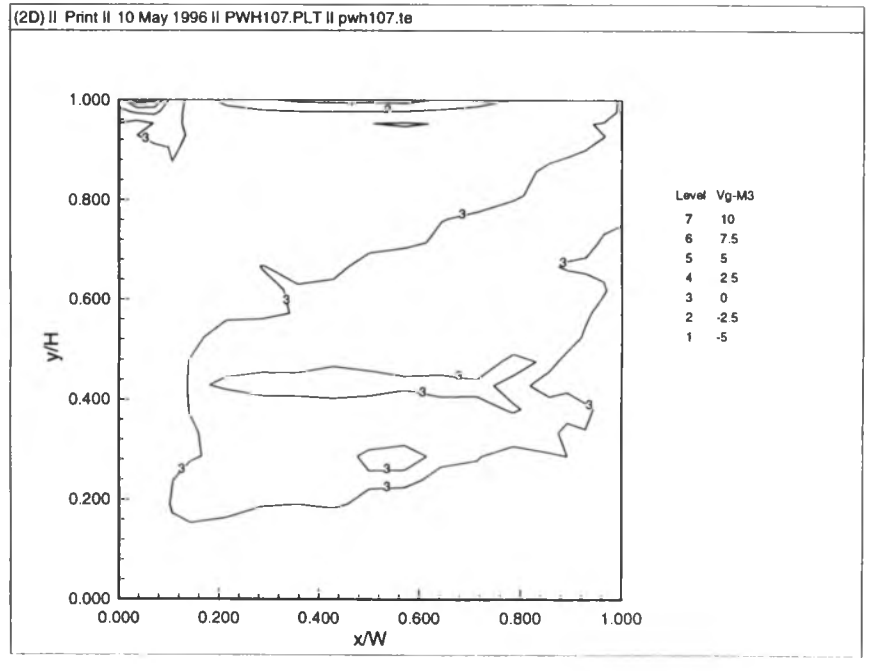

Figure B.11. Means and 1st 3 Mode Shapes of Vertical Pressure Gradients

(60 degrees, open country)

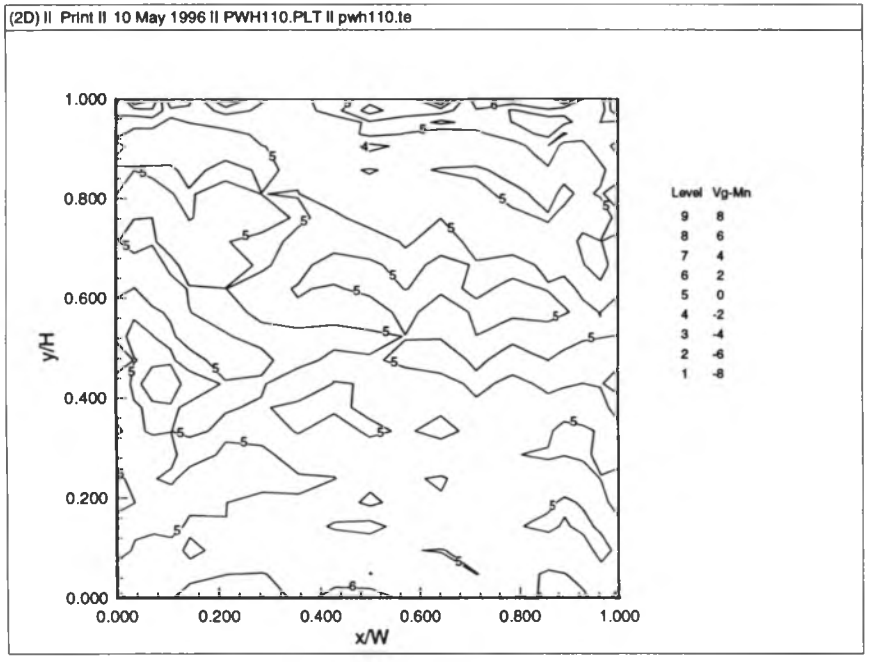

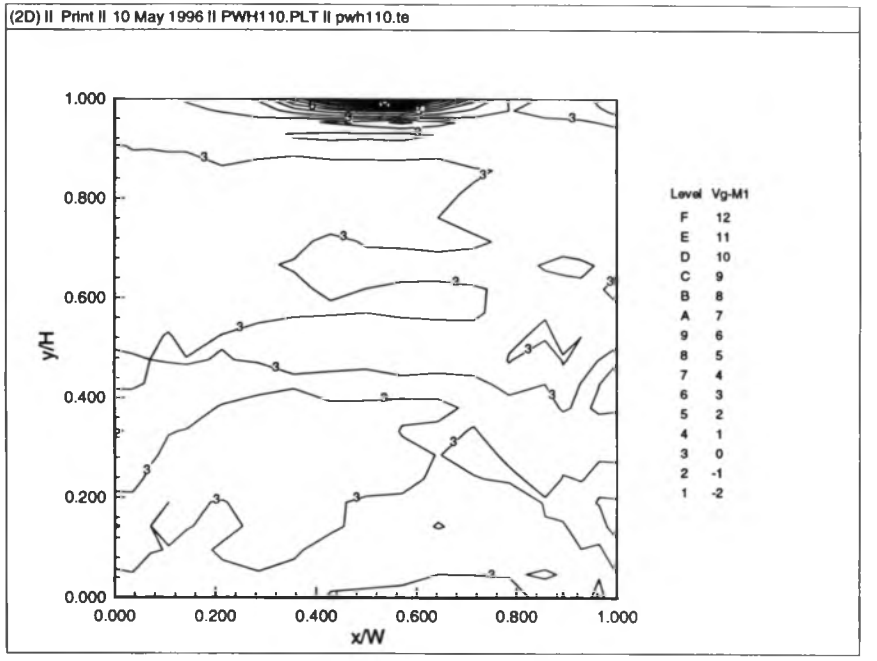

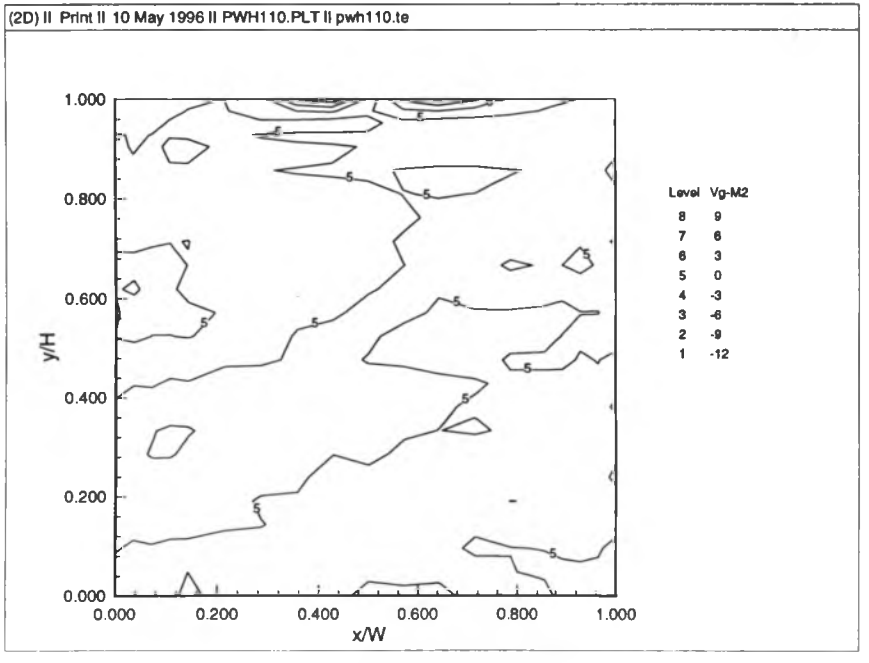

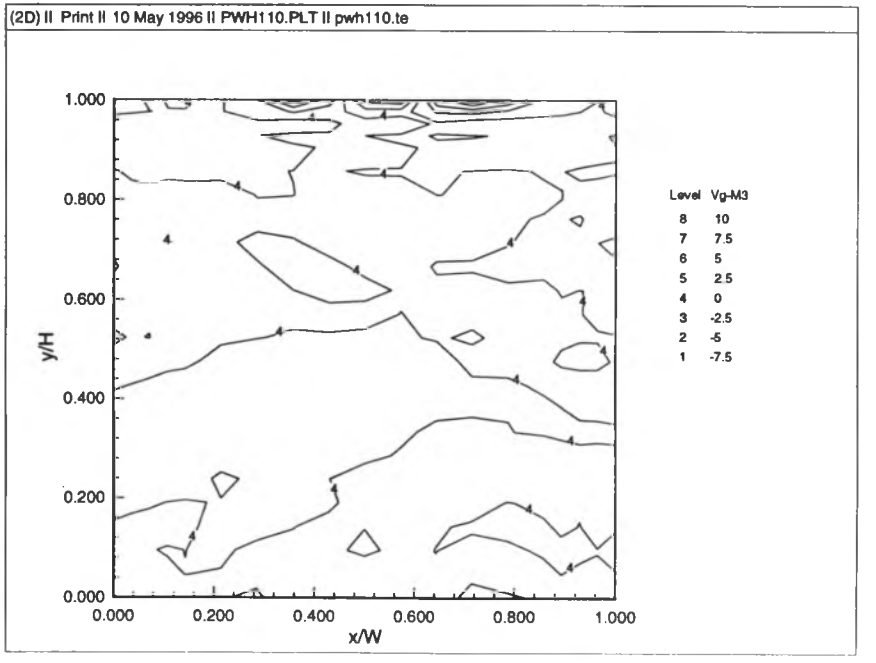

Figure B.12. Means and 1st 3 Mode Shapes of Vertical Pressure Gradients

(90 degrees, open country)

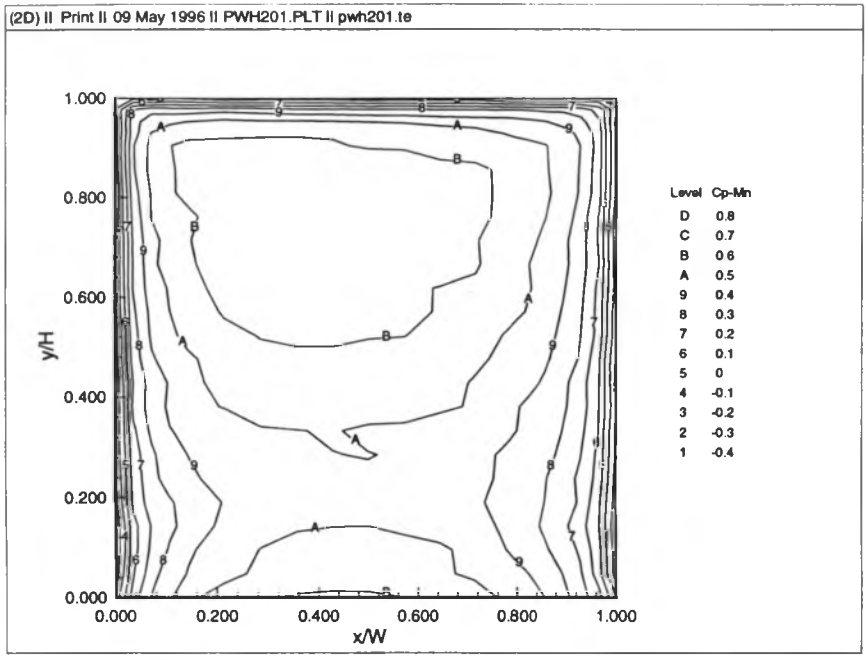

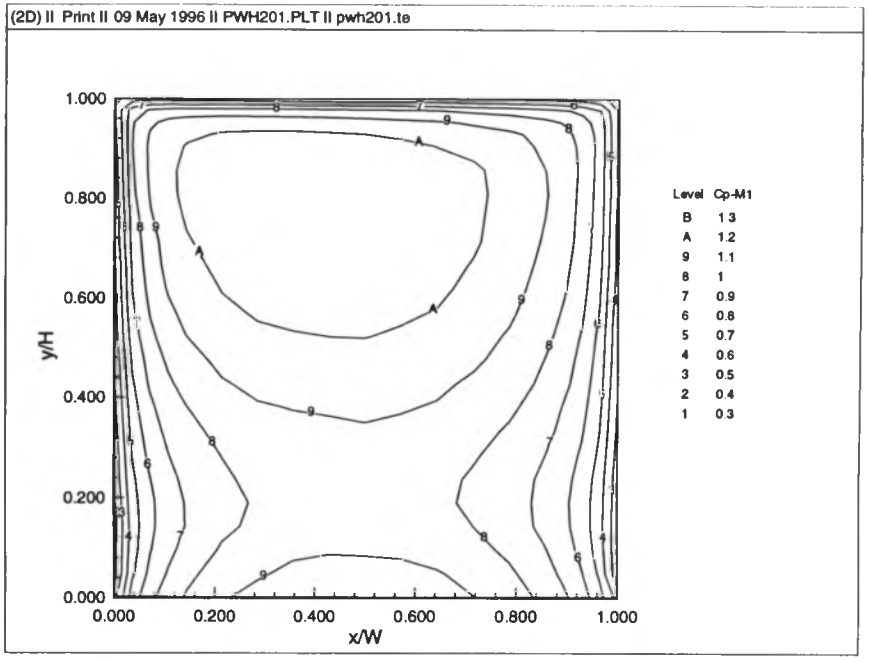

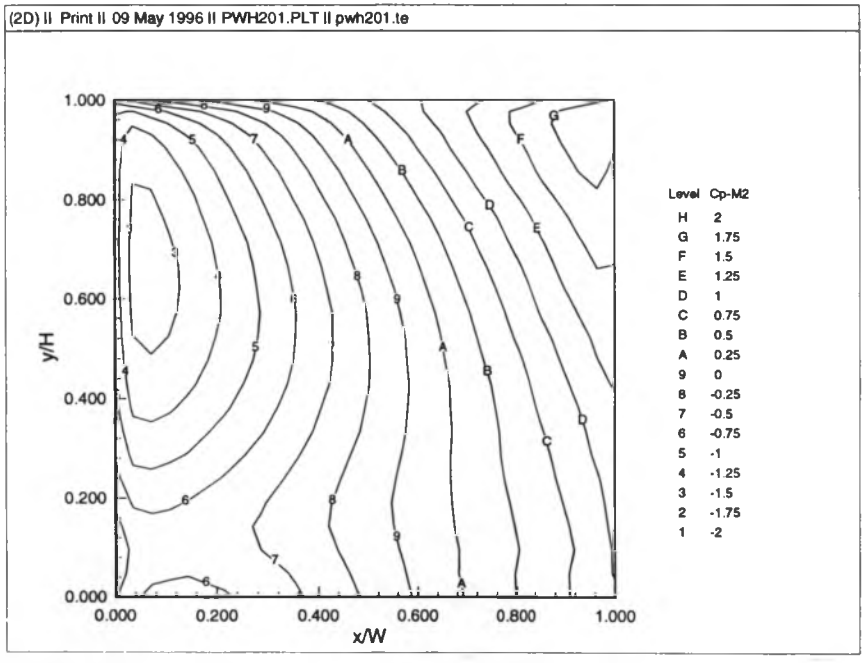

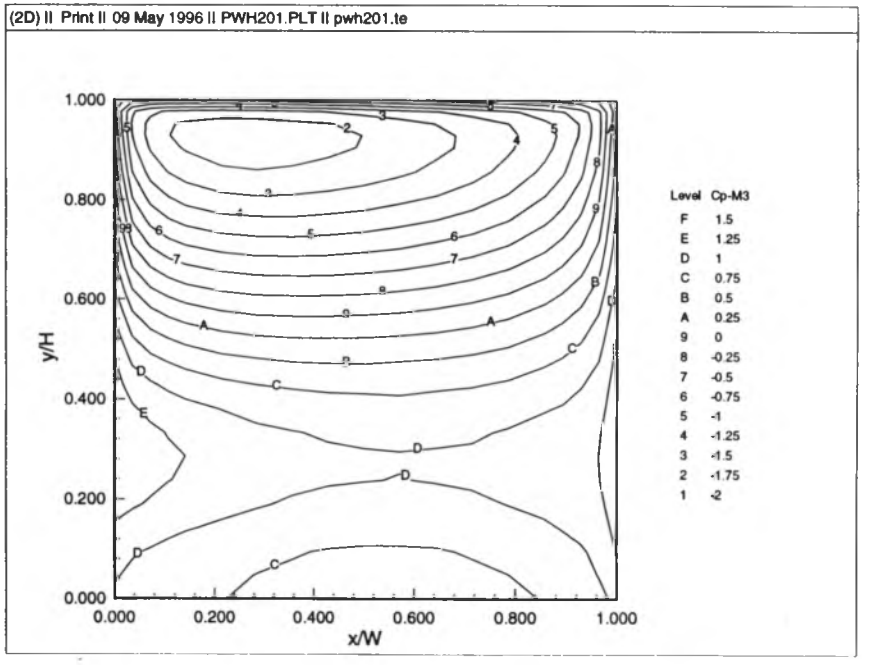

Figure B.13. Means and 1st 3 Mode Shapes of Pressure Coefficients

(0 degrees, suburban)

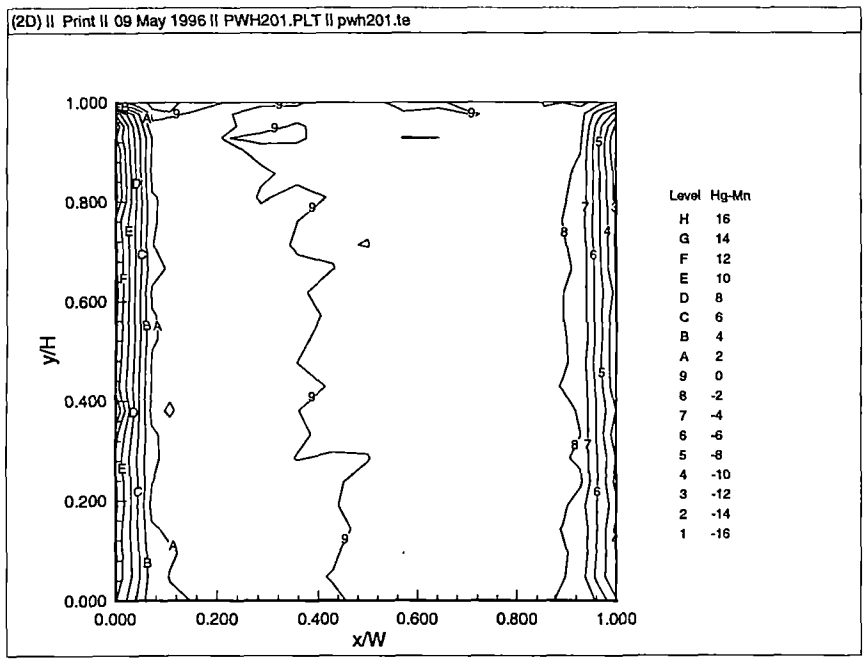

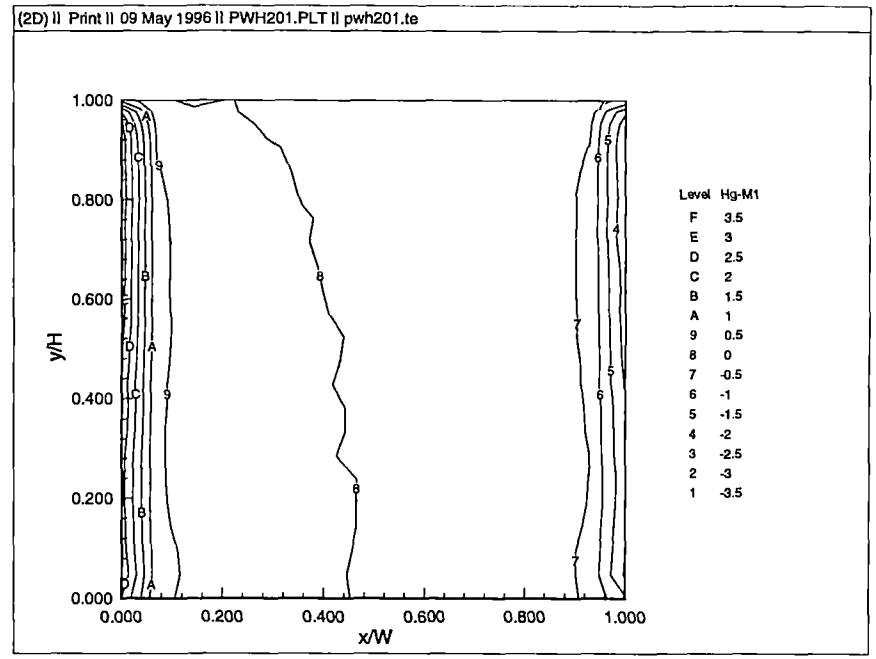

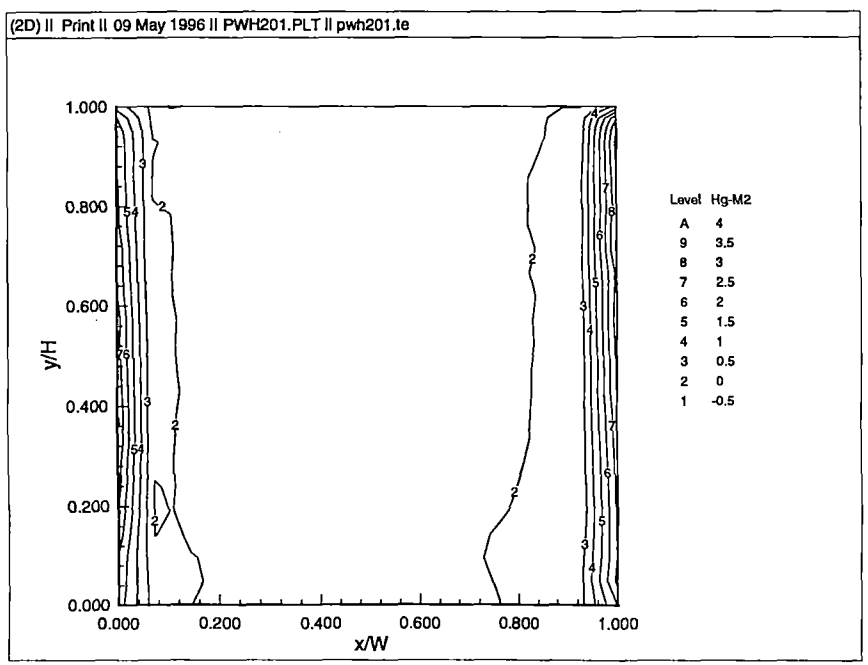

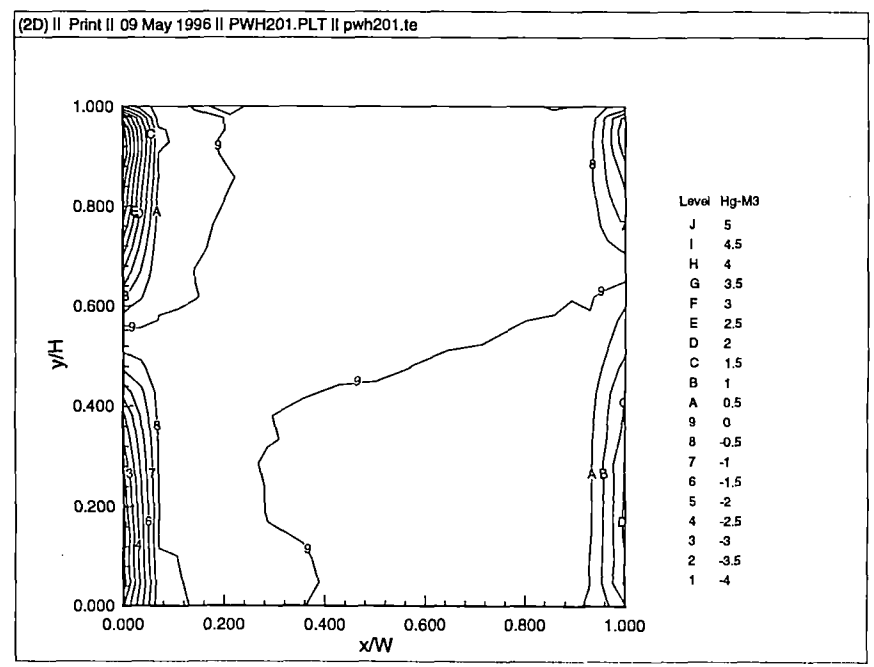

Figure B.14. Means and 1st 3 Mode Shapes of Horizontal Pressure Gradients

(0 degrees, suburban)

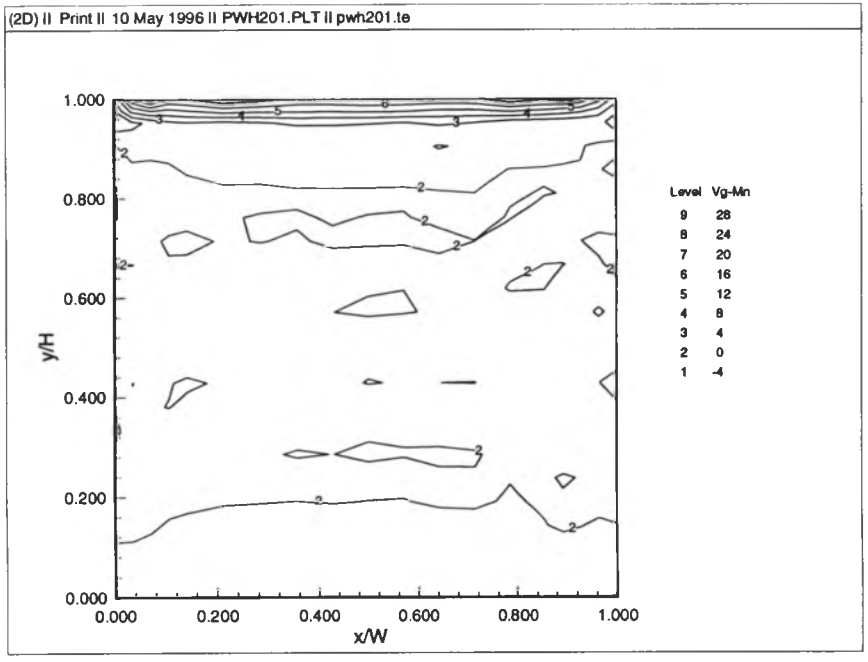

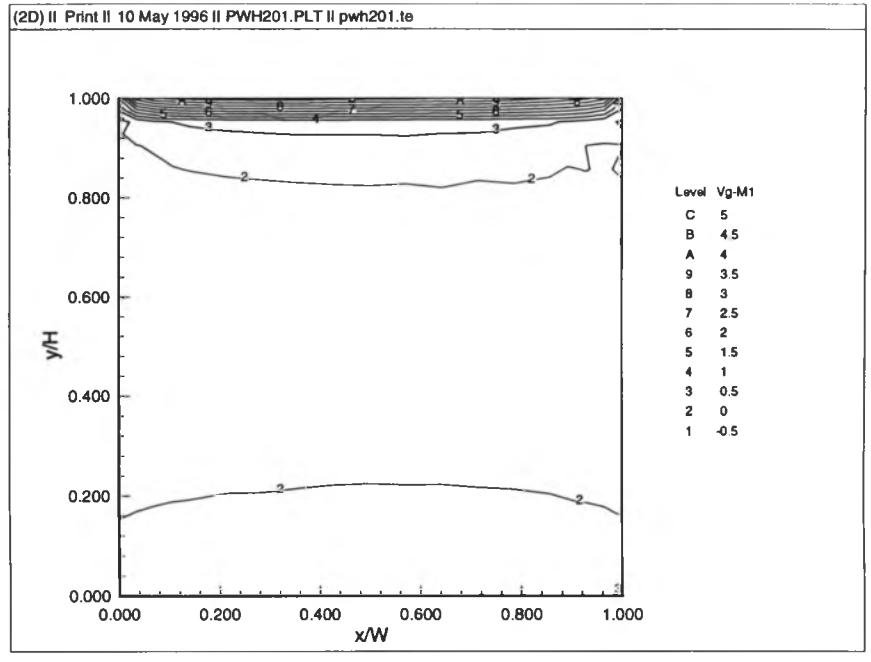

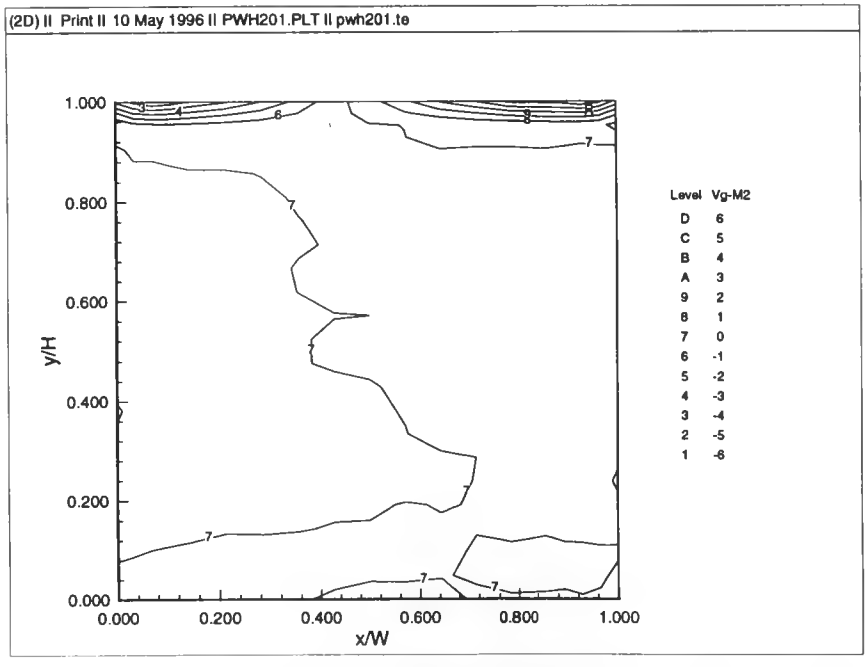

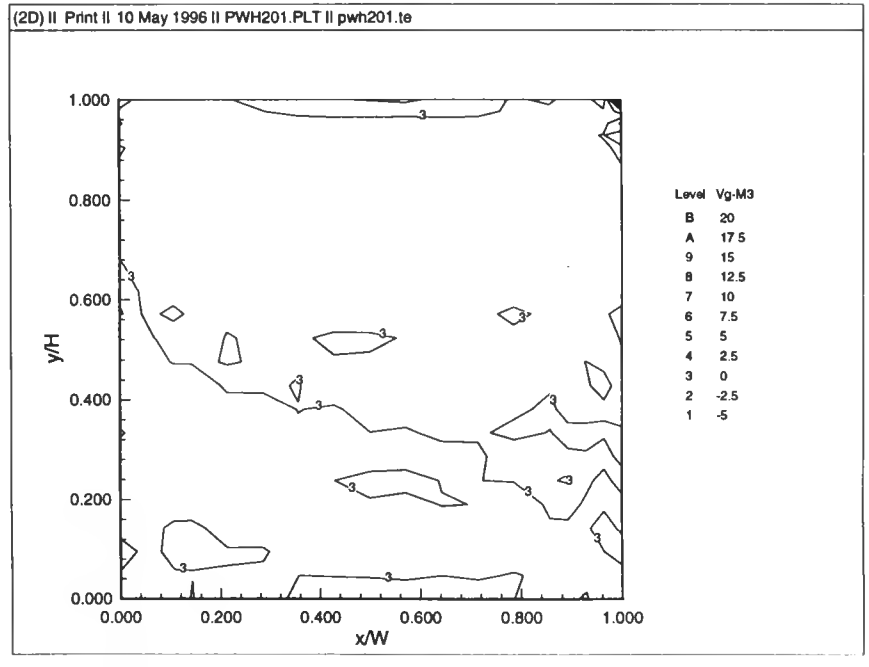

Figure B.15. Means and 1st 3 Mode Shapes of Vertical Pressure Gradients

(0 degrees, suburban)

APPENDIX C

NODAL ENERGY RATIOS
(UNFILTERED & FILTERED)

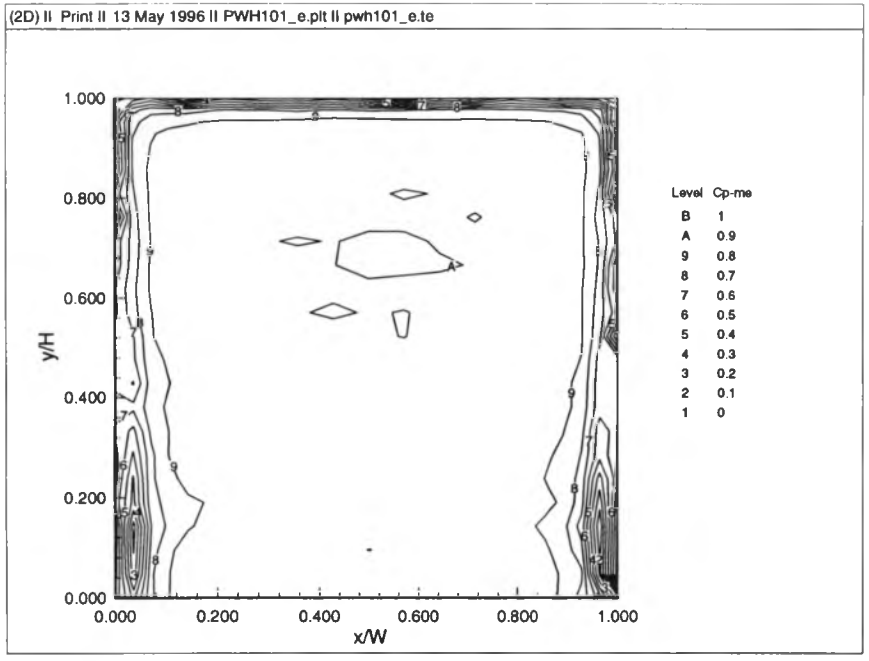

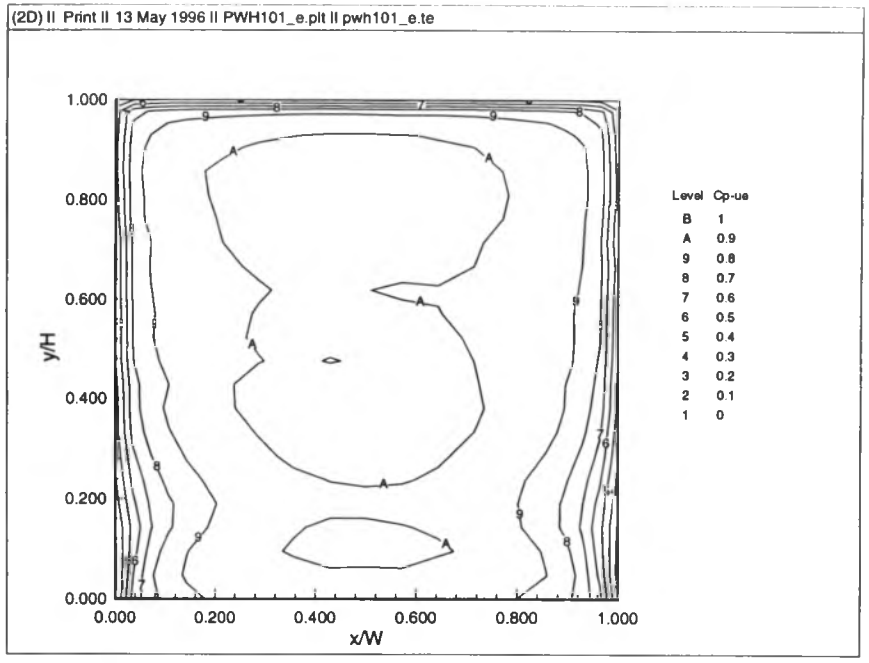

Figure C.1a. Pressures - Energy Contribution of Means [-me] and Nodal Energy Ratios [-ue], unfiltered, (0 degrees, open country)

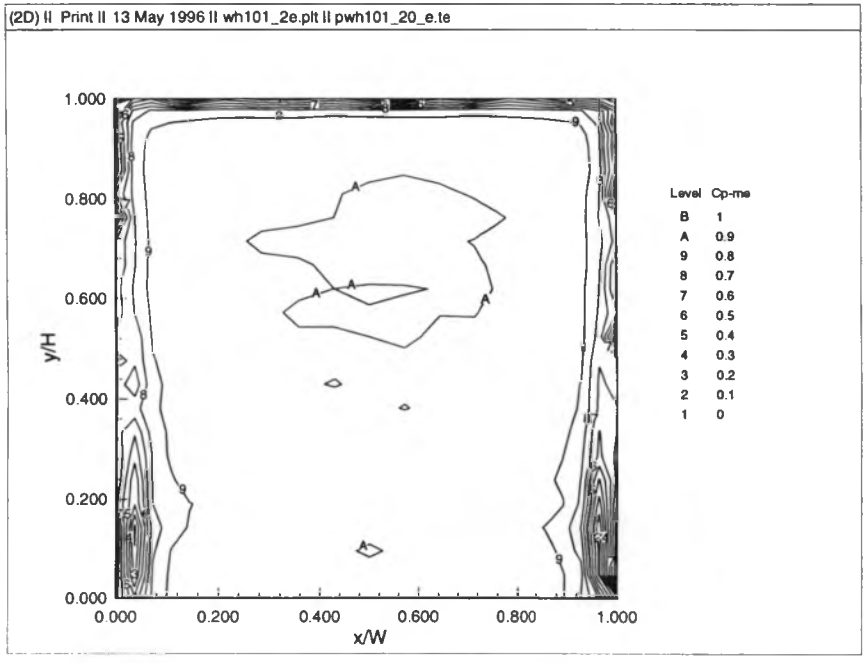

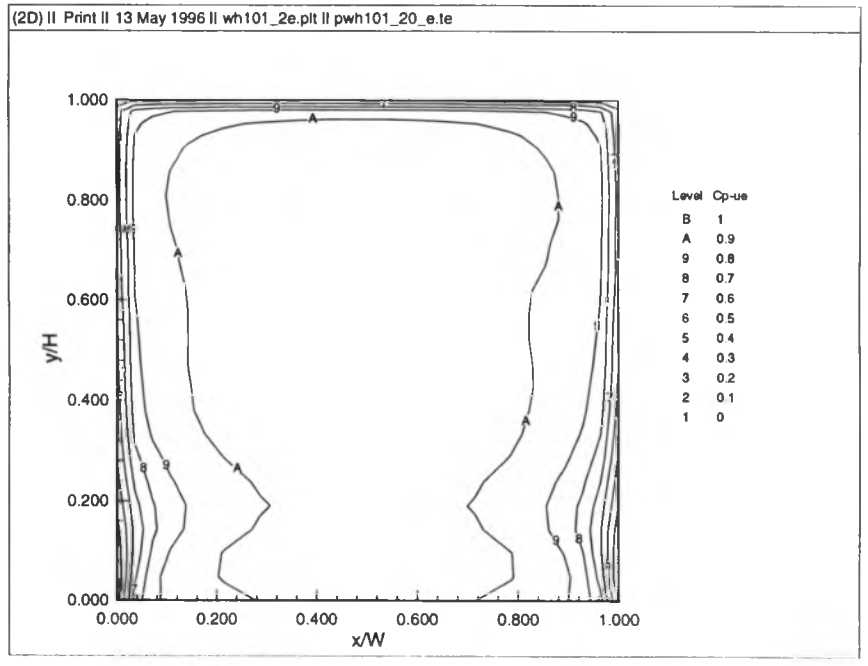

Figure C.1b. Pressures - Energy Contribution of Means [-me] and Nodal Energy Ratios [-ue], filtered, (0 degrees, open country)

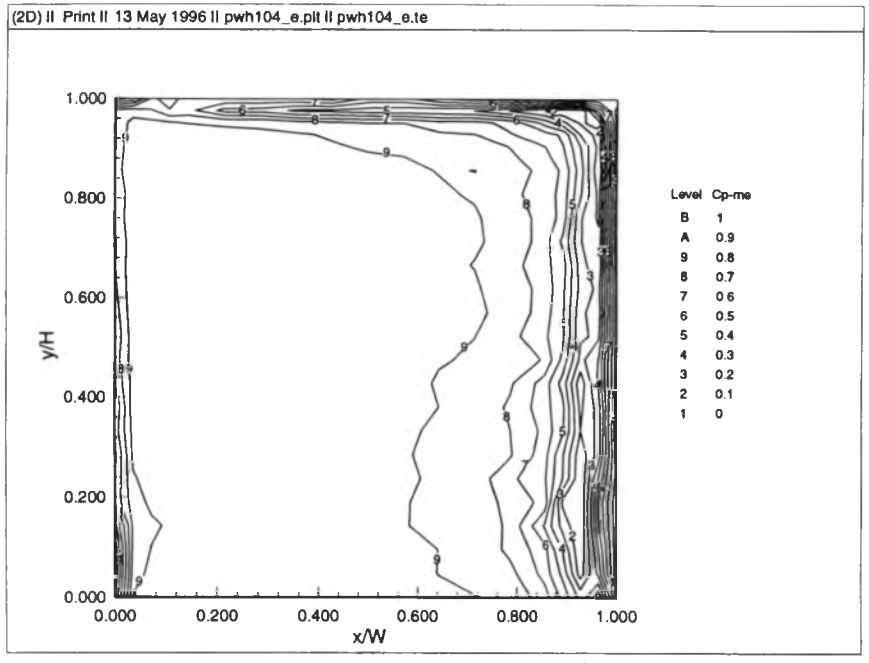

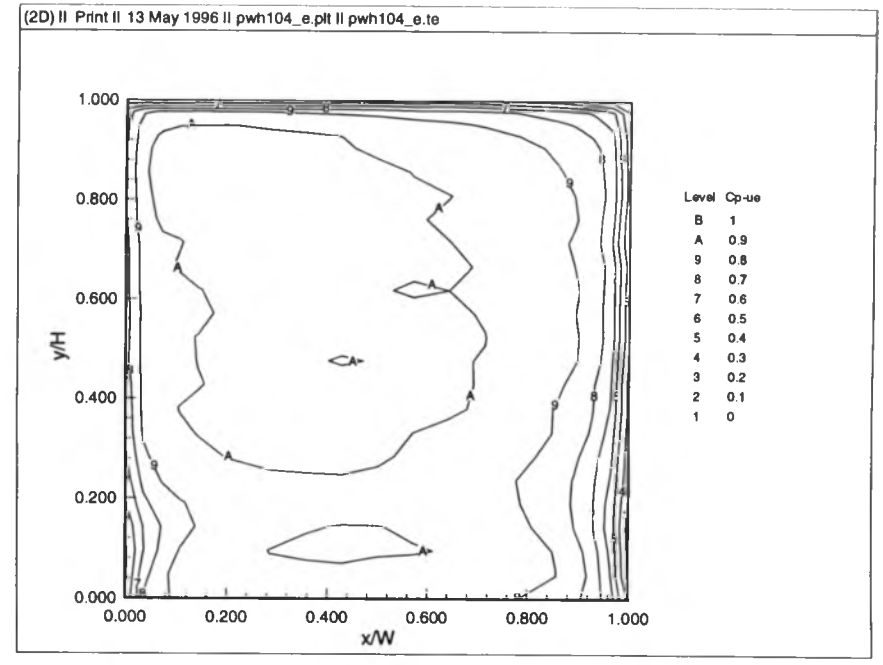

Figure C.2a. Pressures - Energy Contribution of Means [-me] and Nodal Energy Ratios [-ue], unfiltered, (30 degrees, open country)

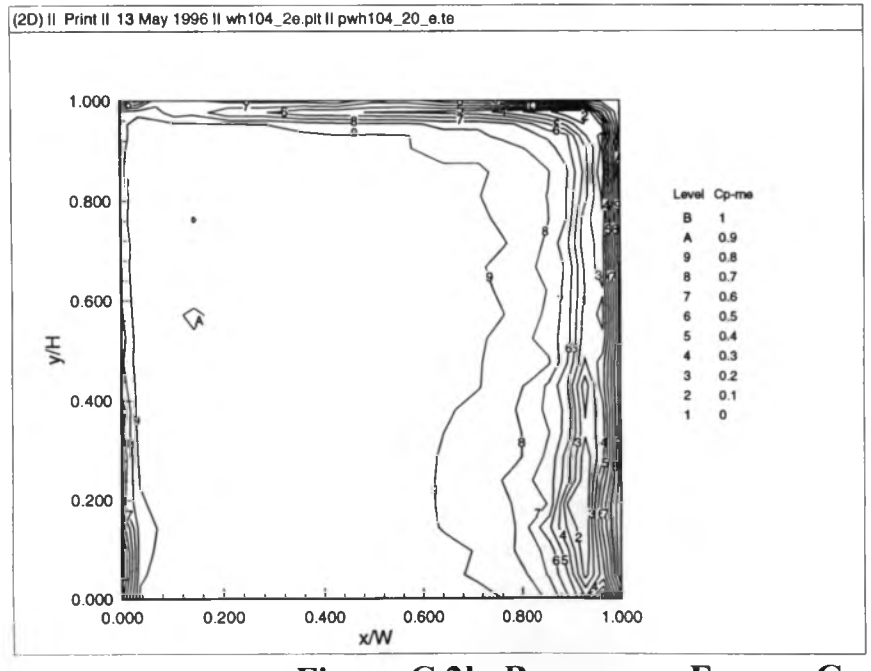

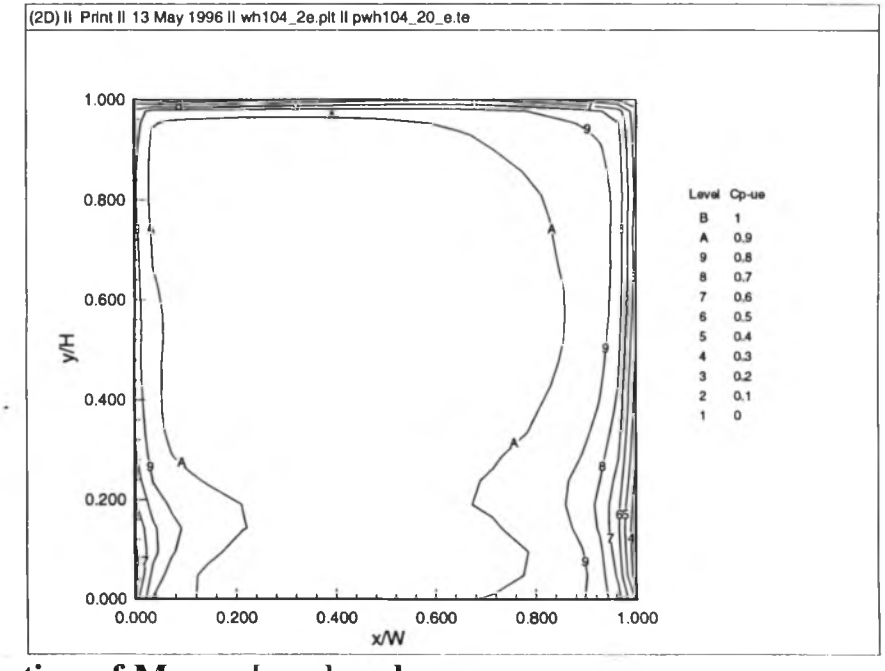

Figure C.2b. Pressures - Energy Contribution of Means [-me] and Nodal Energy Ratios [-ue], filtered, (30 degrees, open country)

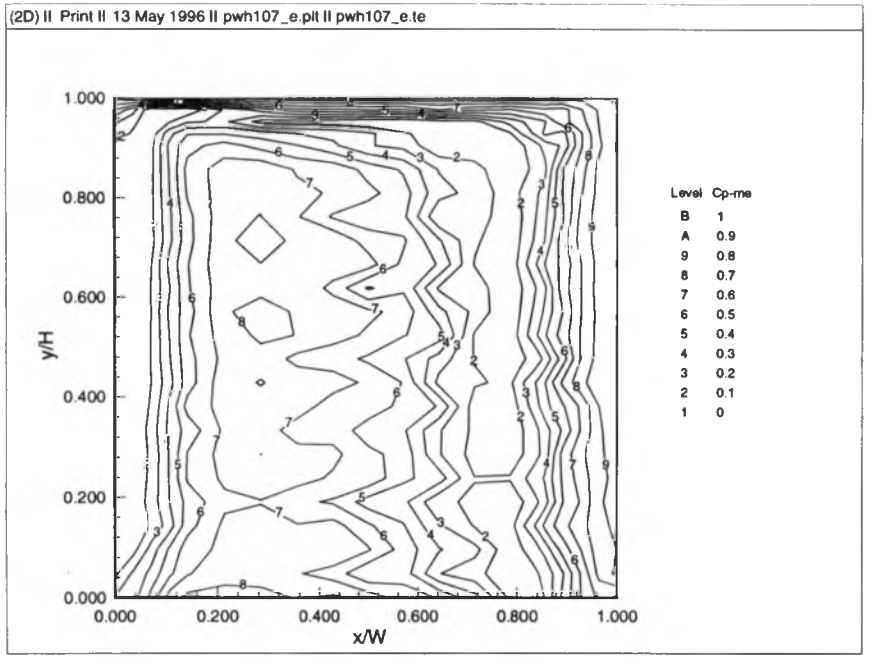

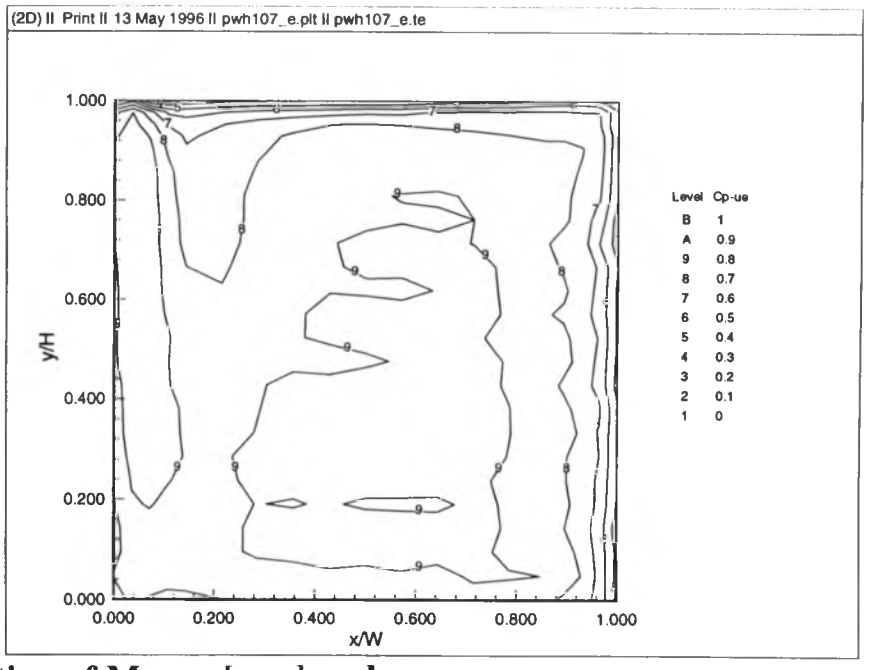

Figure C.3a. Pressures - Energy Contribution of Means [-me] and Nodal Energy Ratios [-ue], unfiltered, (60 degrees, open country)

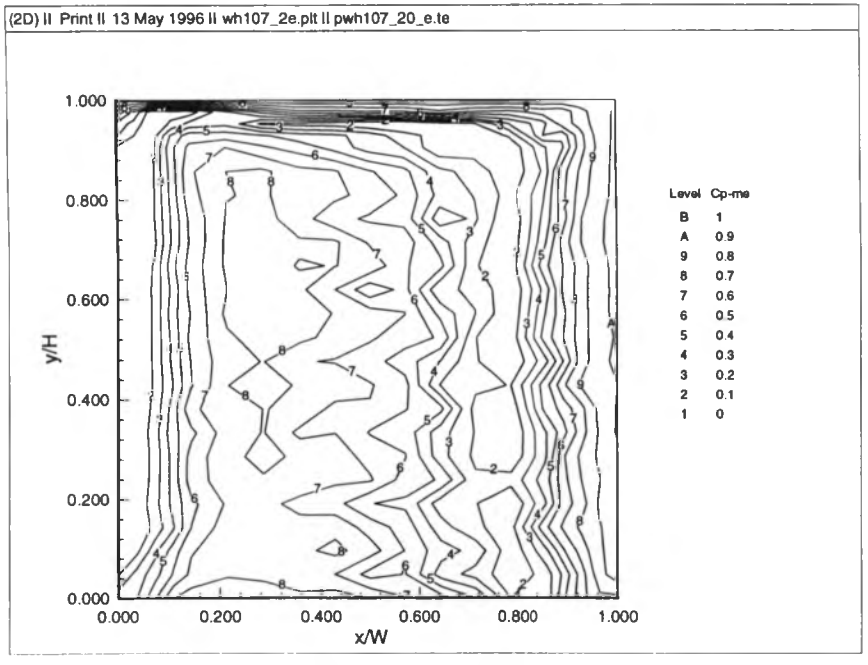

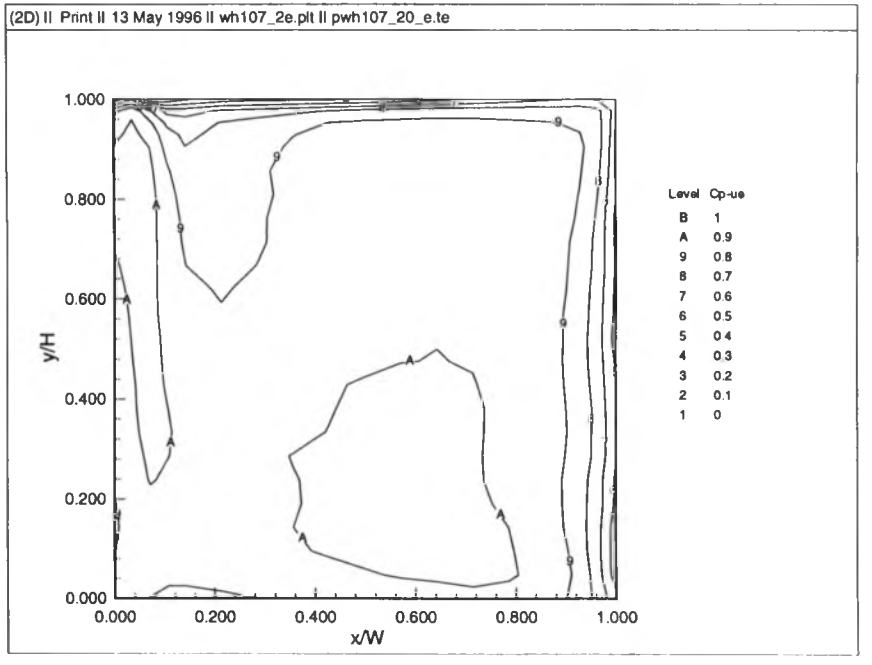

Figure C.3b. Pressures - Energy Contribution of Means [-me] and Nodal Energy Ratios [-ue], filtered, (60 degrees, open country)

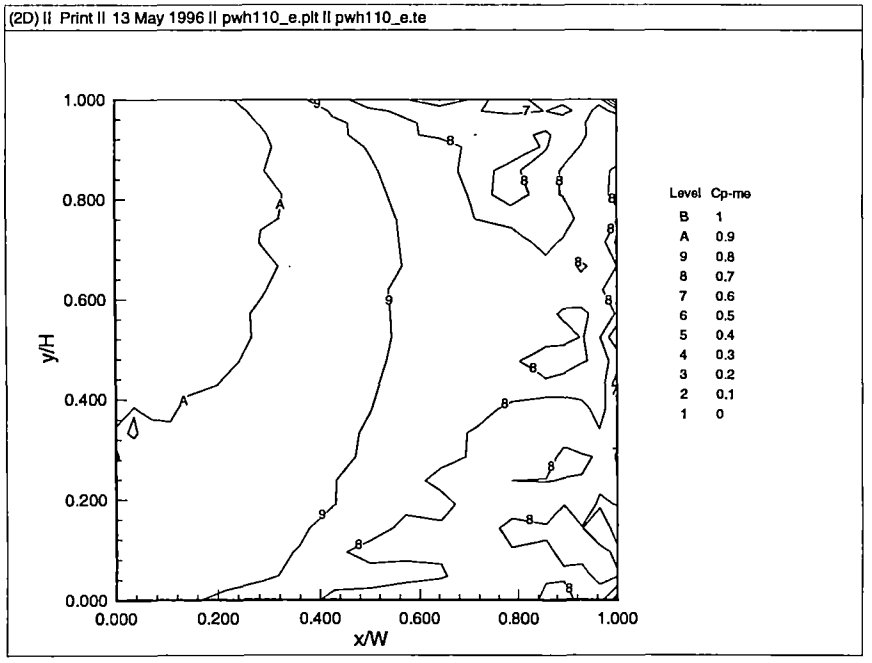

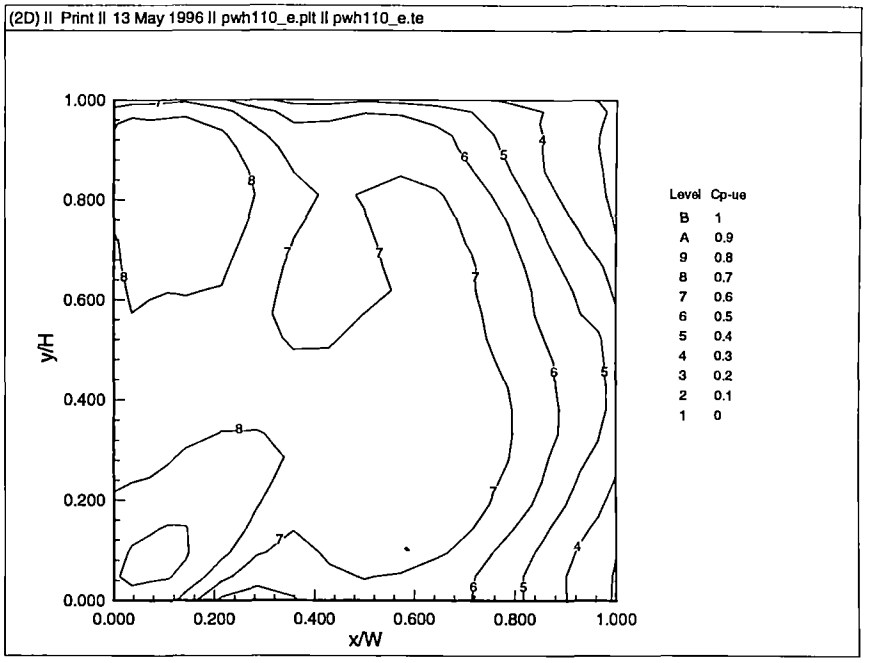

Figure C.4a. Pressures - Energy Contribution of Means [-me] and Nodal Energy Ratios [-ue], unfiltered, (90 degrees, open country)

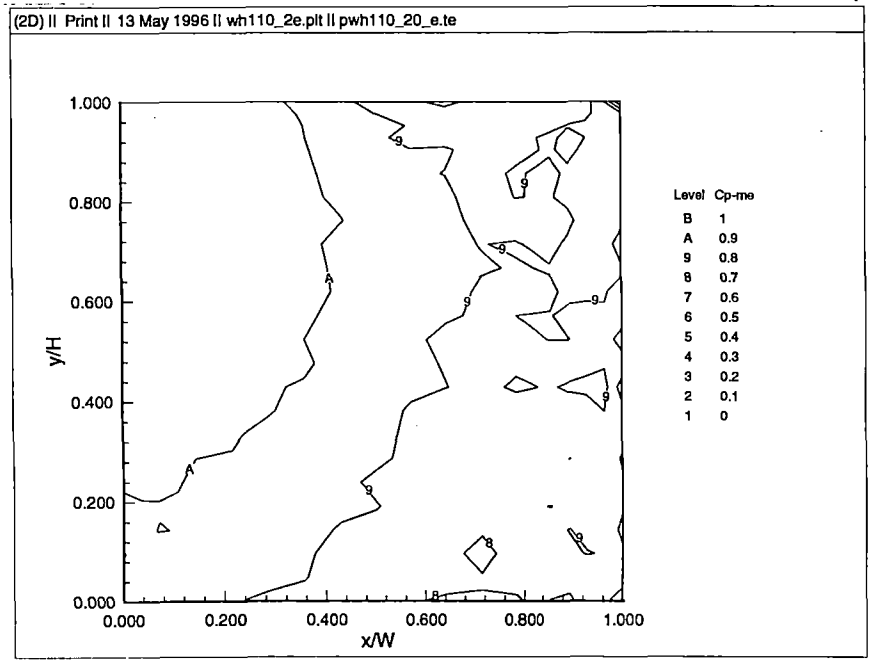

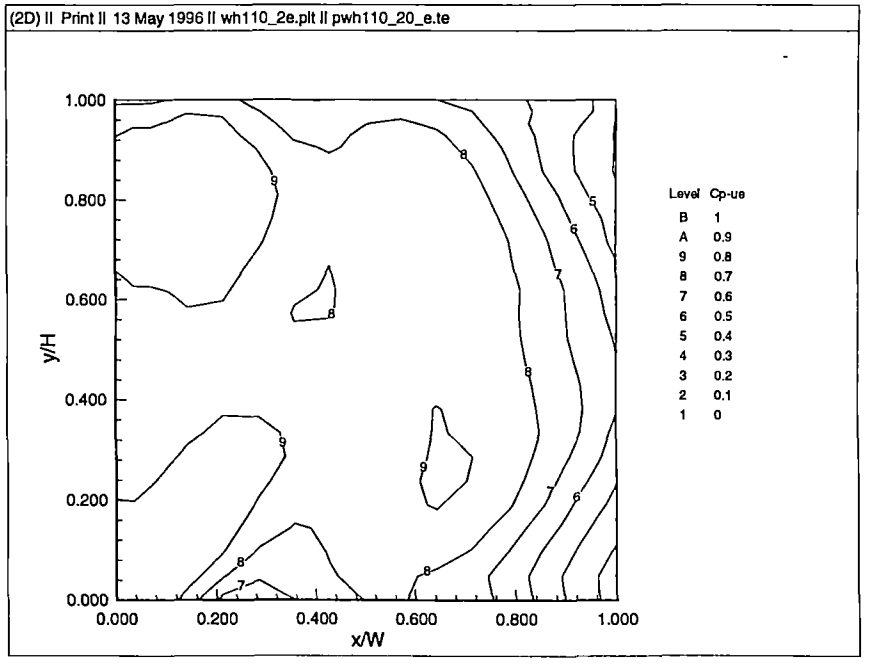

Figure C.4b. Pressures - Energy Contribution of Means [-me] and Nodal Energy Ratios [-ue], filtered, (90 degrees, open country)

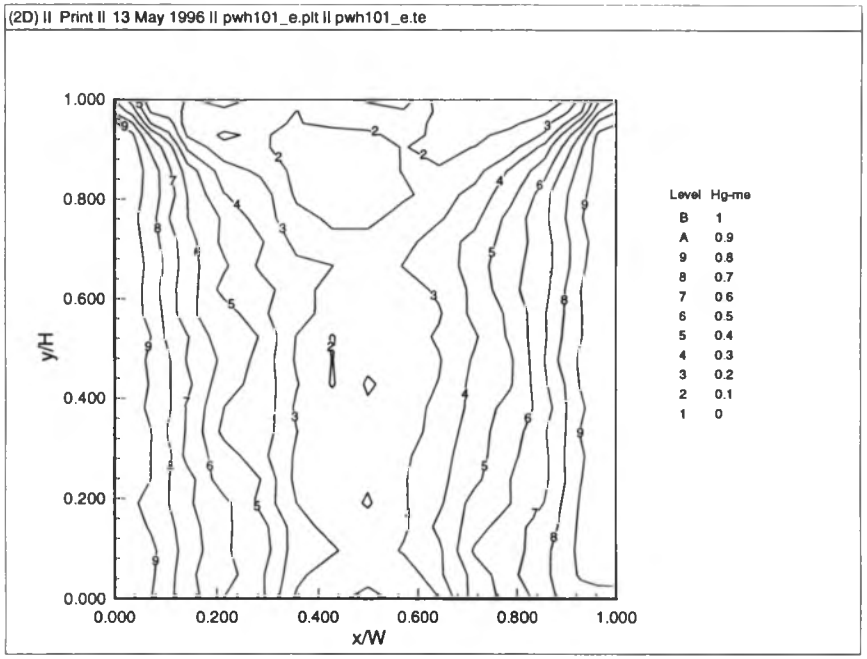

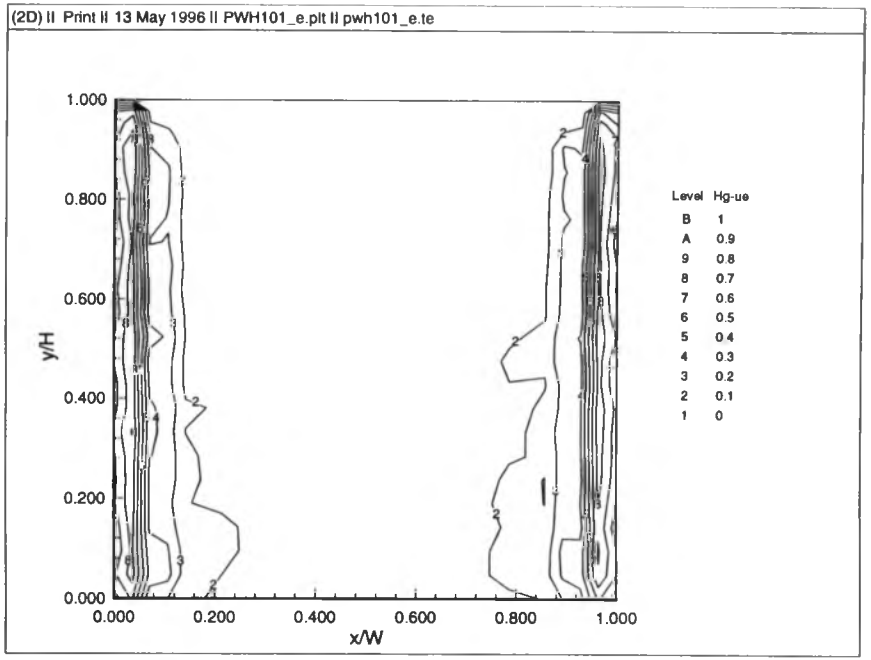

Figure C.5a. Horizontal Gradients - Energy Contribution of Means [-me] and Nodal Energy Ratios [-ue], unfiltered, (0 degrees, open country)

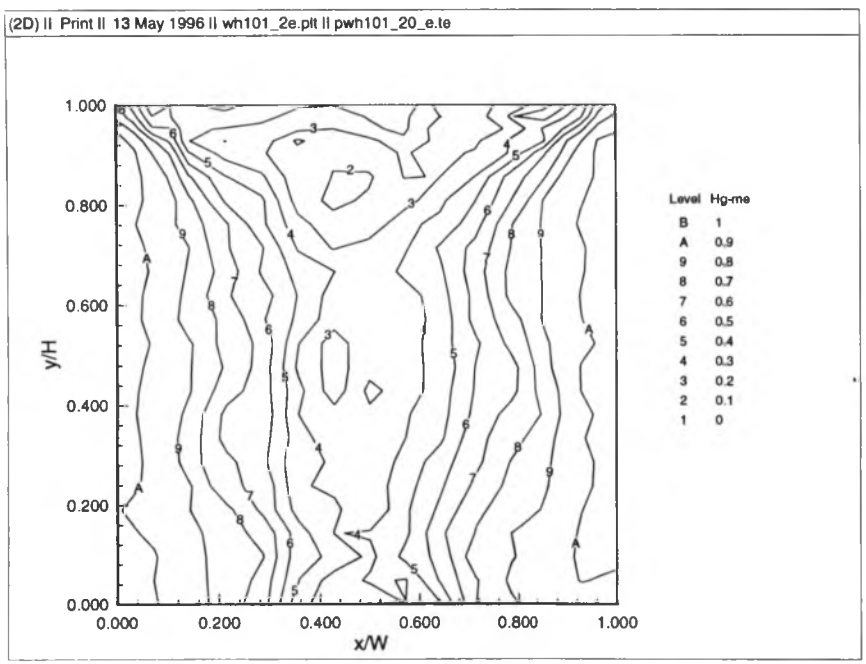

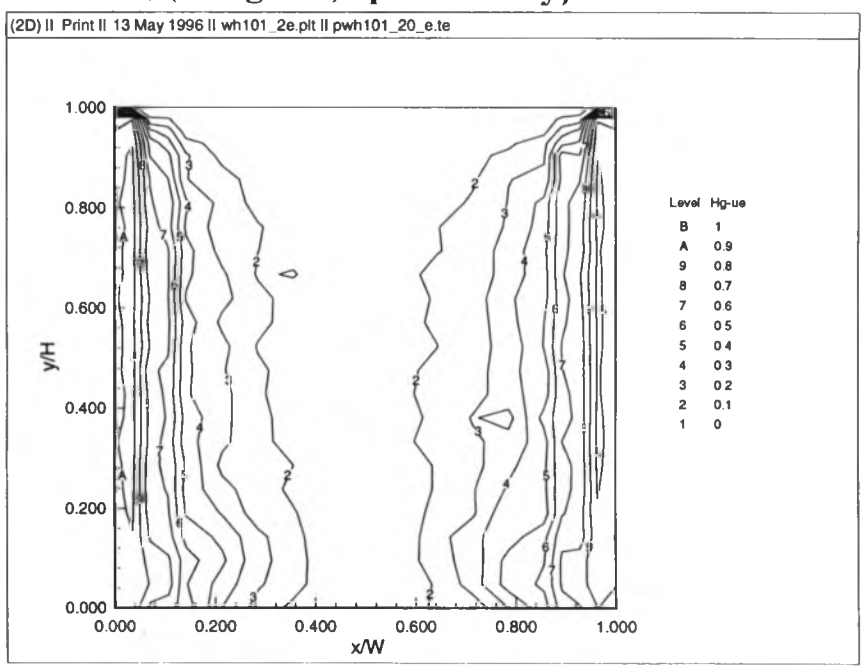

Figure C.5b. Horizontal Gradients - Energy Contribution of Means [-me] and Nodal Energy Ratios [-ue], filtered, (0 degrees, open country)

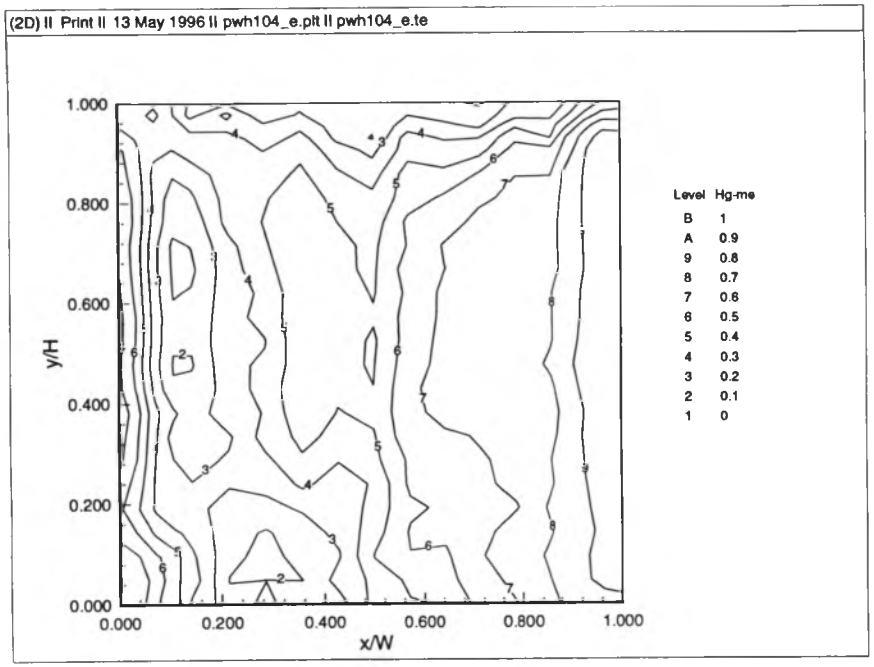

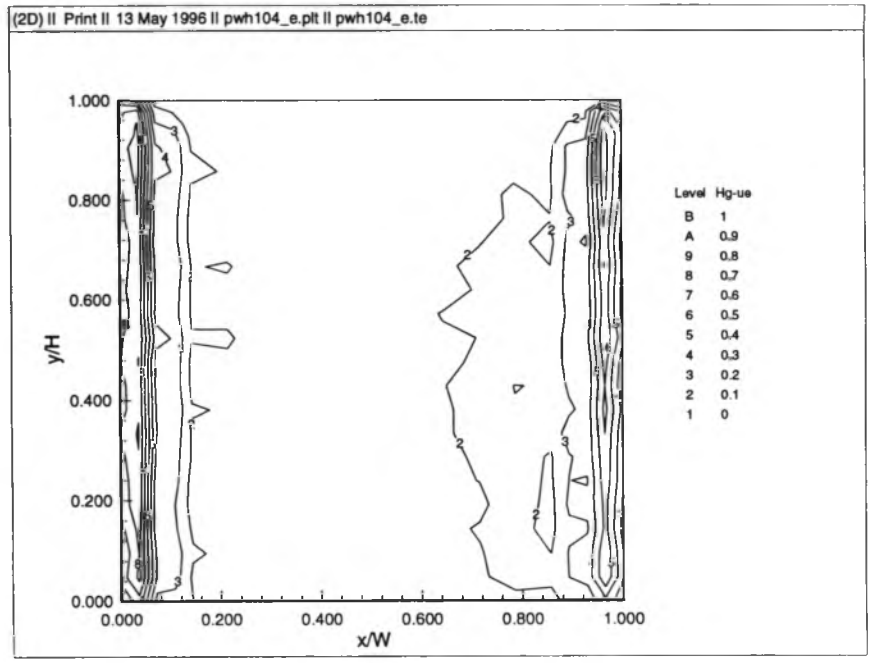

Figure C.6a. Horizontal Gradients - Energy Contribution of Means [-me] and Nodal Energy Ratios [-ue], unfiltered, (30 degrees, open country)

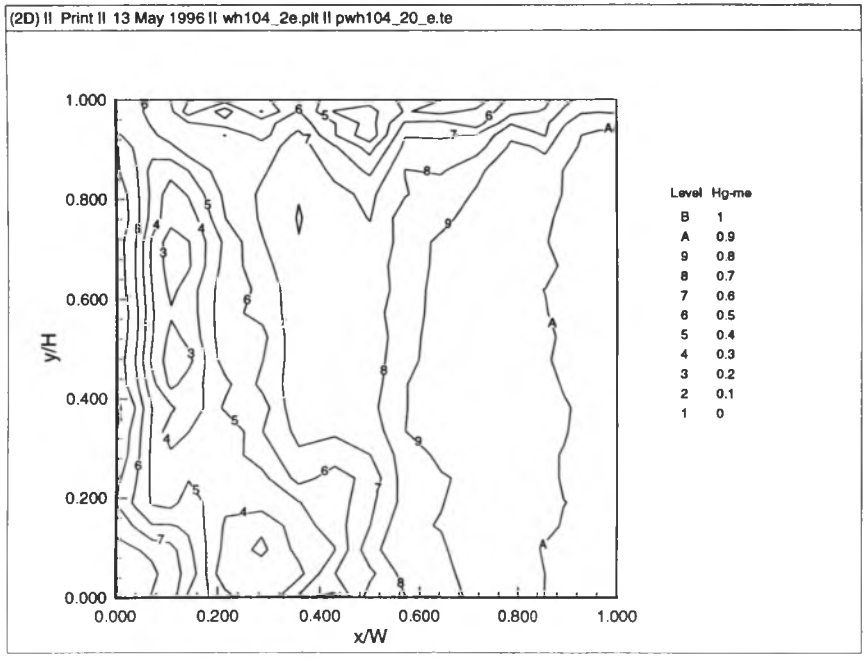

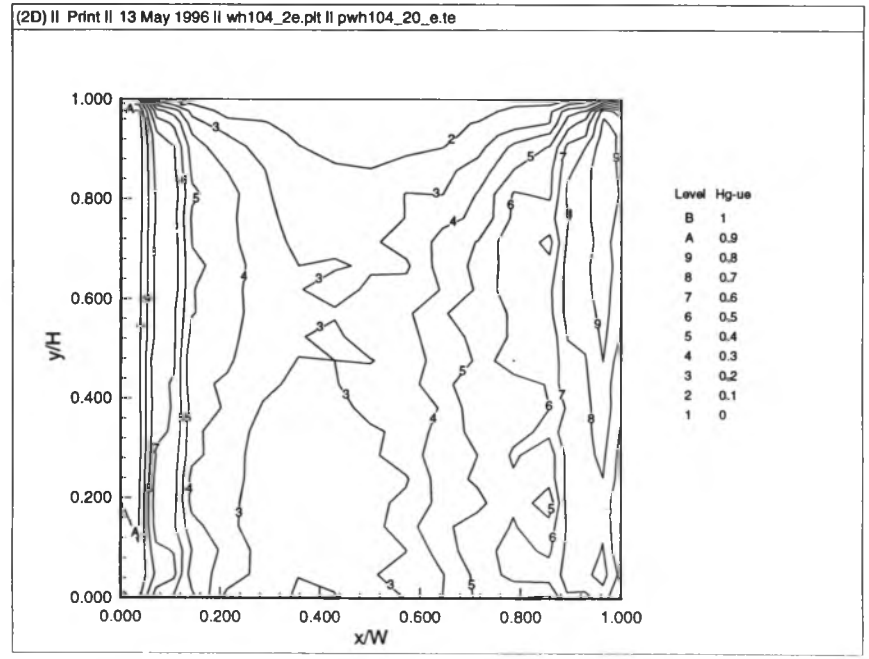

Figure C.6b. Horizontal Gradients - Energy Contribution of Means [-me] and Nodal Energy Ratios [-ue], filtered, (30 degrees, open country)

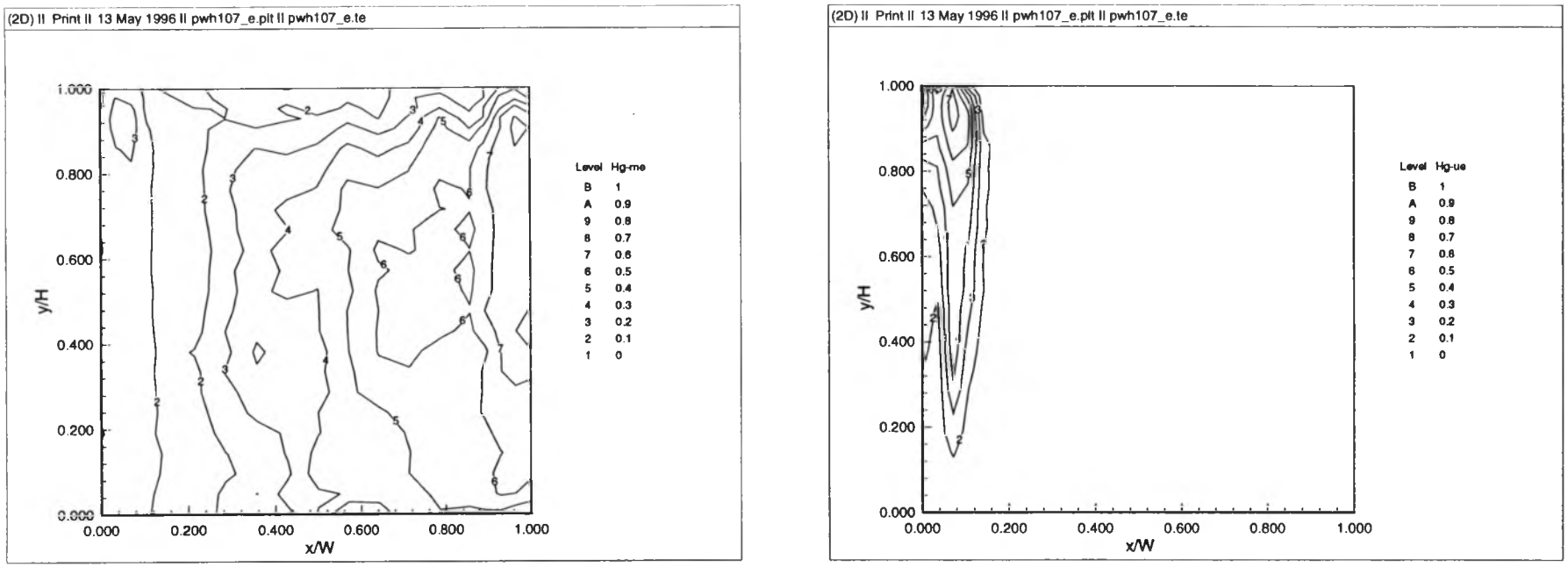

Figure C.7a. Horizontal Gradients - Energy Contribution of Means [-me] and Nodal Energy Ratios [-ue], unfiltered, (60 degrees, open country)

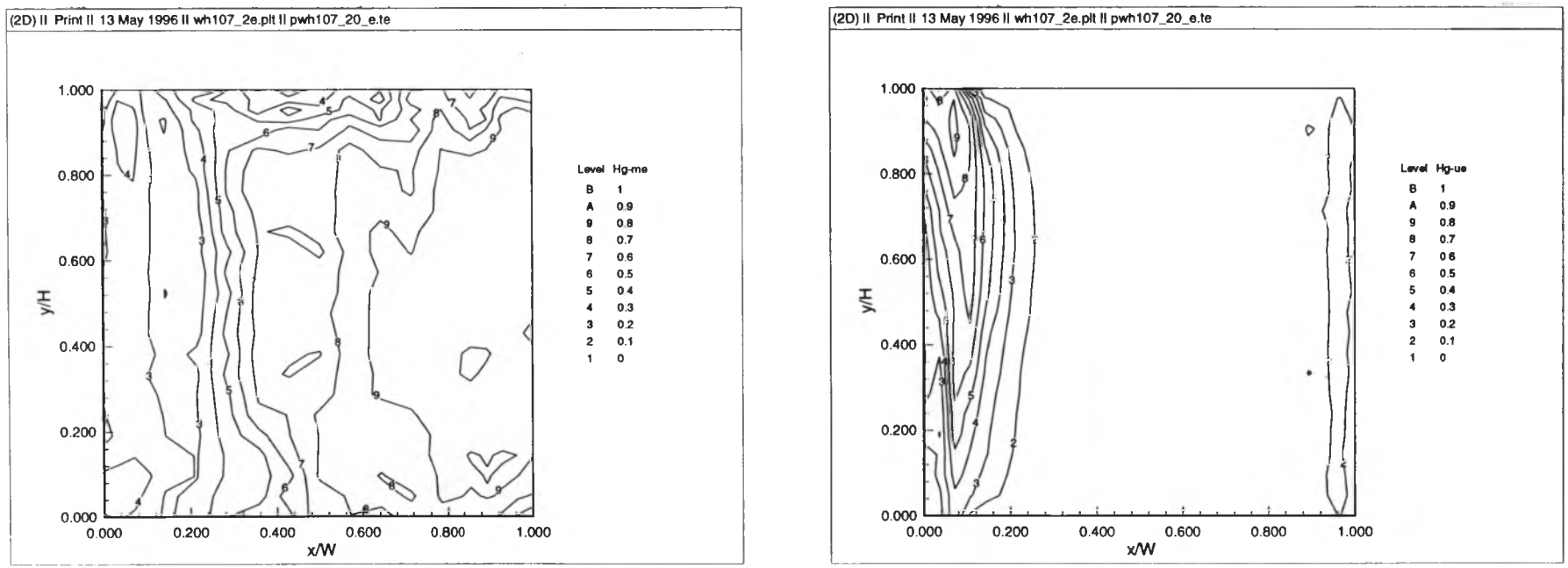

Figure C.7b. Horizontal Gradients - Energy Contribution of Means [-me] and Nodal Energy Ratios [-ue], filtered, (60 degrees, open country)

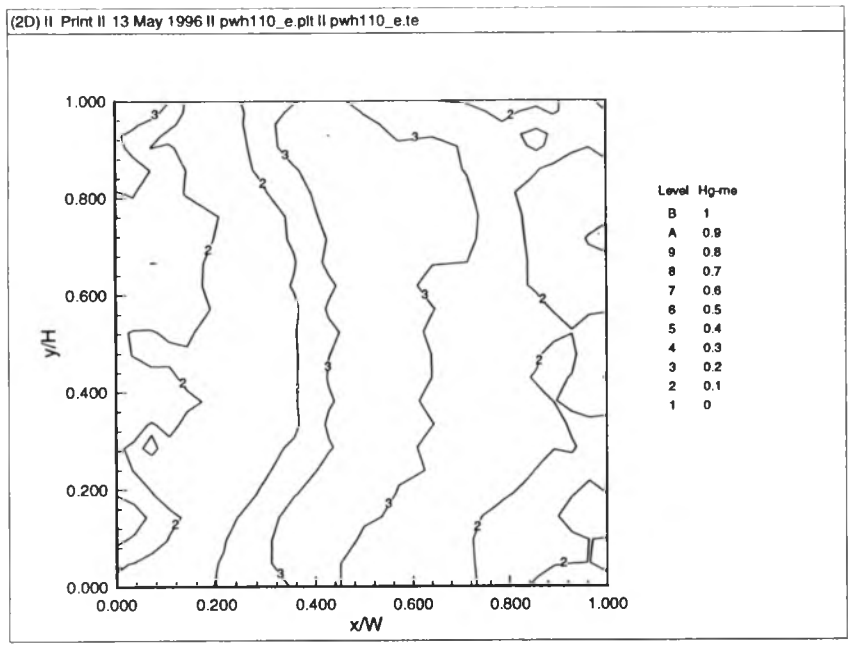

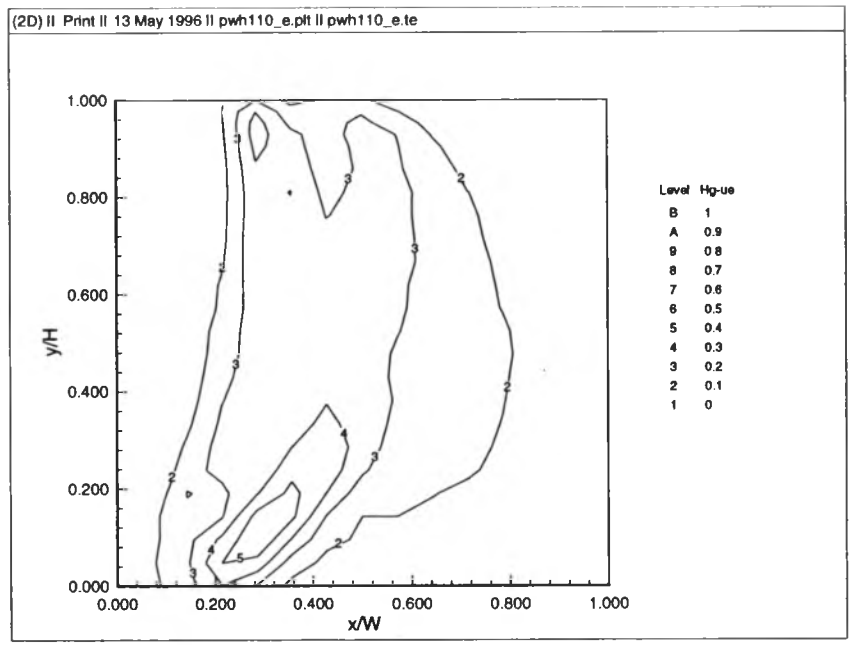

Figure C.8a. Horizontal Gradients - Energy Contribution of Means [-me] and Nodal Energy Ratios [-ue], unfiltered, (90 degrees, open country)

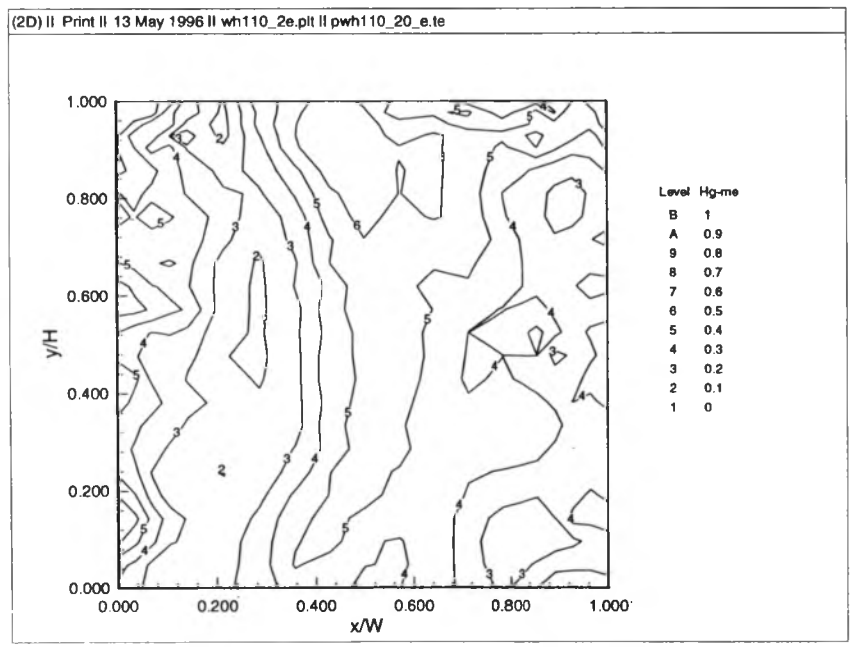

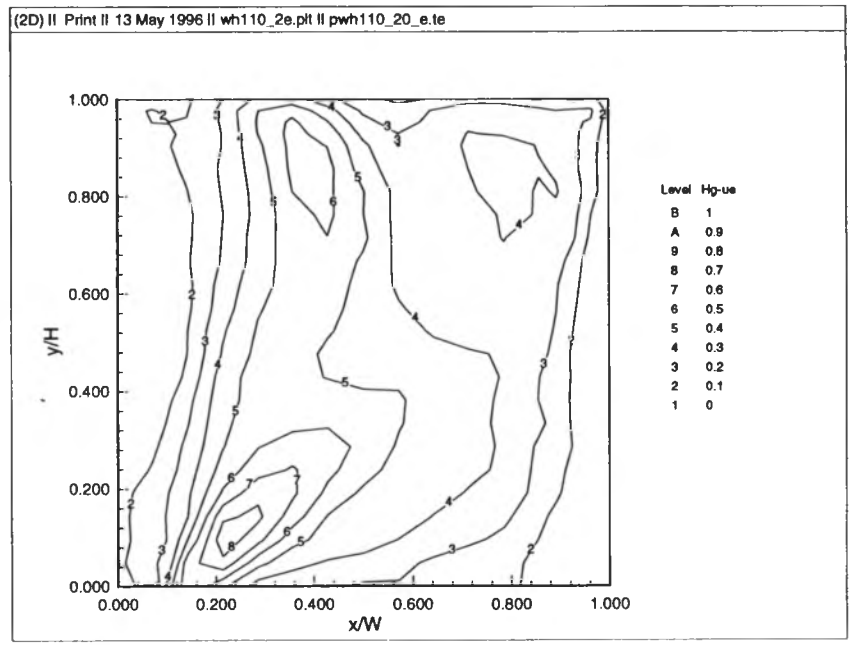

Figure C.8b. Horizontal Gradients - Energy Contribution of Means [-me] and Nodal Energy Ratios [-ue], filtered, (90 degrees, open country)

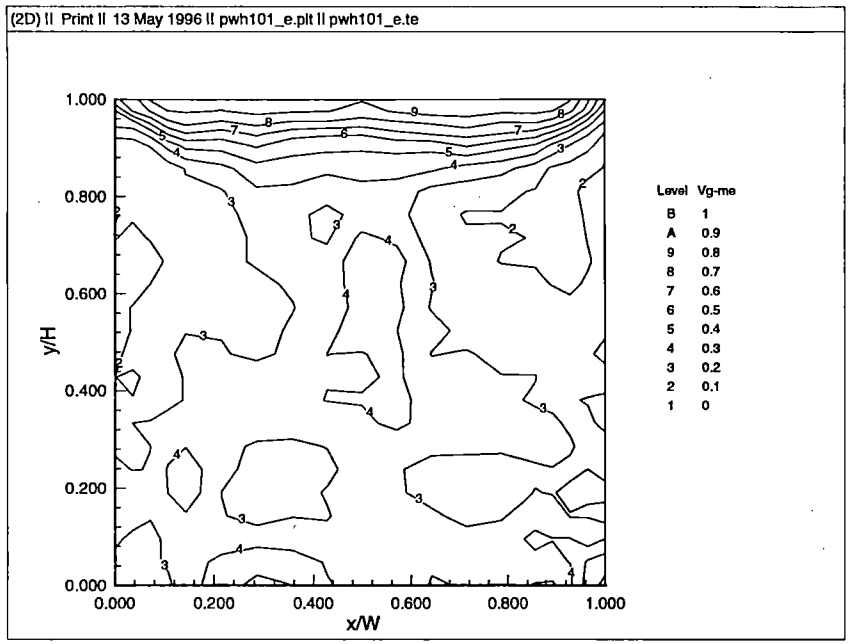

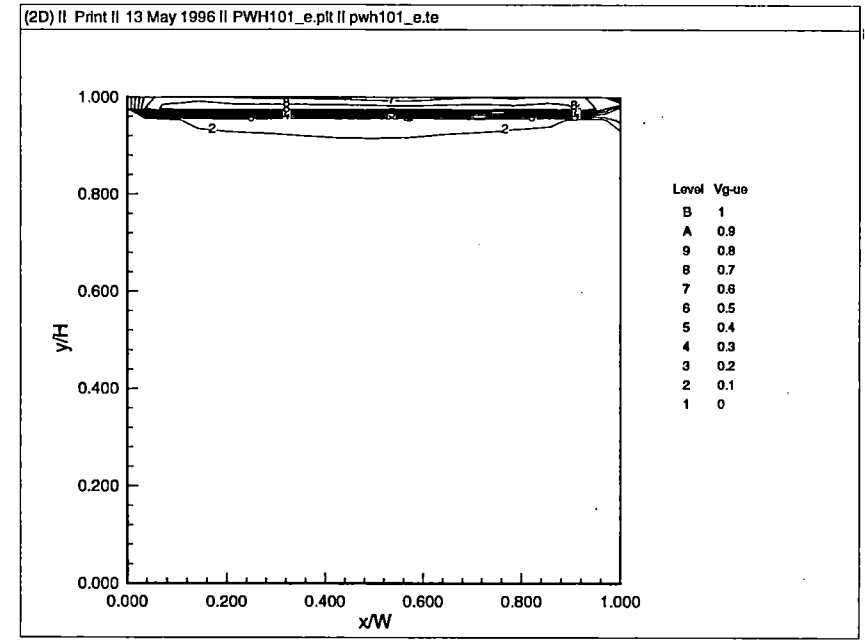

Figure C.9a. Vertical Gradients - Energy Contribution of Means [-me] and Nodal Energy Ratios [-ue], unfiltered, (0 degrees, open country)

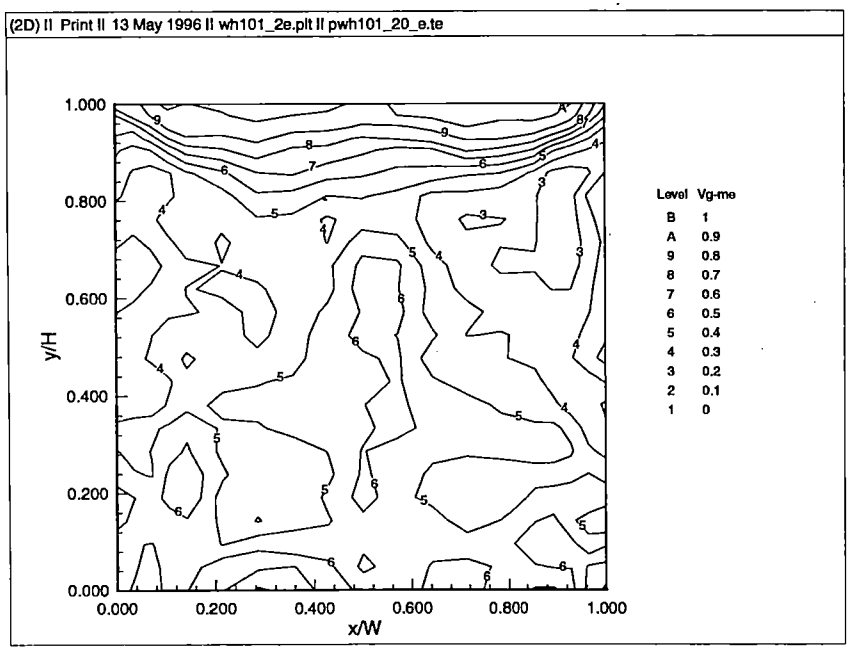

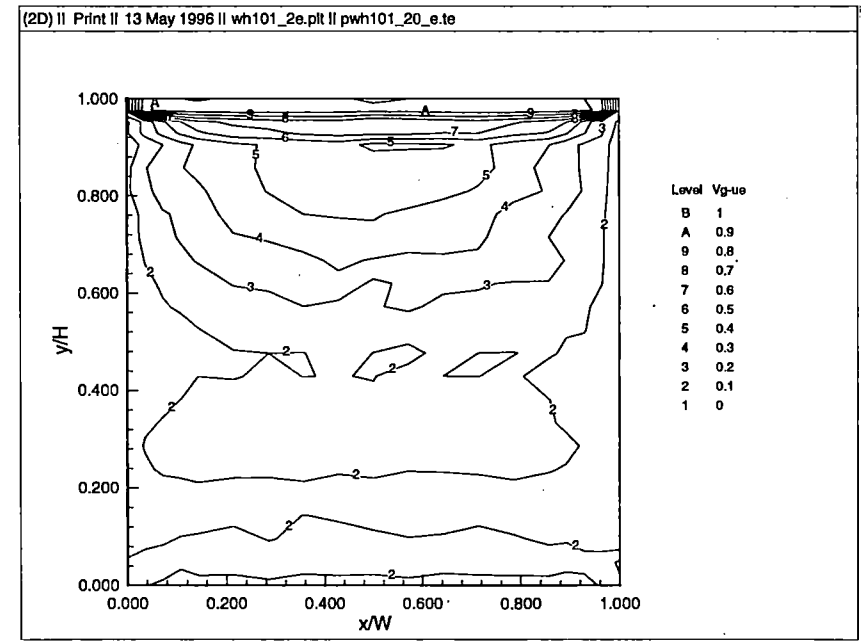

Figure C.9b. Vertical Gradients - Energy Contribution of Means [-me] and Nodal Energy Ratios [-ue], filtered, (0 degrees, open country)

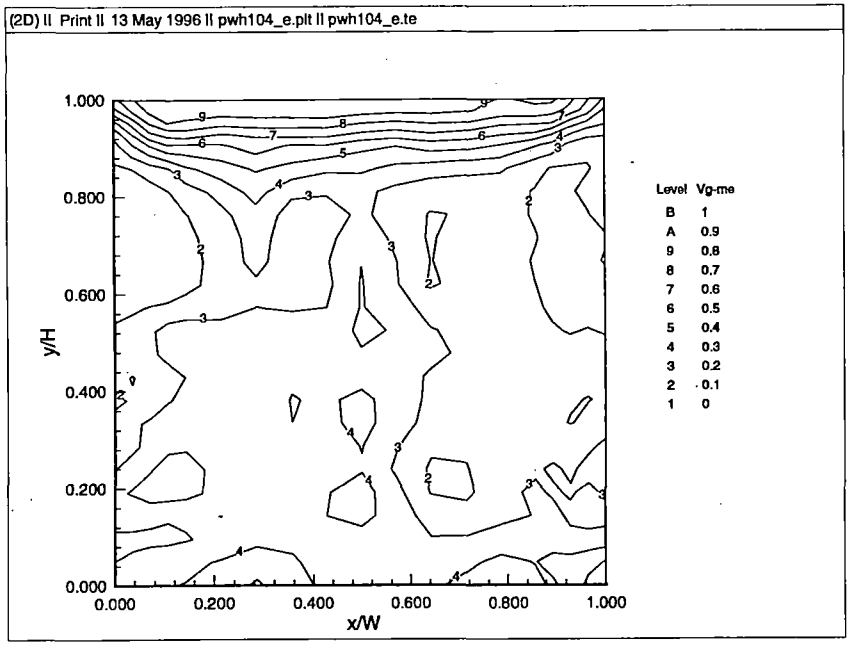

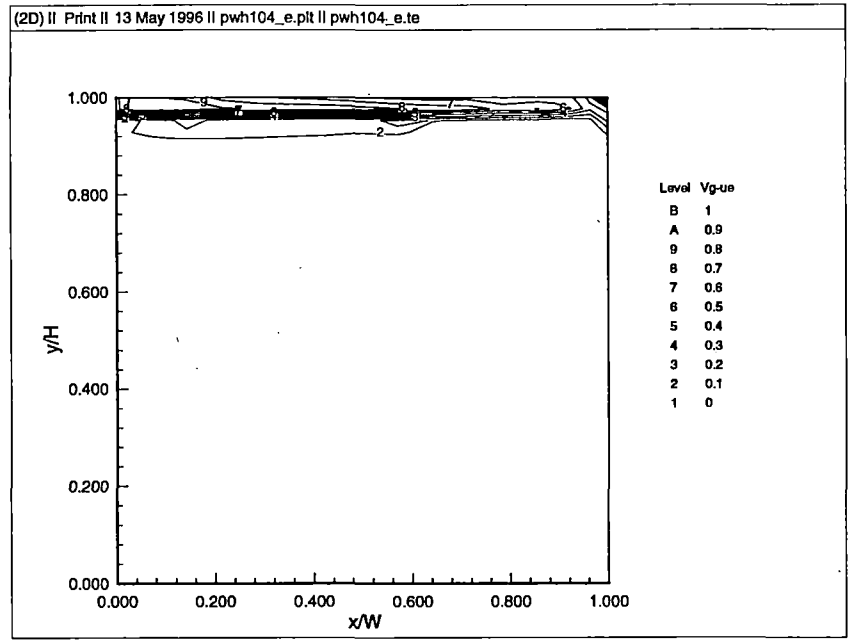

Figure C.10a. Vertical Gradients - Energy Contribution of Means [-me] and Nodal Energy Ratios [-ue], unfiltered, (30 degrees, open country)

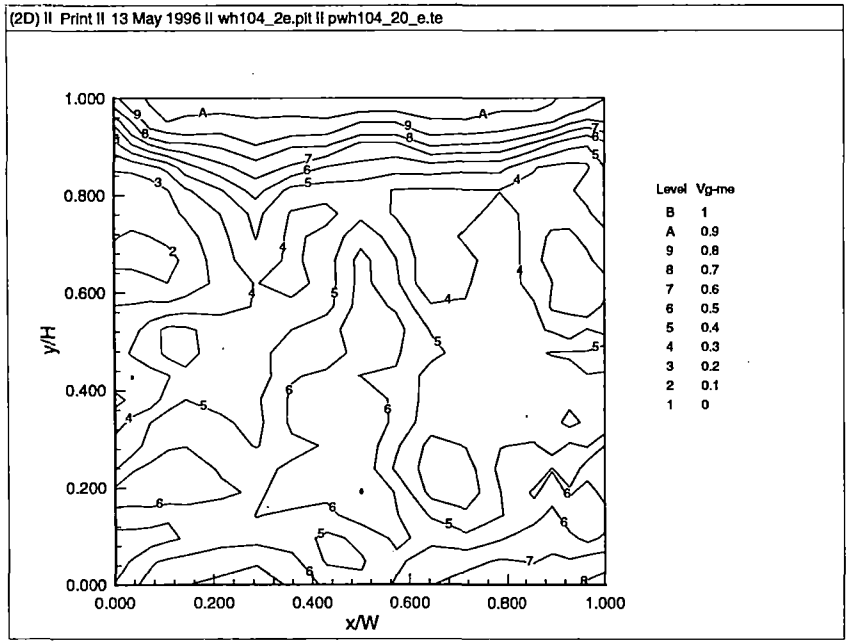

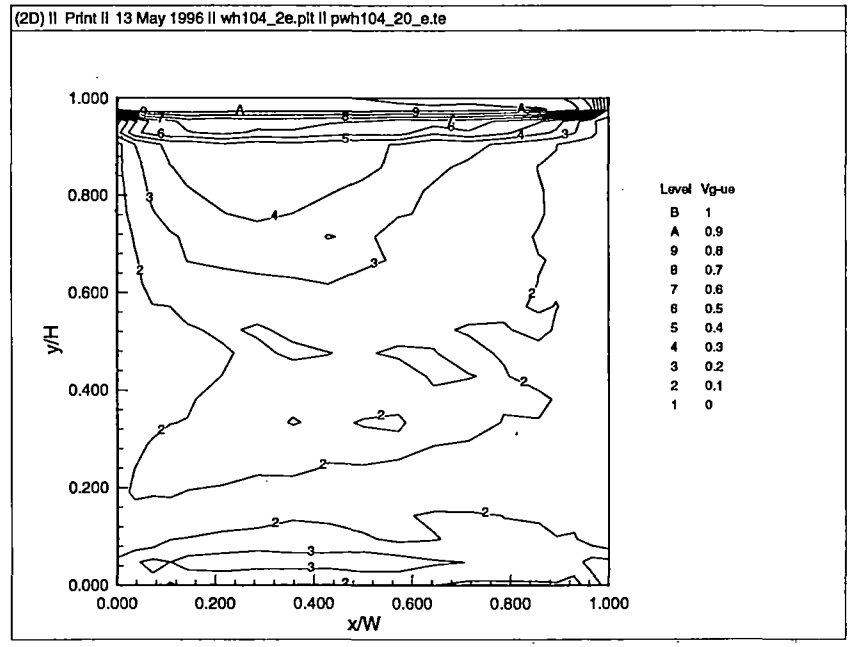

Figure C.10b. Vertical Gradients - Energy Contribution of Means [-me] and Nodal Energy Ratios [-ue], filtered, (30 degrees, open country)

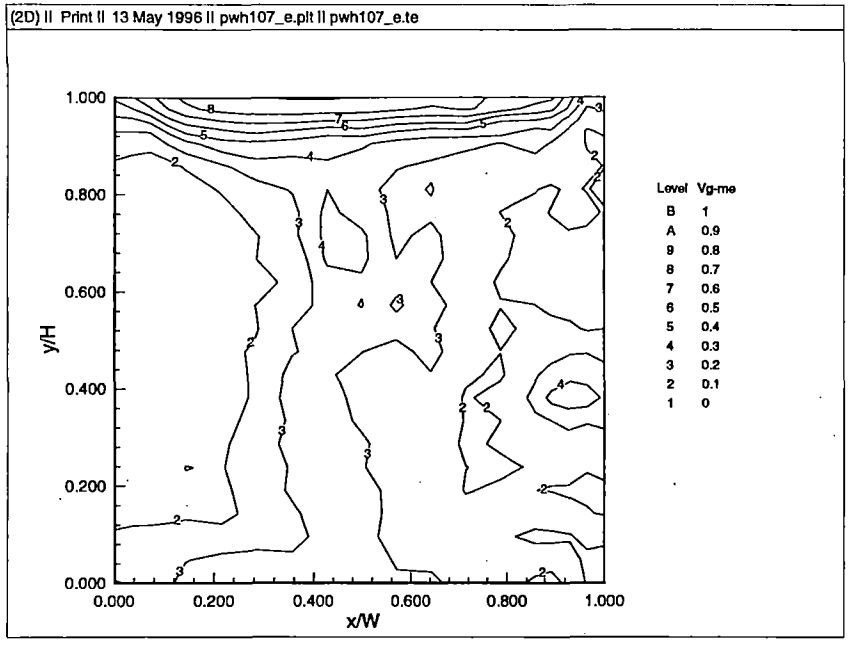

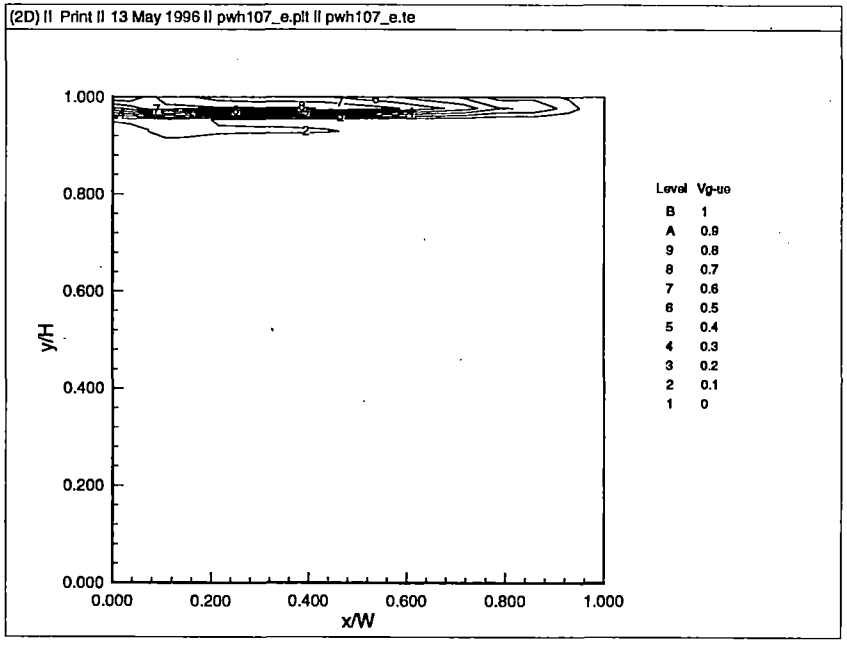

Figure C.11a. Vertical Gradients - Energy Contribution of Means [-me] and Nodal Energy Ratios [-ue], unfiltered, (60 degrees, open country)

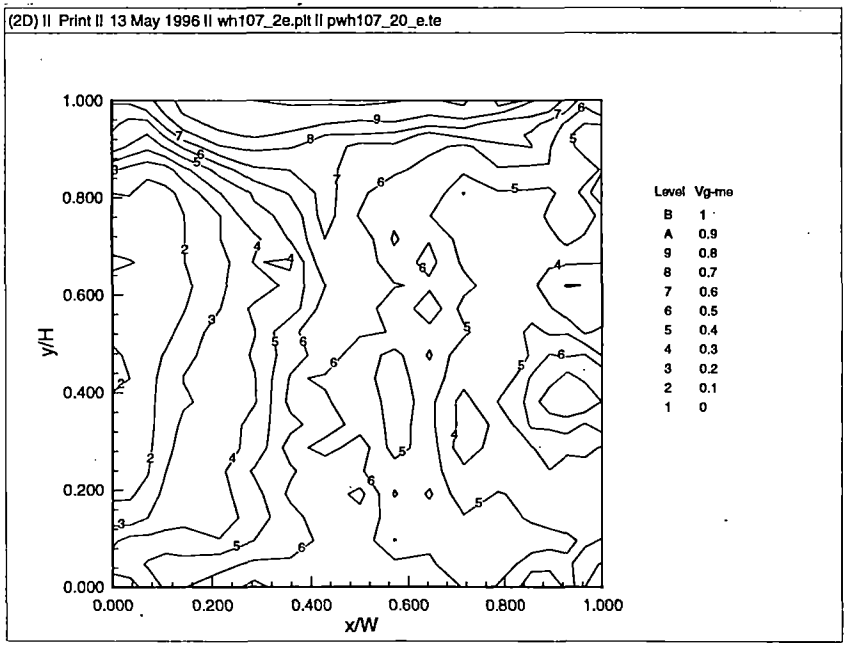

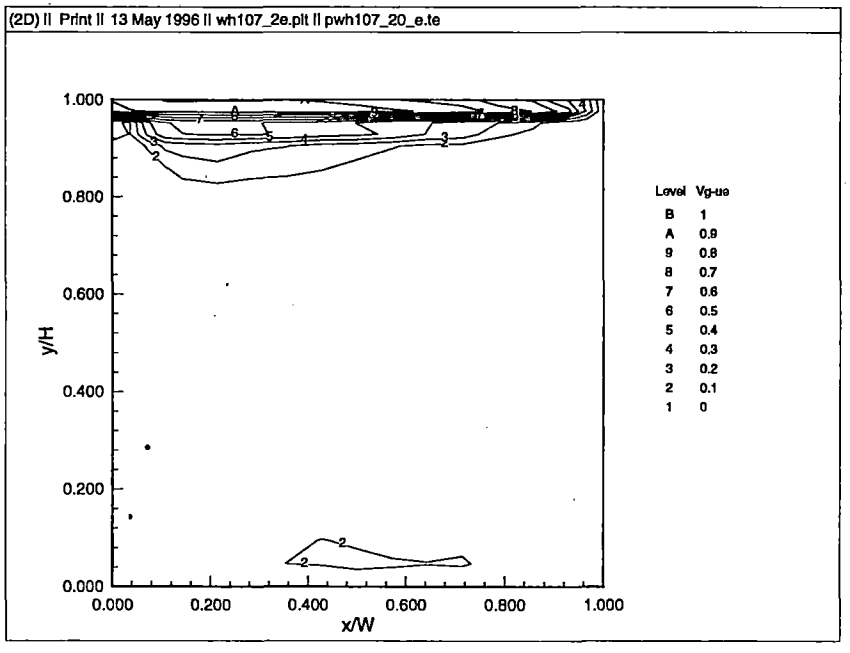

Figure C.11b. Vertical Gradients - Energy Contribution of Means [-me] and Nodal Energy Ratios [-ue], filtered, (60 degrees, open country)

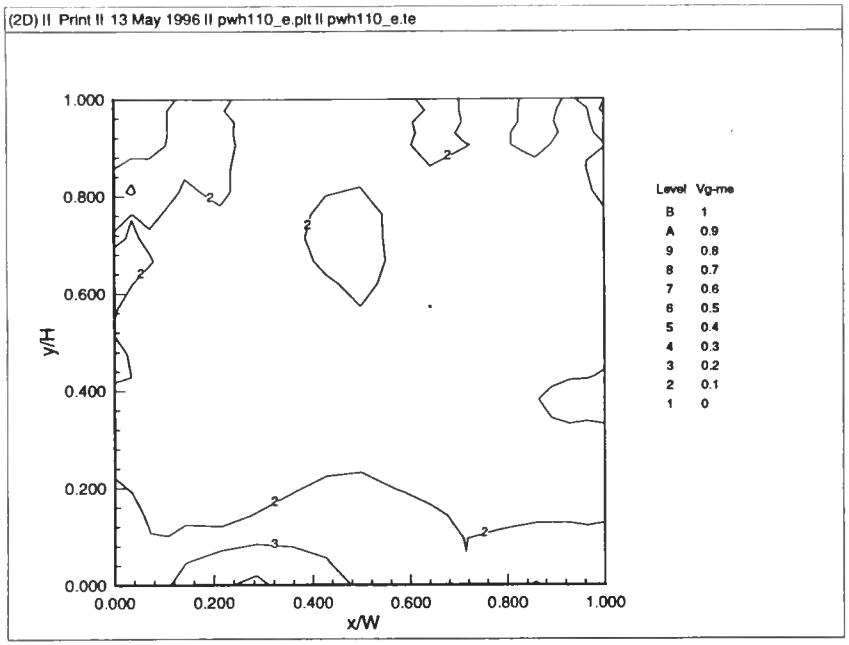

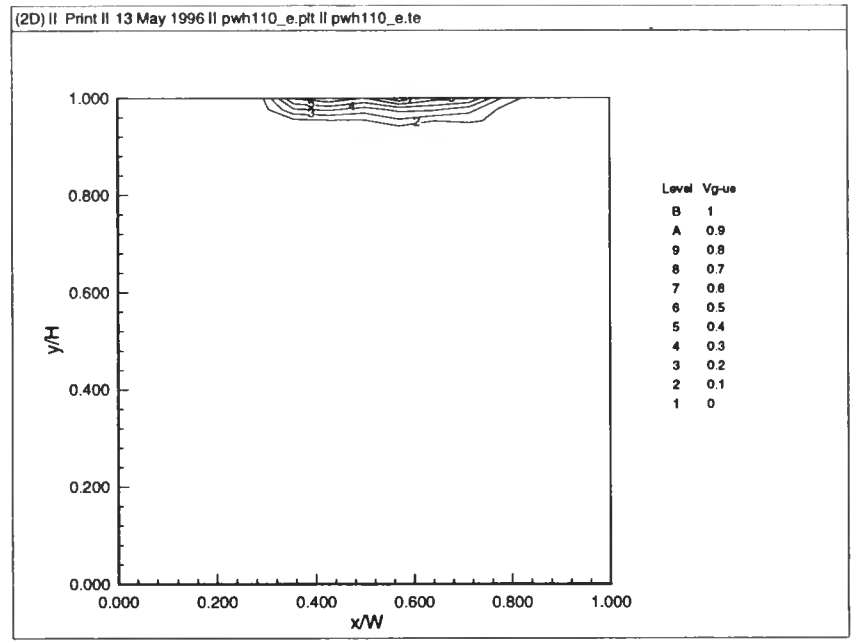

Figure C.12a. Vertical Gradients - Energy Contribution of Means [-me] and Nodal Energy Ratios [-ue], unfiltered, (90 degrees, open country)

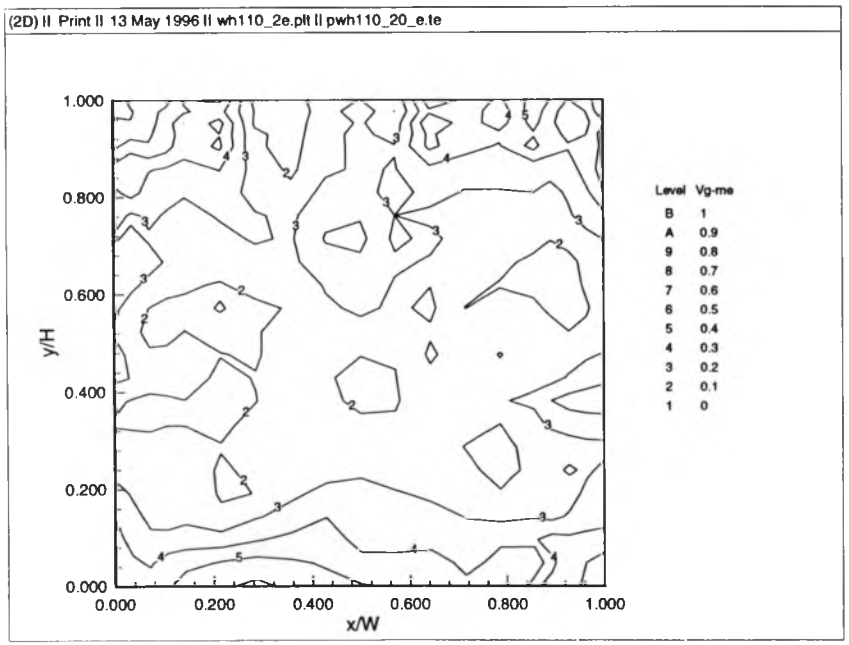

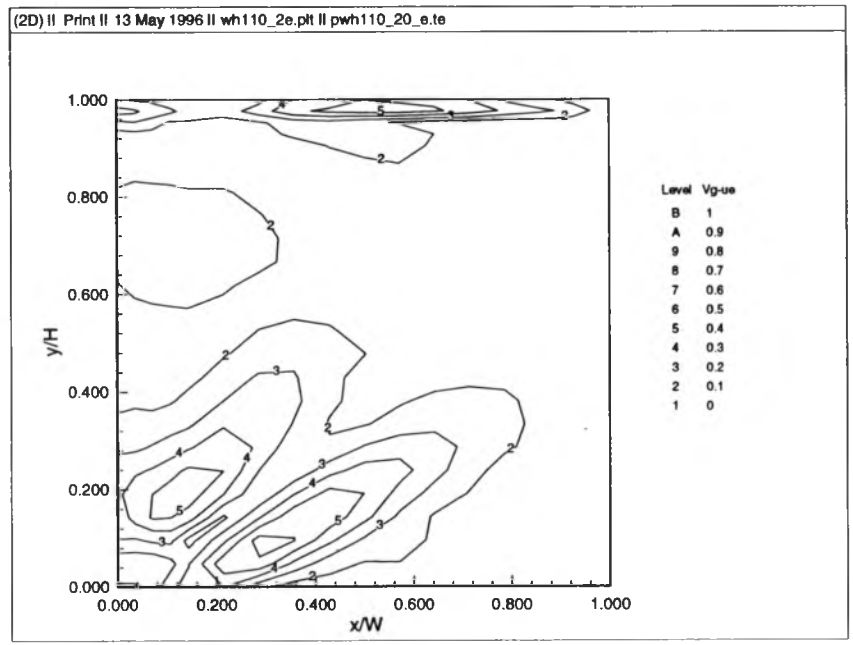

Figure C.12b. Vertical Gradients - Energy Contribution of Means [-me] and Nodal Energy Ratios [-ue], filtered, (90 degrees, open country)

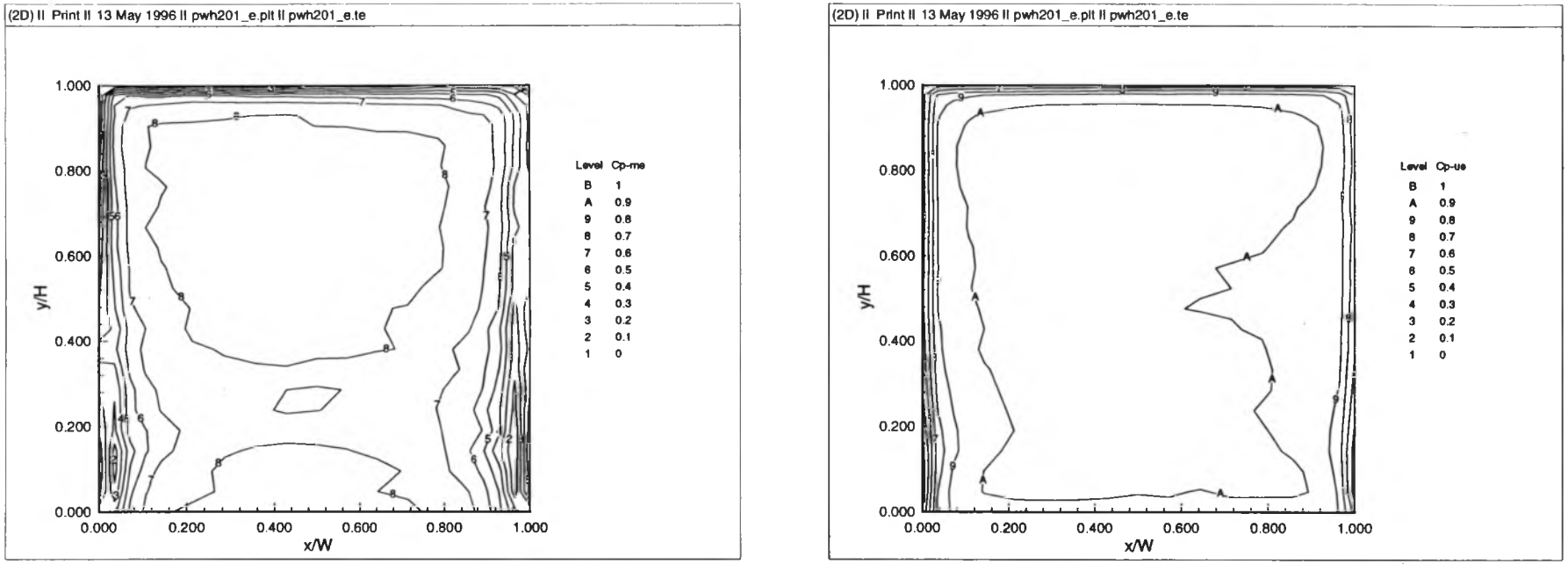

Figure C.13a. Pressures - Energy Contribution of Means [-me] and Nodal Energy Ratios [-ue], unfiltered, (0 degrees, suburban)

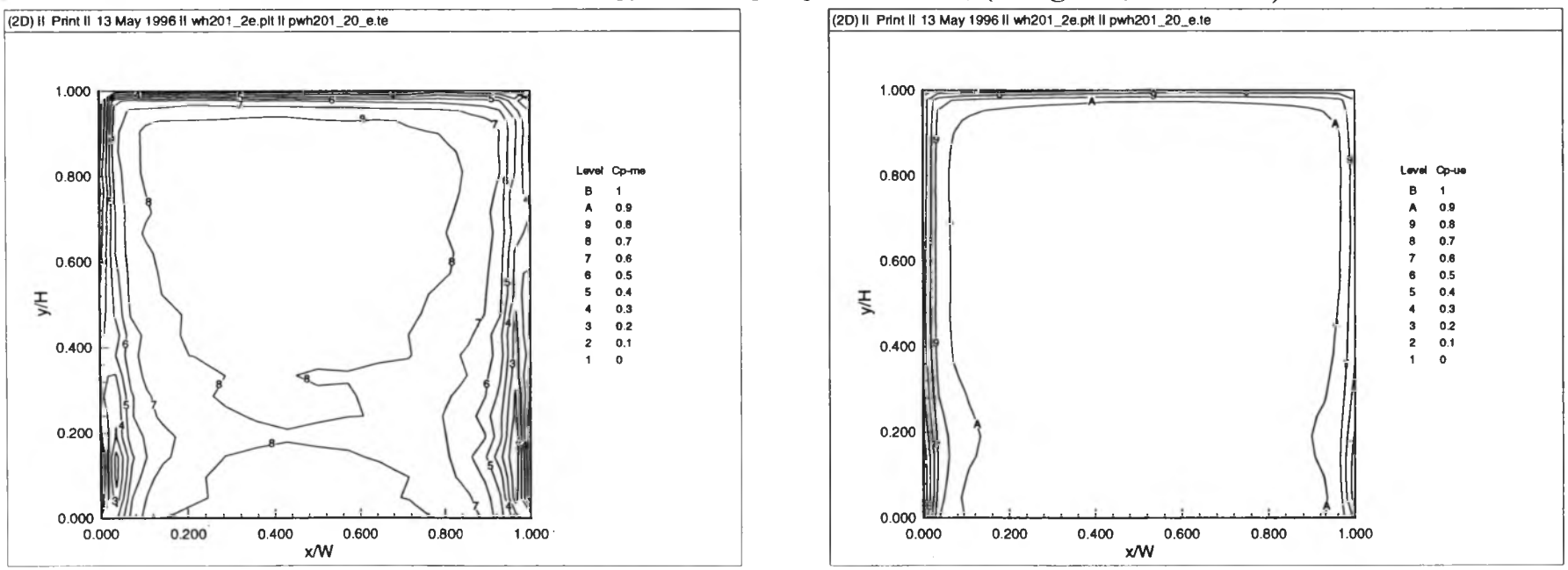

Figure C.13b. Pressures - Energy Contribution of Means [-me] and Nodal Energy Ratios [-ue], filtered, (0 degrees, suburban)

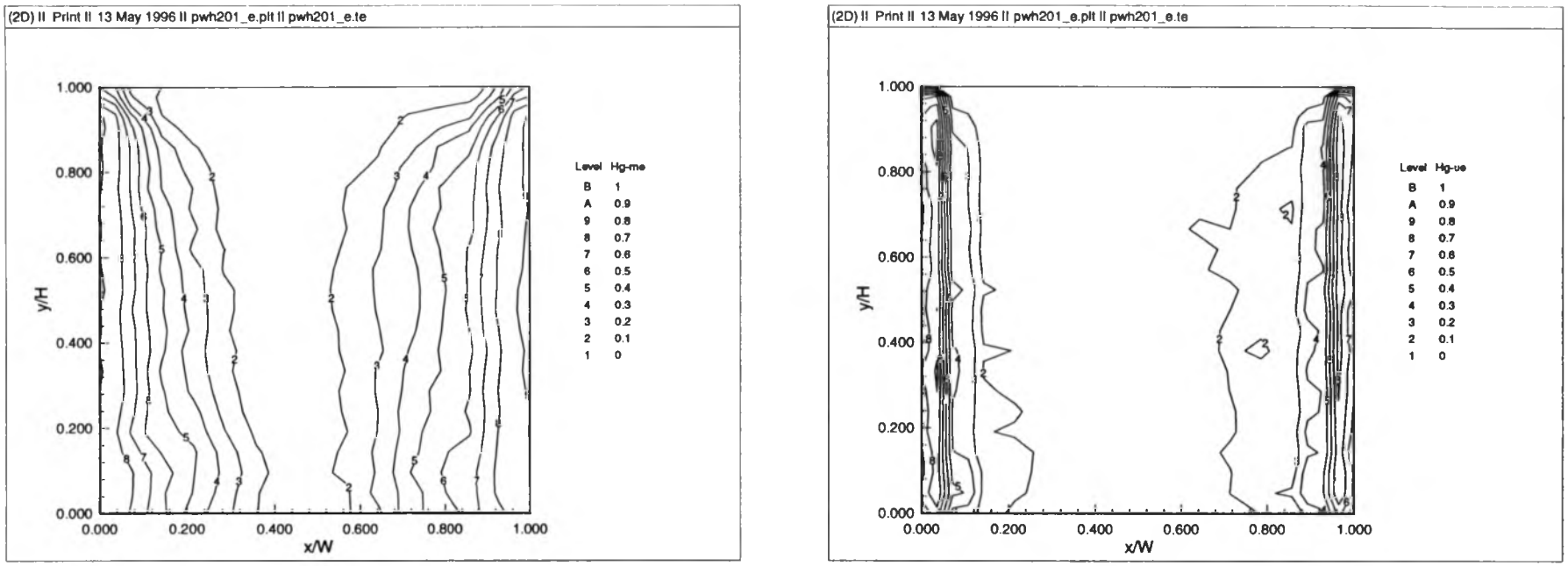

Figure C.14a. Horizontal Gradients - Energy Contribution of Means [-me] and Nodal Energy Ratios [-ue], unfiltered, (0 degrees, suburban)

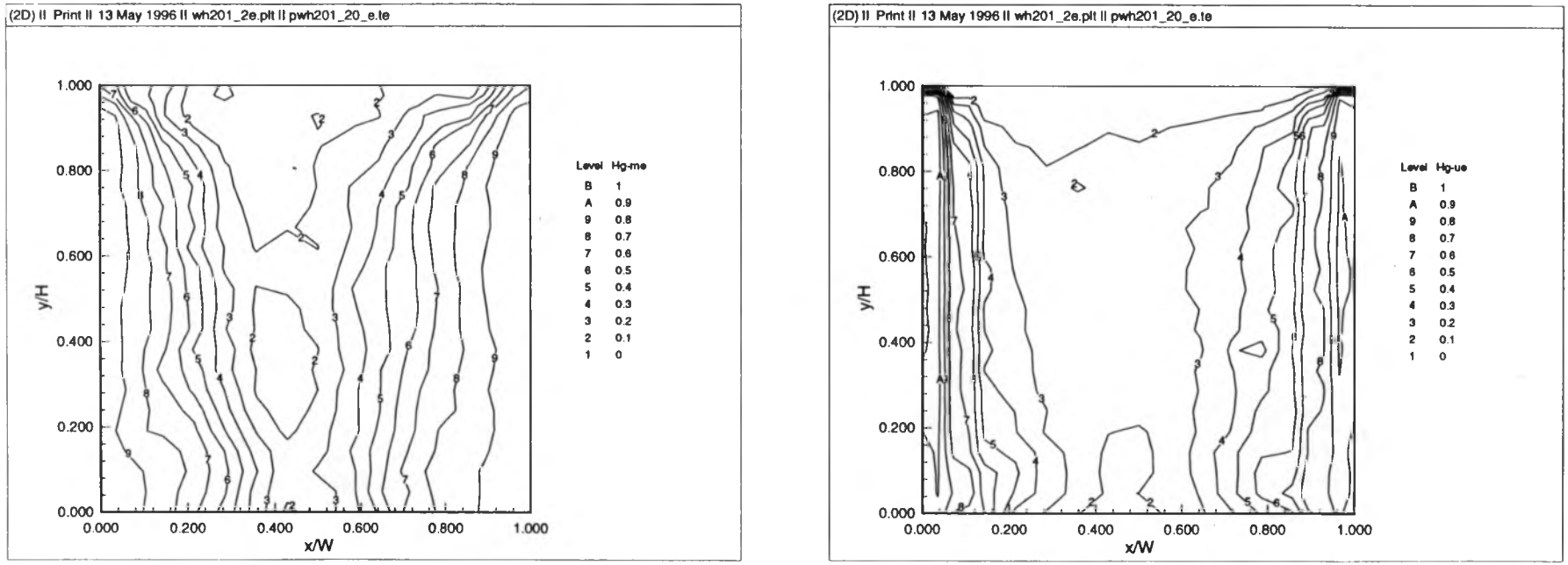

Figure C.14b. Horizontal Gradients - Energy Contribution of Means [-me] and Nodal Energy Ratios [-ue], filtered, (0 degrees, suburban)

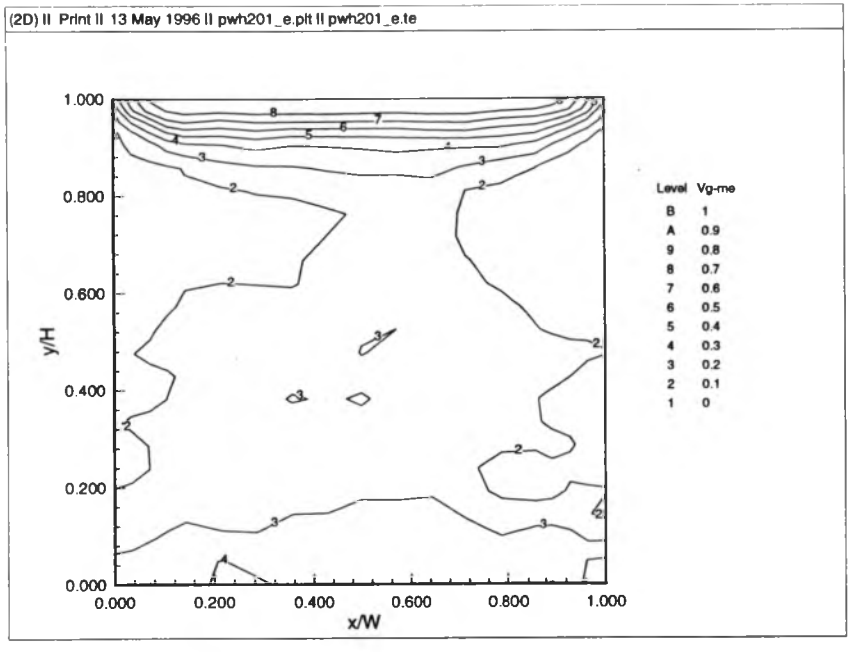

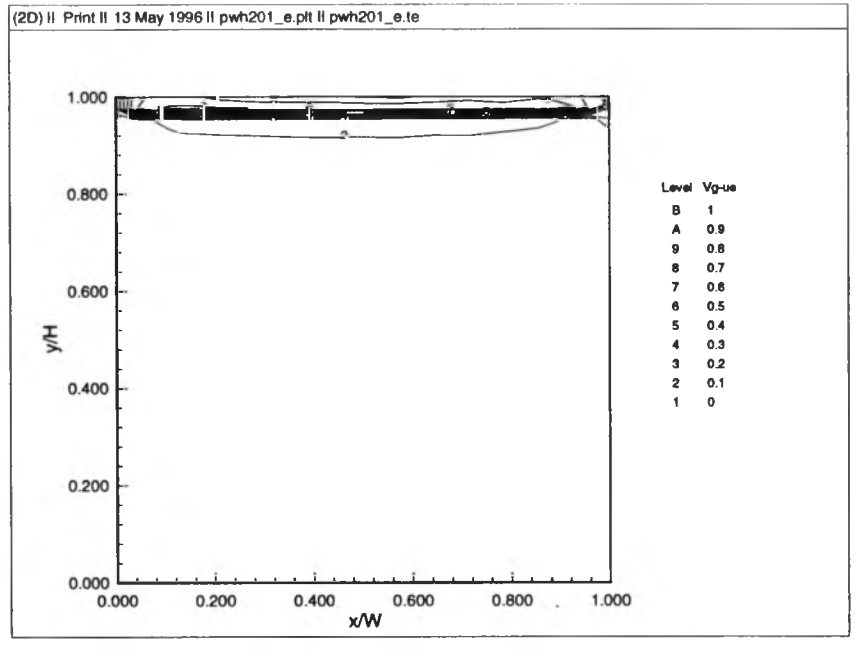

Figure C.15a. Vertical Gradients - Energy Contribution of Means [-me] and Nodal Energy Ratios [-ue], unfiltered, (0 degrees, suburban)

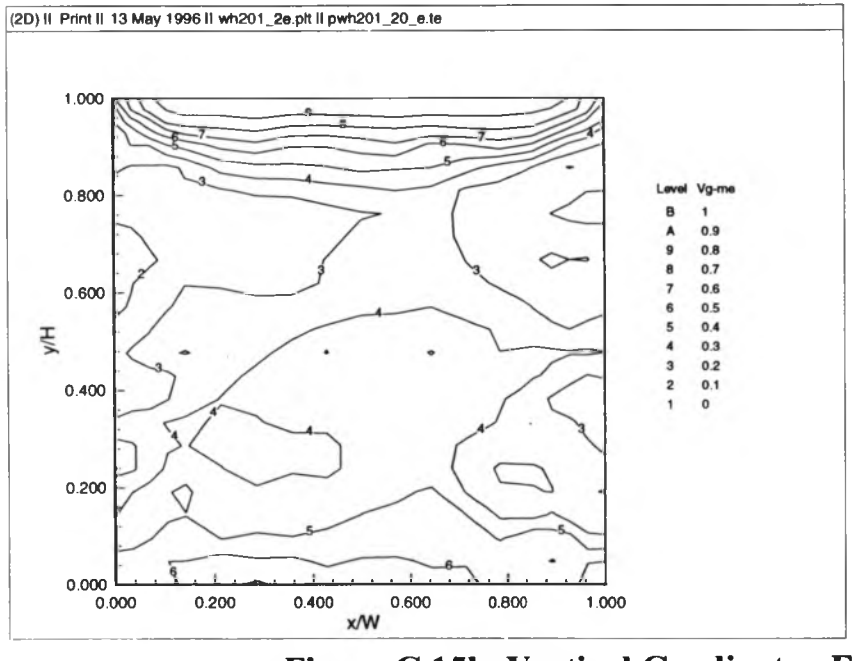

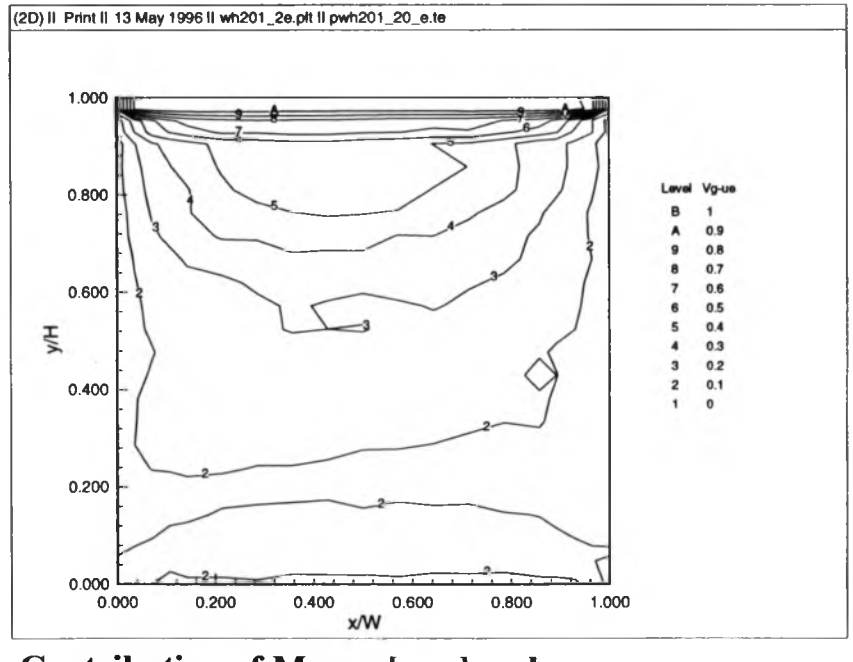

Figure C.15b. Vertical Gradients - Energy Contribution of Means [-me] and Nodal Energy Ratios [-ue], filtered, (0 degrees, suburban)

APPENDIX D

INSTANTANEOUS DISTRIBUTIONS

(FILTERED)

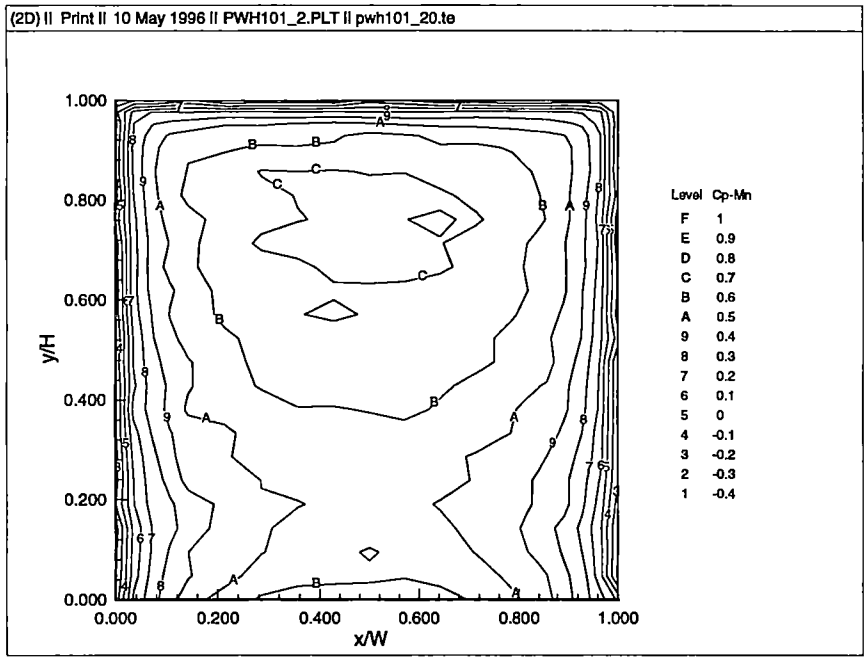

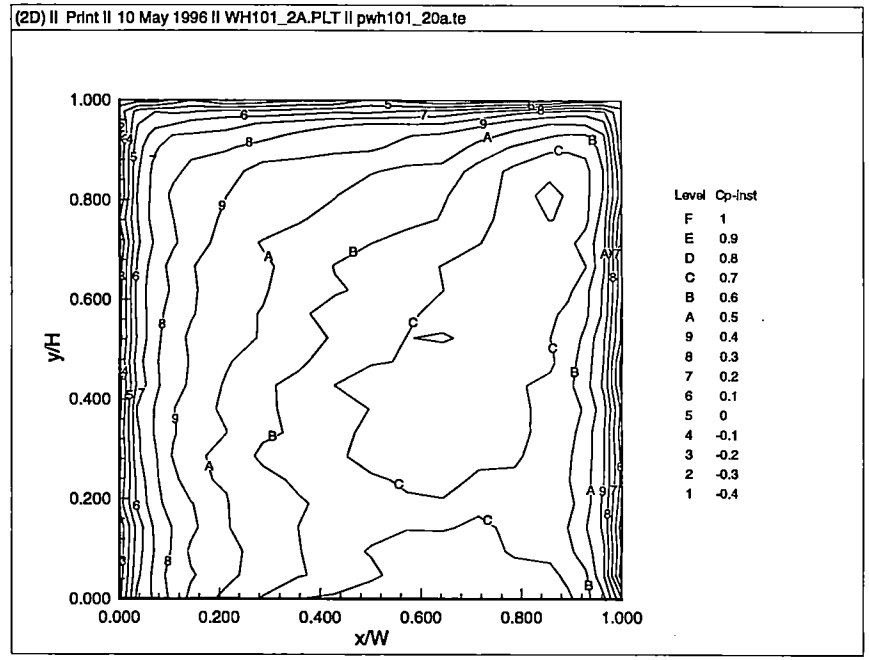

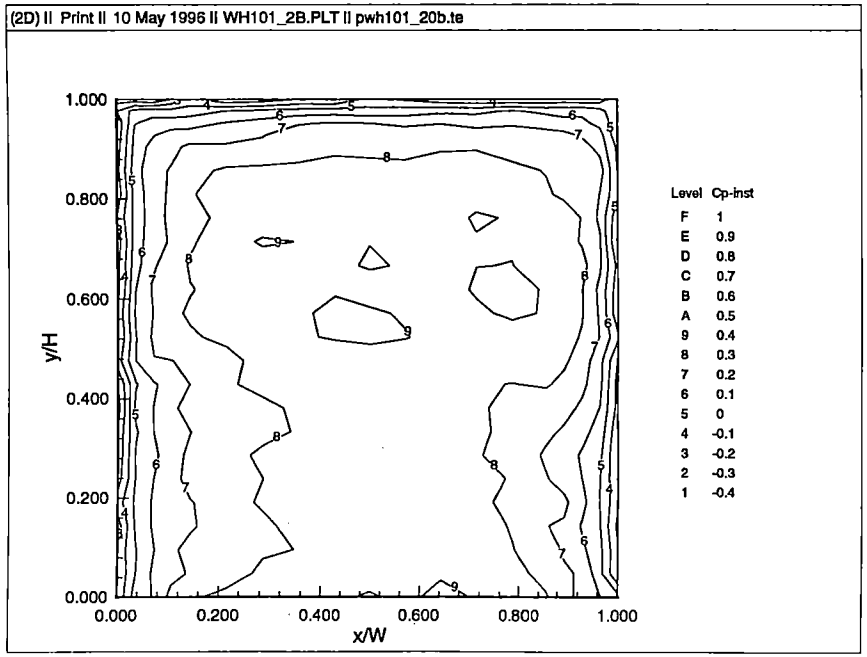

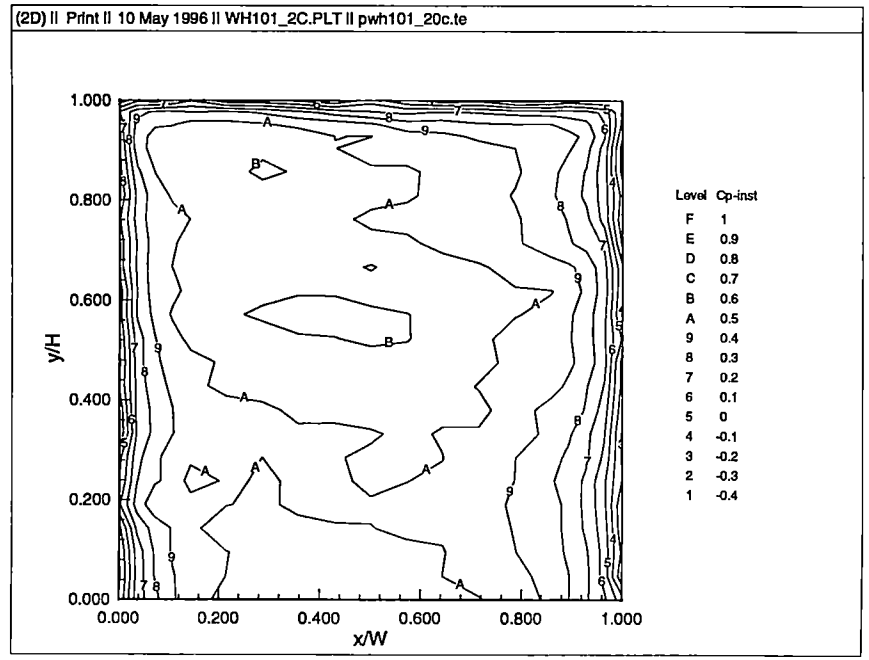

Figure D.1a. Instantaneous Pressure Coefficients, filtered

(0 degrees, open country)

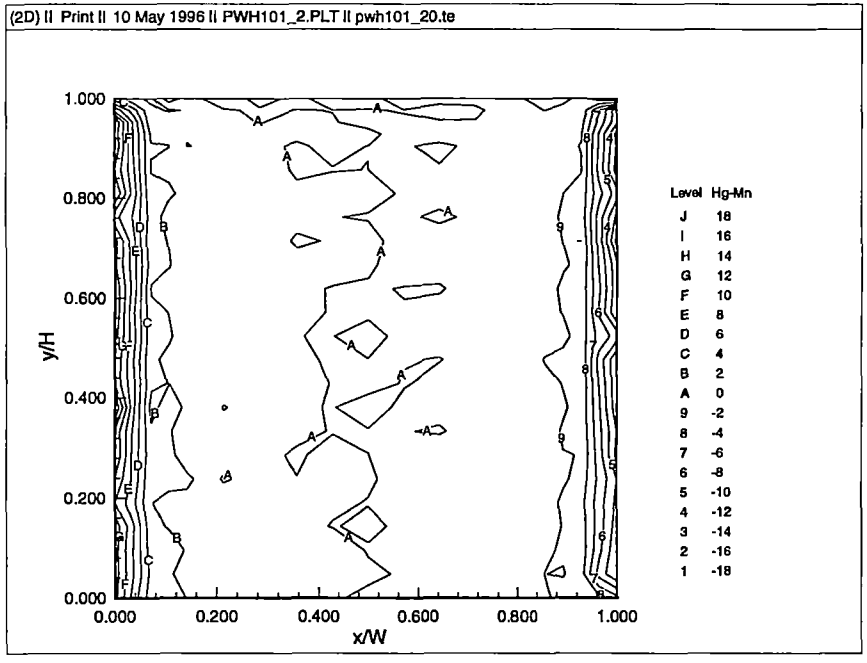

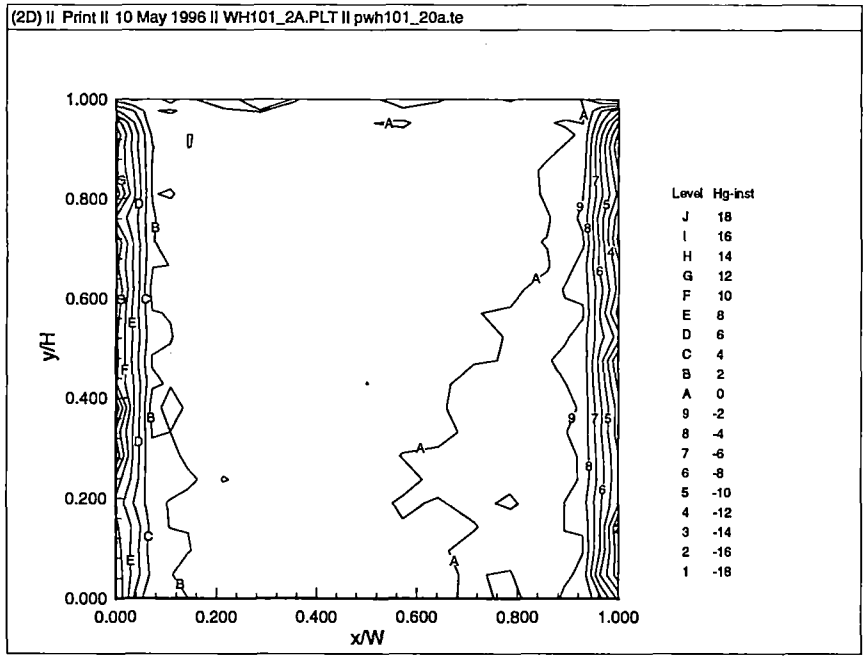

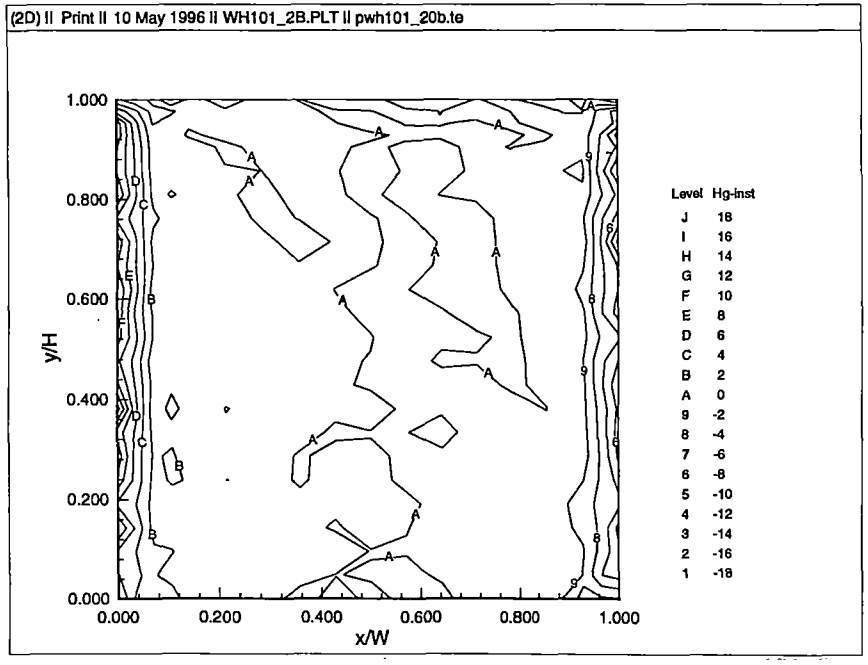

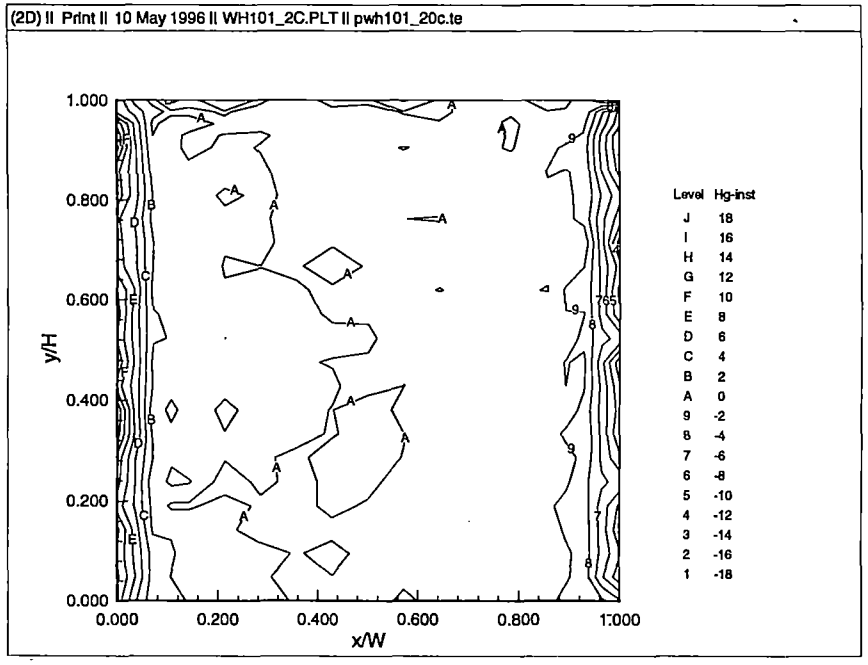

Figure D.1b. Instantaneous Horizontal Pressure Gradients, filtered

(0 degrees, open country)

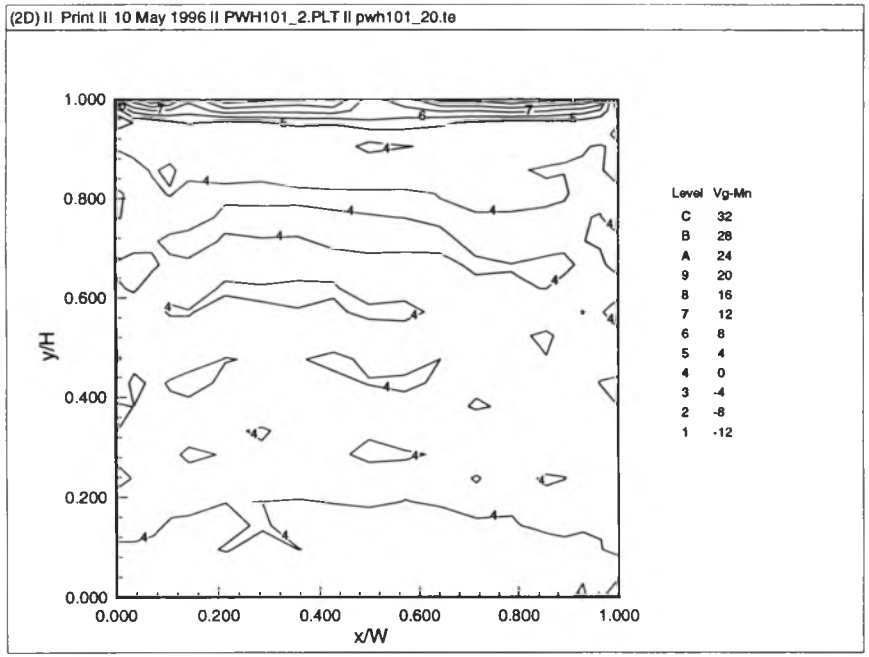

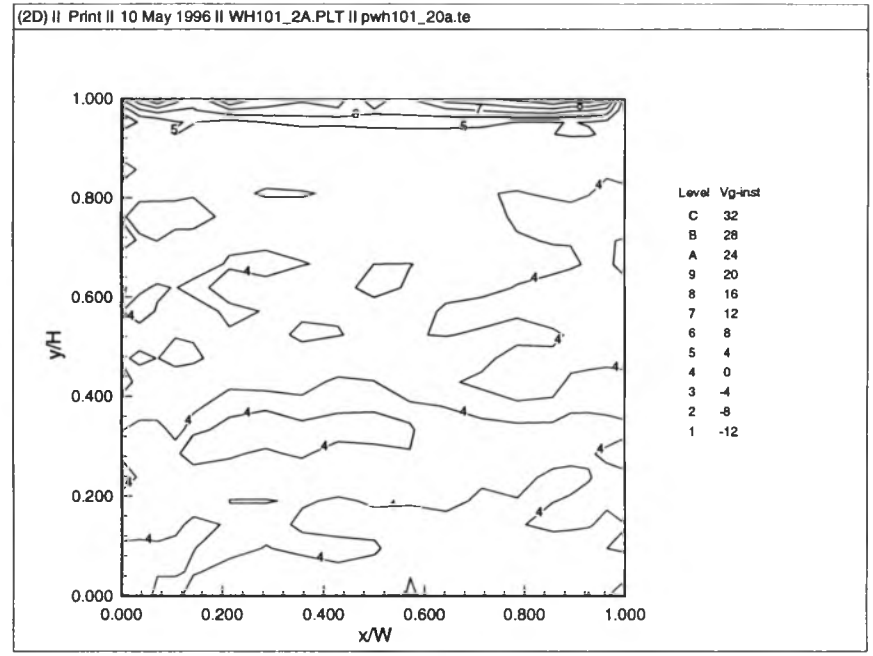

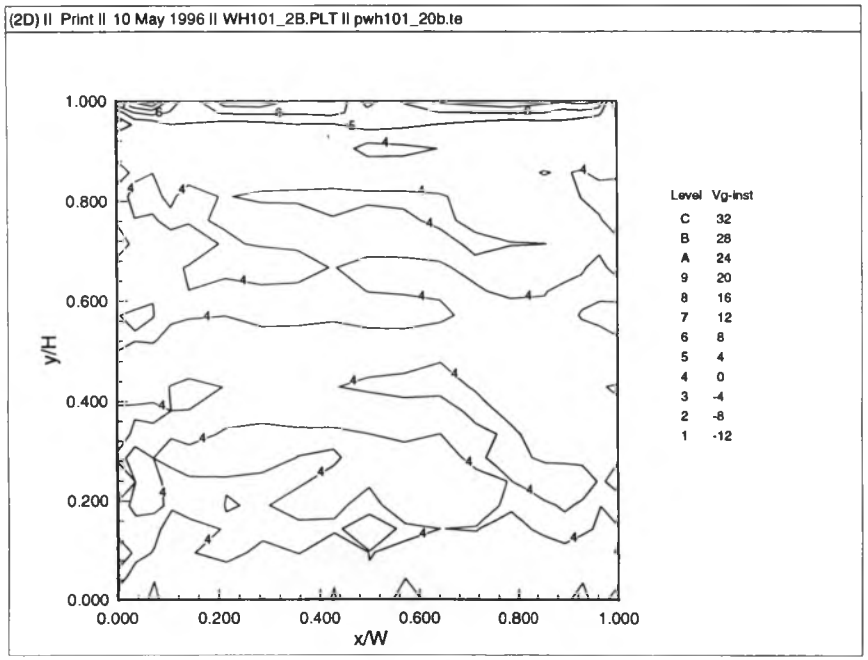

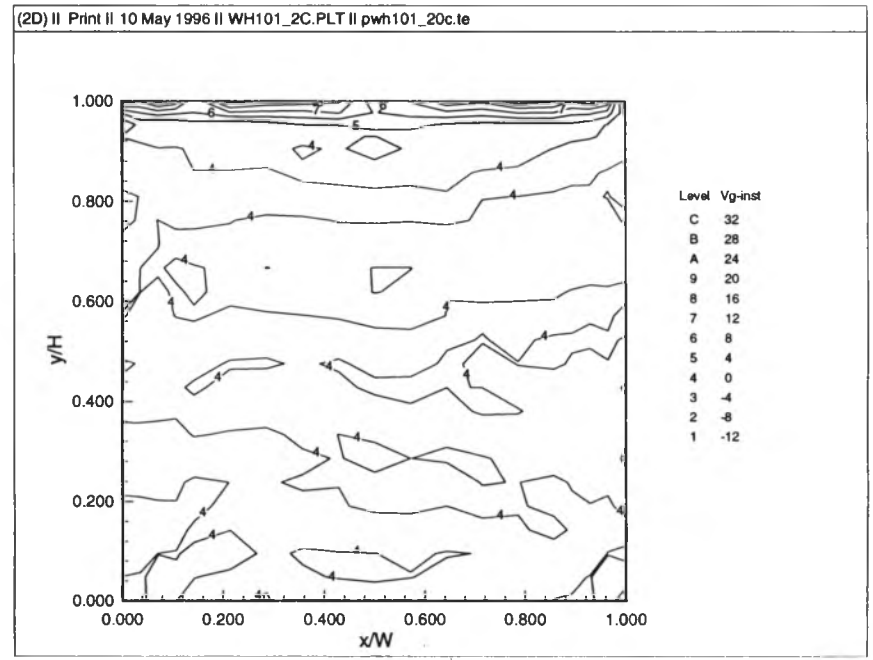

Figure D.1c. Instantaneous Vertical Pressure Gradients, filtered

(0 degrees, open country)

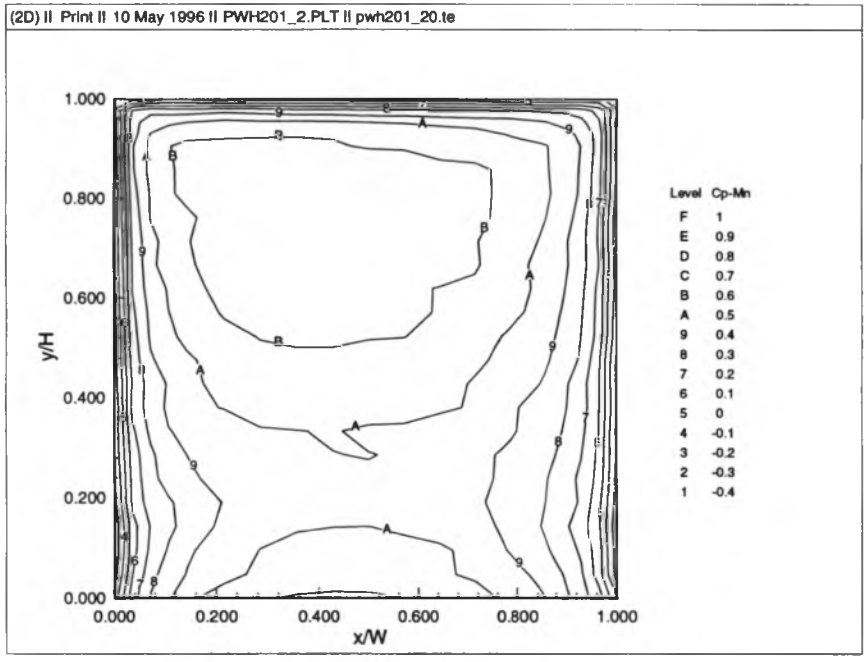

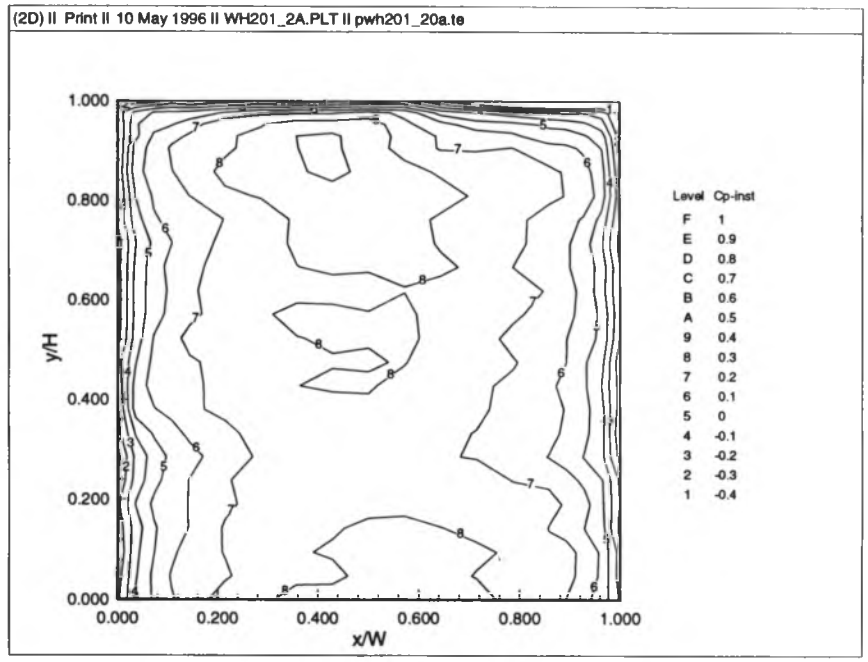

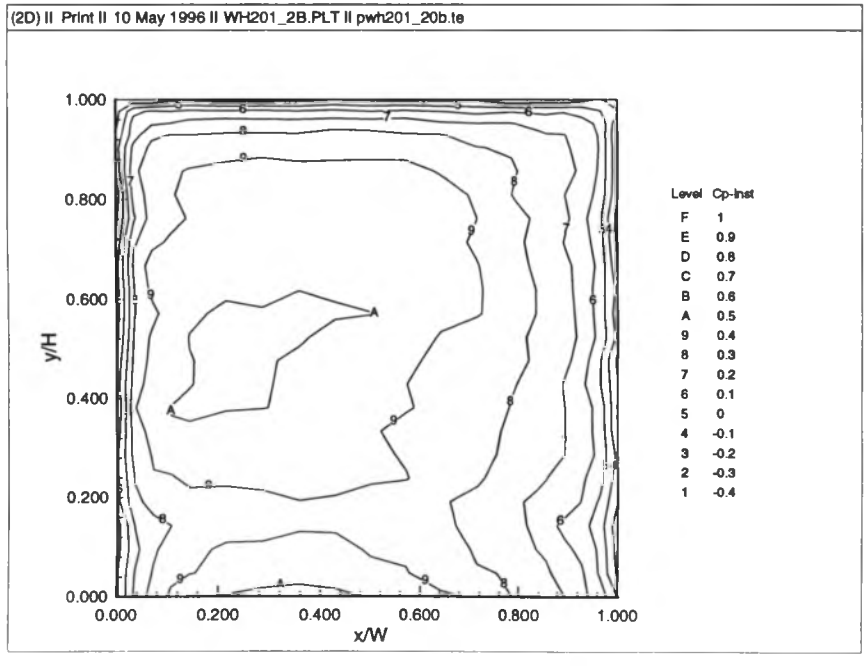

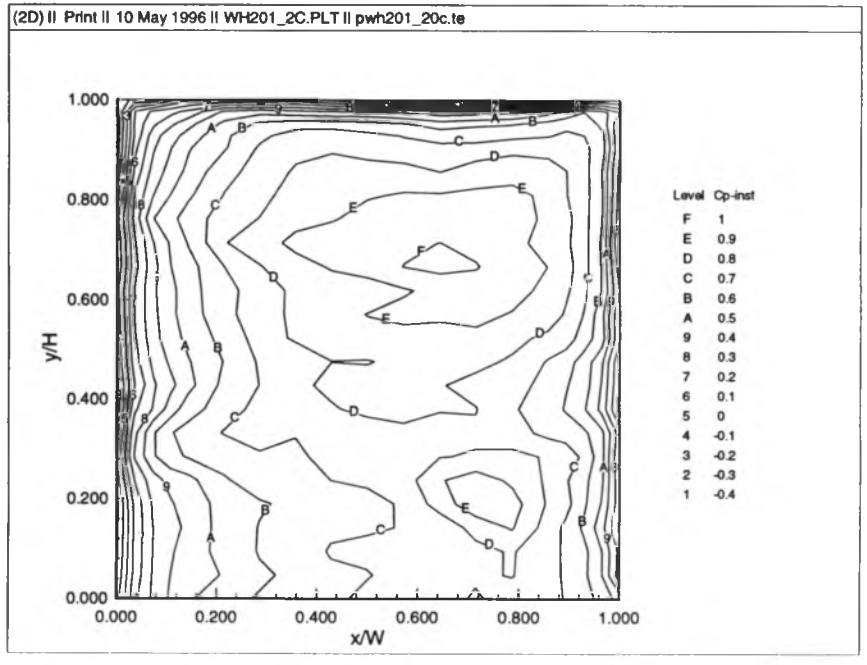

Figure D.2a. Instantaneous Pressure Coefficients, filtered

(0 degrees, suburban)

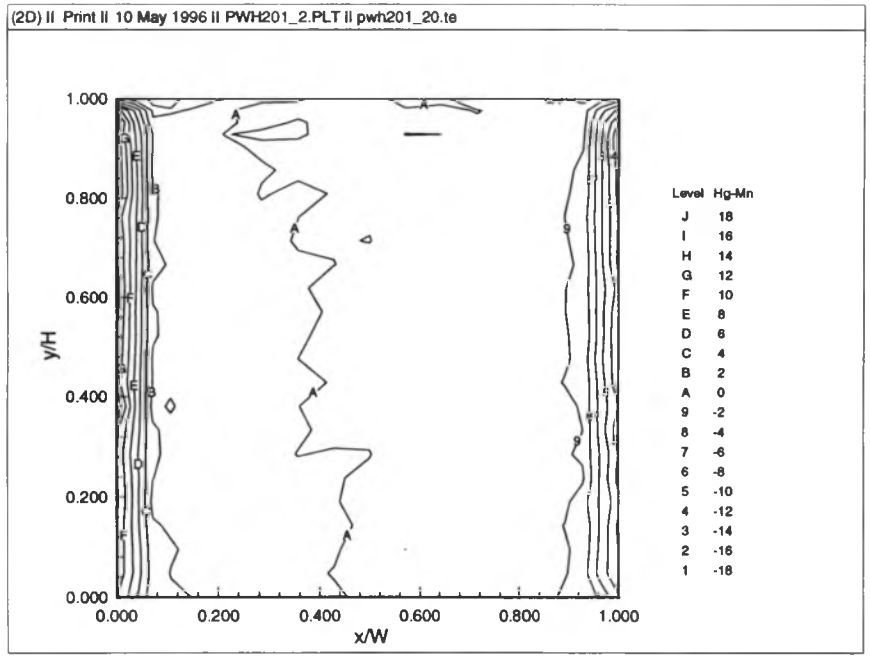

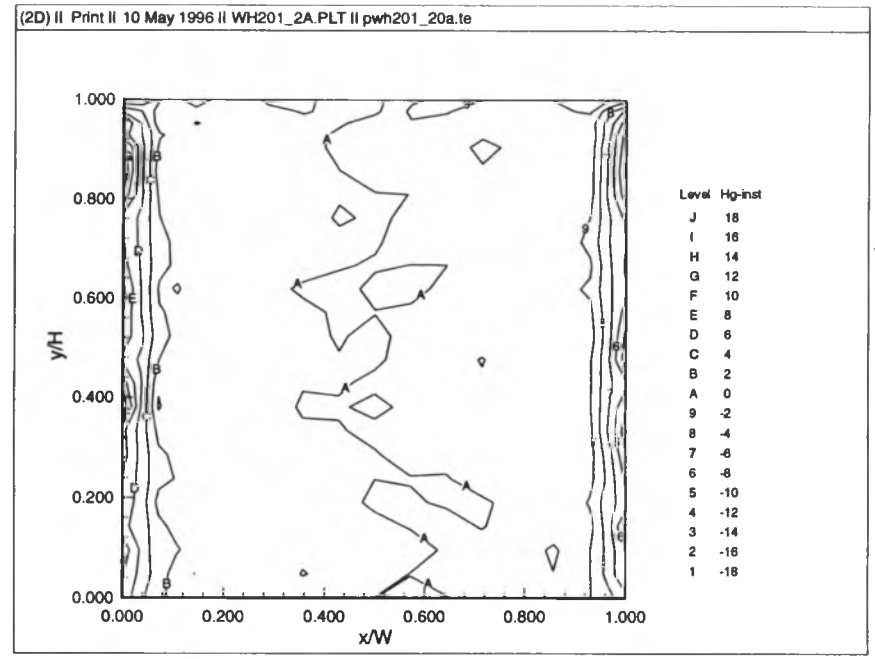

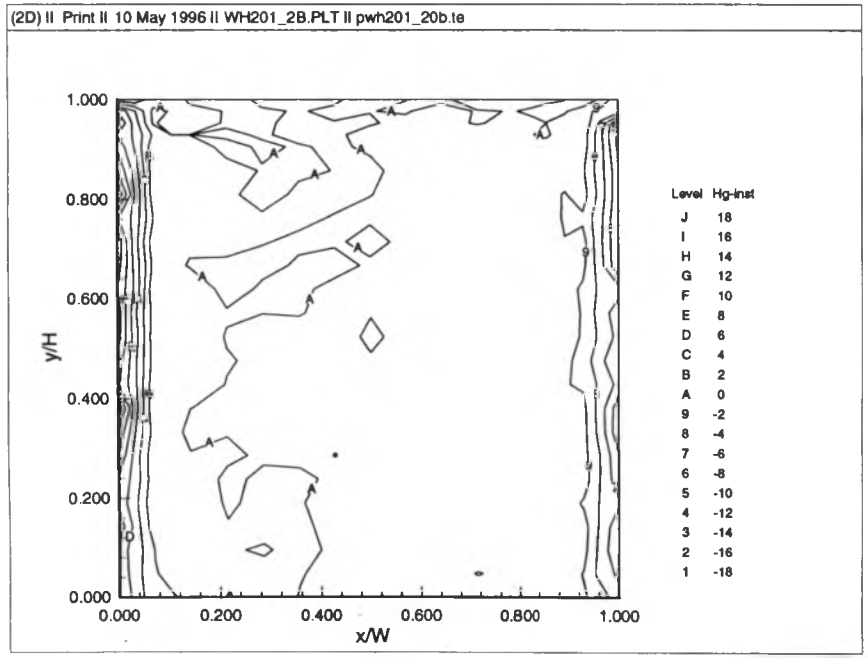

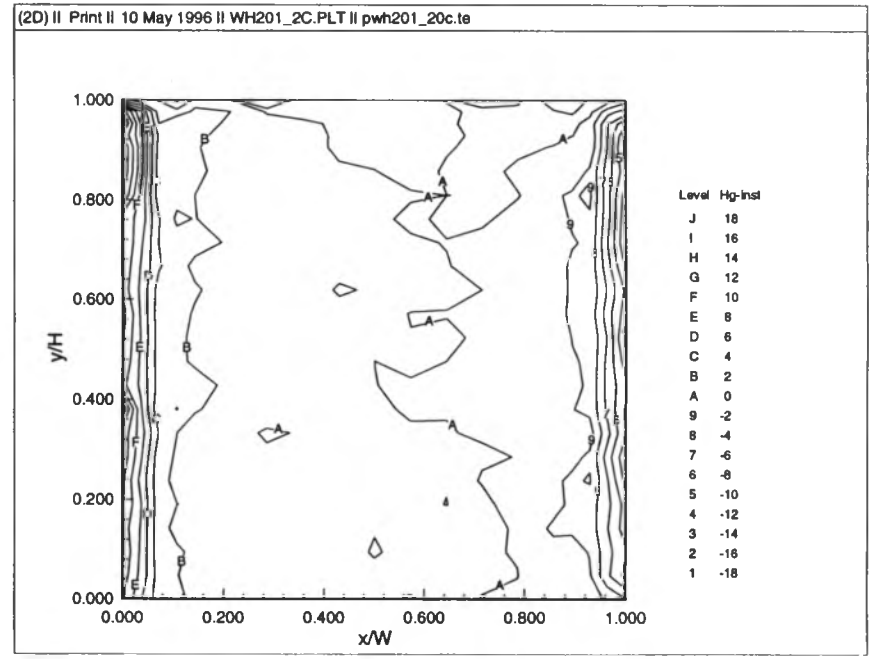

Figure D.2b. Instantaneous Horizontal Pressure Gradients, filtered

(0 degrees, suburban)

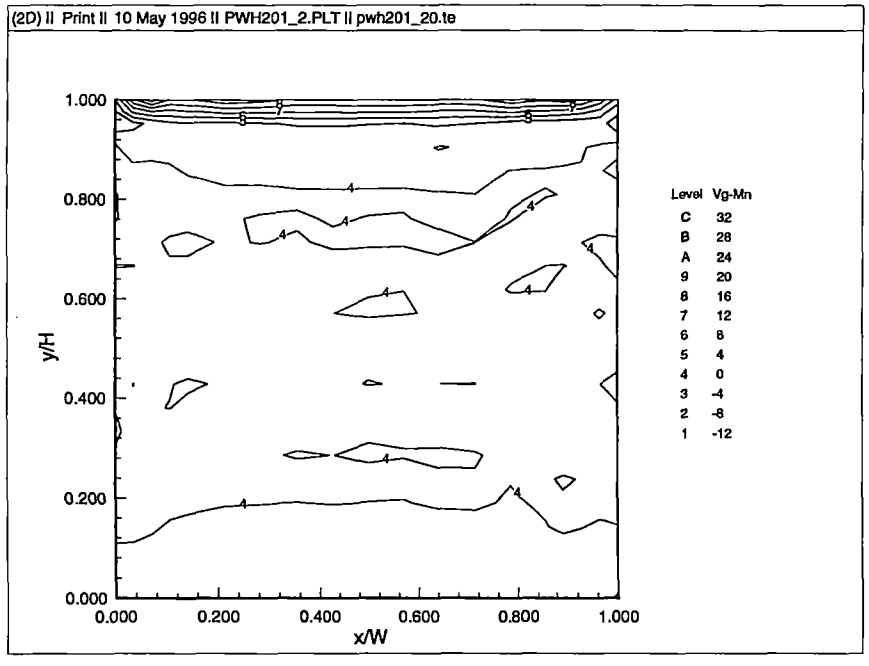

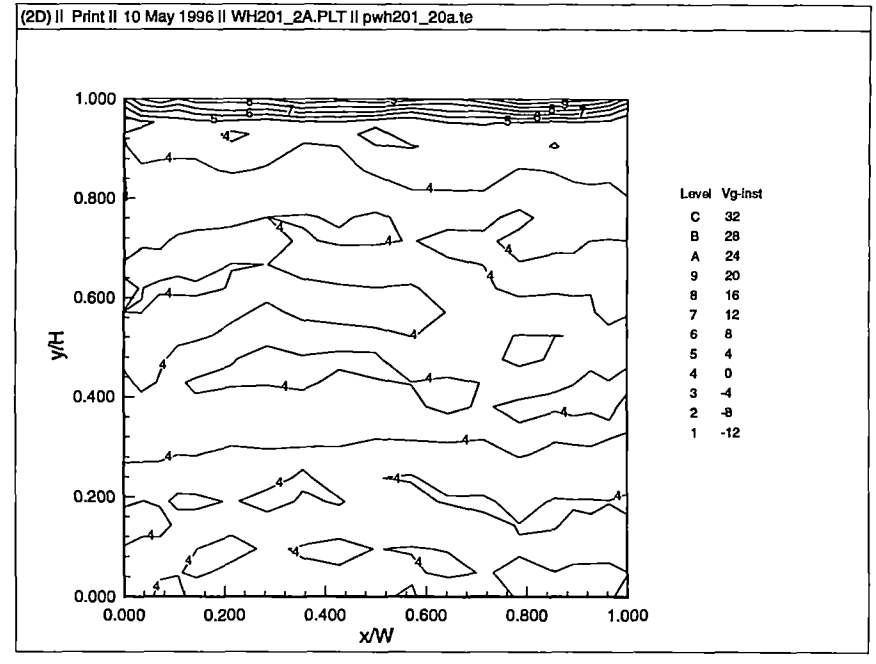

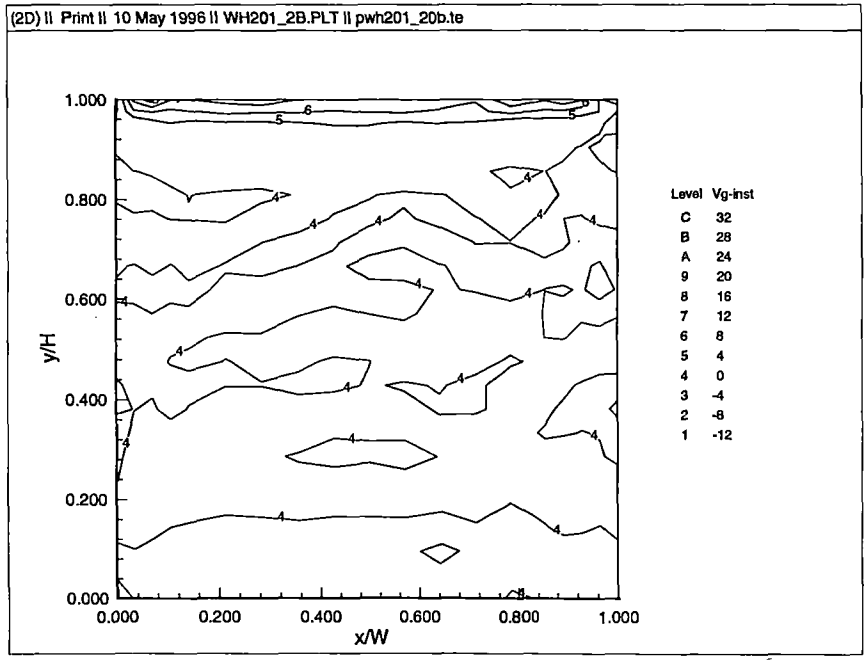

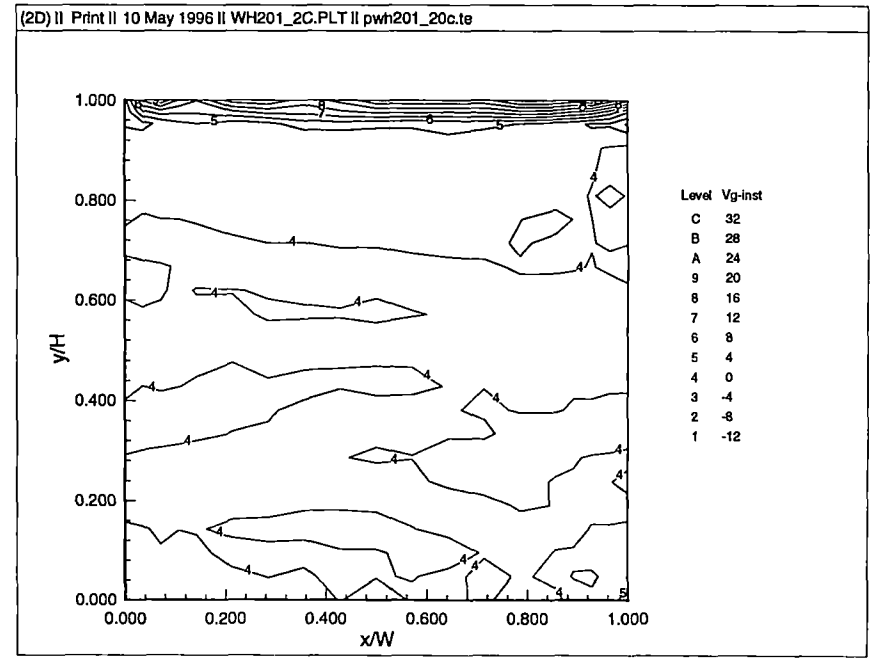

Figure D.2c. Instantaneous Vertical Pressure Gradients, filtered

(0 degrees, suburban)

APPENDIX E

TABLE E.1 - MODAL AMPLITUDES

TABLE E.2 - COLLECTIVE ENERGY RATIOS

MEANS AND 1ST 3 MODE SHAPES

(FILTERED)

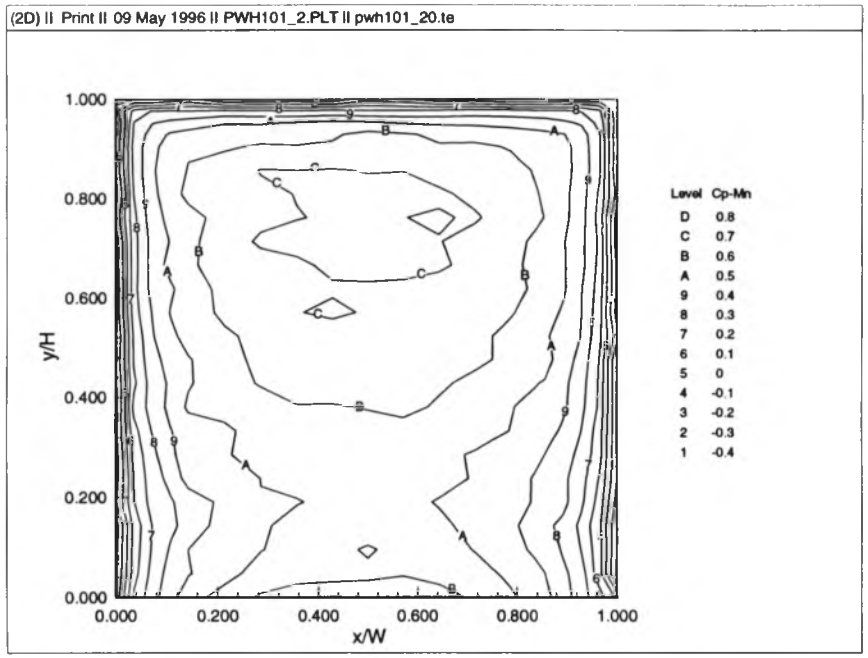

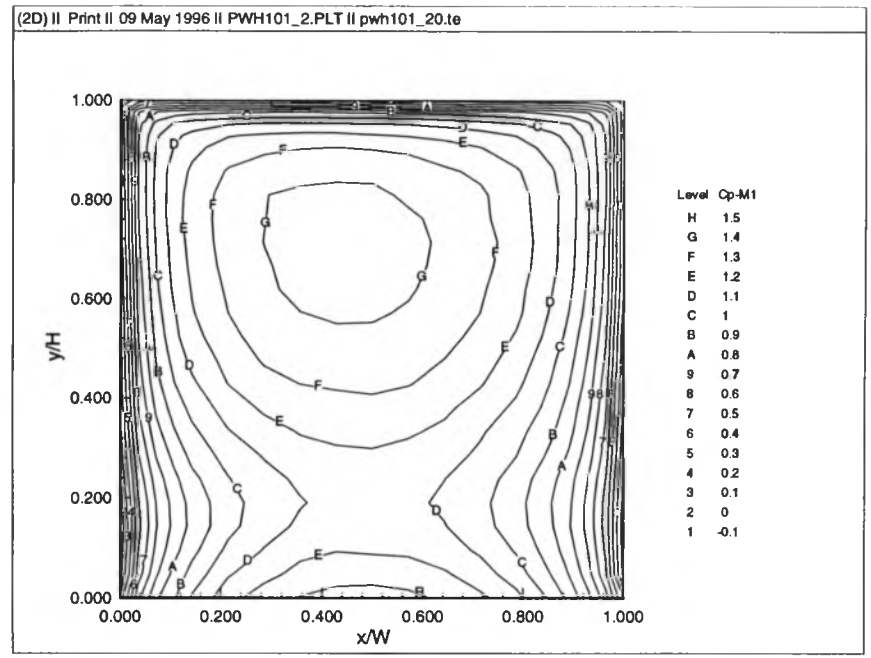

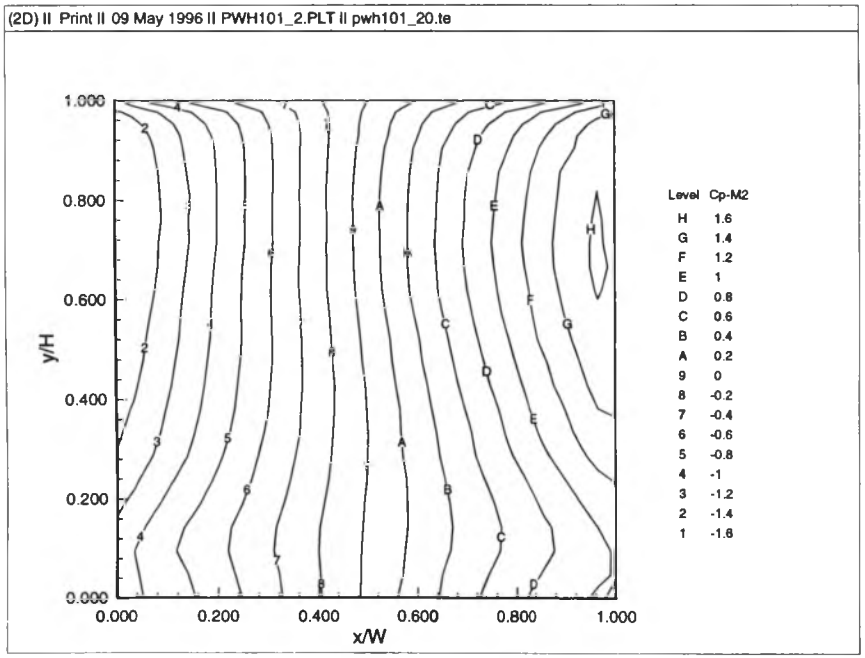

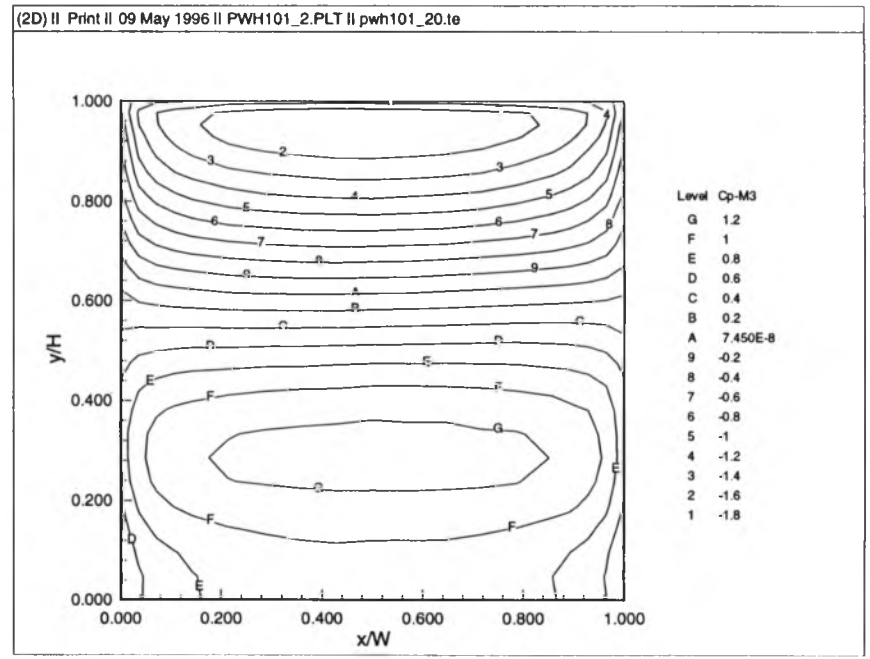

Figure E.1. Means and 1st 3 Mode Shapes of Pressure Coefficients, filtered

(0 degrees, open country)

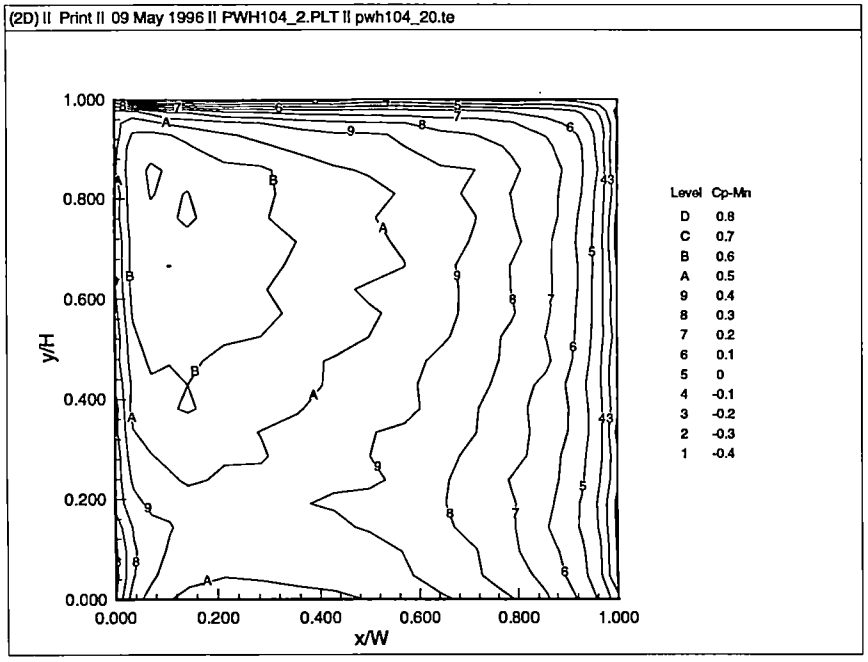

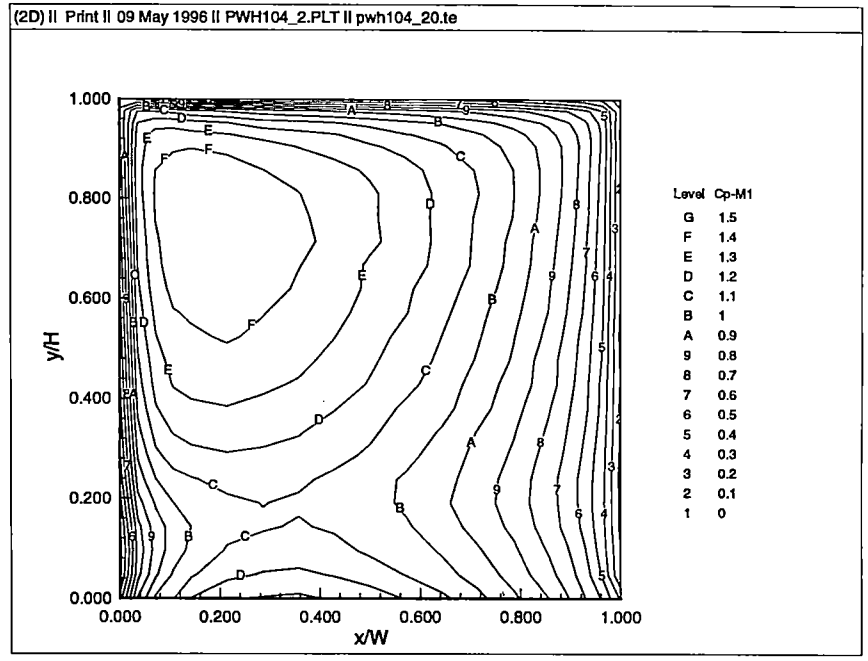

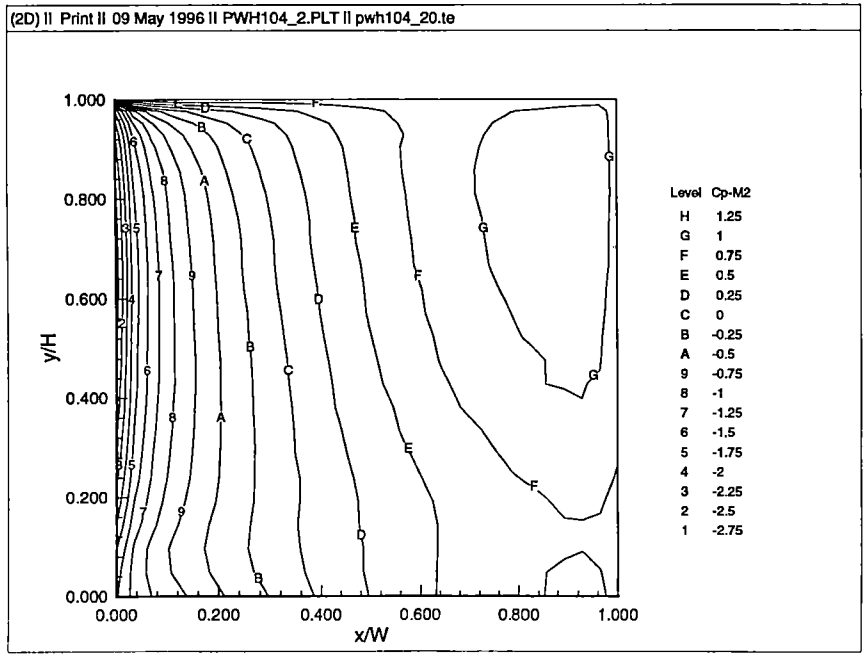

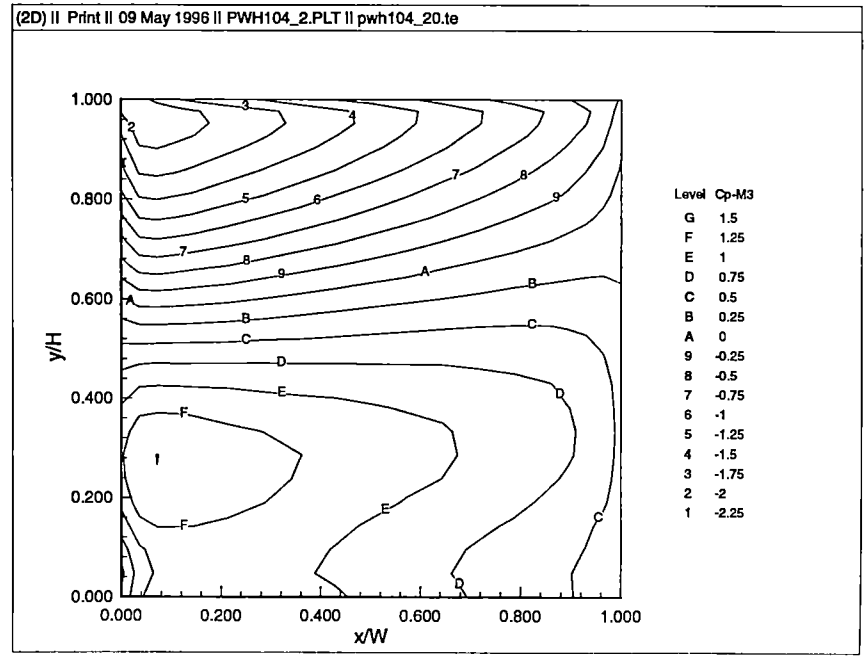

Figure E.2. Means and 1st 3 Mode Shapes of Pressure Coefficients, filtered (30 degrees, open country)

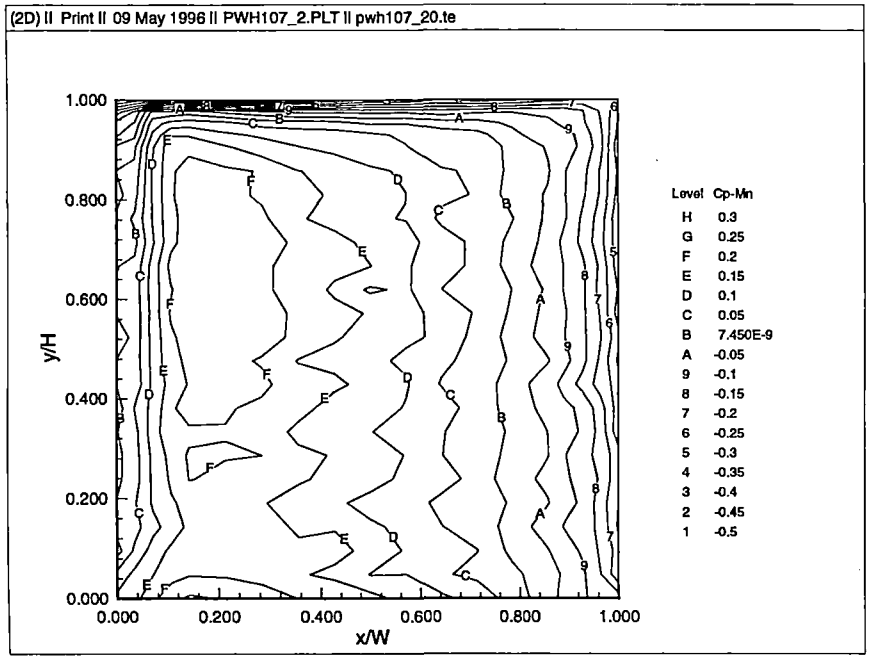

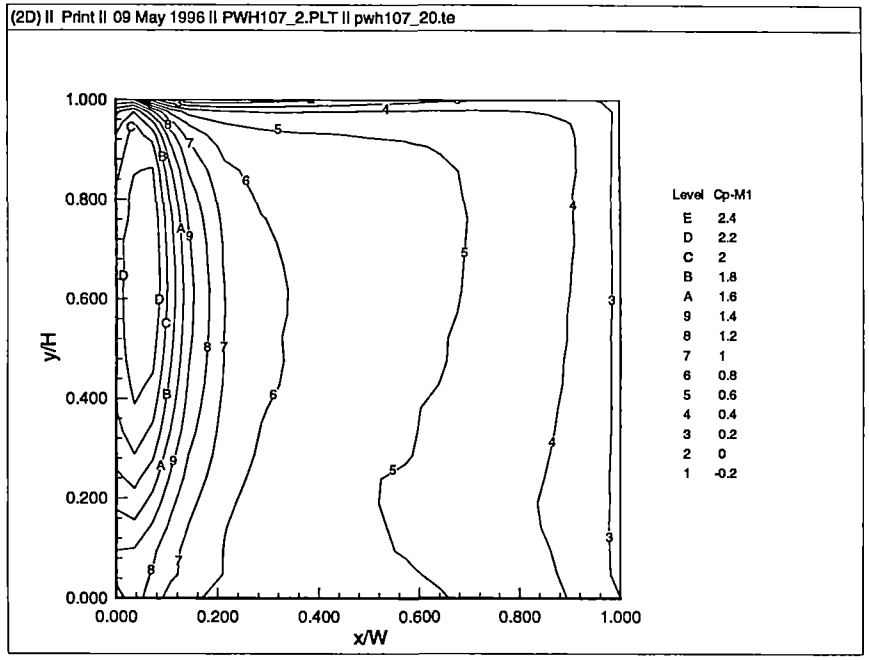

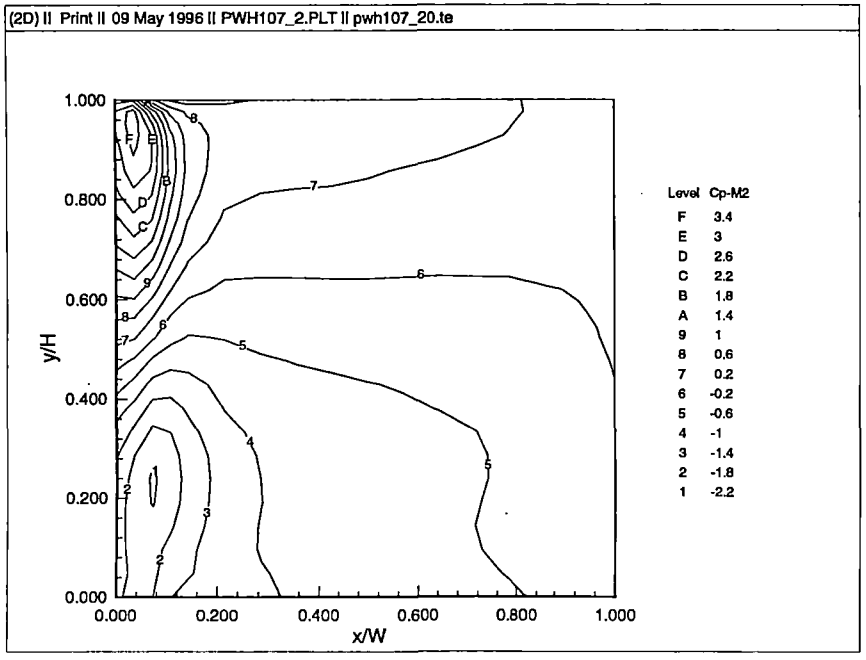

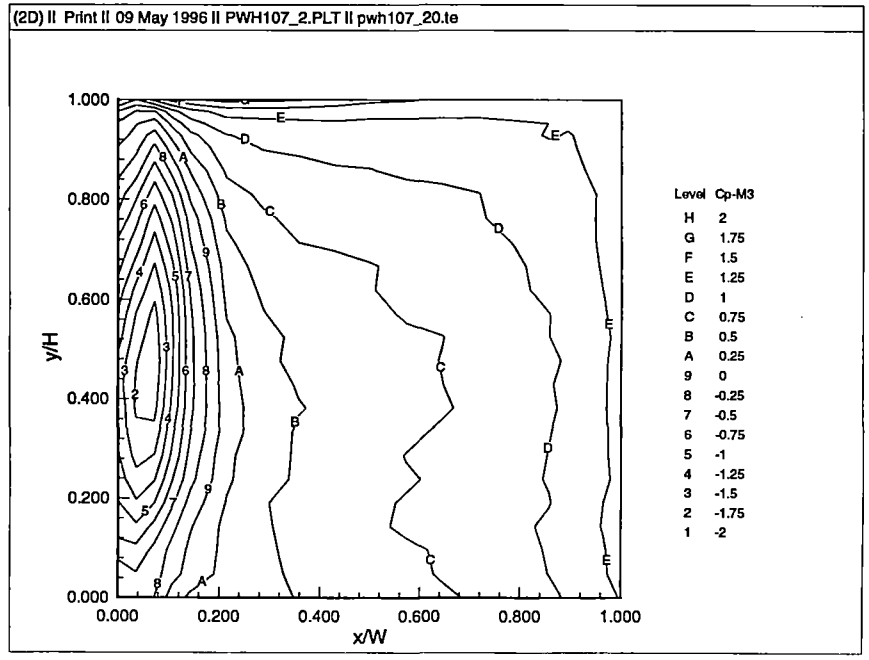

Figure E.3. Means and 1st 3 Mode Shapes of Pressure Coefficients, filtered (60 degrees, open country)

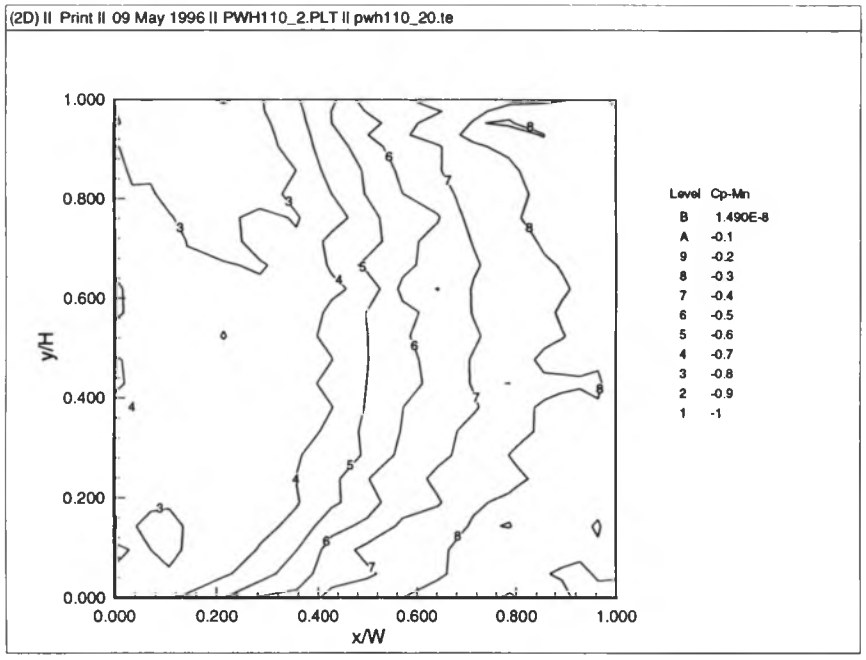

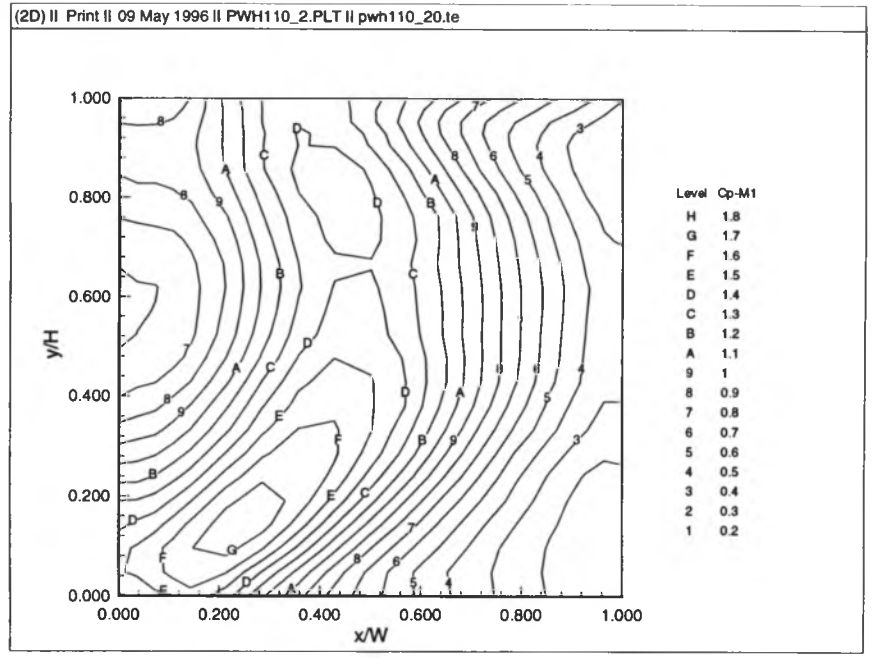

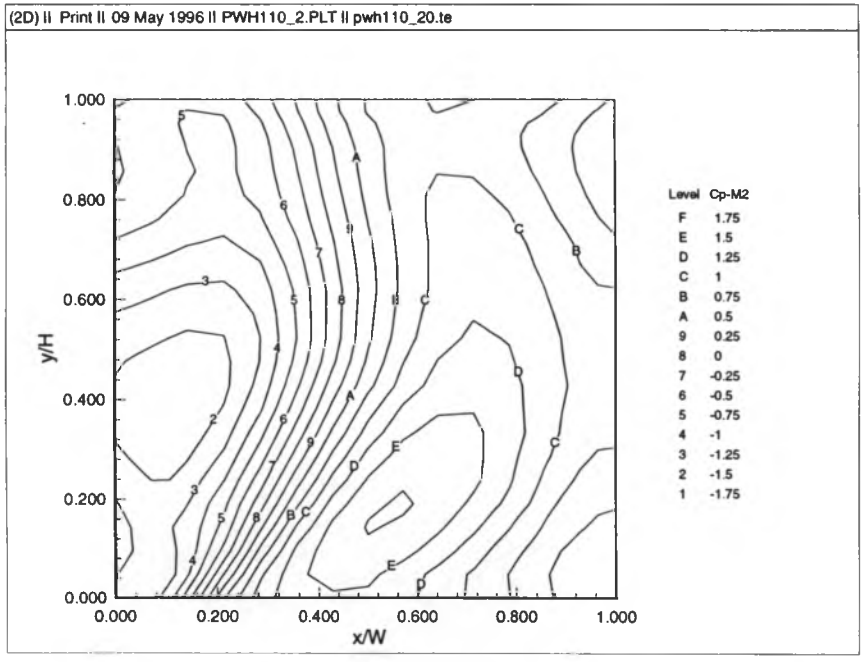

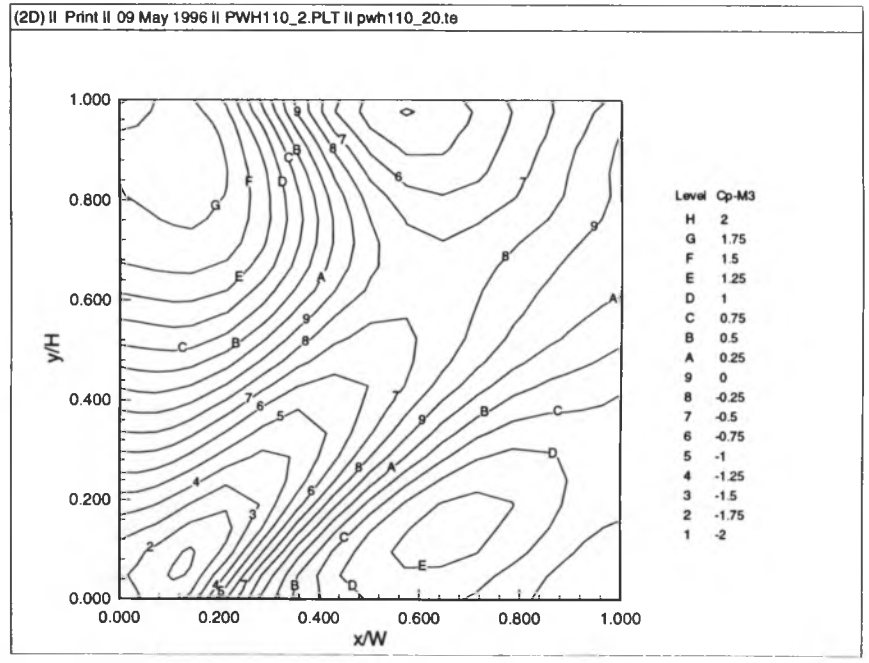

Figure E.4. Means and 1st 3 Mode Shapes of Pressure Coefficients, filtered

(90 degrees, open country)

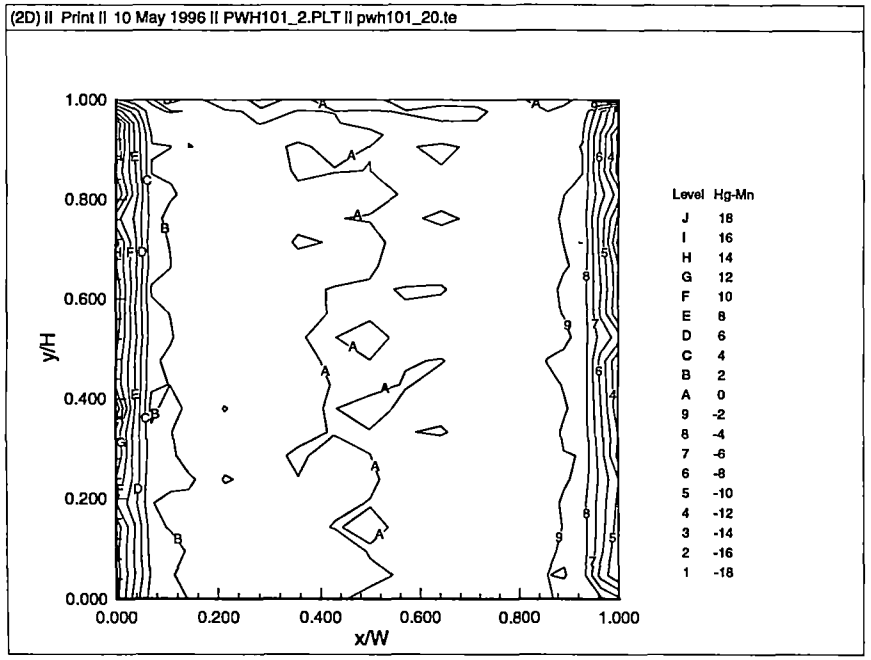

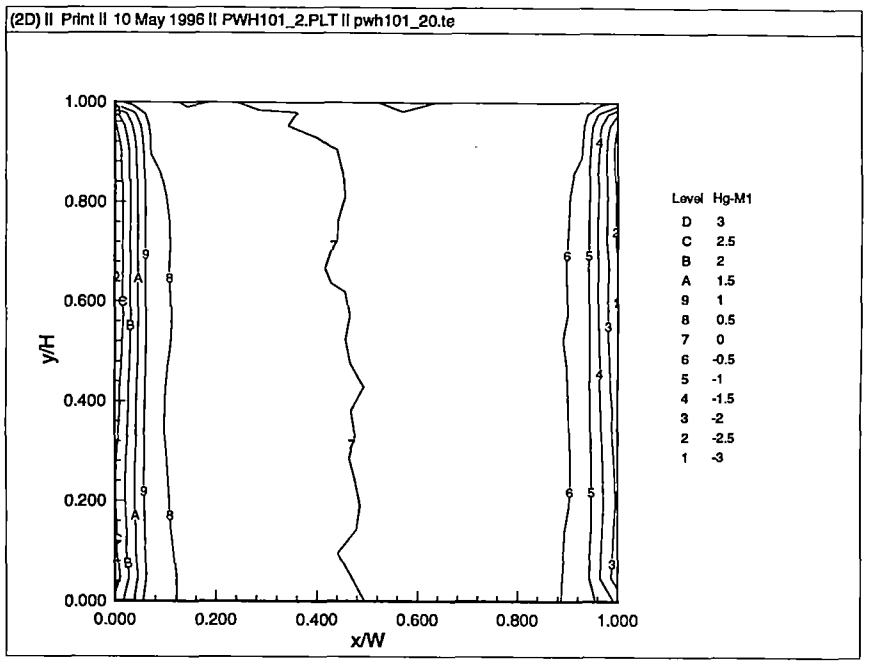

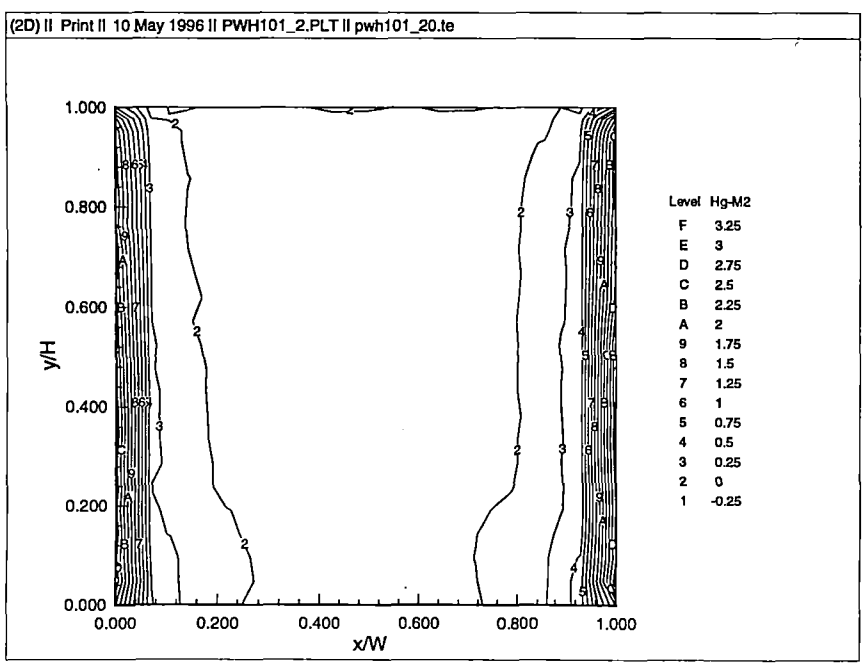

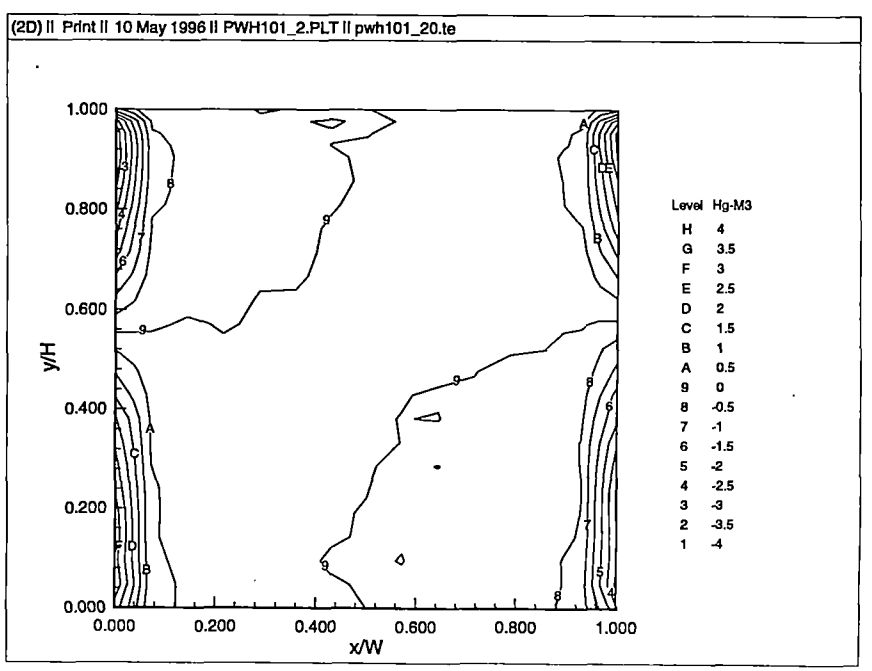

Figure E.5. Means and 1st 3 Mode Shapes of Horizontal Pressure Gradients, filtered (0 degrees, open country)

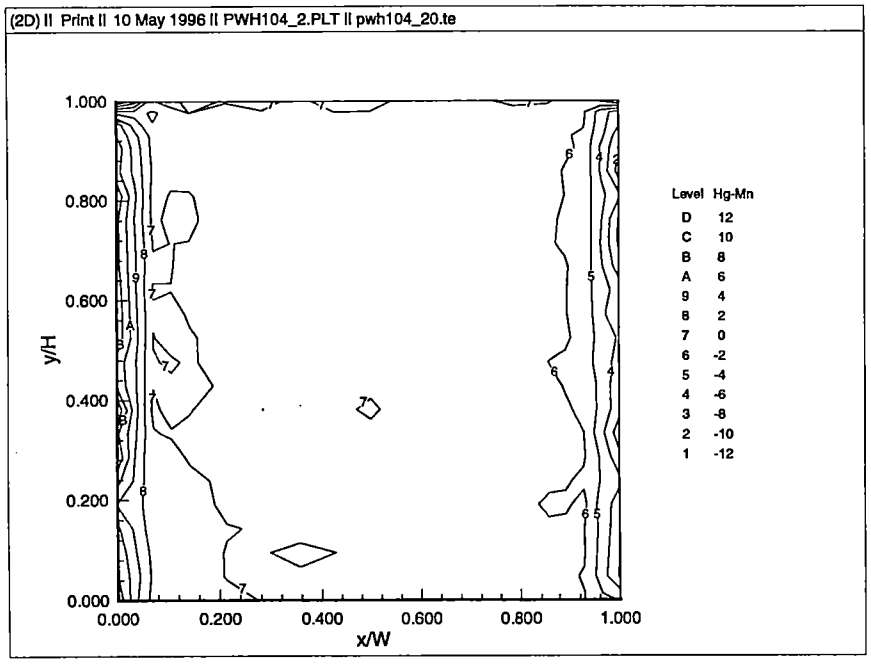

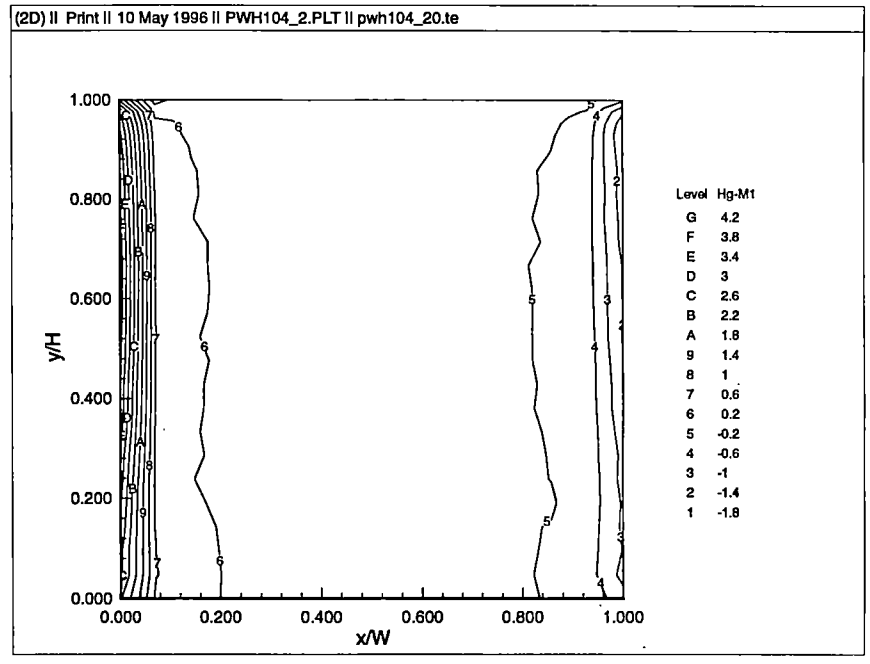

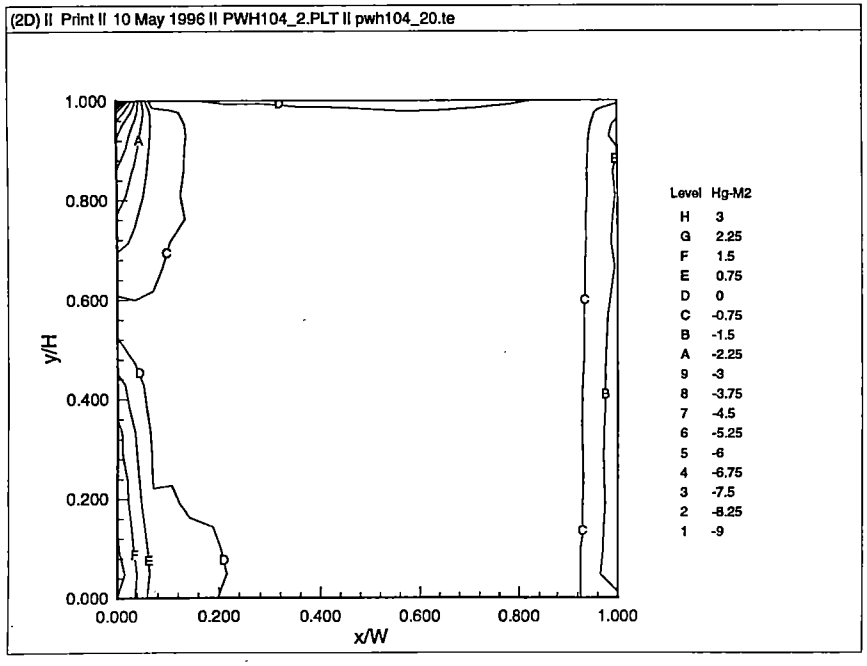

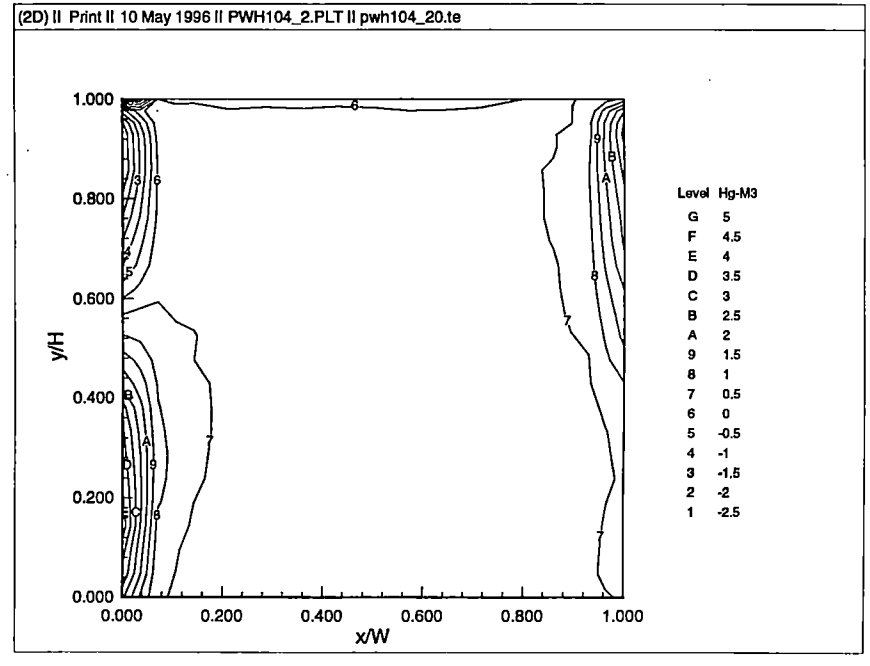

Figure E.6. Means and 1st 3 Mode Shapes of Horizontal Pressure Gradients, filtered (30 degrees, open country)

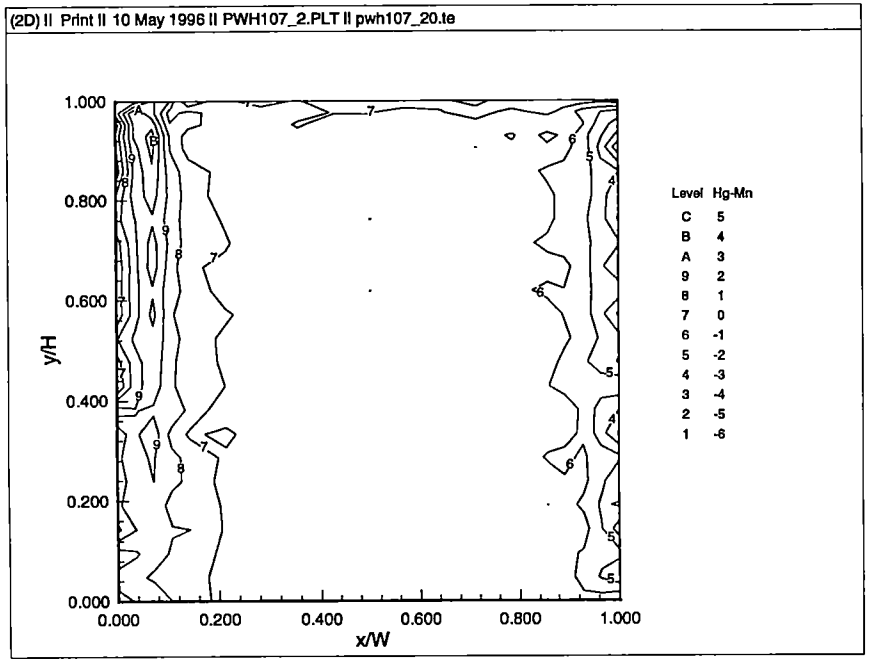

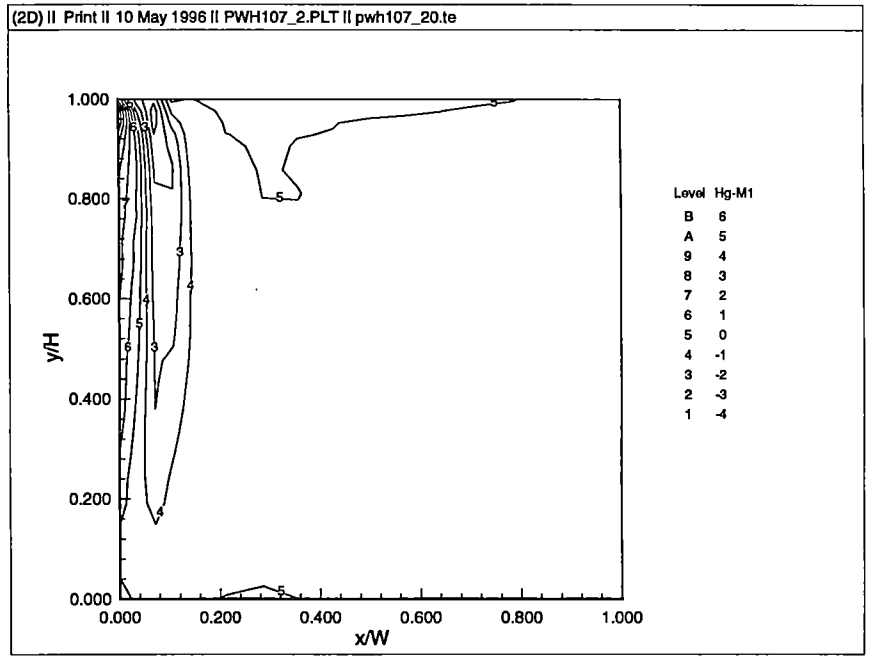

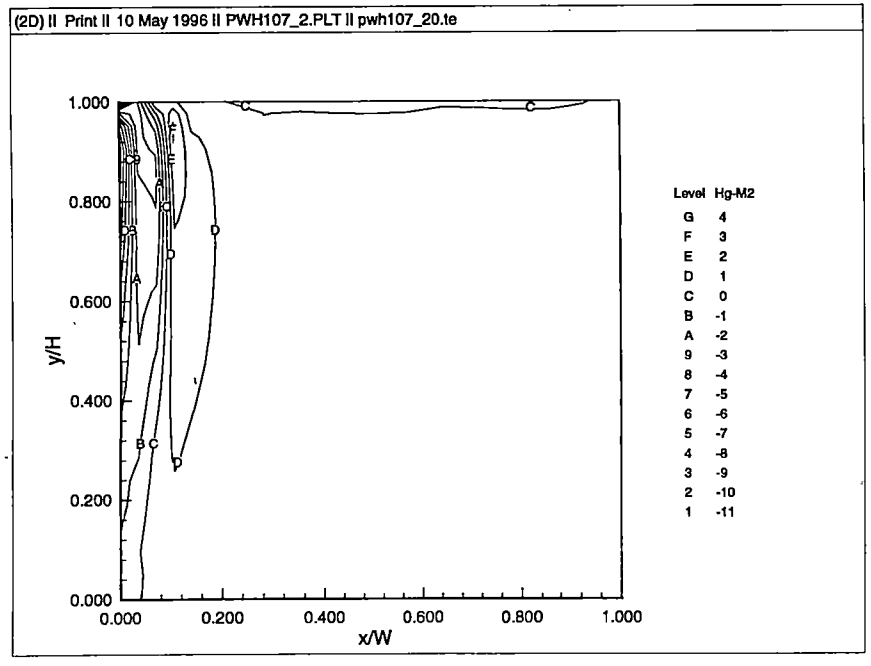

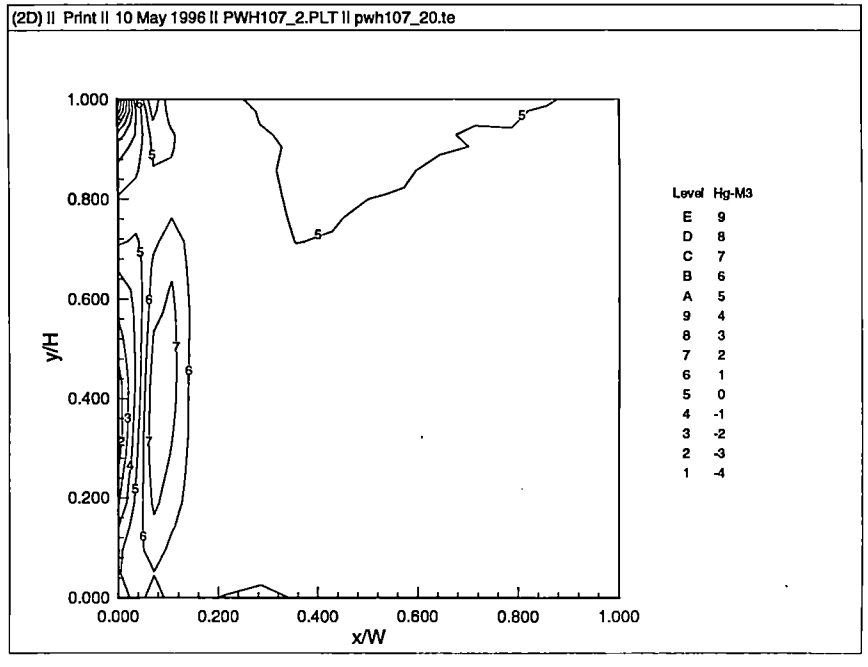

Figure E.7. Means and 1st 3 Mode Shapes of Horizontal Pressure Gradients, filtered (60 degrees, open country)

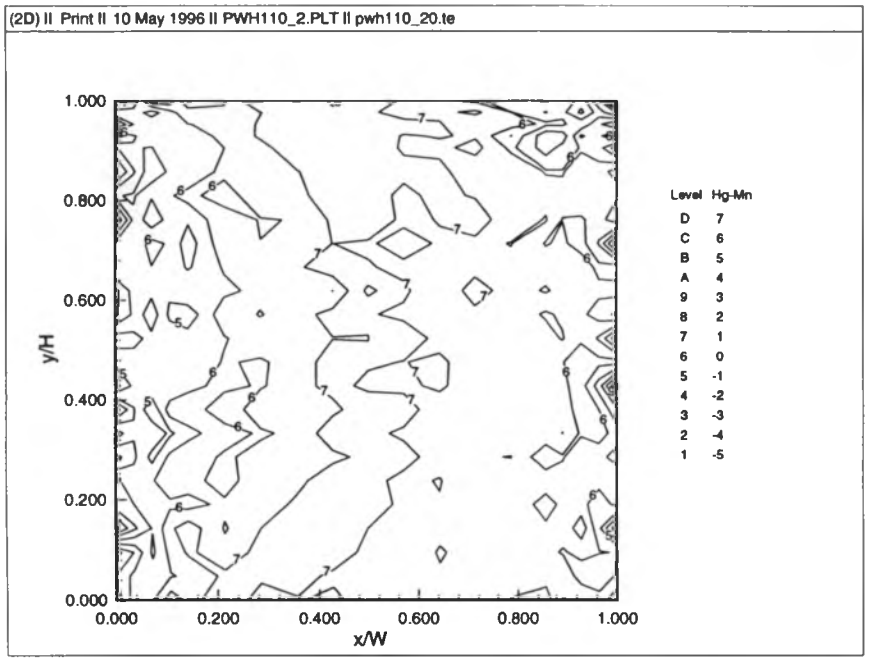

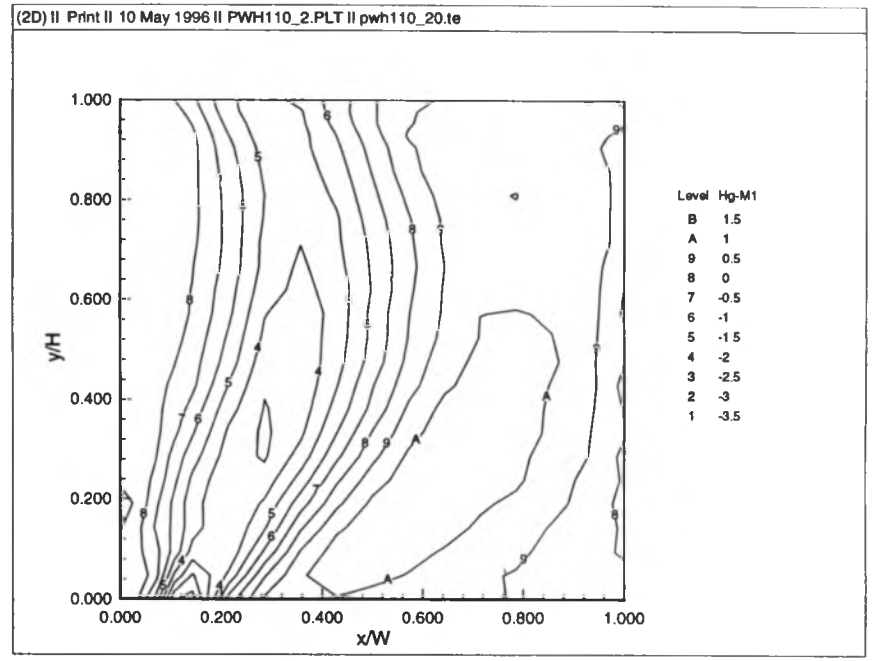

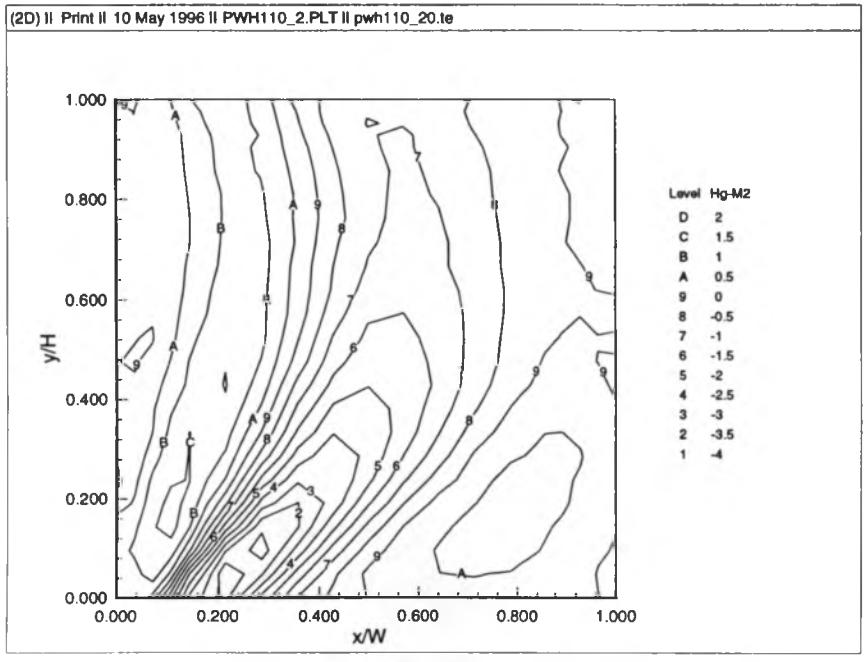

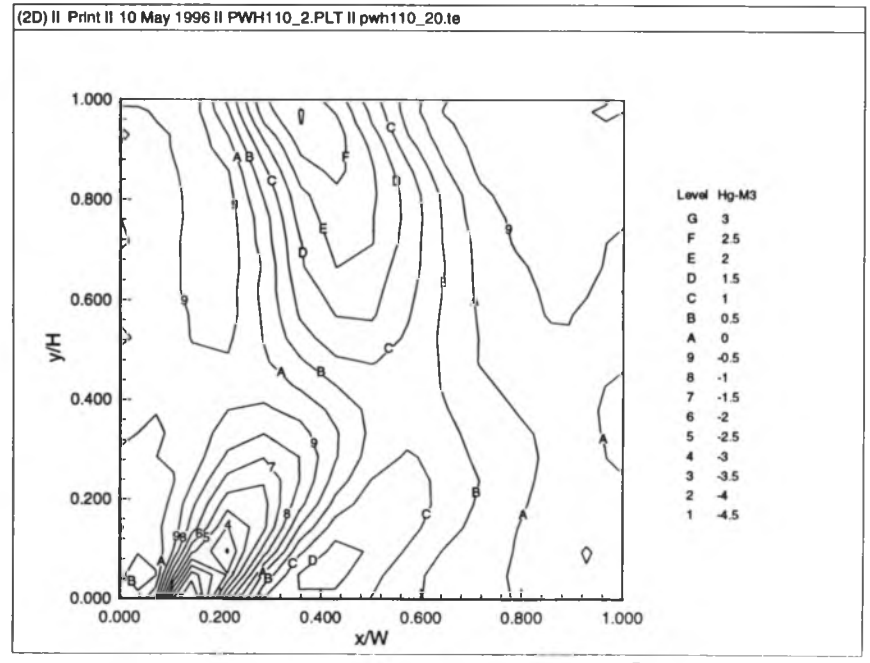

Figure E.8. Means and 1st 3 Mode Shapes of Horizontal Pressure Gradients, filtered (90 degrees, open country)

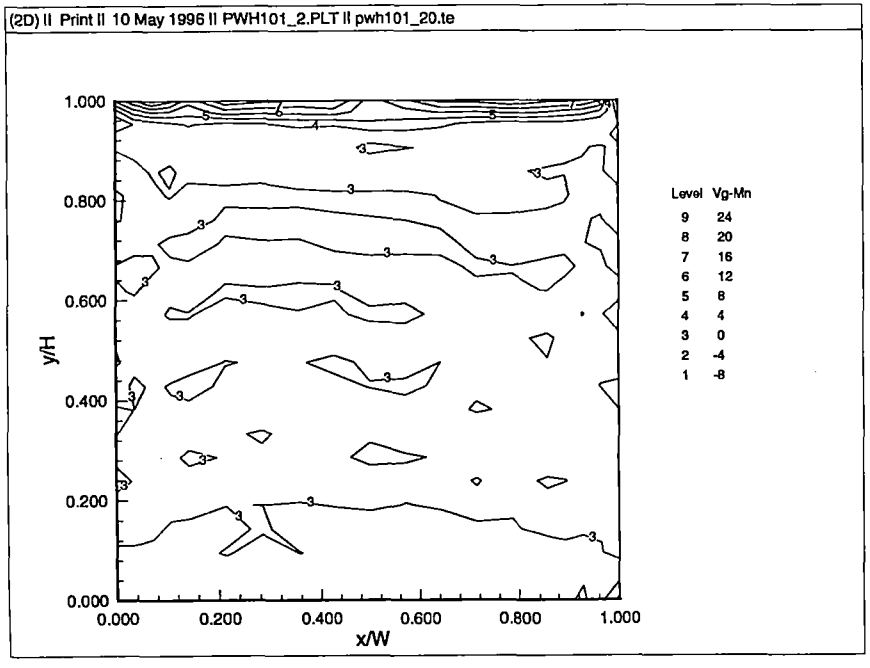

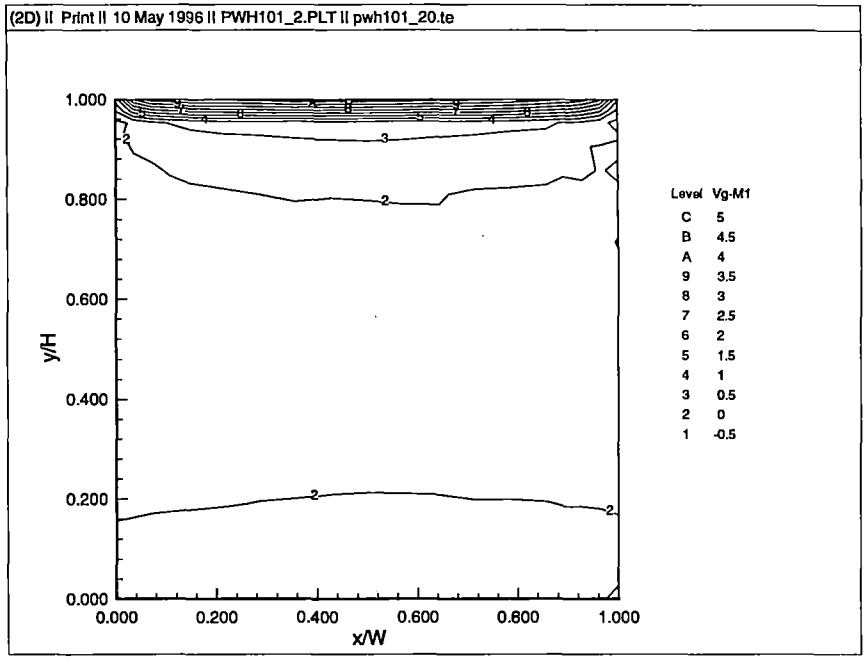

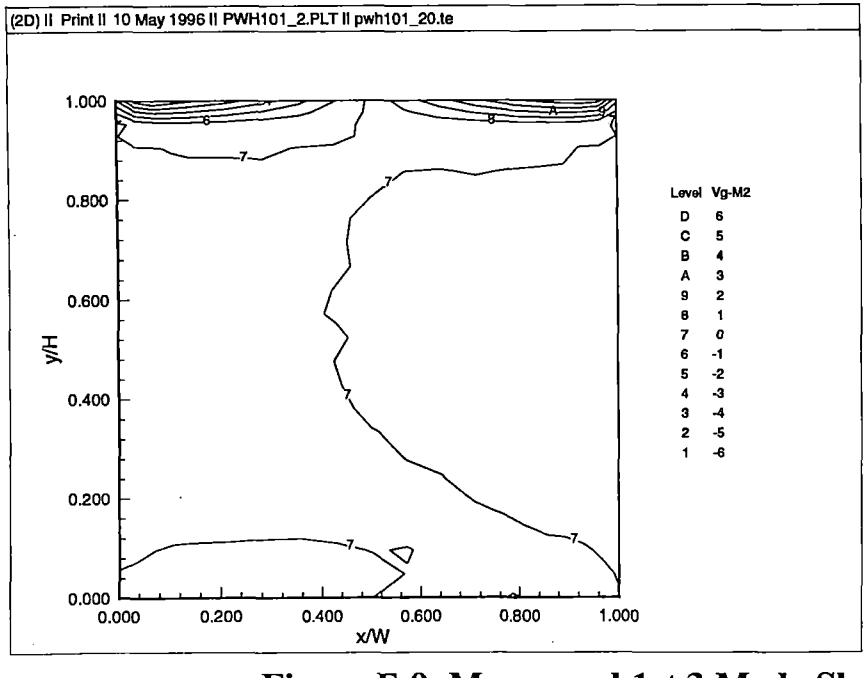

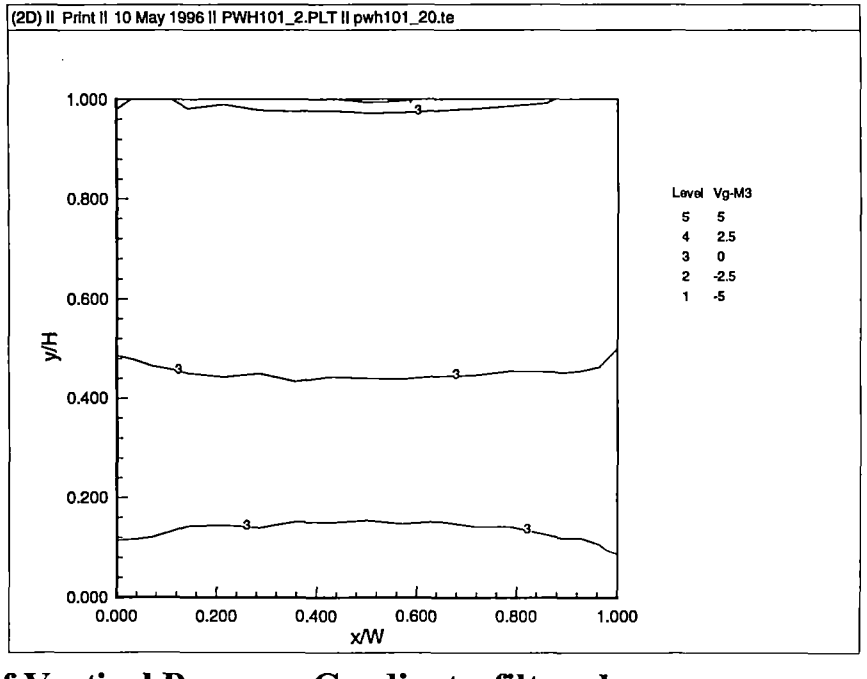

Figure E.9. Means and 1st 3 Mode Shapes of Vertical Pressure Gradients, filtered (0 degrees, open country)

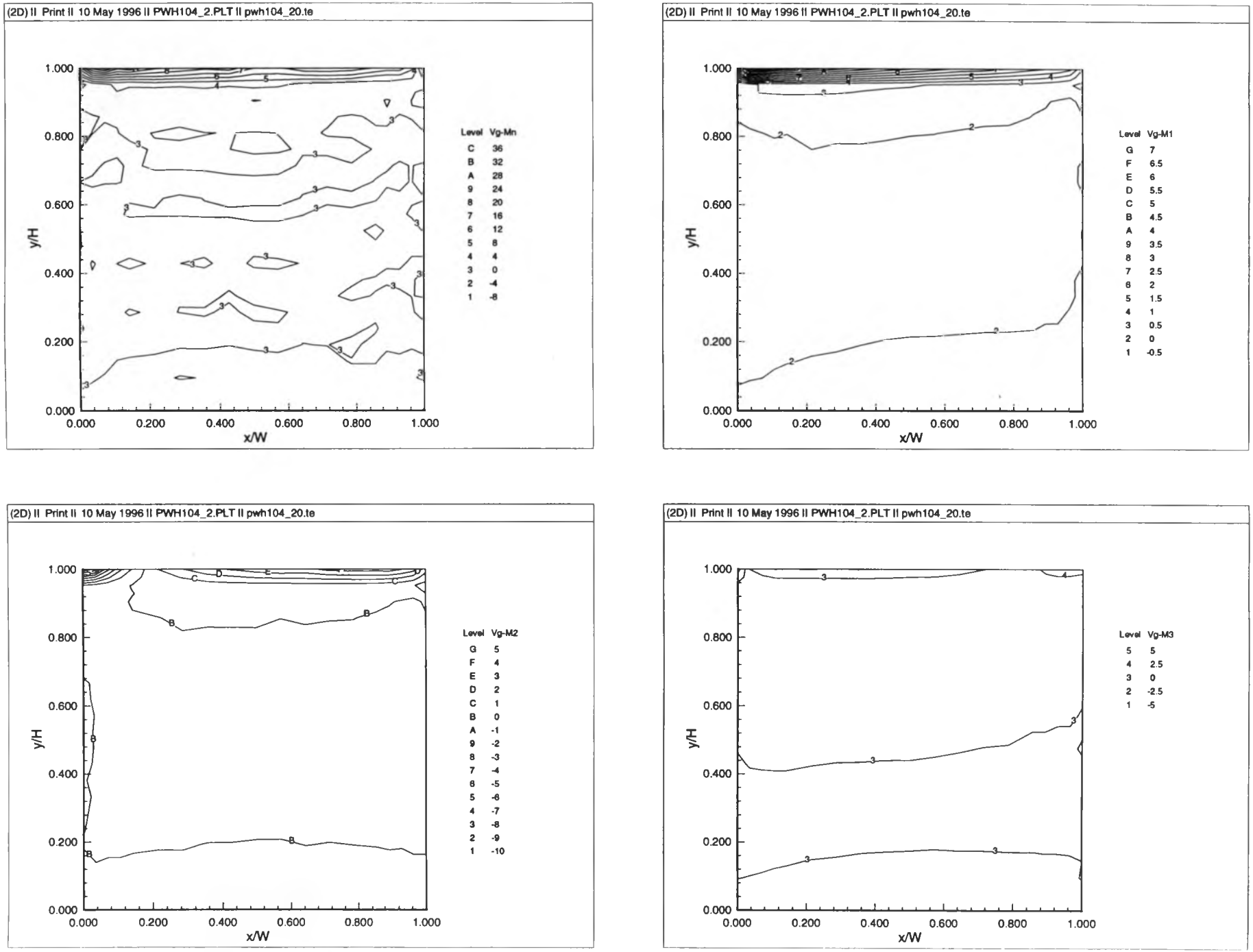

Figure E.10. Means and 1st 3 Mode Shapes of Vertical Pressure Gradients, filtered (30 degrees, open country)

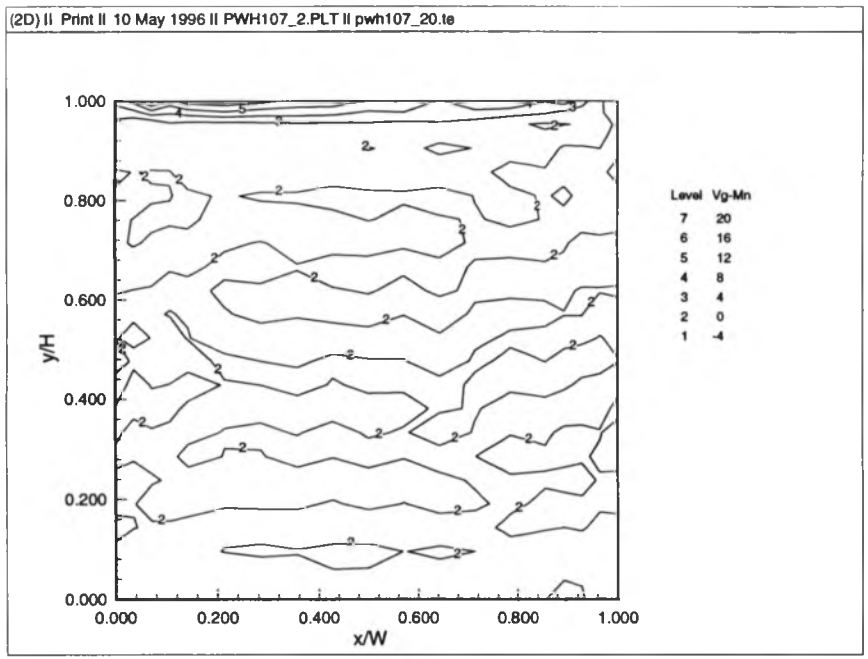

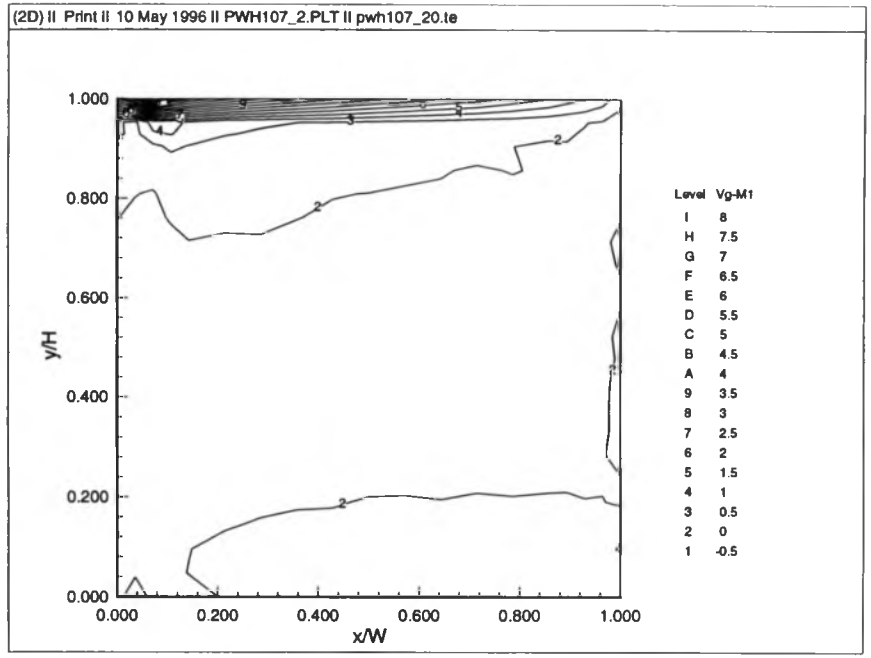

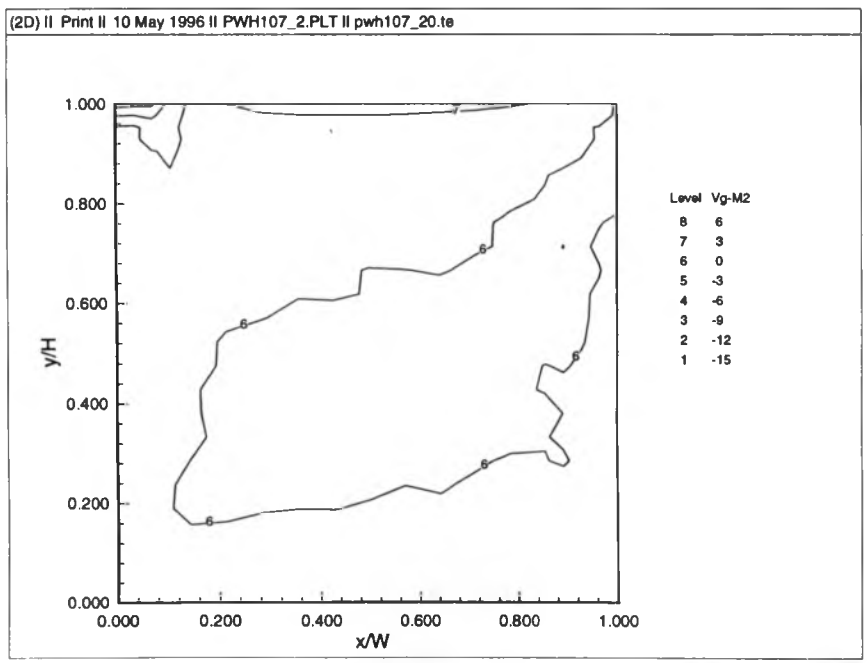

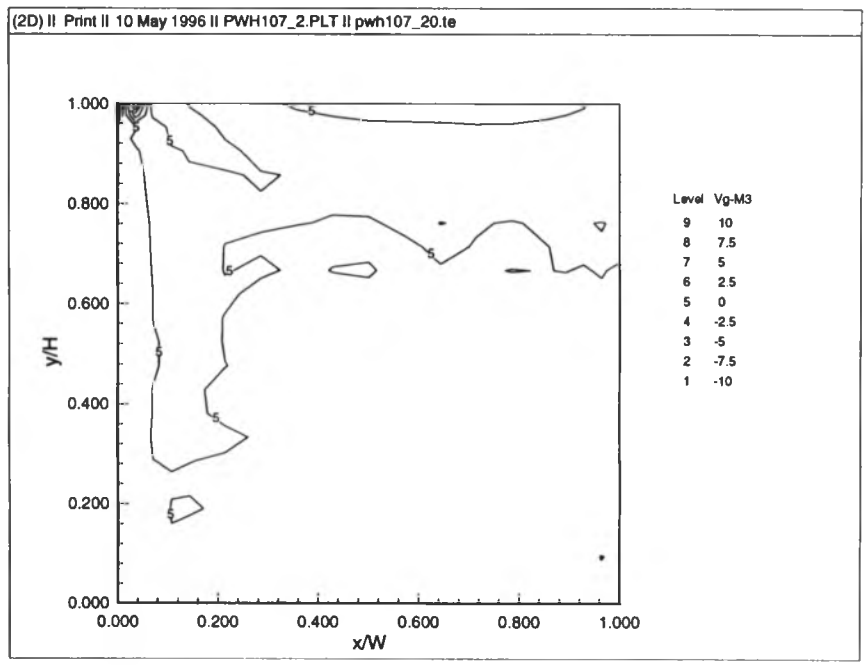

Figure E.11. Means and 1st 3 Mode Shapes of Vertical Pressure Gradients, filtered (60 degrees, open country)

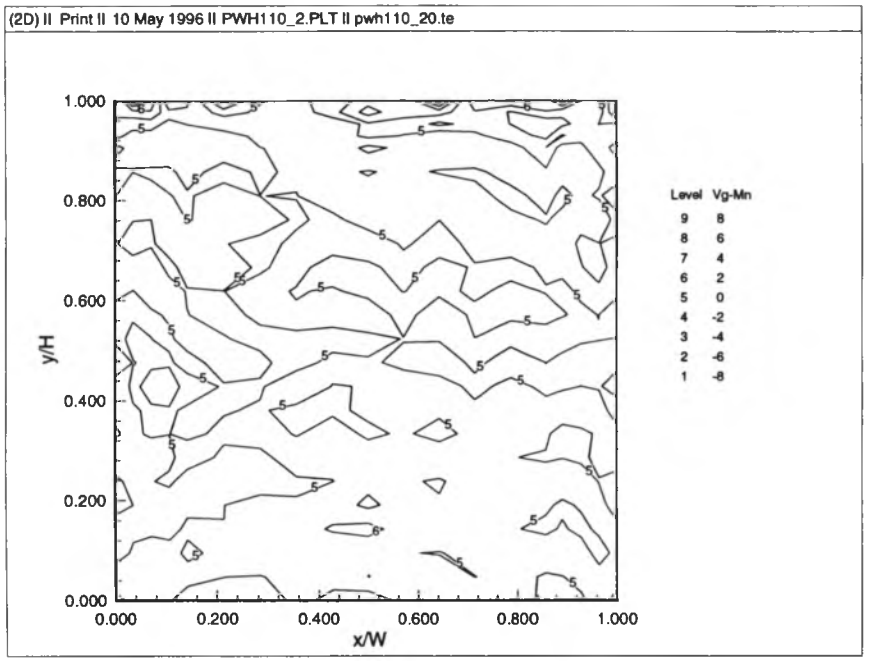

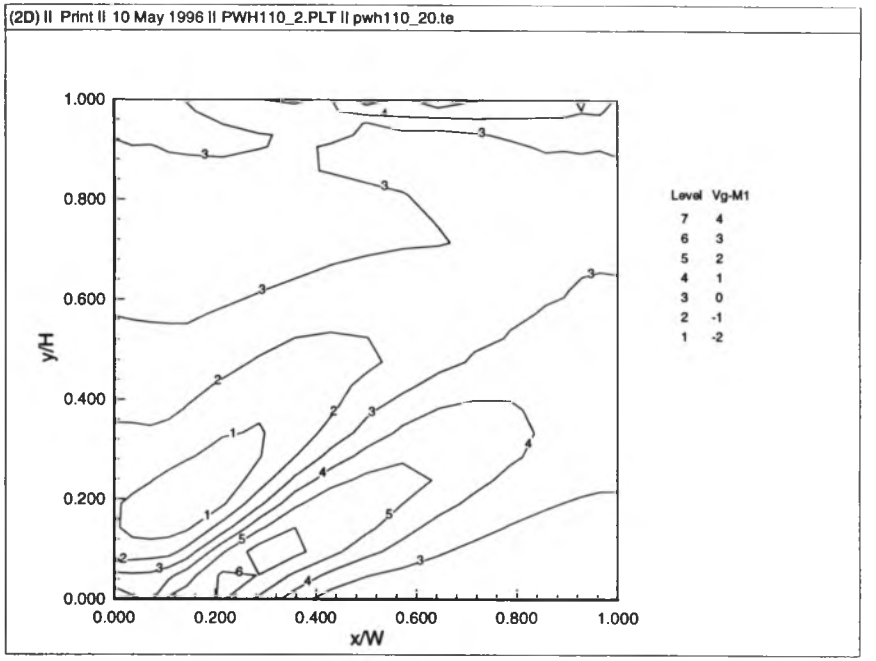

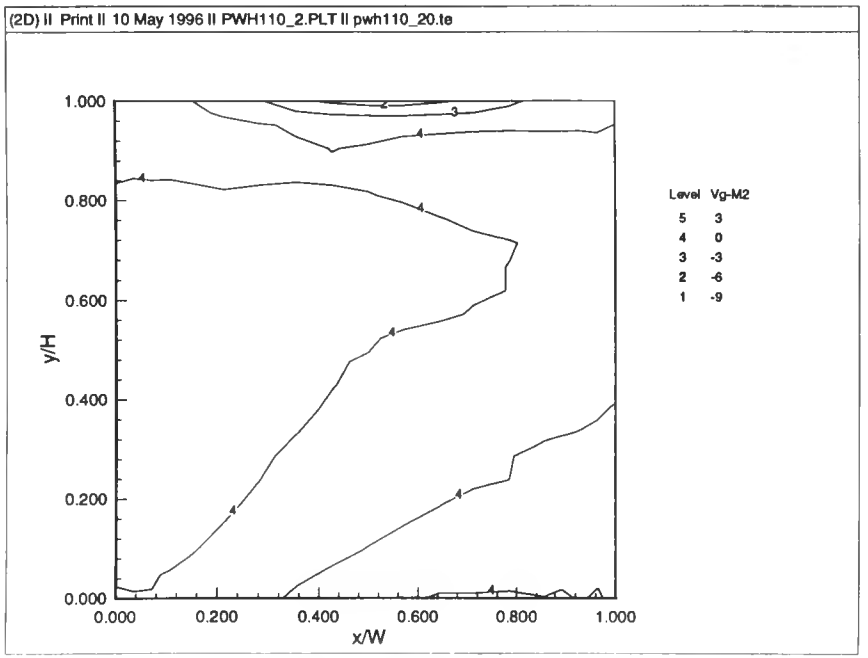

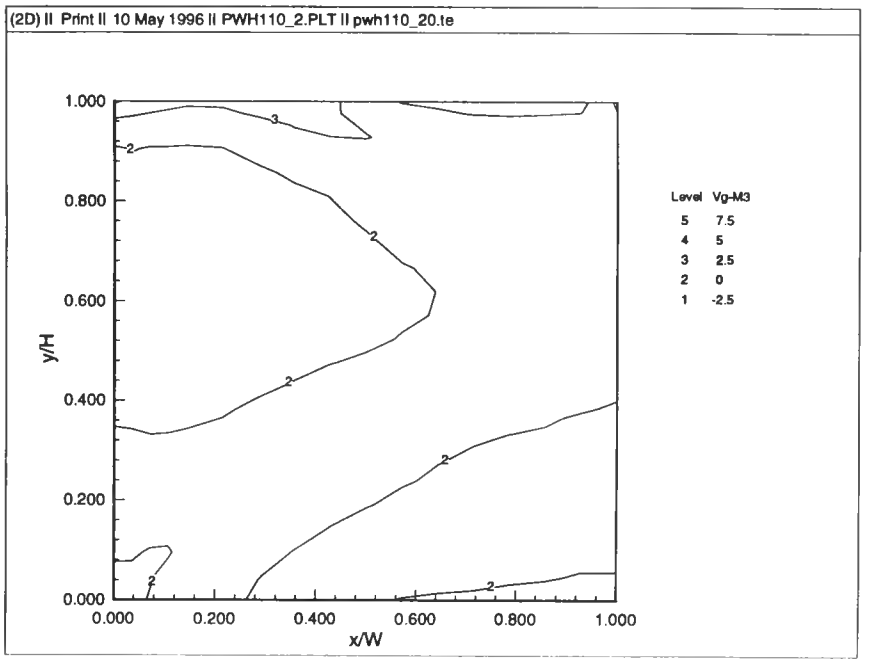

Figure E.12. Means and 1st 3 Mode Shapes of Vertical Pressure Gradients, filtered (90 degrees, open country)

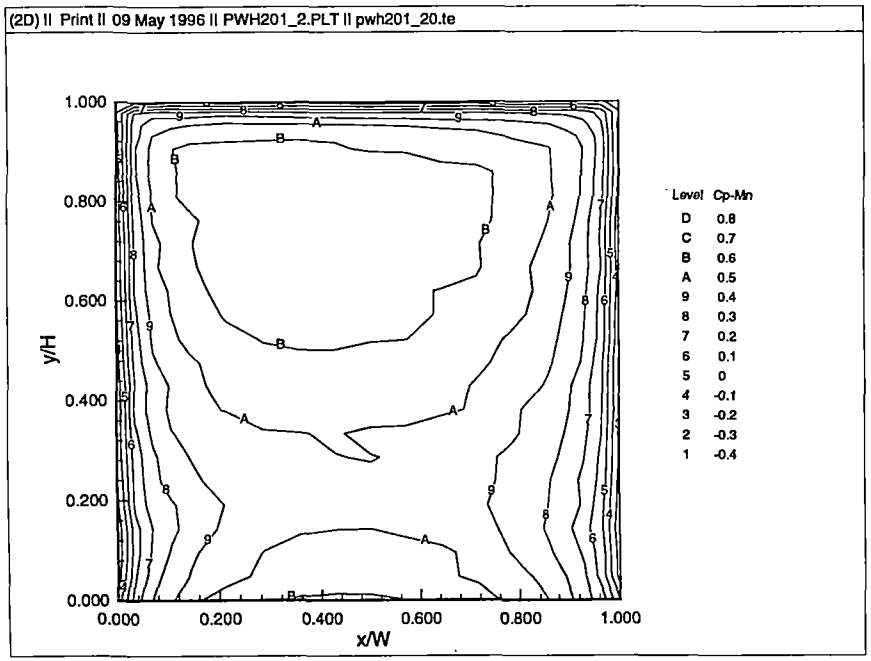

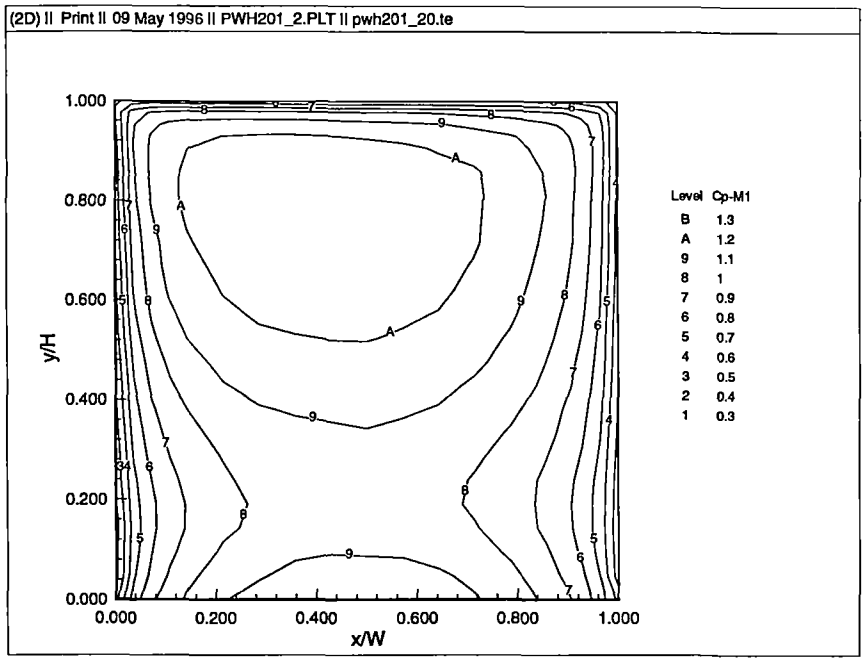

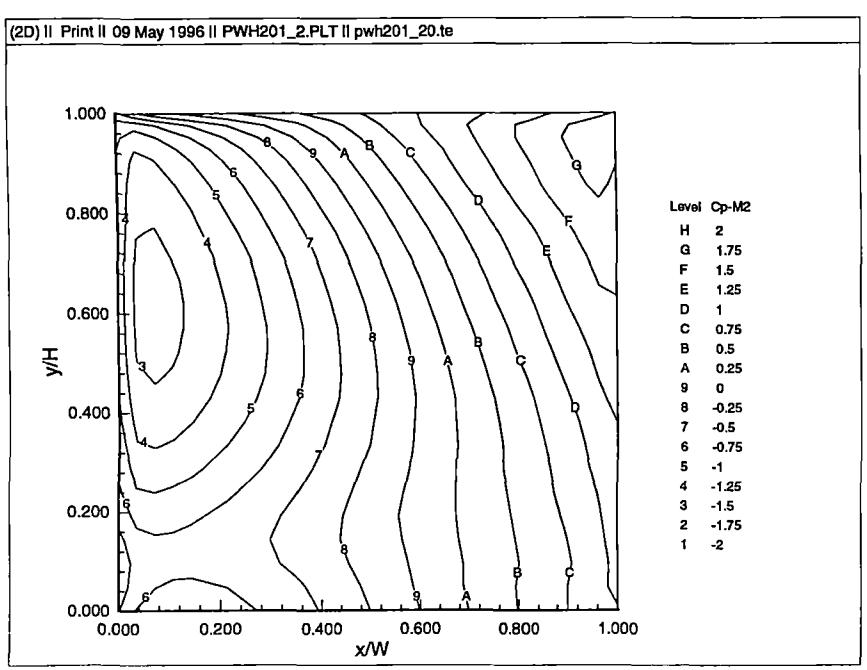

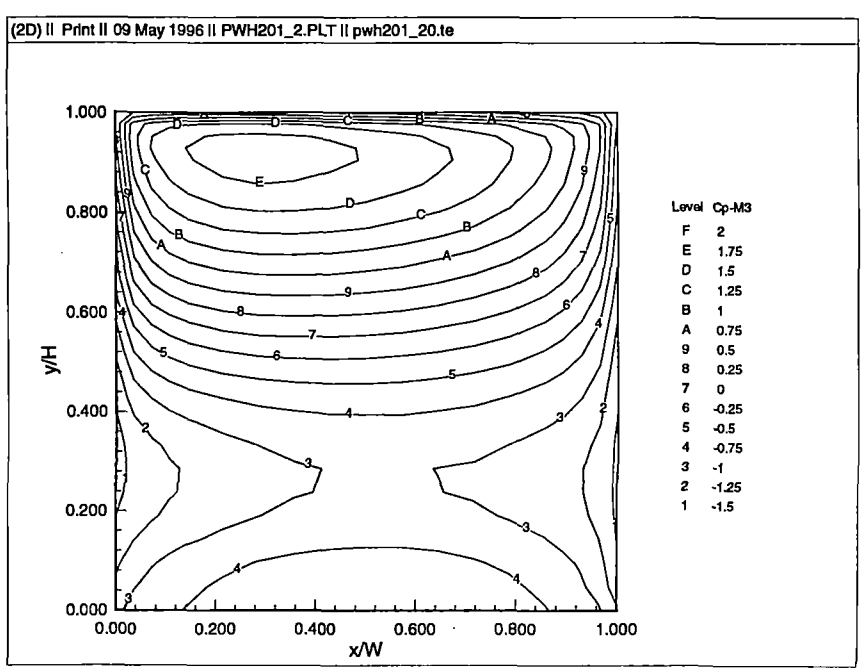

Figure E.13. Means and 1st 3 Mode Shapes of Pressure Coefficients, filtered (0 degrees, suburban)

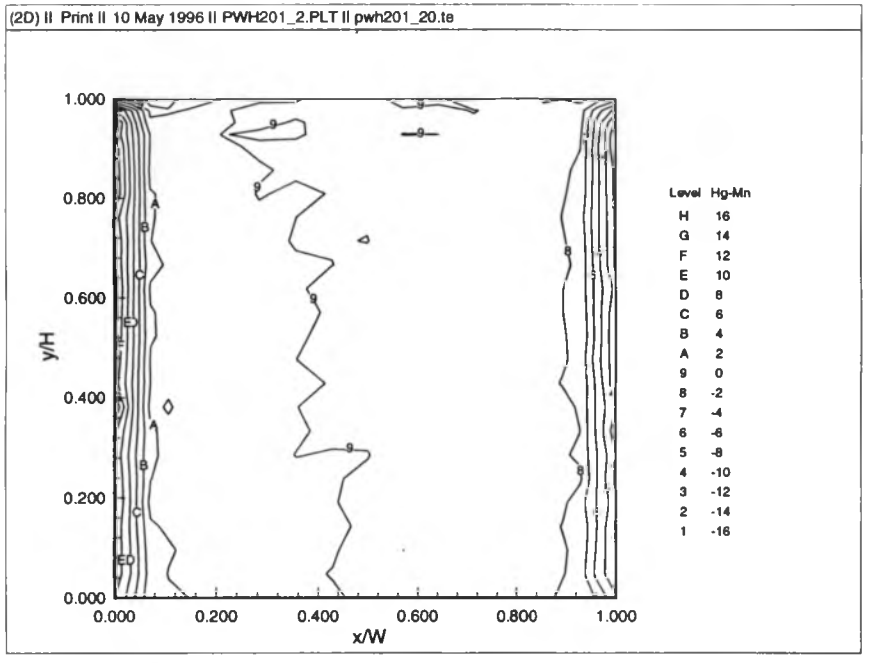

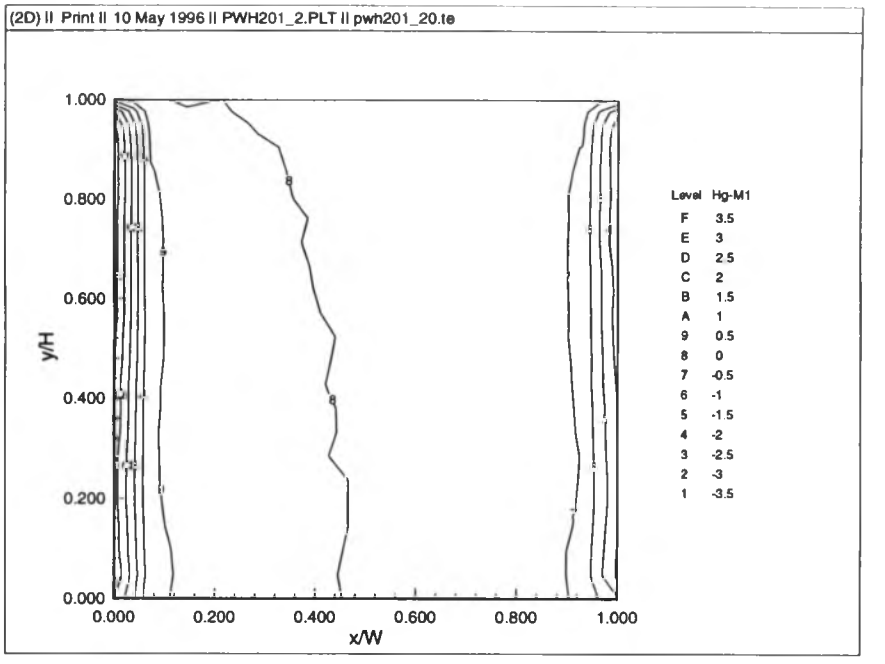

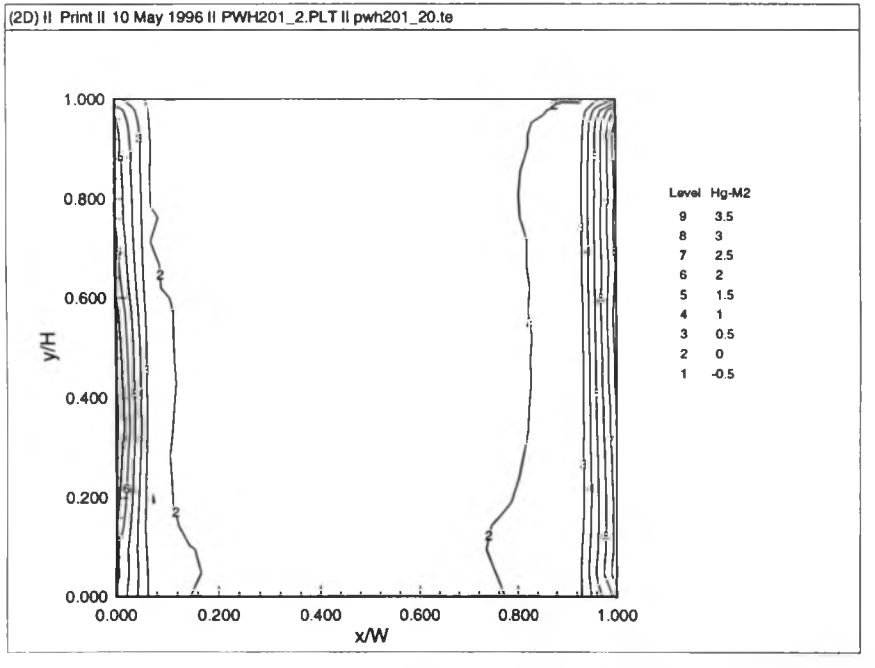

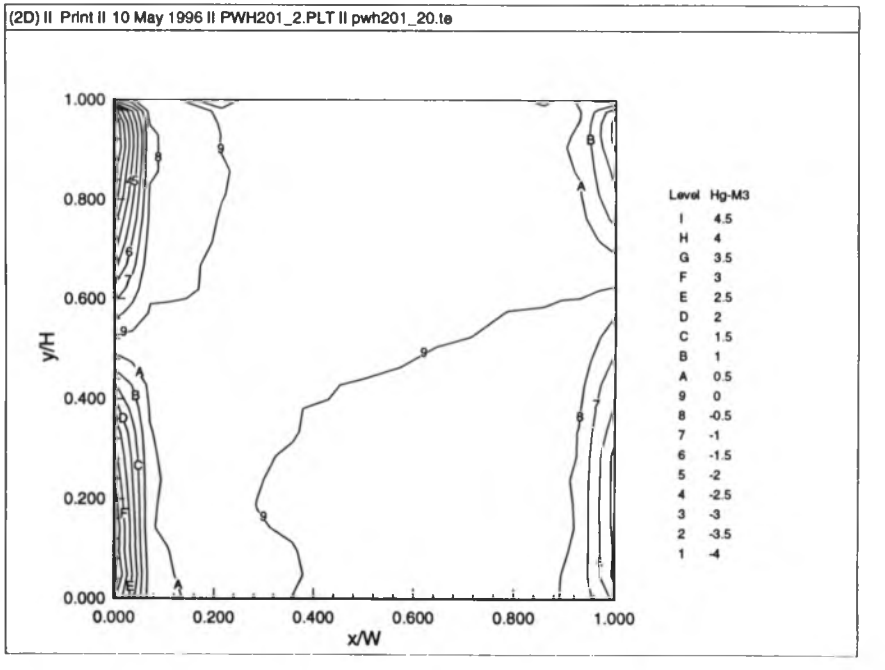

Figure E.14. Means and 1st 3 Mode Shapes of Horizontal Pressure Gradients, filtered (0 degrees, suburban)

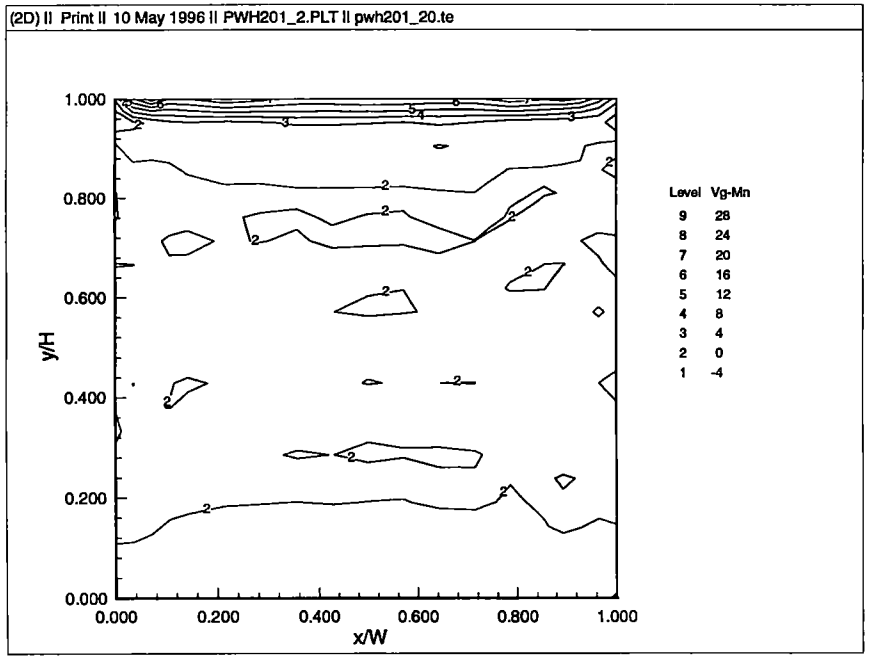

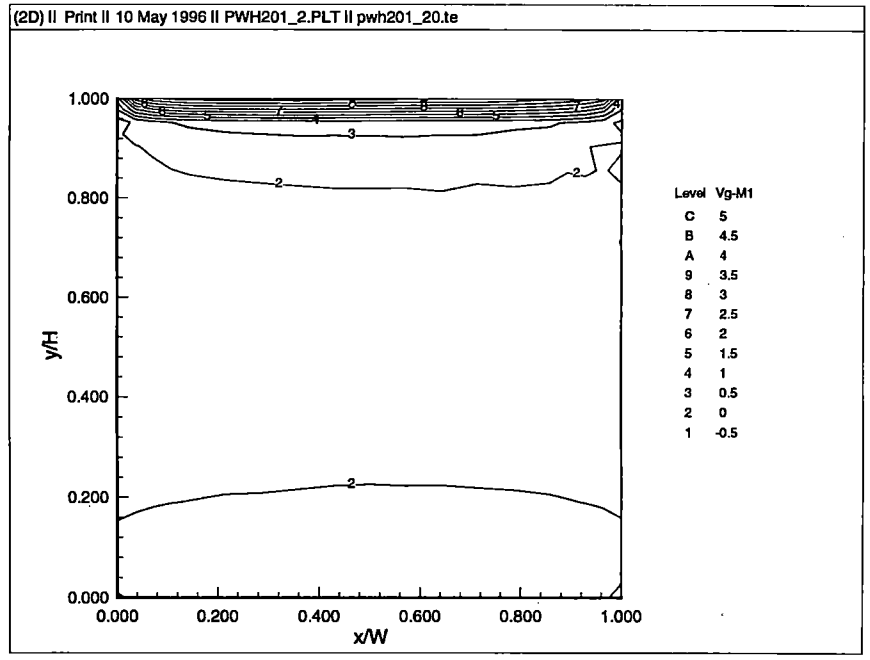

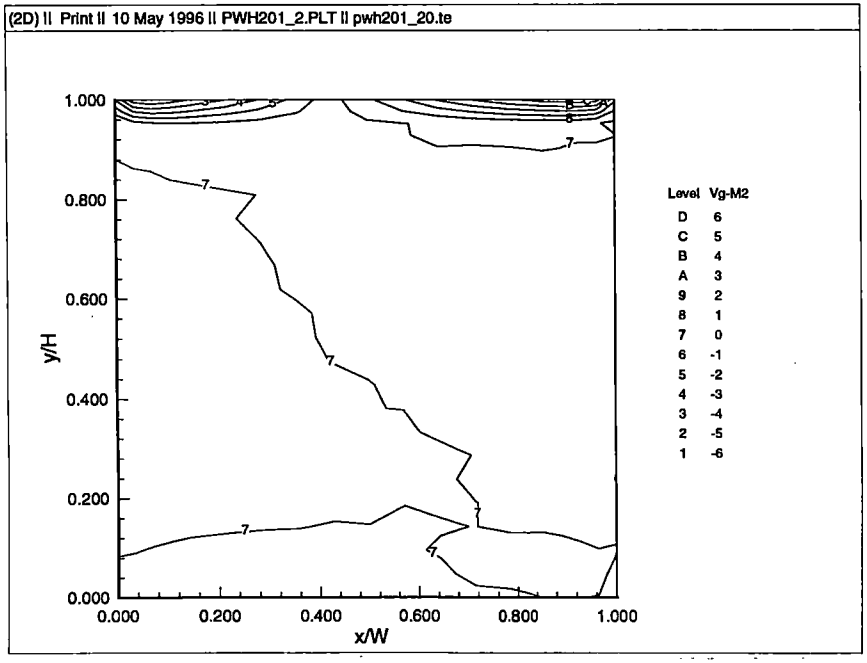

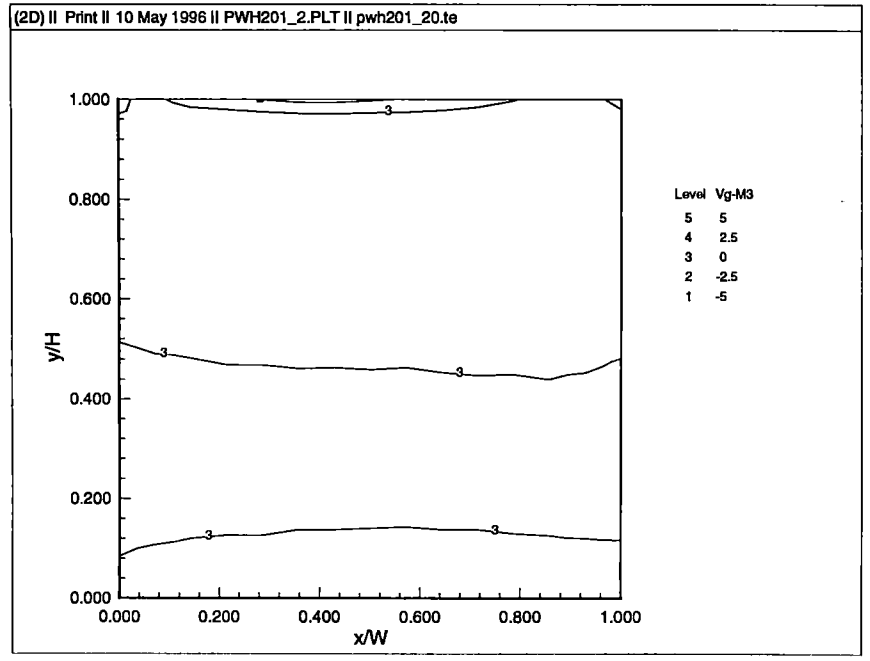

Figure E.15. Means and 1st 3 Mode Shapes of Vertical Pressure Gradients, filtered (0 degrees, suburban)

Open Country Exposure:

Wind Angle	Pressure Coefficients				Horizontal Gradients				Vertical Gradients			
	mode 1	mode 2	mode 3	mode 4	mode 1	mode 2	mode 3	mode 4	mode 1	mode 2	mode 3	mode 4
0	0.155	0.067	0.06	0.035	1.083	0.623	0.317	0.249	1.135	0.413	0.26	0.215
30	0.149	0.069	0.05	0.031	1.154	0.429	0.314	0.203	1.293	0.552	0.223	0.204
60	0.133	0.049	0.043	0.031	0.894	0.688	0.519	0.436	1.122	0.422	0.332	0.207
90	0.144	0.085	0.066	0.047	0.404	0.364	0.28	0.267	0.368	0.347	0.306	0.281

Suburban Exposure:

Wind Angle	Pressure Coefficients				Horizontal Gradients				Vertical Gradients			
	mode 1	mode 2	mode 3	mode 4	mode 1	mode 2	mode 3	mode 4	mode 1	mode 2	mode 3	mode 4
0	0.28	0.083	0.077	0.065	1.519	0.677	0.422	0.311	1.571	0.571	0.345	0.26

Table E.1 Root-Mean-Square Modal Amplitudes (filtered signals)

* wide face of building, aspect ratio H:W of 3:2

OPEN COUNTRY EXPOSURE:

Wind Angle	Pressure Coefficients				Horizontal Gradients				Vertical Gradients			
	mode 1	mode 2	mode 3	mode 4	mode 1	mode 2	mode 3	mode 4	mode 1	mode 2	mode 3	mode 4
0	0.635	0.12	0.096	0.033	0.563	0.186	0.048	0.03	0.601	0.08	0.032	0.022
30	0.655	0.143	0.075	0.028	0.675	0.093	0.05	0.021	0.655	0.119	0.02	0.016
60	0.681	0.091	0.073	0.038	0.259	0.153	0.088	0.062	0.581	0.082	0.051	0.02
90	0.473	0.164	0.1	0.051	0.111	0.09	0.054	0.049	0.062	0.055	0.043	0.037

SUBURBAN EXPOSURE:

Wind Angle	Pressure Coefficients				Horizontal Gradients				Vertical Gradients			
	mode 1	mode 2	mode 3	mode 4	mode 1	mode 2	mode 3	mode 4	mode 1	mode 2	mode 3	mode 4
0	0.765	0.067	0.058	0.041	0.641	0.126	0.05	0.027	0.646	0.086	0.031	0.018

Table E.2 Collective Energy Ratios (filtered signals)

* wide face of building, aspect ratio H:W of 3:2

APPENDIX F

EXPECTED PRESSURES AND GRADIENTS FROM ORTHOGONAL DECOMPOSITION

(FILTERED)

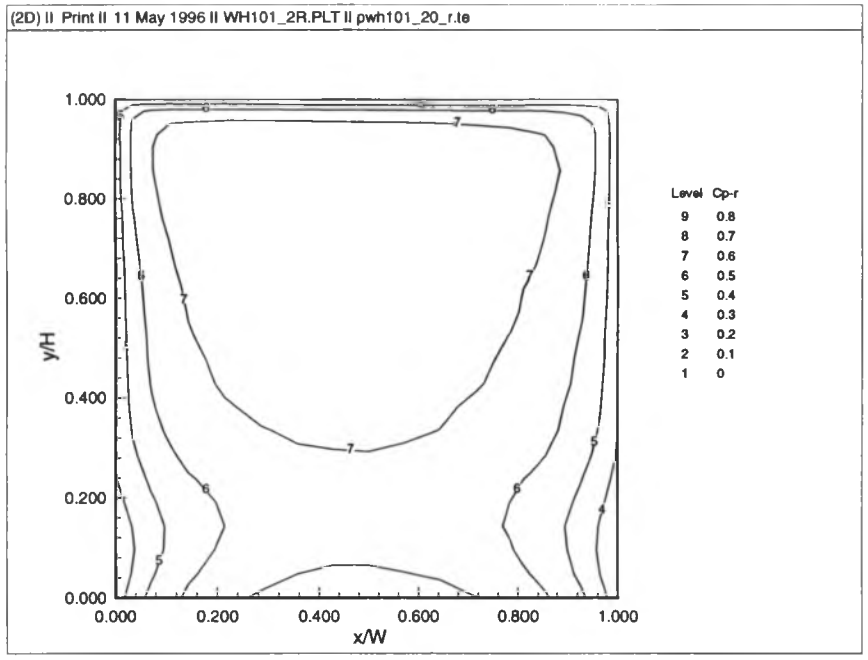

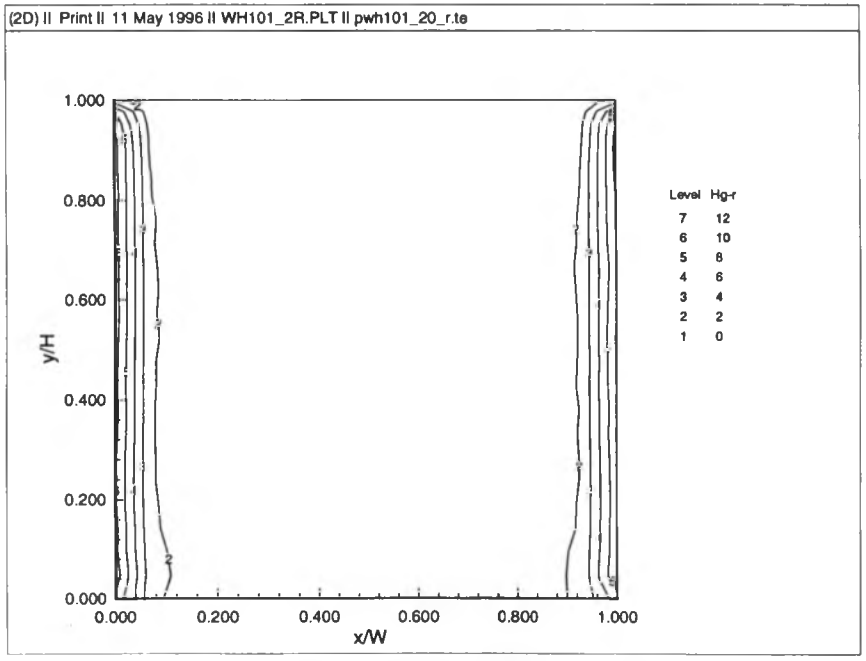

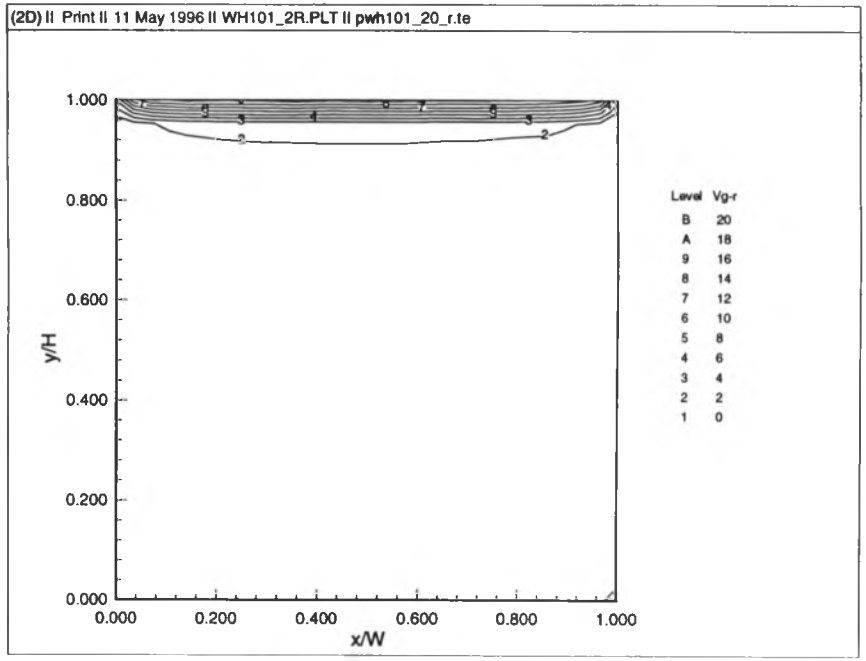

Figure F.1. Expected Unsteady Pressures and Gradients, 3 modes, *B*=3, filtered

(0 degrees, open country)

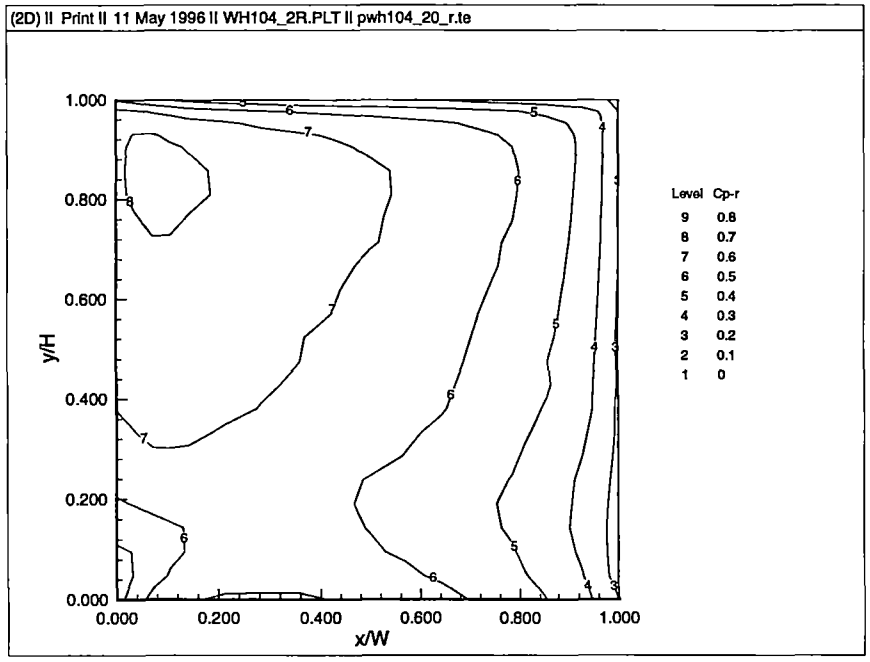

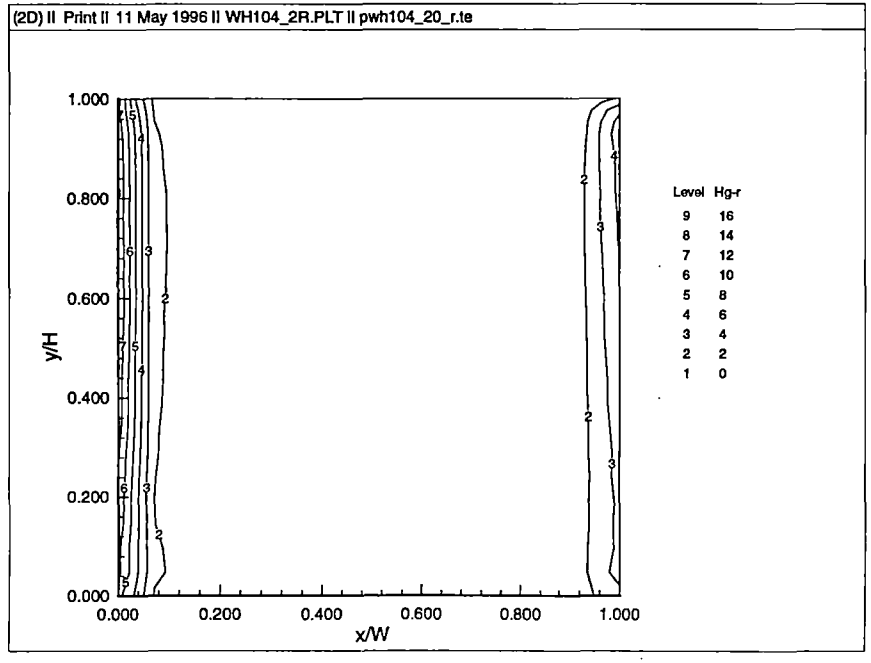

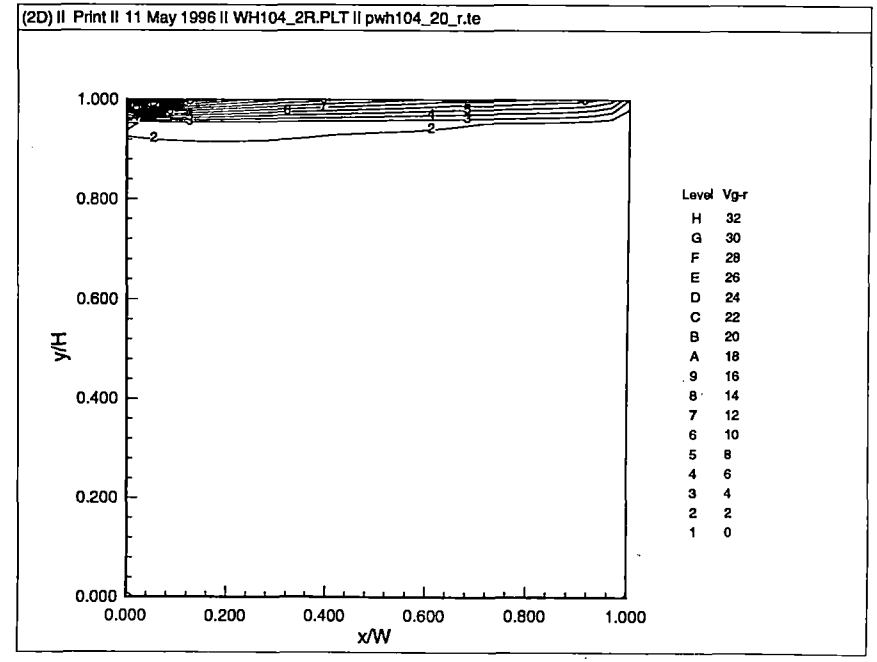

Figure F.2. Expected Unsteady Pressures and Gradients, 3 modes, *B*=3, filtered (30 degrees, open country)

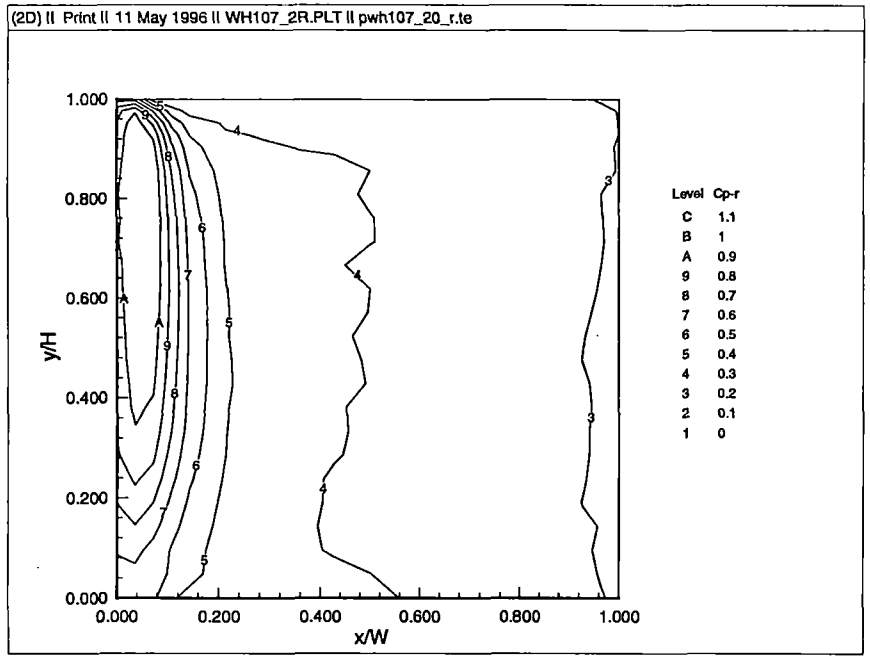

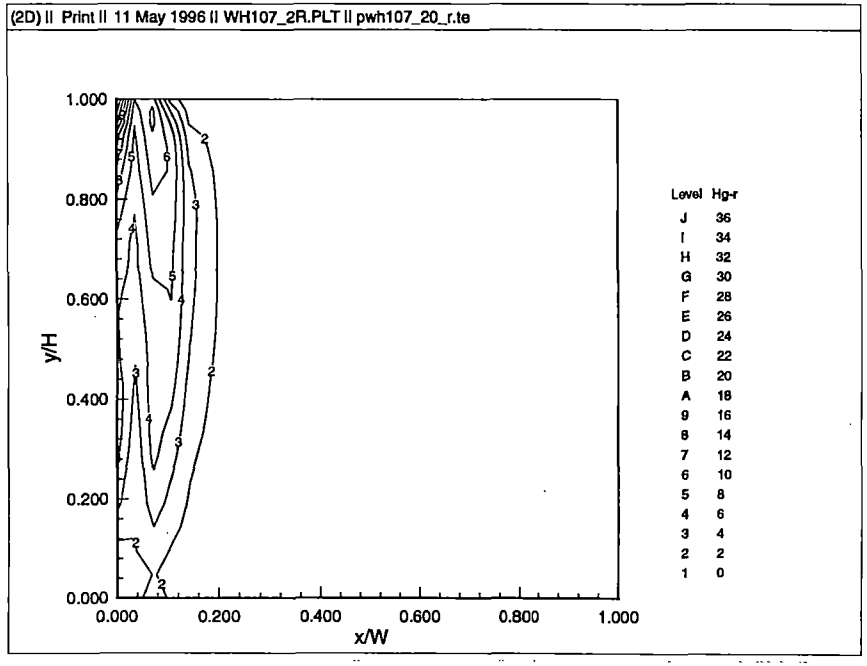

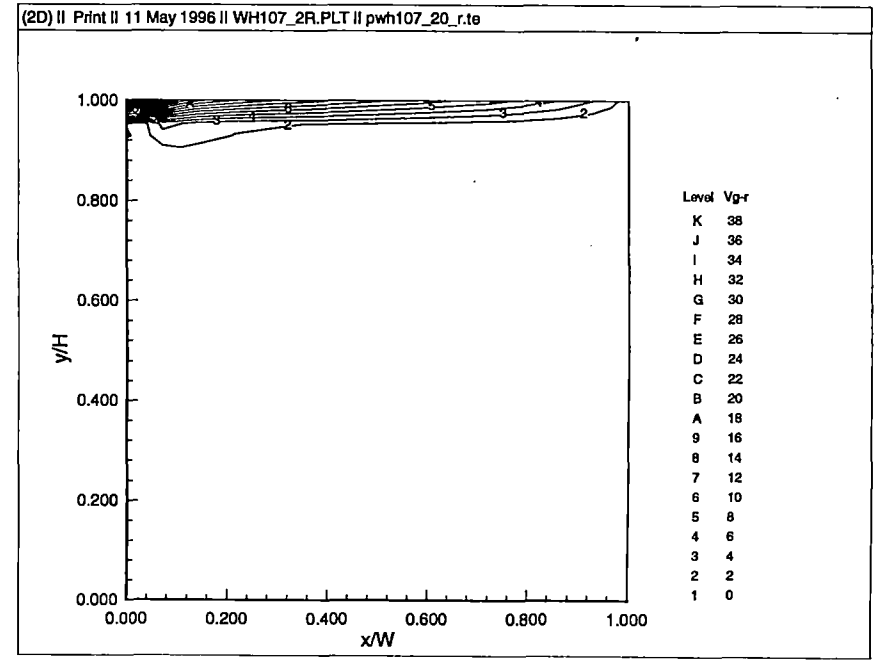

Figure F.3. Expected Unsteady Pressures and Gradients, 3 modes, *B*=3, filtered (60 degrees, open country)

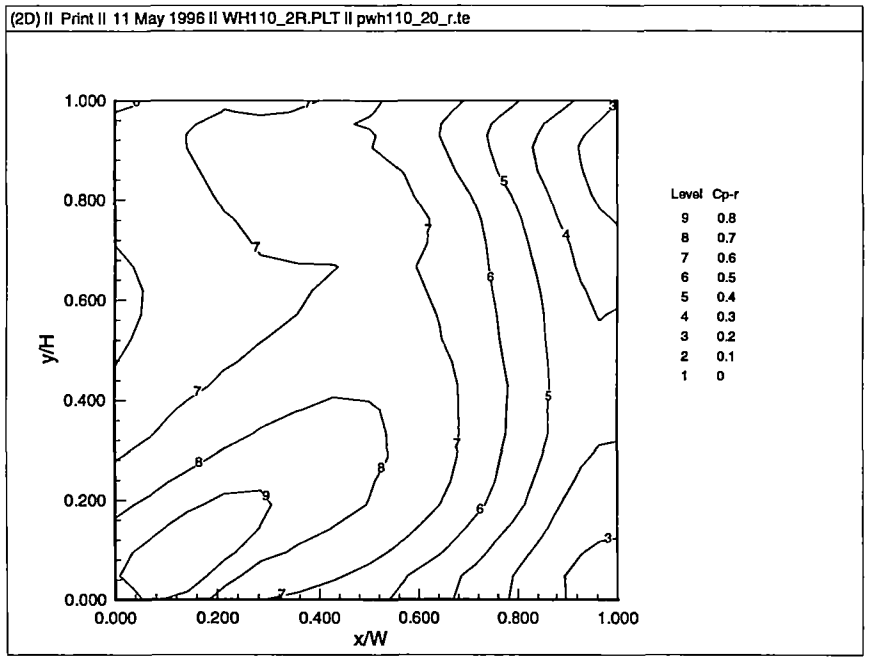

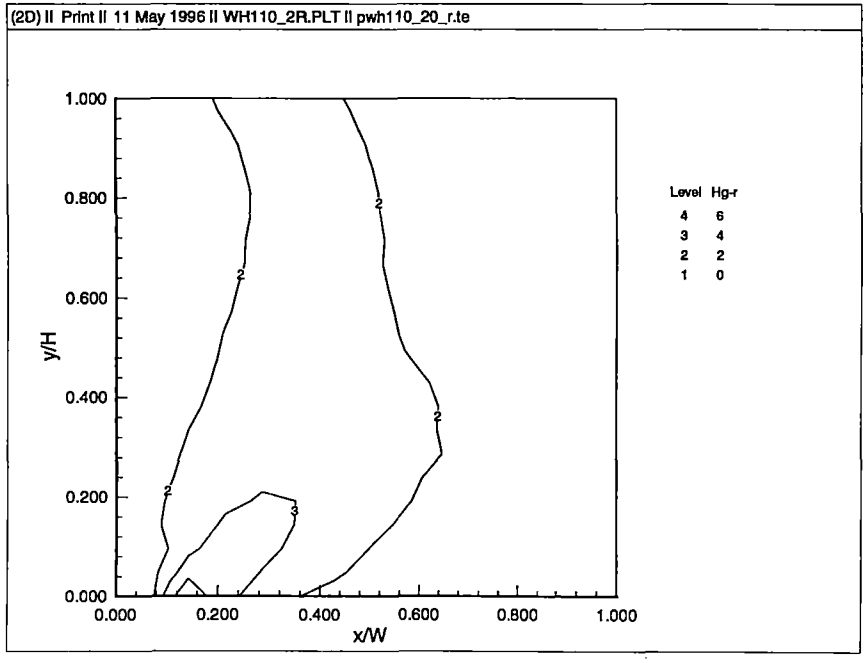

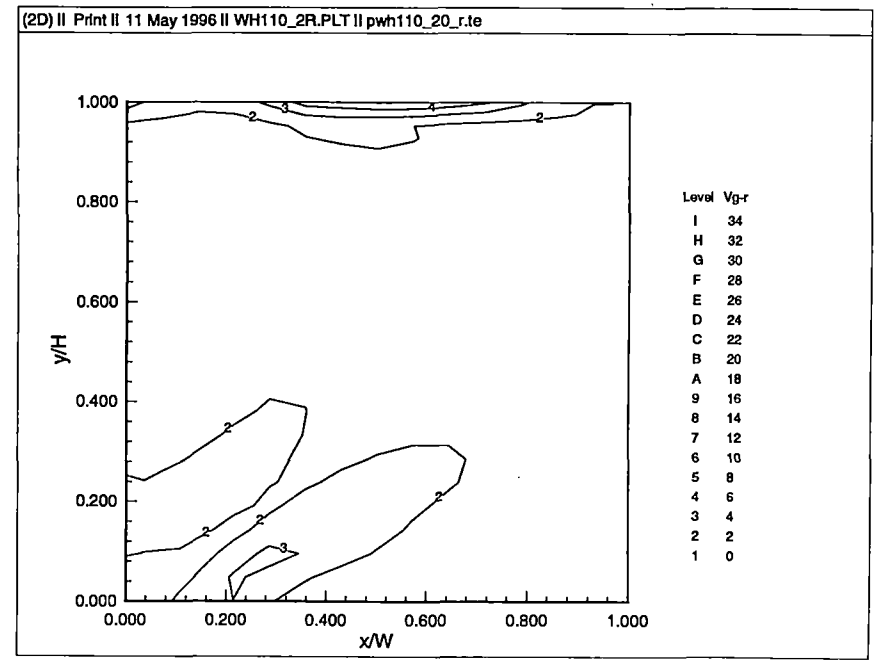

Figure F.4. Expected Unsteady Pressures and Gradients, 3 modes, *B*=3, filtered (90 degrees, open country)

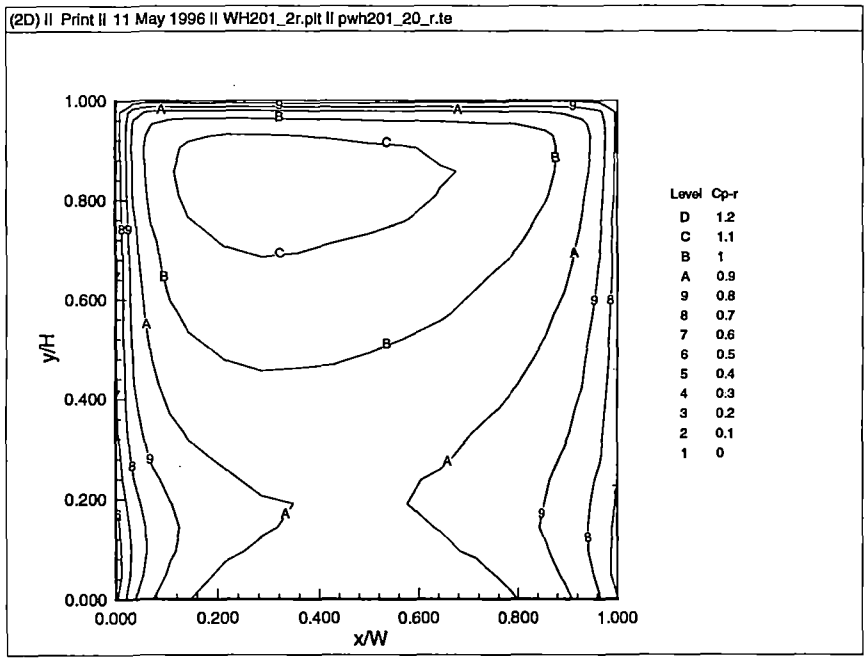

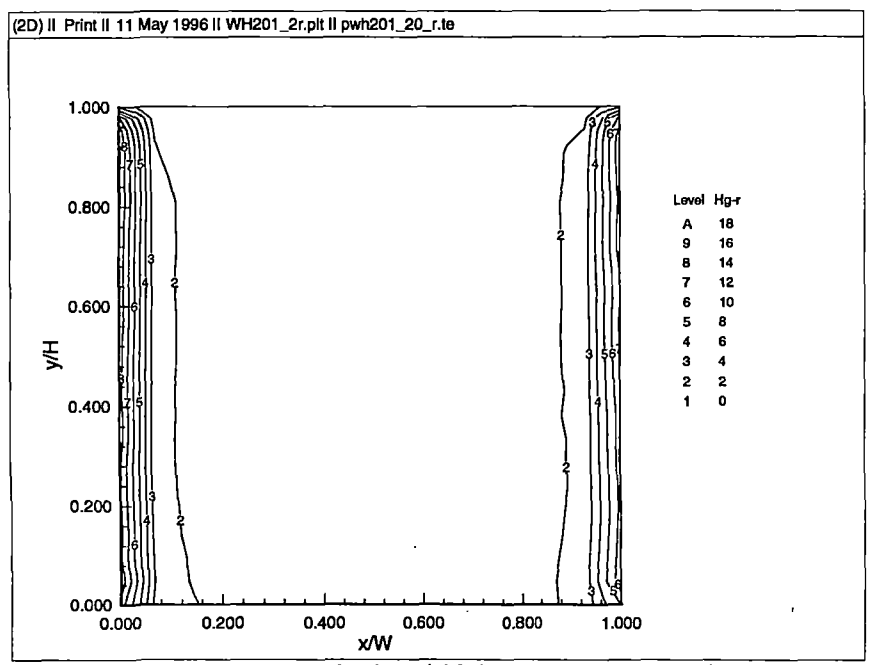

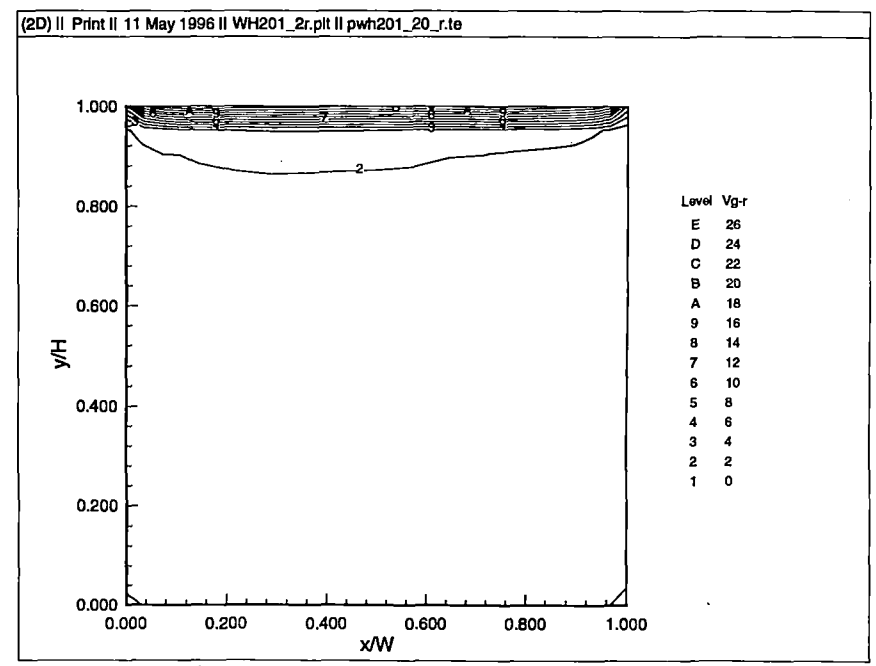

Figure F.5. Expected Unsteady Pressures and Gradients, 3 modes, *B*=3, filtered (0 degrees, suburban)

APPENDIX G

MEASURED PEAK GRADIENTS

(FILTERED)

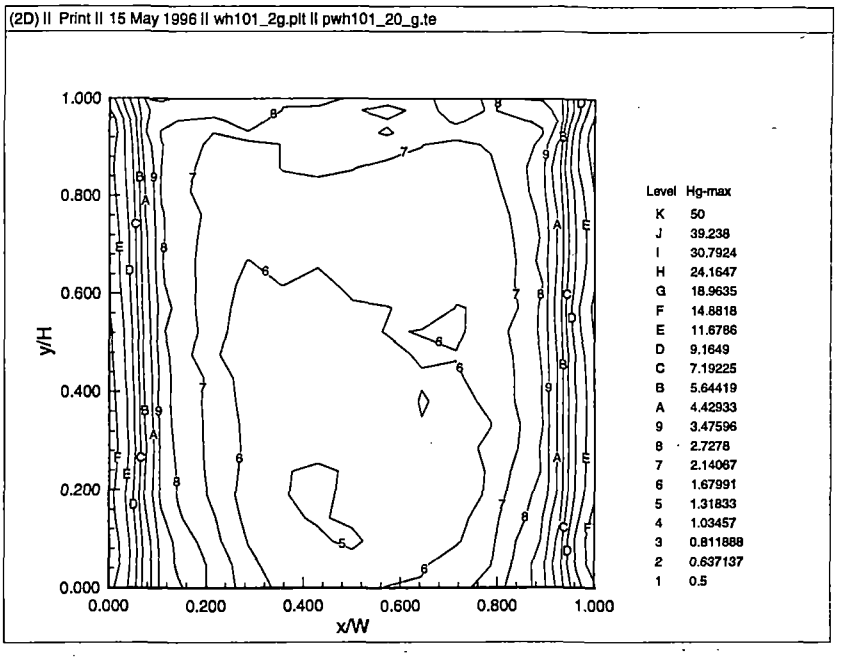

Figure G.1a. Peak Unsteady Horizontal Pressure Gradients, filtered (0 degrees, open country)

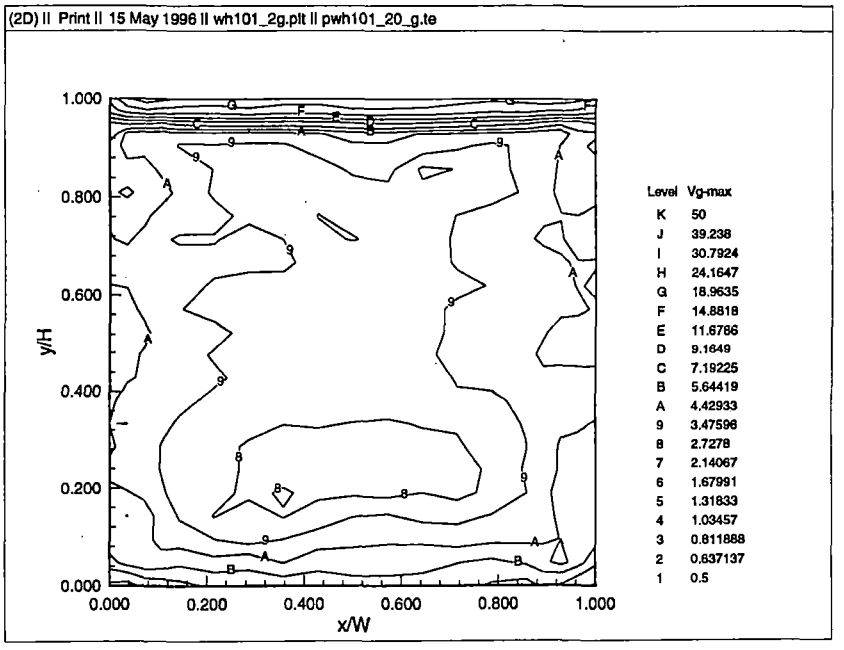

Figure G.1b. Peak Unsteady Vertical Pressure Gradients, filtered (0 degrees, open country)

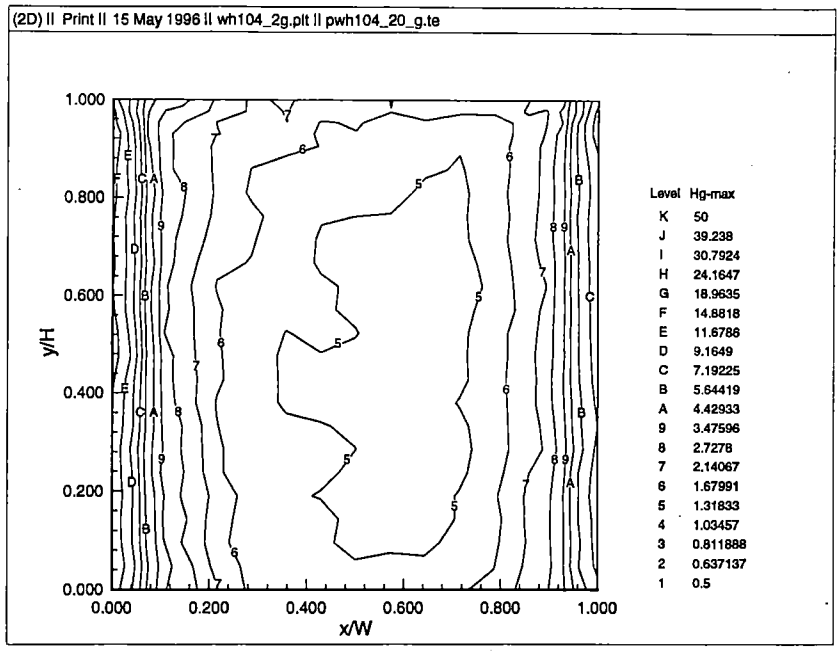

Figure G.2a. Peak Unsteady Horizontal Pressure Gradients, filtered (30 degrees, open country)

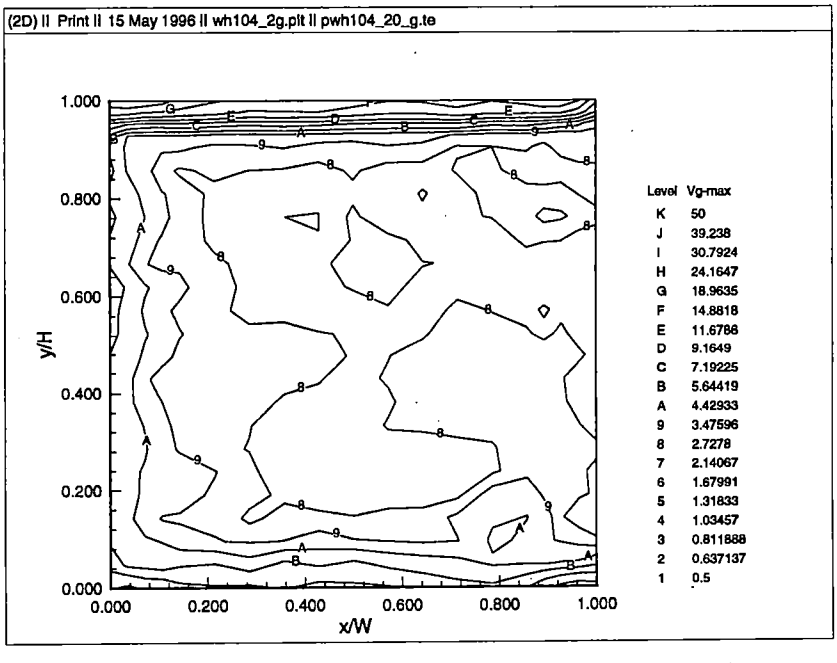

Figure G.2b. Peak Unsteady Vertical Pressure Gradients, filtered (30 degrees, open country)

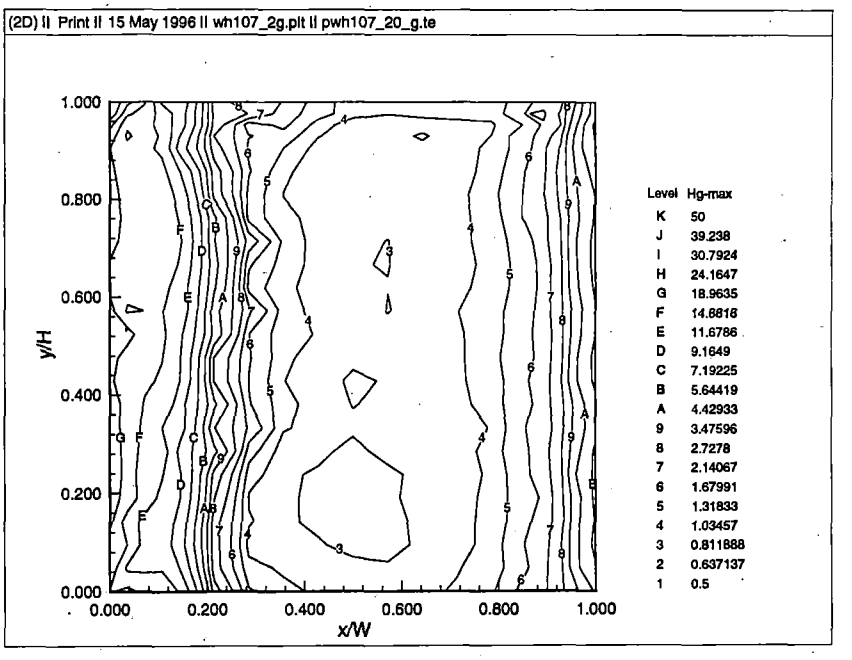

Figure G.3a. Peak Unsteady Horizontal Pressure Gradients, filtered (60 degrees, open country)

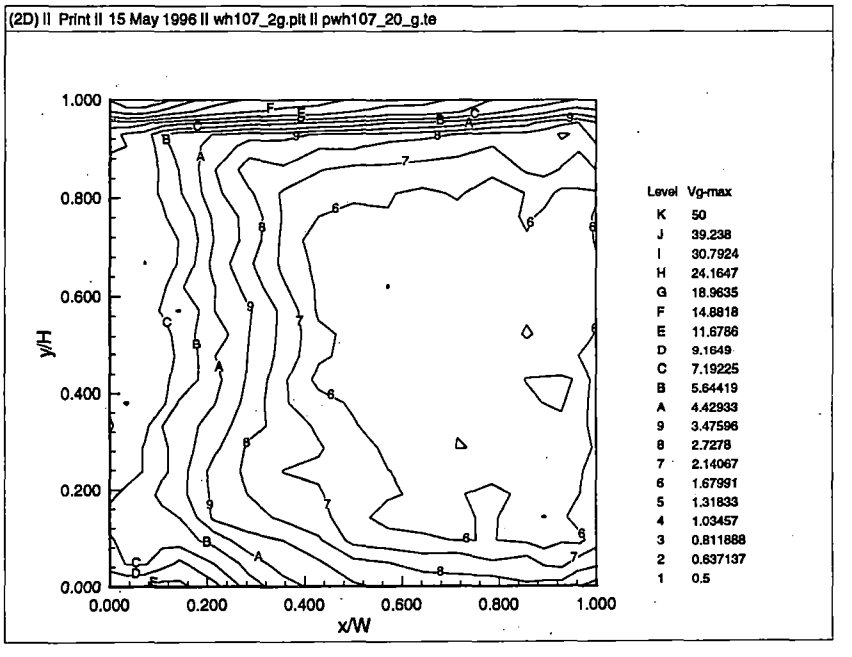

Figure G.3b. Peak Unsteady Vertical Pressure Gradients, filtered (60 degrees, open country)

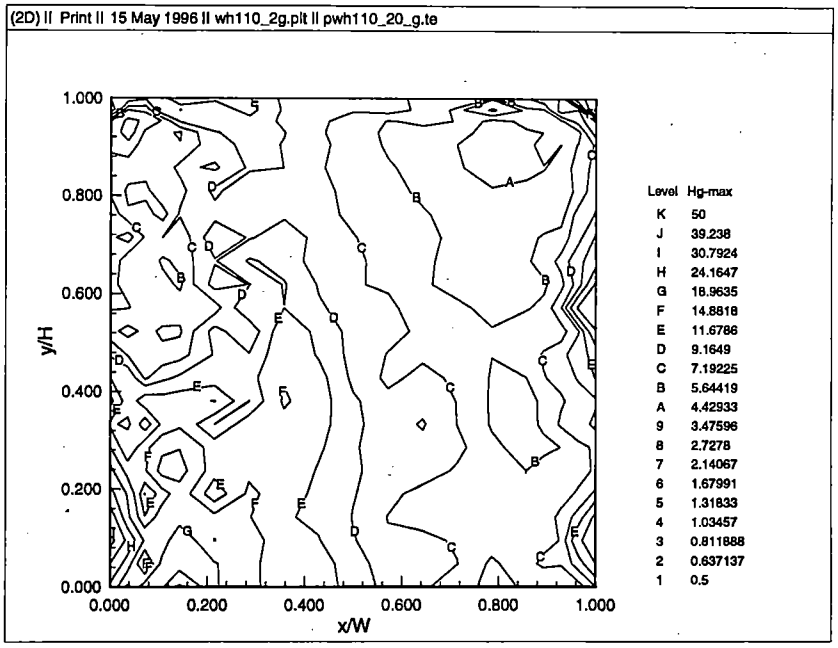

Figure G.4a. Peak Unsteady Horizontal Pressure Gradients, filtered (90 degrees, open country)

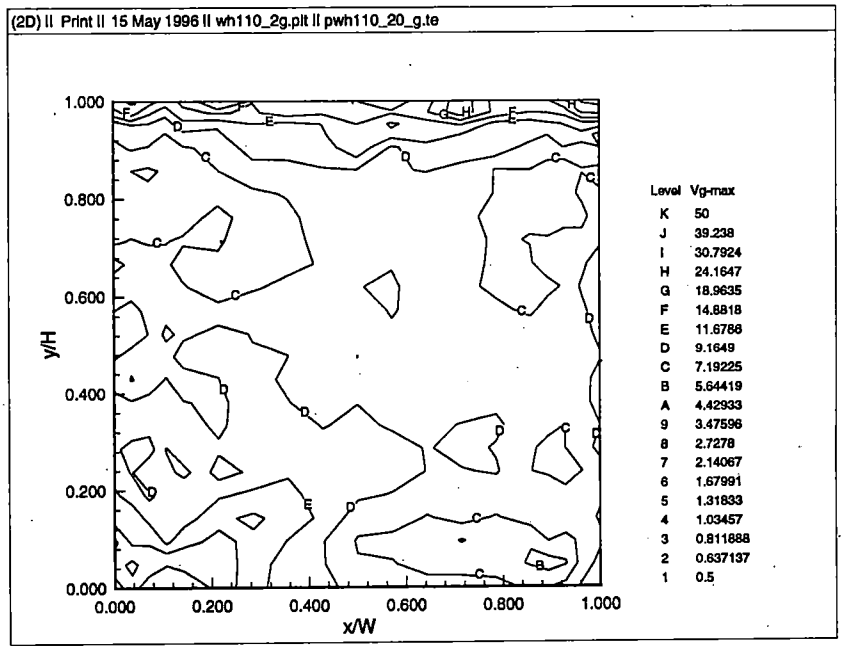

Figure G.4b. Peak Unsteady Vertical Pressure Gradients, filtered (90 degrees, open country)

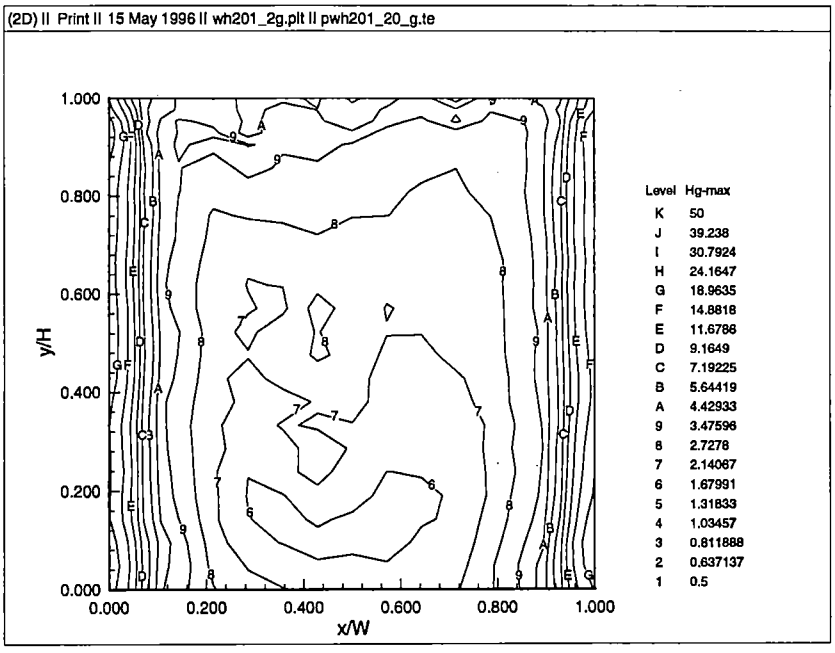

Figure G.5a. Peak Unsteady Horizontal Pressure Gradients, filtered (0 degrees, suburban)

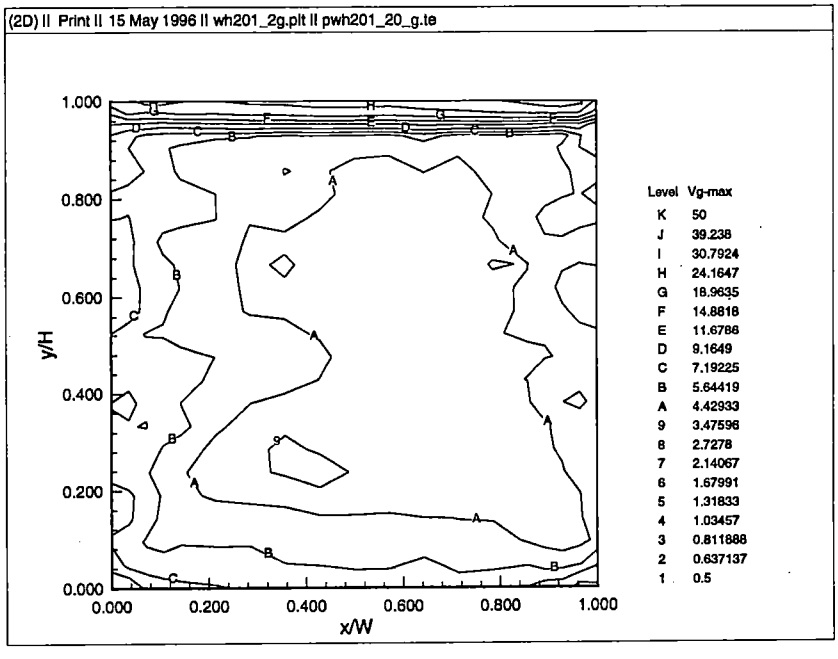

Figure G.5b. Peak Unsteady Vertical Pressure Gradients, filtered (0 degrees, suburban)